UNIVERSITÀ DEGLI STUDI DI MILANO
FACOLTÀ DI FARMACIA

Dipartimento di Scienze Farmaceutiche "Pietro Pratesi"

DOCTORATE SCHOOL IN CHEMICAL SCIENCES AND TECHNOLOGIES
Curriculum
Pharmaceutical Sciences (XXIV Cycle)
CHIM/08

Design, synthesis and biological evaluation of potential STAT3 inhibitors as anticancer agents

Daniela Masciocchi
R08261

Tutor: Dr. Arianna GELAIN
Coordinator: Prof. Ermanno VALOTI

Academic year 2010/2011

ABSTRACT

Signal Transducers and Activators of Transcription factors (STATs) are a class of latent cytoplasmic proteins that regulate cell growth and survival by modulating the expression of specific target genes. One member of the STAT family, STAT3, has received particular attention since it has been found constitutively activated in a broad spectrum of cancer cell lines and human tumors. These compelling results, combined with a well-known selectivity of STAT3 inhibitors for tumor cells, validated STAT3 as a promising anticancer drug target. Although the experimental studies on STAT3 inhibitors seem very interesting, to date, there is no evidence in literature of any impending clinical development.

The aim of this research project was the identification of new small molecules able to inhibit STAT3 activity through the direct binding to STAT3 protein. Starting from the structures of molecules which were known in the literature for their STAT3 inhibitory activity, three classes of compounds were developed: the oxadiazoles, the pyridazinones and the *ortho*-quinone derivatives. The oxadiazoles were structurally related to **AVS-0288**, which was identified through a screening of a Korean chemical library for its ability to inhibit STAT3 activity, although the exact mechanism of action had not been clarified yet. These derivatives were designed using the most classical approaches for a 'hit to lead generation': bioisosterism, vinilogy, homology. The second series of molecules, the pyridazinones, derived from the natural compound **Cryptotanshinone**, a direct STAT3 inhibitor, and was designed with the support of molecular modeling studies. These latter studies suggested a structural similarity between Cryptotanshinone and a series of pyridazinone derivatives, previously investigated by our research group.

Moreover, in order to combine the structural characteristics of the two series of molecules above, chimeric compounds, on the basis of an accurate conformational analysis, were designed and synthesized. Finally, with the aim to understand the mode of interaction of the parent compound Cryptotanshinone with the SH2 domain of STAT3, docking studies and *in vitro* screening were carried out. These suggested a key role of the *ortho*-quinone moiety, since it resembled the phosphotyrosine of the natural peptide able to bind SH2 domain. Therefore, *ortho*-quinone compounds, derived from a simplification of Cryptotanshinone

structure, were synthesized. However, due to the instability and high volatility of some of the designed compounds, only two representative terms have been prepared to date.

All synthesized molecules were evaluated by a cell-based preliminary screening, the dual-luciferase assay, which selected for compounds able to exert an inhibition on STAT3 activity. Although some of these assays showed interesting preliminary results, a deeper investigation was fundamental, in order to determine their target and/or mechanism of action. With this aim, an *in vitro* competitive binding assay, the AlphaScreen technology system, was performed to check the ability of these compounds to bind the SH2 domain of STAT3 and inhibit its dimerization, a crucial step for STAT3 activation.

This biological investigation led to the identification of the oxadiazole amidic derivative **F2e**, which was found to exert positive results both in the luciferase assay (20% inhibition at 5 μM) and in the AlphaScreen-based assay (IC_{50} = 17.7 μM), and moreover, its inhibitory activity was found to be dose-dependent. The effect of **F2e** on the tumor cell growth was also checked and shown to have a good profile of inhibitory activity on cell proliferation, with an GI_{50} around 2 μM for most of the screened tumor cell lines. Due to these encouraging results, **F2e** is considered the lead compound for the development of a new series of derivatives.

CONTENTS

Abbreviations

ALK - Anaplastic lymphoma kinase

ALL - Acute lymphoblastic leukemia

APRF - Acute-phase response factor

Boc - *tert*-Butoxycarbonyl

CAS - Cellular apoptosis susceptibility protein

CIS - Cytokine-inducible SH2 domain protein

CLL - Chronic lymphoblastic leukemia

CML - Chronic myeloblastic leukemia

CNTF - Ciliary neurotrophic factor

Crm1 - Chromosome region maintenance 1

DMF - Dimethylformaldehyde

DPPA - diphenylphosphorylazide

EAE - Experimental Allergic Encephalomyelitis

EDAC - 1-Ethyl-3-[3-dimethylaminopropyl]carbodiimide hydrochloride

EGFR - Epidermal growth factor receptor

ELISA - Enzyme-linked immunosorbent assay

ES cell- Embryonic stem cell

ETS - E-twenty six

FAS - Factor related apoptosis

Gbr2 - Growth factor receptor-bound protein 2

GH - Growth hormone

HATU - 2-(1H-7-Azabenzotriazol-1-yl)--1,1,3,3-tetramethyl uronium hexafluorophosphate

HDAC - Histone deactylases

HSF1 - Heat shock factor protein 1

HTS - High-throughput screening

IBX - 2-Iodoxybenzoic acid

IGF - Insulin-like growth factor

IGFBP - Insulin-like growth factor binding protein

ISRE - Interferon-stimulated response elements

JAB - JAK-binding proteins

JAK – Janus-family kinase

LIF - Leukemia inhibitory factor

MAPK - Mitogen-Activated Protein Kinase

MMP - Matrix metalloproteinase

NCS - *N*-chlorosuccinimmide

NES - Nuclear export signal

NGF - Nerve growth factor

NLS - Nuclear Localization Signals

NMR - Nuclear magnetic resonance

NOESY - Nuclear overhauser effect spectroscopy

NPC - Nuclear pore complex

ODN - Oligonucleotides

PC12 cells - Pheochromocytoma 12 cells

PDB - Protein data bank

PDGFR - Platelet-derived growth factor receptor

PIAS - Proteins that inhibit activated STATs

POM - pivaloyloxymethyl

PPA - Poliphosphoric acid

PPI - Protein-protein interactions

ppm - Parts per million

PTPases - Protein tyrosine phosphatases

*p*Tyr – Phosphotyrosine

rt - Room temperature

SHP - SH2-containing phosphatase

SOCS - Suppressors of cytokine signaling

SSI - STAT-induced STAT inhibitors

STAT3DN - STAT3 dominant negative protein

SUMO - Small ubiquitin-related modifier

TBAF - Tetra-*n*-butylammonium fluoride

TBTU - *O*-(Benzotriazol-1-yl)-*N*,*N*,*N*',*N*'-tetramethyluronium tetrafluoroborate

TFs - transcription factors

THF - Tetrahydrofuran

TYK - Tyrosine kinase

UV - Ultraviolet

VEGF - Vascular endothelial growth factor

Y* - Phosphotyrosine

1. INTRODUCTION

The proliferation and differentiation of mammalian cells is modulated by a number of specific signal molecules that regulate gene expression. Among these signals are: *i*) the steroid hormones *(e.g.* glucocorticoids, mineralocorticoids, estrogens, progestins, and androgens), chemical messengers produced by the body in response to a variety of stimuli; *ii*) small-molecule hormones including thyroid hormone, calcitriol (a vitamin D3 metabolite), and the retinoids; and *iii*) the cytokine superfamily of proteins. The latter cytokines are a large and diverse family of circulating polypeptides produced by many different cell types. They include various types of interferons (*e.g*. IFN-α, -β, -γ) the interleukins (*e.g*. IL-6), the colony-stimulating factors (*e.g*. granulocyte colony-stimulating factor, G-CSF), and growth factors (*e.g*. epidermal growth factor, EGF). Individual cytokines act upon a variety of cell types. As polypeptides, cytokines cannot freely enter into the cells, but instead act by binding to specific cell surface receptors. Thus they can indirectly initiate a chain of events that culminate in changes in the pattern of cellular gene expression, causing cells to alter their metabolism in many different ways. The understanding of biochemical events by which some of the cytokines achieve their distinctive biological effects has increased significantly in the early 1990's, when the first signaling pathway was unearthed in detail: IFN signaling.[1, 2, 3] This involved JAK tyrosine kinases and the activation of latent cytoplasmic transcription factors termed STATs (Signal Transducers and Activators of Transcription). STAT proteins were activated through phosphorylation on a tyrosyl residue within minutes after the binding of an extracellular protein to its cell surface receptor. This phophorylation of STAT was mediated by specific tyrosine kinases (such as JAKs) and resulted in their conversion from latent to active transcription factors, which migrated into the nucleus and affected transcription of specific target genes. Afterwards, STATs were found to mediate signal transduction for the majority of the cytokines, and it was surprising the similarity in the way that cytokines, with their myriad of distinctive biological effects, acted to control gene expression. Since STATs discovery, a great deal of infomation has accumulated about the specificity in their activation, their functional domains and the variety of their biological functions, as well as their effect on transcriptional changes. Although this thesis will concentrate on the role of STAT3 in cancer and on the development of STAT3 inhibitors, it

will be useful first to summarize the structure of the STATs, and their interaction with other proteins, as they function in transcriptional control.

1.1 The Signal Transducers and Activators of Transcription (STATs) family

STAT members (STAT1, STAT2, STAT3, STAT4, STAT5a, STAT5b, and STAT6), encoded in distinct genes, have been identified in various mammalian cells.[4] With the exception of STAT4, which is expressed mainly in the thymus and testes,[5] the other STAT proteins are ubiquitous. They range in size from 750 and 900 amino acids and have a molecular weight from 90 to 115 kDa. Despite functional differences of individual STAT proteins, crystallographic studies of the cores of STAT1 and STAT3 (from residues 130-712; lacking an *N*-terminal proteins are a family of latent transcription factors that are abundantly produced in many cell types. So far a total of seven different STAT family and C-terminal domain) and the NH_2 terminus of STAT4, as well as sequence comparisons and deletion mutagenesis experiments, has revealed common STAT structural features. The overall amino acid sequence identity between STATs is 28-54% (**Table 1**).[6]

	STAT1	**STAT2**	**mSTAT3**	**mSTAT4**	**sSTAT5**	**STAT6**
STAT1	100%	44.1%	52.8%	53.5%	32.2%	31.5%
STAT2	62.3%	100%	41.0%	40.9%	28.3%	30.2%
mSTAT3	70.9%	61.3%	100%	47.3%	30.5%	28.2%
mSTAT4	71.6%	60.0%	70.0%	100%	32.8%	30.3%
sSTAT5	55.2%	50.0%	53.2%	53.9%	100%	39.5%
STAT6	52.3%	52.2%	50.7%	51.6%	59.6%	100%

Table 1. Amino acid sequence similarity and identity of STATs.[6]
Per cent identity is above the 100% line, per cent similarity below.

Seven structurally and/or functionally conserved domains can be identified (**Figure 1**).

i) The *amino terminal domain* (NH_2; ~125 amino acids) is well conserved and is important for dimer-dimer interactions to form tetrameric STAT molecules. The tetramer formation has

been shown to be necessary for a strong STAT–DNA interaction at adjacent sites and is important for maximal transcriptional stimulation.[7] Additionally it has been shown that the *N*-terminus is involved in receptor recognition, phosphorylation, nuclear translocation, and dephosphorylation.[8] The crystal structure of the amino terminus of STAT4 was solved independently of the core structure and comprises a series of eight short interactive helices (**Figure 1**, **b**). Other STAT amino termini probably have similar structures, because of the similarity of structurally important amino acid residues in their amino termini, although experiments in which the domains were swapped indicate that they might not be completely equivalent.[9]

ii) The *coiled-coil domain* (amino acids ~135 to ~315) consists of a potentially dynamic four-helix bundle that protrudes laterally (~80 Å) from the core. This domain associates with regulatory proteins and has also been implicated in controlling the process of nuclear import and export.[10, 11]

iii) The *DNA Binding Domain* (DBD; amino acids ~320 to ~480) is also well conserved and mediates a robust binding to GAS palindromes. All activated STAT homodimers, except STAT2, directly bind GAS elements. The DBD has also been implicated in the regulation of nuclear import and export.[11,12]

iv) The *Linker Domain* (amino acids ~480 to ~575) structurally translates active dimerization to the DNA binding motif. Studies also suggest that it regulates a process of continual basal (*i.e*. in resting cells) nuclear export.[13]

v) The *SH2 Domain* (amino acids ~575 to ~680) is the most highly conserved motif. It mediates specific recruitment to receptor chains, as well as the formation of active STAT dimers.[14,15]

vi) The *Tyrosine Activation Motif* consists of a conserved tyrosine along with 5-7 specific carboxy terminal amino acids, usually near residue 700: like the corresponding SH2 domain, this motif resides on the exposed surface of the inactive homodimer, facilitating its JAK-dependent phosphorylation during receptor recruitment.[16] Upon phosphorylation, this motif is recognized and bound by the corresponding SH2 domain of the partner STAT, directing the critical structural changes required for an active conformation.[17]

vii) The *Transcriptional Activation Domain* (TAD) resides at the carboxy terminus and is highly variable in length and sequence between STAT family members. However, for each specific STAT, except STAT2, this sequence is conserved in humans and mice.[10,18] Many TADs include conserved serine phosphorylation sites that facilitate the recruitment of coactivators (e.g. CBP, p300 and the MCM complex).[19] Moreover, the phosphorylation of this specific serine residue (Ser727 in STAT3) contributes to maximal STAT3 transcriptional activity.[20] The STAT TAD also appears to regulate protein stability. Specifically, STAT4, STAT5 and STAT6 can be targeted for ubiquitin-dependent destruction, whereas STAT1, STAT2 and STAT3 are more stable.[21, 22]

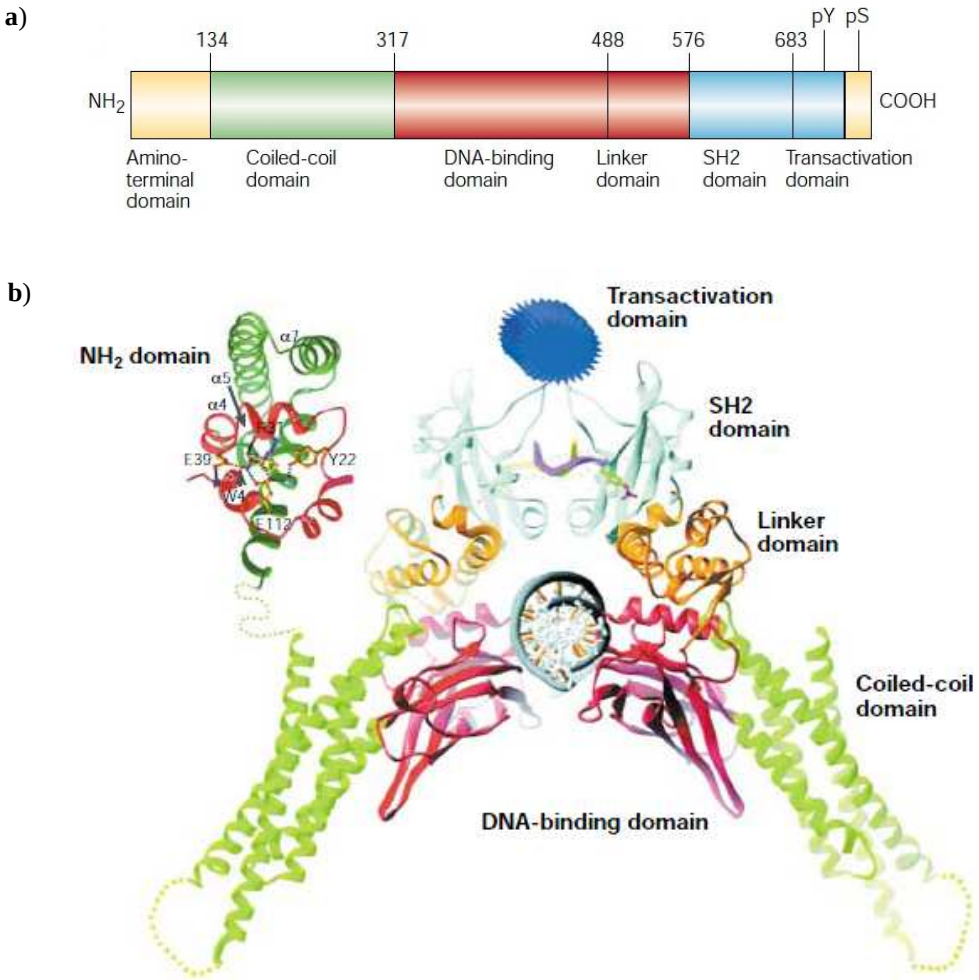

Figure 1. STATs structure. a) Functional domains of STAT proteins. **b**) Core structure (amino acids ~130-712) of STAT1 dimer bound to DNA. The placement of the amino-terminal domain in the intact structure in undefined.[23]

Finally, a number of native carboxy terminally truncated STAT isoforms have been shown to direct unique programs of gene expression through their association with other transcription factors (*e.g*. STAT1b with STAT2 in ISGF-3 and STAT3b with *c*-jun[24, 25]). These truncated isoforms still get tyrosine phosphorylated, dimerize and bind DNA, but they exert a dominant negative effect by blocking the DNA-binding sites in STAT responsive gene promoter elements. So far, splice variants of STAT1, STAT3 and STAT5 have been identified, namely STAT1β, STAT3β, and STAT5β, and are generated by two distinct mechanisms: alternative mRNA splicing and proteolytic processing. [26] As an example, compared to wild-type STAT3, STAT3β has seven new amino acids and lacks an internal domain of 50 base pairs from the C-terminal of STAT3. This splice product is a naturally occurring isoform of STAT3 and encodes a 80 kDa protein which also lacks the Ser727 phosphorylation site. STAT3β has been and still is widely considered as a dominant negative factor, because its overexpression can suppress specific STAT3 functions. However, STAT3β activities have not only been linked to repression. Although STAT3β is not required for viability, it is also involved in inflammatory processes. Moreover, the observation that both up and downregulation of genes occurs in mice specifically lacking STAT3β also indicates its transcriptional activator properties.[27]

1.2 Mechanism of STATs activation and regulation

STATs are activated by over 40 different polypeptides binding cytokine receptors, G-protein-coupled receptors, receptor tyrosine kinases like epidermal growth factor receptor and platelet-derived growth factor receptor (EGFR and PDGFR), as well as numerous non-receptor tyrosine kinases (*e.g*. Src and Abl) (**Figure 2**).

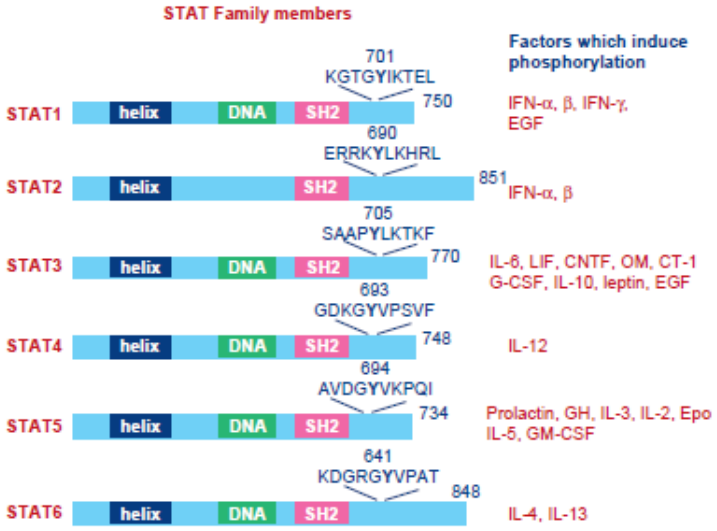

Figure 2. Schematic illustration of STAT family members and factors that induce phosphorylation. EGF: epidermal growth factor; LIF: leukemia inhibitory factor; CNTF: ciliary neutrophic factor; OM: oncostatin M; CT-1: cardiotrophin 1; G-CSF: granulocyte colony-stimulating factor; GM-CSF: granulocyte-macrophage colony stimulating factor; Epo: erythropoietin.[28]

The best-studied pathway for STAT activation is through the JAKs (Chapter 1.2.1), otherwise known as the JAK/STAT pathway (**Figure 3**).

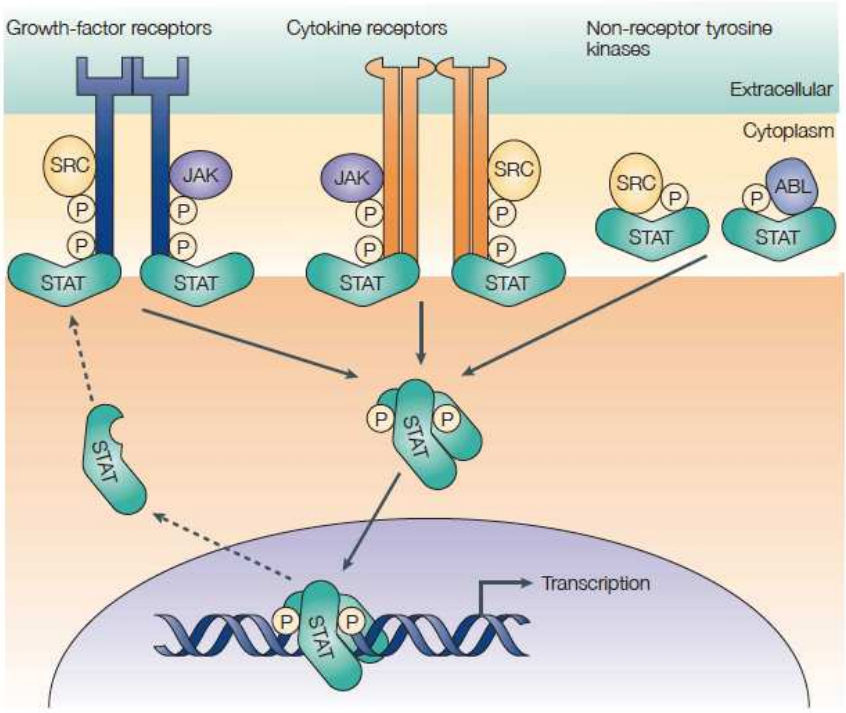

Figure 3. Signaling pathways that converge on STATs.[29] Binding of growth factors or cytokines to their receptors results in the activation of intrinsic receptor tyrosine-kinase activity or of receptor-associated kinases, such as the Janus kinase (JAK) or Src tyrosine kinases. Non-receptor tyrosine kinases, such as the oncoproteins Src and Bcr-Abl can phosphorylate STATs independently of receptor engagement. Phosphorylated STATs dimerize and translocate to the nucleus, where the dimers directly regulate gene expression.

Cytokine receptors (e.g. IL-6R and IFNgR) have constitutive association of JAKs within the intracytoplasmic portion of the receptor.[30] Ligand binding leads to dimerization of the receptor and activation of the JAKs, which *trans*-phosphorylate tyrosine residues within the intracytoplasmic portion of the receptor chains. The tyrosine phosphorylated receptor allows for docking of STATs through their SH2 domains. The JAKs subsequently phosphorylate the recruited STAT on a specific tyrosine residue near the carboxy terminus (*e.g.* position 701 for STAT1[31] and position 705 for STAT3[2]). STAT activation is not mediated exclusively by cytokine receptors that lack intrinsic tyrosine kinase domains. STAT proteins are also activated by receptor tyrosine kinases such as epidermal growth factor-receptor (EGF R), PDGF-R,[32] and colony stimulating factor-1R (CSF-1R),[33] seven transmembrane G-protein-coupled receptors such as angiotensin II receptor[34] and serotonin 5-HT2A receptor[35], and through the T cell receptor complex[36] and the CD40 receptor[37]. Both the EGF and PDGF receptors are capable of directly phosphorylating STAT proteins in the absence of JAK activation. In addition, other TKs, such as Src and Abl, were found to directly phosphorylate STATs. Upon tyrosine phosphorylation, STATs form homodimers (most commonly) as well as heterodimers (e.g. STAT1/STAT2 in response to IFN-α/β activity, STAT1/STAT3 in response to IL-6 activity and STAT5a/STAT5b in response to growth hormone activity[38]) and are subsequently released from the receptor. Dimeric STATs enter the nucleus (Chapter 1.2.2) where they bind to specific DNA-binding elements (Chapter 1.2.3) and activate transcription of target genes. STATs activation is normally rapid and transient, lasting from several minutes to a few hours, and is usually quickly down-regulated to keep cytokine responses under control (Chapter 1.2.4).

1.2.1 Janus Kinases (JAKs)

The JAKs proteins are highly related intracellular protein tyrosine kinases of about 1200 amino acids (120-140 kDa) and are able to activate a large number of receptors. JAKs are characterized by an amino-terminal portion of approximately 600 amino acids and two kinase domains, each of about 250 residues, separated by a short hinge region[39] (**Figure 4**).

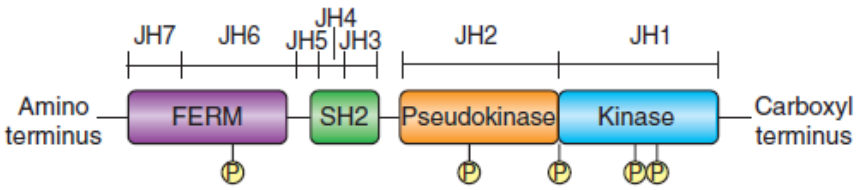

Figure 4. Schematic representation of the primary structure of Janus kinases (JAKs).[40] JAKs are made up of FERM, SH2-like, pseudokinase and kinase domains. An alternative nomenclature for the putative domains is as a series of Janus homology (JH) domains. The FERM domain mediates binding to cytokine receptors. Both the FERM and the pseudokinase domains regulate catalytic activity and appear to interact with the kinase domain. JAKs autophosphorylate at multiple sites (P), including two in the activation loop of the kinase domain, but the precise function of these modifications is just beginning to be understood.

A canonical tyrosine kinase domain (JAK homology region 1 or JH1), located at the carboxyl end of the protein, is constituted by a central kinase-like domain (also referred to as pseudokinase or JH2 domain) unique to the family. The function of the kinase-like domain in the catalytic activation of JAKs remains unknown: it seems to regulate catalysis negatively and might have a role in substrate recognition.[41] Despite considerable sequence similarity with other kinase domains, the kinase-like domain lacks key motifs essential for phosphate transfer. A non-conserved amino terminus of approximately 30-50 amino acids is followed by five JH regions of variable lengths and degrees of identity (JH3-JH7). Among these, the most conserved is JH4 which has a central core of 18 residues identical in all family members.

There are four members that belong to these family of proteins: JAK1, JAK2, JAK3 and Tyk2. JAK1, JAK2 and Tyr2 were identified through different cDNA-cloning approaches. Their ubiquitous expression gave no hint to their function. JAK3, was cloned on the basis of similarity, and was found to be expressed predominantly in haematopoietic cells. The four mammalian JAKs are activated upon high-affinity binding of a variety of cytokines to their multimeric cell-surface receptors. Ligand-induced conformational changes and the increased local concentration of JAKs promoted by receptor dimerization could lead to their activation. A critical determinant of the involvement of a JAK family member in cytokine signaling pertains to its ability to associate with the intracellular portion of receptor components. Therefore, much effort has been recently devoted to determine the structural features of this interaction. Closer inspection of the intracellular portions of cytokine receptors has revealed the presence of short membrane-proximal motifs that were originally found to be required for

induction of proliferative signals. In a number of cases, these variably conserved motifs were found to mediate JAK2 activation. JAK activation is generally measured as an increase in the tyrosine phosphorylation of the protein, which correlates with its increased catalytic activity. A first level of control of the catalytic activity of the JAKs appears common to that of most protein kinases and involves auto(trans)phosphorylation of a conserved activation loop of the kinase domain. Phosphorylation of critical tyrosine residues might relieve steric blocking in the catalytic site and allow access of the substrate. The activated JAK protein kinases are likely to act on a multiple substrate, among which are juxtaposed JAKs, receptor components and signaling proteins that are recruited to the receptor-JAK complex upon ligand binding. STATs are among the best characterized substrates. Currently, they do not seem to have specificity for a particular STAT protein. For example, different receptors can activate the same STAT molecule through phosphorylation of the same tyrosine site, even though they activate distinct JAKs. The interchangeability of the JAKs in heterodimeric receptors suggests that, to some extent, what governs substrate specificity is not the JAK itself, but rather the receptor component to which the JAK is associated. When JAKs are overexpressed and hyperphosphorylated in mammalian cells, they were shown to phosphorylate STATs in a ligand-independent manner, possibly through a direct interaction. Involvement of aberrant JAK activation in human cancer is linked to a chromosomal abnormality in acute lymphocytic leukemia (ALL).[11] Chromosomal translocation of the short arm of chromosome 9, containing the kinase domain of JAK2, to the short arm of chromosome 12, containing the oligomerization domain of the ETS transcription factor, results in a fusion protein (Tel-JAK2) possessing constitutive kinase activity.[42]

1.2.2 STAT nucleocytoplasmic transport

The translocation of STATs into the nucleus dependents on active transport through the nuclear pore complex (NPC), since STAT dimers are too large (~180 kDa) for passive diffusion. The mechanism of nuclear translocation has been unknown for several years. Subsequent studies have demonstrated that nuclear import of STAT proteins is directed by short amino acid sequences, rich in arginine and lysine, termed Nuclear Localization Signals (NLSs). These latter are recognized by specific cytoplasmic receptors, called importins. Importins are constituted by two subunits, importin α and importin β. To date, six human

importin α isoforms have been identified: importin α1, α3, α4, α5, α6 and α7. Upon binding with NLS of the STAT, importin α binds to importin β, which docks the importin-cargo complex on the cytoplasmic side of the nuclear pore complex and mediates the movement of the complex into the nucleus.[43] The energy for this active nuclear transport is provided by the small G protein, Ran (**Figure 5, a**).[44]

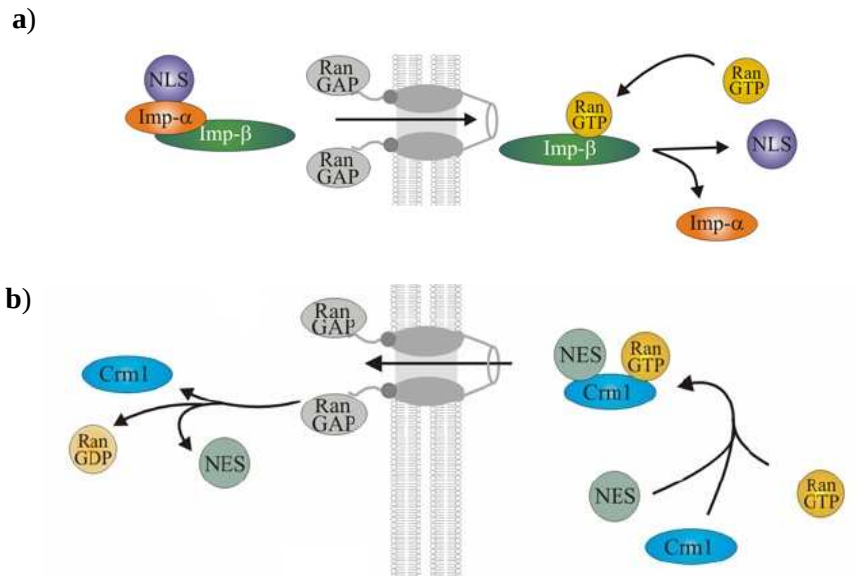

Figure 5. a) Nuclear import of Nuclear Localization Sequence (NLS) cargo mediated by the importin α/β. **b**) Nuclear export of NES cargo mediated by Crm1. [45] See text for details.

Classical NLSs have not been identified in STATs. The first report of the existence of NLS signals in STAT molecules emerged when an unconventional, structural and dimer-specific NLS was identified in STAT1 and STAT2.[46] This structural NLS is situated in the DNA-binding domain of the molecule, and two of these elements, one in each monomer, were shown to be required for nuclear import of STAT1 and STAT2. The amino acids required for nuclear import were mapped to lysines 410 and 413 of STAT1, and to arginine 409 and lysine 415 of STAT2. Another study has described leucine 407 to be essential for STAT1 nuclear import.[47] STAT3 has been shown to contain two distinct arginine-rich sequence elements, which are required for its nuclear import.[48] These elements are situated in the coiled-coil (arginines 214 and 215) and DNA-binding (arginines 414 and 417) domains of STAT3. The NLSs of STAT1, STAT2 and STAT3 differ from the classical NLS signals to some extent.

They do not resemble the consensus sequences of classical mono- or bi-partite NLSs, and they become active only in dimers. Recently, it has been presented that the nuclear import of STAT3 is mediated by importin α5 and importin α7 in a cytokine-stimulation dependent fashion.[49] However, it has also been suggested that signal-dependent nuclear import of STAT3 is mediated by other importin α isoforms.[50] In addition, it has been proven that nuclear import of STAT3 is independent of tyrosine phosphorylation and mediated by importin α3.[51] At present, there is no detailed information describing the molecular mechanisms of nuclear import of STAT4, STAT5a, STAT5b or STAT6. It has been suggested that unphosphorylated STATs shuttle continuously between the nucleus and cytoplasm. It has also been proposed that the nuclear import of unphosphorylated STATs and tyrosine phosphorylated STAT dimers are mechanistically distinct from each other. It was revealed that only unphosphorylated STAT1 could enter the nucleus in the absence of cytosolic proteins, whereas the nuclear import of tyrosine phosphorylated STAT1 dimers required importins and metabolic energy.[52] Similar results were obtained also for unphosphorylated mouse STAT3 and sheep STAT5.[52] These distinct pathways are most likely the consequence of the conformational differences between the unphosphorylated dimers and the phosphorylation-activated STAT dimers.

Nuclear export, similar to the nuclear import, requires the presence of special hydrophobic amino acid sequences, rich in leucine, called Nuclear Export Signal (NES), as well as soluble carriers named exportins. There are specific exportins such as CAS, which are important for export of importins α, and more general exportins like Crm1 (Chromosome region maintenance 1). Crm1 identifies NESs and binds the NES carrying cargo together with Ran-GTP to form a stable ternary complex. The complex travels through the NPC and dissociates in the cytoplasm after the hydrolysis of Ran GTP (**Figure 5**, **b**). STAT1 nuclear export is achieved *via* a NES, residues 399-410, within the DNA binding domain, and Crm1 binding to this area.[53] A second NES domain, a leucine-rich helical segment, has been described in the N terminus of STAT1.[54] However, Crm1 binding to this region has as of yet been reported, which leads to the assumption that this region participates in a different manner in nuclear export. Interestingly, the NES of STAT1 seems to be hidden when STAT1 is bound to the DNA and it is therefore essential to dislodge STAT1 from the DNA for tyrosine

dephosphorylation, which leads to the accessibility of the NES by Crm1 and the nuclear export of STAT1.[55] Regarding STAT3, three nuclear export signal (NES) elements has been identified. Two of these elements, 306-318 and 404-414, correspond to those recently identified in STAT1 399-410, and a third, STAT3 524-535, is novel.[13]

1.2.3 The DNA response elements

Gene	Nucleotide sequence
IFN-α-stimulated response elements (ISRE)	
ISG54	AGTTTCACTTTCCC
ISG15	AGTTTCGGTTTCCC
6–16	AGTTTCATTTTCCC
9–27	AGTTTCTATTTCCT
OAS	GGTTTCGTTTCCTC
GBP	ACTTTCAGTTTCAT
Consensus	AGTTTCNNTTTCNC/T
GAS-like elements	
GBP	TTACTCTAA
cFos-SIE	TTCCCGTCA
M67-SIE	TTCCCGTAA
Ly-6A/E	TTCCTGTAA
FcγR1 (GRR)	TTCCCAGAA
ICSBP	TTCTCGGAA
IRF1	TTCCCCGAA
ICAM-1	TTCCCGGAA
IFP53	TTCTCAGAA
MIG	TTACTATAA
α_2-Macroglobulin	TTCCCGTAA
Acid glycoprotein	TTCCCAGAA
Rat β-casein gene	TTCTTGGAA
Bovine β-casein gene	TTCTAGGAA
Consensus	TTNNNNNAA

Table 2. Response elements.[6]

The DNA sequence elements in the promoters of genes that bind STAT3 proteins can be classified into two groups (**Table 2**). The prototype of the first class is the interferon-stimulated response elements (ISRE). The second class comprises the GAS-like response elements. The IFN-γ activation site (GAS) was originally identified as the IFN-γ response element in the promoter of the GBP gene.[6] An ever-growing number of GAS-like sequences have been identified in promoters of genes activated by hormones, growth factors, cytokines and interleukines. STAT1 homodimers, STAT1-STAT3 dimers, STAT3 homodimers, STAT4 homodimers, STAT5 homodimers and STAT6 homodimers have been shown to bind to at least one of the GAS-like elements.[56, 57] All these elements have the palindromic core sequence TTNNNNNAA, but differ in the five inner nucleotides (**Table 2**). Variations of the inner nucleotides between different elements have been shown to influence the binding affinity towards specific STAT dimers. A STAT1 homodimer binds to the GAS element found in the promoter of the FcγR1 gene, whereas STAT3 homodimer does not.[58] The STAT3 homodimer, however, binds the SIE (sis-inducible element) element found in the promoter of the *c-fos* gene.[59] Selective and specific activation of genes by different STAT dimers could therefore stem from differential binding affinities to slightly different response elements.

1.2.4 STAT inactivation

The transient nature of STAT activation suggests that nature has also invented sophisticated mechanisms to turn off the signaling pathway. In fact, recent studies have shown that STAT activation is negatively regulated by several mechanisms, including proteolytic degradation via ubiquitin-proteasome pathway and dephosphorylation of JAKs and STATs, as well as inhibition of STAT activity *via* two different protein families: the suppressors of cytokine signaling family (SOCS) and proteins that inhibit activated STAT proteins family (PIAS).

Proteolytic degradation

Ubiquitin-proteosomal degradation is essential for the degradation of proteins whose levels have to be regulated either constitutively, or in response to extracellular stimuli and changes in the cellular environment and is thus an important mechanism for the downregulation of JAK/STAT signaling pathways. It was demonstrated that JAK1, JAK2 and JAK3 are targets for degradation,[60] as well as tyrosine phosphorylated STAT1, STAT4, STAT5 and STAT6, with only marginal effects on STAT2 and STAT3.[61, 62]

Protein tyrosine phosphatases (PTPases)

Dephosphorylation is an important way to inhibit the STAT signaling pathway and can occur both in cytoplasm, where the JAKs and the STATs are targets, and in the nucleus where dephosphorylation of the STATs takes place. Several PTPs have been identified that negatively regulate the JAK/STAT pathway (**Table 3**). The cytoplasmic tyrosine phosphatases found to be involved in inhibiting JAK/STAT activity were the closely related SH2-containing phosphatases (SHP), SHP1 and SHP2.[63] SHP1 is mainly expressed in hematopoietic tissues, whereas SHP2 is ubiquitously expressed. All tyrosine-phosphorylated signaling molecules, such as receptors, JAKs or STATs, have to be considered as possible targets for SHP2. However, direct interaction has only been shown for SHP1 with JAK1 and JAK2,[64] and for SHP2 with JAK1 and STAT5.[65] PTP1B has also been implicated in the dephosphorylation of STAT5 under overexpression conditions.[66] However, whether STAT5 is a physiological substrate of PTP1B remains to be established. Earlier studies indicated the existence of a PTP activity in the nucleus to inactivate STAT1. Through biochemical purification, TC45, the nuclear isoform of TCPTP, has been identified as a STAT1 PTP.[67]

Inhibitor	Target
JAK PTPs	**JAKs**
SHP1	JAK2, JAK1
SHP2	JAK1
CD45	JAK1, JAK2, JAK3, TYK2
PTP1B	JAK2, TYK2
TCPTP	JAK1, JAK3
Cytoplasmic STAT PTPs	**STATs**
SHP2	STAT5
PTP1B	STAT5
TCPTP	STAT1, STAT3
Nuclear STAT PTPs	**STATs**
SHP2	STAT1
TCPTP	STAT1, STAT3

Table 3. Negative regulation of JAK-STAT signaling.[63] JAK, Janus-family kinase; PTP, protein tyrosine phosphatase; SHP, SH2-domain-containing PTP; TCPTP, T-cell PTP; TYK2, tyrosine kinase 2.

TC45 can directly dephosphorylate STAT1. In addition to TC45, SHP2 is also involved in the nuclear dephosphorylation of STAT1.[68] How other STATs become dephosphorylate remains unknown, but recent studies have shown that there is specificity in the dephosphorylation of STATs by PTPs. For example, it has been shown that TCPTP is involved in the dephosphorylation of both STAT1 and STAT3, but not STAT5 or STAT6.[67]

The SOCS family of inhibitors

The suppressors of cytokine signaling (SOCS) are a family of intracellular proteins that play a crucial role in negatively regulating the response of the immune system to cytokines. These inhibitors have been variously named by independent discoverers as suppressor of cytokine signaling (SOCS), JAK-binding proteins (JABs), STAT-induced STAT inhibitors (SSIs) or cytokine-induced SH2 (CIS) proteins. The eight proteins that belong to the SOCS family include cytokine-inducible SH2 domain protein (CIS) and SOCS1-SOCS7. SOCS proteins contain a central SH2 domain, an amino-terminal domain of variable length and a divergent sequence that carries, in the case of SOCS1 and SOCS3, a kinase inhibitory region and a carboxy-terminal 40 amino-acid module known as the SOCS box[69] (**Figure 6**, **a**). The SOCS

box can bind to elongins B and C, which are known components of the ubiquitin E3 ligase complex, suggesting that SOCS proteins may target signaling molecules like JAK2, to the proteasome for degradation.[70] SOCS proteins are generally expressed at low levels in unstimulated cells and expression is largely increased upon cytokine, insulin and EGF stimulation. The fact that they subsequently inhibit JAK/STAT signaling leads to the conclusion that they act as classical feedback loop inhibitors.[71] The mechanism of inhibition varies between the different SOCS proteins (**Figure 6**, **b**). SOCS1 binds directly *via* its SH2 domain to tyrosine phosphorylated JAKs, and as a consequence, JAK activity is directly inhibited. SOCS3 uses a different mechanism for inhibition of JAKs: it binds to the activated receptor directly.[72] By contrast, CIS does not affect the activity of JAKs. Instead, CIS inhibits STATs by competing with STATs for docking sites on the receptor.[73]

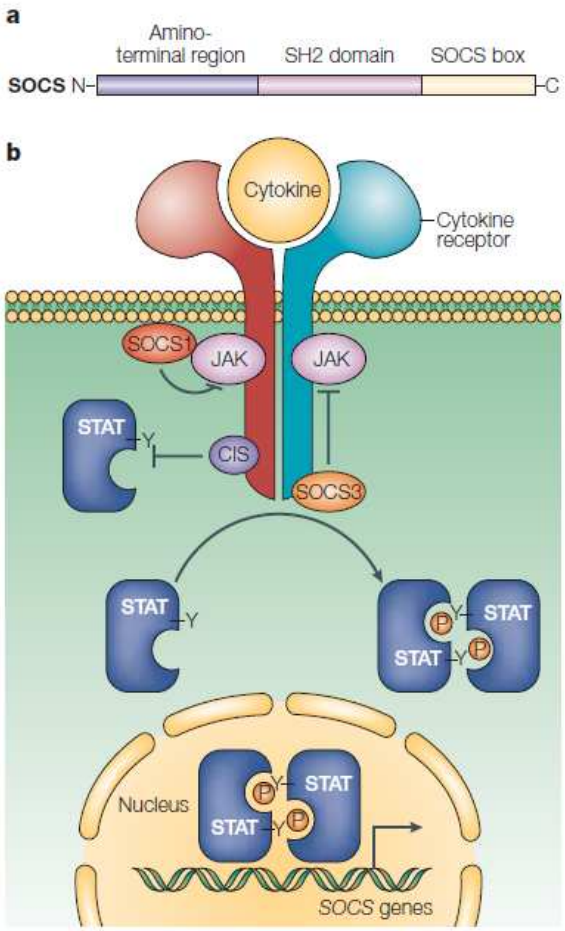

Figure 6. The SOCS family of proteins. a) Domain structure of suppressor of cytokine signaling (SOCS) proteins. **b**) Inhibition of the Janus kinase (JAK)- and the signal transducer and activator of transcription (STAT)-signaling pathway by SOCS proteins through distinct mechanisms.[63]

The PIAS family of inhibitors

In the nucleus, protein inhibitors of activated STATs (PIAS) inhibit the DNA binding of active STATs. The mammalian PIAS family consists of four members: PIAS1, PIAS3, PIASX and PIASY.[74] After cytokine stimulation, PIAS1, PIAS3 and PIASX interact with STAT1, STAT3 and STAT4 respectively.[75, 76, 77] In addition, PIASY has also been shown to be associated with STAT1. The PIAS–STAT interaction is cytokine dependent and PIAS proteins do not interact with STATs in unstimulated cells. The cytokine dependency of the interaction might be explained by the finding that PIAS1 can bind to the dimeric, but not the monomeric, form of STAT1.[78] Each member of the PIAS family has been shown to inhibit STAT-mediated gene activation. Distinct mechanisms for PIAS-mediated inhibition of STATs have been indicated (**Figure 7**).

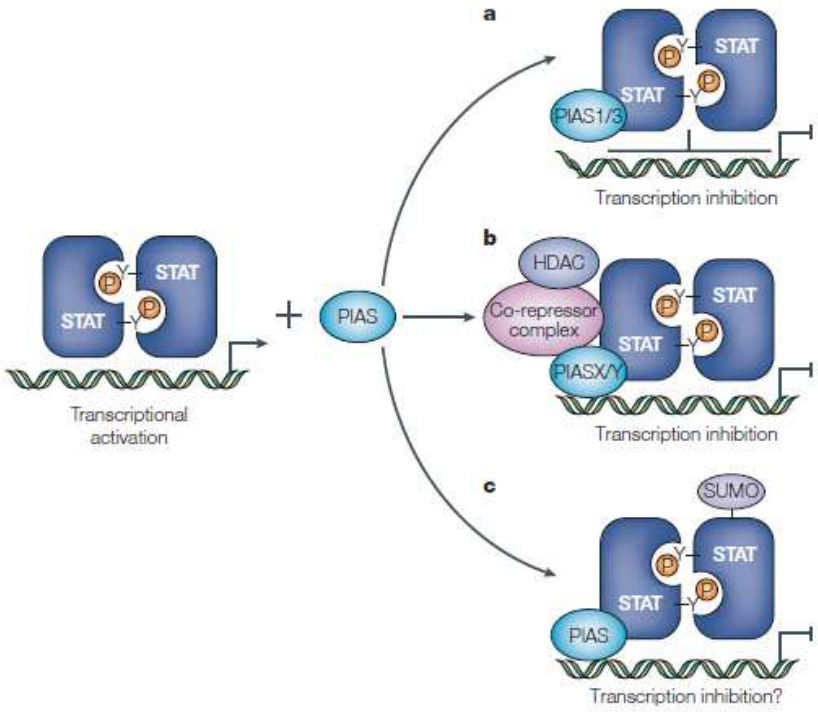

Figure 7. Proposed mechanisms for inhibiting the JAK–STAT pathway by PIAS proteins. a) PIAS1 and PIAS3 block the DNA-binding activity of STAT dimers. **b**) PIASX and PIASY might act as transcriptional co-repressors of STAT by recruiting other co-repressor proteins, such as histone deacetylase (HDAC). **c**) PIAS proteins can promote the conjugation of small ubiquitin-related modifier (SUMO) to STAT1. The significance of STAT1 sumoylation in regulating STAT1 activity is controversial and needs to be clarified.[63]

PIAS1 and PIAS3 can inhibit the DNA binding activity of STAT1 and STAT3, respectively.[75, 76] By contrast, PIASX and PIASY can inhibit STAT4- and STAT1-dependent transcription without affecting the DNA-binding activity of STAT4 and STAT1.[77,79] The interaction of PIAS proteins with histone deactylases (HDACs) has been described. PIASX has been shown to interact with HDAX3.[80] PIASY has also been found to interact with HDAC1.[81] So, it is probable that PIASX and PIASY function as transcriptional co-repressors of STATs, possibly by recruiting HDACs and other co-repressor molecules. Interestingly, PIAS proteins have been shown to have SUMO E3 ligase activity.[82] It has been suggested that PIAS proteins might regulate transcription by promoting SUMO conjugation of transcription factors.

1.3 Roles of STATs in physiological processes

Activation of STATs results in the expression of genes that control critical cellular functions, including cell proliferation, survival, differentiation and development, as well as specialized cellular functions, such as those associated with immune responses. The contribution of specific STAT family members to control the normal cellular processes has been elucidated on the base of studies of homozygous deletion, or more recently, by tissue-specific, conditional knockout of each STAT family member in mice. These studies indicate that STAT proteins are highly specific in their function and that they are responsible for mediating the immune response in mammals (**Table 4**).

STAT1

STAT1 knockout mice are viable and fertile and display no developmental defects. However, STAT1-/- mice failed to induce transcription of target genes after stimulation with IFNα/β and IFNγ; these mice are highly susceptible to microbial and viral infections.[83, 84] Atypical susceptibility to mycobacterial, but not to viral infection, has also been identified in patients suffering with a natural heterozygous germline STAT1 mutation, further strengthening the importance of STAT1 in contributing to immune responses.[85] Interestingly, STAT1 deficient mice also showed sensitivity for both spontaneous tumor development and tumor

development after methylcholanthrene treatment.[86] This suggests that STAT1 has a proapoptotic function.

STAT protein	Phenotype of null mice
STAT1	Impaired responses to interferons; increased susceptibility to tumours; impaired growth control
STAT2	Impaired responses to interferons
STAT3	Embryonic lethality; multiple defect in adult tissues including impaired cell survival (both positive and negative) and impaired response to pathogens
STAT4	Impaired T_H1 differentiation owning to loss of IL-12 responsiveness
STAT5a	Impaired mammary gland development owing to loss of prolactin responsiveness
STAT5b	Impaired growth owing to loss of growth hormone responsiveness
STAT6	Impaired T_H1 differentiation owning to loss of IL-4 responsiveness

T_H1: T helper 1 cell; IL: interleukin

Table 4. Role of STAT proteins as revealed by gene-targeting in mice[23]

STAT2

STAT2 is a particular member of the STAT family, since it does not bind to GAS elements and it does not homodimerize. Instead, upon activation by IFNα STAT2 forms the transcription factor complex ISGF3, together with STAT1 and p48/ISGF3γ. Therefore, it is not surprising that the STAT2 knockout exhibits similarities with the STAT1 knockout. The mice are viable, fertile and display no developmental defects. Nevertheless, they are also susceptible to viral infections due to their impaired ability to respond to IFNα/β signaling. Additionally, STAT1 tyrosine phosphorylation and activation after IFNα stimulation is weakened in the STAT2 deficient mice, arguing for an enhancer effect of STAT2 in binding to the receptor complex in the STAT1/STAT2 heterodimers.[87]

STAT3

Will be discussed in detail in Chapter 2.

STAT4

STAT4 is only expressed in natural killer cells (NK cells), dentritic cells and T lymphocytes, and is mainly activated by IL-12. CD4+ T cells differentiate with the help of IL-12 to Th1 cells, which in turn leads to the expression of IFNγ. Th1 cells are involved in hostdefense against intracellular pathogens and tumors, and in the development of autoimmune diseases, for example, rheumatoid arthritis, diabetes and multiple sclerosis. Consequently, it was no surprise that the STAT4 and IL-12 deficient mice show a similar phenotype, *i.e.*, loss of Th1 differentiation, loss of IFNγ expression and enhanced tendency towards Th2 differentiation, which is usually inhibited by Th1 cells.[88] Recent data indicate that STAT4 deficient mice show a resistance to autoimmune diseases like rheumatoid arthritis, diabetes and experimental allergic encephalomyelitis (EAE).[89] In humans, it was shown that IFNα/β can stimulate T cells to drive Th1 development, bypassing the need for IL-12-induced signaling. In contrast, IFNα does not cause Th1 differentiation in mice.[90] The reason for this is that IFNα/β is able to activate STAT4, by recruitment of STAT4 to the IFNα receptor complex exclusively via the C-terminus of STAT2 in human cells. The difference between mouse and human signaling is that the mouse STAT2 gene harbors a minisatellite insertion, which changes the C terminus sequence and selectively disrupts its ability to activate STAT4, but not other STATs.[91]

STAT5

STAT5 was originally characterized as a prolactin-responsive transcription factor in sheep, and exists as two closely related isoforms, STAT5a and STAT5b, which share 95% identity at the *N*-terminus and some variability at the *C*-terminus.[92, 93] Both genes are expressed in all tissues and are activated by a wide variety of cytokines. Given the broad range of activation it might be thought that the knockout of these proteins would have many effects. However, the STAT5 specific knockouts exhibited a very precise phenotype for the individual gene. Both of the STAT5a and STAT5b deficient mice are viable, fertile and display no developmental defects. STAT5a -/- mice are impaired in prolactin activated mammary gland development, necessary for lactation[94] while STAT5b -/- mice have impaired GH signaling effects, similar to GH deficient mice.[94] Since high GH levels are mainly observed in males, female STAT5b -/- showed almost no phenotype, whilst males were smaller and revealed the loss of male-specific liver genes (as MUP and CYP2D9). Interestingly the STAT5a/b double knockout

mice are infertile, small, die after a few weeks of birth, and are defective in the development of the mammary gland and the corpus luteum.[94]

STAT6

STAT6 is ubiquitously expressed and is mainly activated by IL-4 and IL-13.[95] IL-4 is expressed by activated T and B cells, and regulates differentiation of CD4+ T cells to Th2 cells and class switching of B cells, which results in the secretion of IgE. Th2 helper cells are essential for host defense against helminthes and further allergic responses. STAT6 and IL-4 deficient mice show similar phenotypes; neither are able to differentiate into Th2 cells and are inoperative to class switch to IgE. Otherwise they are viable, fertile and display no developmental defects.[96, 97, 98] In addition, STAT6 deficient mice, have a predominantly Th1 phenotype, experience a severe clinical course of EAE, are inhibited in host defense against helminthes, are resistant to septic peritonitis because of enhanced local bacterial clearance, show resistance to tumor recurrence and deregulated activation of NF-κB, leading to reduced expression of proinflammatory cytokines and chemokines induced by endotoxins.[99, 100]

2. STAT3 PROTEIN

2.1 Influence of STAT3 on biological functions

STAT3 was initially identified as the acute-phase response factor (APRF), activated by IL-6.[101] The authors further showed that STAT3 activation through phosphorylation occurred in the cytoplasm and that STAT3 migrates into the nucleus and binds IL-6 response elements of various acute-phase protein genes (e.g., the alpha 2-macroglobulin, fibrinogen, and alpha 1-acid glycoprotein genes).[101] The STAT3 cDNA was cloned one year later and encodes an open reading frame of 770 amino acids resulting in a protein of 88 kDa.[102] STAT3 is ubiquitously expressed and its expression starts very early during post-implantation development in the mouse. STAT3 can be activated by many different cytokines, growth factors and oncogenes (**Figure 2**). The IL-6 family of cytokines has many biological functions and STAT3 plays a major role in these processes.[103] IL-6 activation in mouse myeloid leukemia M1 cells has been shown to lead to growth arrest and terminal differentiation into macrophages. Overexpression of STAT3DN (a STAT3 dominant negative protein which lacks the C-terminal portion and is able to block STAT3 transcriptional activity) abrogated the IL-6 induced effects, leading to the inhibition of IL-6-induced repression of c-myb and c-myc.[104] These experiments demonstrated for the first time that STAT3 activation is essential for IL-6 mediated growth arrest. Conversely, other studies demonstrated that STAT3 is involved in anti-apoptosis, proliferation and upregulation of Bcl-2 by overexpression of STAT3DN in mouse pro-B (BAF/B03) cells.[105] It has been demonstrated in the following years that STAT3 activation was not only essential for cell survival but also required for cell cycle transition, *via* STAT3 mediated upregulation of cyclins D2, D3 and A, and cdc25A, and the associated downregulation of p21 and p27.[105] Interestingly, in a few cases STAT3 was also able to inhibit cell differentiation, following its activation with IL-6 or LIF. IL-6 was shown to induce differentiation of PC12 cells that have been pretreated with nerve growth factor (NGF). Stimulation of the MAPK pathway is important for neurite outgrowth, since cells overexpression gp130 mutants incapable of activating the MAPK cascade, or cells treated with the MEK inhibitor PD98059 treatment with IL-6, both failed to induce

differentiation of PC12. Conversely, overexpression of a mutant gp130, which is defective in STAT3 signaling but not in SHP2 signaling, did not inhibit, but rather stimulated neurite outgrowth. NGF pretreatment inhibited the IL-6-induced activation of STAT3 and overexpression of STAT3DN did not require NGF pretreatment for neurite outgrowth. These facts indicate that STAT3 is negatively involved in PC12 differentiation.[106] Likewise, STAT3 is essential for self renewal of embryonic stem (ES) cells, that are continuously propagated in an undifferentiated pluripotent state with LIF, since overexpression of a dominant negative STAT3 is able to abrogate LIF mediated self-renewal and promote differentiation.[107, 108, 109] Concordant with this finding is a study of ES cells expressing a fusion protein composed of the entire coding region of STAT3 and the ligand binding domain of the estrogen receptor (STAT3ER), that can be activated by the synthetic ligand 4-hydroxytamoxifen (4HT), maintained an undifferentiated state upon stimulation with 4HT.[110]

STAT3 knockout mice

STAT3 is the only STAT family member whose knockout leads to embryonic lethality.

STAT3 deficient mice develop into the egg cylinder stage but show a rapid degeneration between embryonic days 6.5 and 7.5. This is probably due to nutritional insufficiency, since STAT3 is expressed at day 7.5 in the embryonic visceral endoderm, which is important for nutrient exchange between the maternal and embryonic environment.[111] Some knockouts of components of STAT3 activating pathways also lead to embryonic lethality, such as gp130 and LIFRβ. STAT3-deficient T cells showed a loss of proliferative response due to a defect in IL-6 mediated prevention of apoptosis. The anti-apoptotic protein, Bcl-2, is normally upregulated in response to IL-6 even in STAT3-deficient T cells.[112] This suggests that STAT3 has a Bcl-2 independent anti-apoptotic function. Targeted STAT3 knockout in macrophages and neutrophils results in mutant mice that are highly susceptible to endotoxin shock and develop chronic enterocolitis with age, due to abolished inhibitory effects of IL-10 on inflammatory cytokine production.[113] In addition, STAT3 -/- plus IL-10 -/- mice show similar phenotypes and it has been shown that IL-10 suppresses expression of TNF-α via STAT3.[114] STAT3 phosphorylation occurs at the onset of mammary gland involution and STAT3 null mammary glands show a decrease in apoptosis and a dramatic delay of involution, a stage of mammary gland development that is characterized by an extensive apoptosis of the epithelial

cells. In normal glands involution is accompanied by increase in insulin-like growth factor binding protein (IGFBP5) levels, which binds the survival factor insulin-like growth factor (IGF1) and inhibits IGF1. There was evidence to suggest that IGFBP-5 is a direct or indirect target for STAT3, since IGFBP5 upregulation is not observed in STAT3 null mammary glands.[115] These data have showen for the first time that STAT3 is important for apoptosis *in vivo*.

Mice with STAT3 deficient epidermal and follicular keratinocytes were viable and did not have any defects in the development of epidermis and hair follicles. However, the mice had sparse hair, their wound-healing processes were severely impaired and they spontaneously developed ulcers with age. Considering that migration and proliferation are essential for wound healing, motility and growth of keratinocytes were examined. Results illustrated that migration of STAT3-disrupted keratinocytes in response to growth factor stimulation, *in vitro*, was impaired while proliferation was not disturbed. Furthermore, the mice exhibited a normal first hair cycle (morphogenesis), but an impaired second hair cycle (skin remodeling).[116] This analysis provided the first *in vivo* data showing that STAT3 has a function in cell migration and that STAT3 is necessary for skin remodeling, including hair cycle and wound healing.

STAT3 is required for the neurotrophic actions of CNTF and LIF on developing cytokine dependent sensory neurons: STAT3-deleted nodose neurons showed a reduced response to CNTF and LIF *in vitro* and they had an enhanced death rate *in vivo.* These results provide the first evidence for a role for STAT3 signaling in regulating neuronal survival.[117, 118] Knockout of STAT3 in cardiomyocytes showed that STAT3 is involved in regulation of inflammatory responses and survival.[119] STAT3 deficient hepatocytes severely impaired IL-6 induced acute-phase response in the liver during inflammation.[120] Interestingly, STAT3β deficient mice exhibited reduced recovery from endotoxic shock and showed hyperresponsiveness to a subset of endotoxin-inducible genes in the liver. These findings revealed a critical negative regulatory role for STAT3β in the control of systemic inflammation.[121]

Considering all knockout data together it is surprising that STAT3 has such mild phenotypes in the conditional knockout mice compared to the early embryonic lethality in the full knockout. The data suggests that the STAT3 activators in early development are different from the known activators in the adult and it will be of interest to identify them. Moreover, STAT3 elicits diverse functions in various cell types since the readout of the STAT3 tissue

deficient mice is diverse and ranges from apoptosis, survival, and effects on migration up to proliferation. It will be a challenge to solve the riddle why STAT3 activation has diverse biological functions and the more information will be gained about the different sets of genes that are regulated by STAT3, in different cell types, the more it will be possible to understand the function of STAT3 molecule.

2.2 Validation of STAT3 as a target for cancer therapy

STAT3 is persistently activated in over a dozen types of human cancers, including all the major carcinomas as well as some hematologic tumors. In some cancers, enough clinical samples have been examined to state the approximate frequency of persistently active STAT3, which occurs in more than half of breast and lung cancers, hepatocellular carcinomas, multiple myelomas and more than 95% of head and neck cancers (**Table 5**). Moreover, in cultured tumor cells from several different cancers, interruption of this persistent STAT3 activity, by dominant negative proteins or antisense oligonucleotides, leads to apoptosis.[122] Targeted deletion of STAT3 in skin cells was recently shown to prevent epithelial cancer[123] and in this issue a dependence on STAT3 was demonstrated in lymphomas and myelomas.[124] These studies took advantage of sophisticated genetic manipulations to delete STAT3 specifically in B and T cells, which along with previous experiments deleting STAT3 in epidermal precursor cells, clinches the importance of STAT3 in tumor cells both *in vivo* and *in vitro*. They also showed that administration of antisense oligonucleotides targeted against STAT3 to animals can substantially reduce the growth of the hematologic tumors, highlighting the potential of anti-STAT3 therapy in clinical medicine.
Overactive kinases or dysfunctional receptors are the culprits in head and neck cancer, some multiple myelomas, leukemias and lymphomas. Studies of leukemias, lymphomas, hepatocellular carcinomas and non-small cell lung cancer report the loss of proteins that negatively regulate STAT3, such as PIAS or SOCS (Chapter 1.2.4). [125, 126, 127]

	Activated STAT
Blood tumors	
Multiple myeloma	Stat1, Stat3
Leukemias	
HTLV-I-dependent	Stat3, Stat5
Erythroleukemia	Stat1, Stat5
Acute lymphocytic leukemia	Stat1, Stat5
Chronic lymphocytic leukemia	Stat1, Stat3
Acute myelogenous leukemia	Stat1, Stat3, Stat5
Chronic myelogenous leukemia	Stat5
Megakaryotic leukemia	Stat5
Large granular lymphocyte leukemia	Stat3
Lymphomas	
EBV-related/Burkitt's	Stat3
Mycosis fungoides	Stat3
HSV saimiri-dependent (T-cell)	Stat3
Cutaneous T-cell lymphoma	Stat3
Hodgkin's disease	Stat3
Solid tumors	
Breast cancer	Stat1, Stat3
SCCHN	Stat1, Stat3
Renal cell carcinoma	Stat3
Melanoma	Stat3
Ovarian carcinoma	Stat3
Lung cancer	Stat3
Prostate carcinoma	Stat3
Pancreatic adenocarcinoma	Stat3

Table 5. Activation of STATs in human primary tumors and tumor cell lines.[128]

SCCHN: squamous cell carcinoma of the head and neck; HTLV: human T-cell leukemia-virus type-I

One oncogene that persistently activates STAT3 is ALK kinase, a tyrosine kinase persistently activated in a human disease called anaplastic large cell lymphoma.[129] Chromosomal translocations join the nucleoplasmin gene to the gene that encodes ALK kinase, producing the persistently active NMP-ALK oncogene. To investigate the role of STAT3 in malignant transformation by NMP-ALK and in cancer cell survival, for the first time it has been studied bone marrow-derived cancer cells in which the *STAT3* gene has been deleted.[124] It was showed that fibroblasts containing one functional *STAT3* allele could be transformed by the NMP-ALK oncogene, as measured by growth in soft agar. In contrast, STAT3-deficient fibroblasts could not be transformed. NMP-ALK activity can be expressed in lymphocytes both in cultured cells and in the whole animal. Animals bearing NPM-ALK and molecularly marked *STAT3* genes capable of being deleted specifically in lymphocytes were studied. T lymphocytes retaining a single *STAT3* allele and T lymphocytes lacking both *STAT3* alleles

formed NMP-ALK–induced lymphomas that killed the animals in about 40 weeks. In culture, however, the lymphomas without *STAT3* grew less well than those still retaining one *STAT3* allele. Most important, in the NMPALK-bearing animals with a single *STAT3* allele, every one of the induced lymphomas had persistently active, tyrosine phosphorylated STAT3 and when the lymphoma cells in these animals were engineered to lose the *STAT3* gene, the cells promptly underwent apoptosis. It was demonstrated that NMP-ALK can induce myeloma, a B cell-specific tumor. In mice that had *STAT3* ablated in about 80% of B cells, all NMP-ALK-induced myeloma cells still had *STAT3* and it was persistently activated. These genetic experiments indicate clearly that the presence of persistently active *STAT3* favors the development of T- and B-cell tumors and is required for their maintenance. In additional studies, the injection of antisense oligonucleotides to *STAT3* at a site distant from transplanted lymphoma or myeloma tissue was performed. This treatment successfully restricted growth of either T-cell lymphomas or B-cell myelomas. It is noteworthy that the antisense oligonucleotides against *STAT3* killed tumor cells but had little effect on the animal. These experiments with hematologic tumors build on other studies suggesting that anti-STAT3 therapy would limit tumor growth. For instance, tumors in mice, resulting from transplantation of human head and neck squamous carcinoma cells, shrink when injected directly with an antisense *STAT3* synthetic DNA derivative.[130]

STAT3 activation can suppress apoptosis

In most cells, STAT3 activation can suppress apoptosis.[131] This effect is mediated through the expression of various cell survival gene products, regulated by STAT3, including bcl-xl,[132, 133] bcl-2,[134] survivin,[135] Mcl-1,[136] and cIAP2[13] (**Figure 8**). Additionally, most tumor cells that exhibit constitutive activation of STAT3, also express the above mentioned cell survival gene products:[137, 138] thus, suppression of STAT3 activation can inhibit their expression and potentiate apoptosis.[139] The downregulation of STAT3 also leads to expression of Fas protein, which can promote apoptosis.[25]

Importantly, numerous published reports showed that blocking constitutively activated STAT3 signaling leads to apoptosis of tumor cells[128, 140, 141]. By contrast, the blockage of STAT3 signaling in normal cell does not generally lead to apoptosis[142, 143]. This selective inhibition might reflect an irreversible dependence of tumor cells on high levels of activated

STAT3 for growth and survival, whereas normal cells might be able to withstand lower levels of STAT3 activity or use alternative pathways for growth and survival.

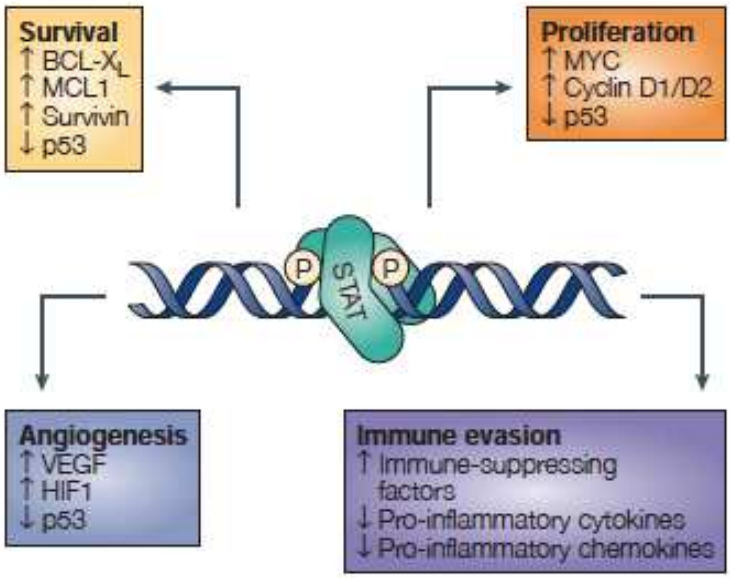

Figure 8. Control of cell growth and survival by STATs.[29]

STAT3 activation can lead to cellular proliferation and cellular invasion.

STAT3 activation has also been linked with proliferation of tumor cells (**Figure 8**). This effect of STAT3 is mediated through its ability to induce the expression of cyclin D1.[144] STAT3 has also been shown to upregulate the expression of several growth-promoting genes, such as myc[145] and pim-1.[146] The pro-apoptotic factors, such as Fas, are downmodulated by STAT3 activation.[25] There are other reports, however, which describe the activation of the expression of the cell cycle inhibitor p21(waf1) by this Fas protein,[147] suggesting that STAT3 can also block cell cycle progression and prevent abnormal cell proliferation.

Numerous studies indicate that STAT3 activation plays a major role in tumor cell invasion, and inhibition of STAT3 reduces it.[131] STAT3 activation regulates the expression of matrix metalloproteinase MMP-1 and MMP-2, which then mediate tumor invasion and metastasis.[148, 149] STAT3 upregulates the transcription of MMP-2 through direct interaction with the MMP-2 promoter. Furthermore, blockage of activated STAT3 in highly metastatic cells significantly suppresses the invasiveness of the tumor cells, inhibits tumor growth, and prevents metastasis in nude mice. Also, overexpression of phosphorylated STAT3 correlates with the invasion

and metastasis of cutaneous squamous cell carcinoma.[150] STAT3, however, is also known to upregulate tissue inhibitors of metalloproteinase (TIMP)-1, a cytokine known to block metalloproteinases and decrease invasiveness in certain cancer cell types.[151] STAT3, moreover, controls the expression of the *MUC1* gene, which can mediate tumor invasion.[152] Thus, STAT3 mediates tumor invasion through numerous mechanisms.

STAT3 can mediate angiogenesis

Most tumors hold their growth unless they are supplied with oxygen and nutrients from newly formed blood vessels. A role of activated oncogene products in stimulating angiogenesis was established (**Figure 8**).[78, 79] The most potent angiogenesis-inducing signal is the vascular endothelial growth factor (VEGF).[80] VEGF is over-expressed in cancer cells and it binds tyrosine kinases receptor of endothelial cells. This activated endothelial-cell migration and proliferation is needed for the formation of new blood vessels[81]. STAT3 activates the transcription of the *VEGF* gene[82, 83] and it has been shown that over-expression of mutant STAT3C increases *VEGF* expression and induces angiogenesis *in vivo.*[82]

All of these results, together with the requirement of STAT3 for survival in many tumor cells in culture, promise that whereas all tumors may not have persistently active STAT3, the very large number that do may well respond to anti-STAT3 therapy. To this end, efforts are underway to discover small molecules capable of directly inhibiting STAT3. Given the preliminary success in developing small molecules, plus experimental evidences, including the effective antisense treatment in whole animals, it is not at all unreasonable to hope that effective anticancer therapy can derive form inhibiting persistently active STAT3.

2.3 Classification of STAT3 inhibitors[153]

There are two different approaches to inhibit STAT signaling:

- direct, by interaction of molecules with the protein;
- indirect, by inhibition of the upstream tyrosine kinases that are responsible for STAT3 activation or by blockage of factors that are involved in the activation of STAT3 signaling.

The **direct inhibitors** can be divided into:

- peptides
- peptidomimetics
- natural compounds
- synthetic compounds
- oligonucleotides.

The **indirect inhibitors** can be classified as either natural or synthetic compounds. However, the poorly specific mechanism of action highlights the limits of the indirect approach.

2.3.1 Direct inhibitors

Peptides

The dimerization of STAT3 is a key event for its activation and to interfere with dimerization can compromise STAT3 biological activity. In particular, the SH2 domain, with *p*Tyr, is crucial for the dimerization process. From this consideration, a phosphopeptide-based compound was initially designed on the basis of molecular modeling of STAT3 docking sites. Its lead sequence PY*LKTK (**1**, **Figure 9**) derives from the consensus sequence in the STAT3-SH2 domain surrounding *p*Tyr-705. Y* (*p*Tyr of the peptide) interacts with STAT3-SH2 domain, and reduces the number of STAT3-STAT3 dimers available to bind DNA, splitting and replacing them with STAT3-phosphopeptide dimers.

Further studies defined the structure activity relationships for this kind of inhibitors:

- XY*L (X is any amino acid) is the basic sequence able to interrupt dimerization and DNA binding: the derived tripeptides PY*L (**2**, **Figure 9**) and AY*L (**3**, **Figure 9**) had different amino acid in (Y*-1) position but comparable activities on STAT3. In particular, the *in vitro* activity of **2** and **3** showed a significant decrease of STAT3-DNA binding in a dose-dependent manner;
- the amidic bond between X and Y* is critical and cannot be substituted;
- lysine (Y*+2 and Y*+4) and threonine (Y*+3) are not essential.
- the corresponding unphosphorylated sequence had no inhibitory effects: this highlights the importance of the phosphate group for SH2-domain recognition.

However, peptides can't be administered orally because of their low stability in the stomach, where they can be hydrolyzed by acidity or peptidase. Moreover, they have poor membrane permeability. Considering PY*LKTK, this latter problem was overcome by linking a hydrophobic sequence to the *C*-terminus; this allowed the entry of the peptide into the cell.

Another phosphopeptide lead was the hexapeptide Ac-Y*LPQTV-NH_2 (**4**, **Figure 9**) derived from the amino acid sequence of receptor docking sites of STAT3 on gp130. It was able to inhibit with high affinity dimer formation and DNA binding. The peptide bound to STAT3-SH2 domain was crystallized and for this reason it was used as a standard.

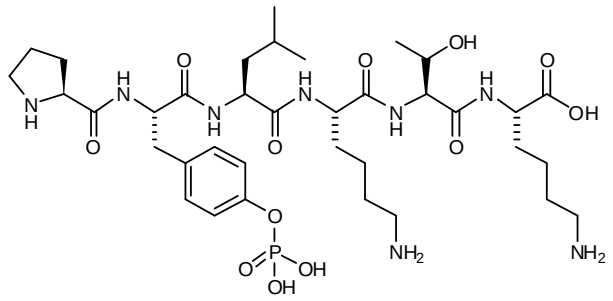

1: PY*LKTK

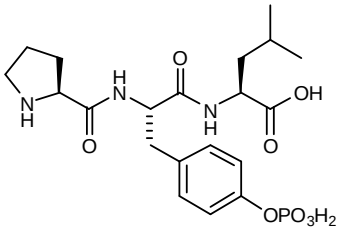

2: PY*L

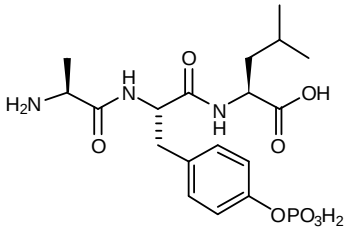

3: AY*L

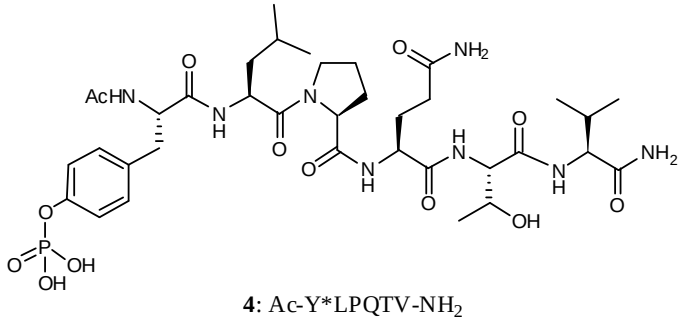

4: Ac-Y*LPQTV-NH_2

Figure 9. Structures of peptide

Peptidomimetics

Peptides present lots of limitations due to low membrane permeability and low stability, that do not allow their use *in vivo* at therapeutic doses. However, the lead compounds of their class provide a starting point for the developement of peptidomimetics with higher membrane permeability.

The indication of the essential tripeptide **2** for the DNA-binding inhibitory activity, led to structural modifications which involved the *N*-terminal proline. This amino acid was replaced with groups of different dimensions, polarity and orientations (**Figure 10**) as:

- 4-cyanobenzoyl or 2,6-dimethoxybenzoyl: a fivefold increase of the inhibition was observed, probably due to the fact that these peptides have access to a hydrophobic domain and are involved in additional H-bonds on the protein surface. Furthermore, these compounds selectively disrupted STAT3-STAT3 dimers with respect to the STAT1 and STAT5 dimers;
- phenyl-(7,8), pyridyl and pyrazinyl-based carboxylic acids were well tolerated; bulky carboxylic acids such as quinoline, naphtalene or biphenyl derivates, led to loss of activity.

Subsequently, derivatives of **5**, which had previously shown the best inhibitory activity, were developed functionalizing the *C*-terminus domain: among these compounds, ISS840 (**6**, **Figure 10**) exhibited 20-fold higher STAT1 (IC_{50} = 31 µM) inhibition activity compared with STAT3 (IC_{50} = 560 µM).

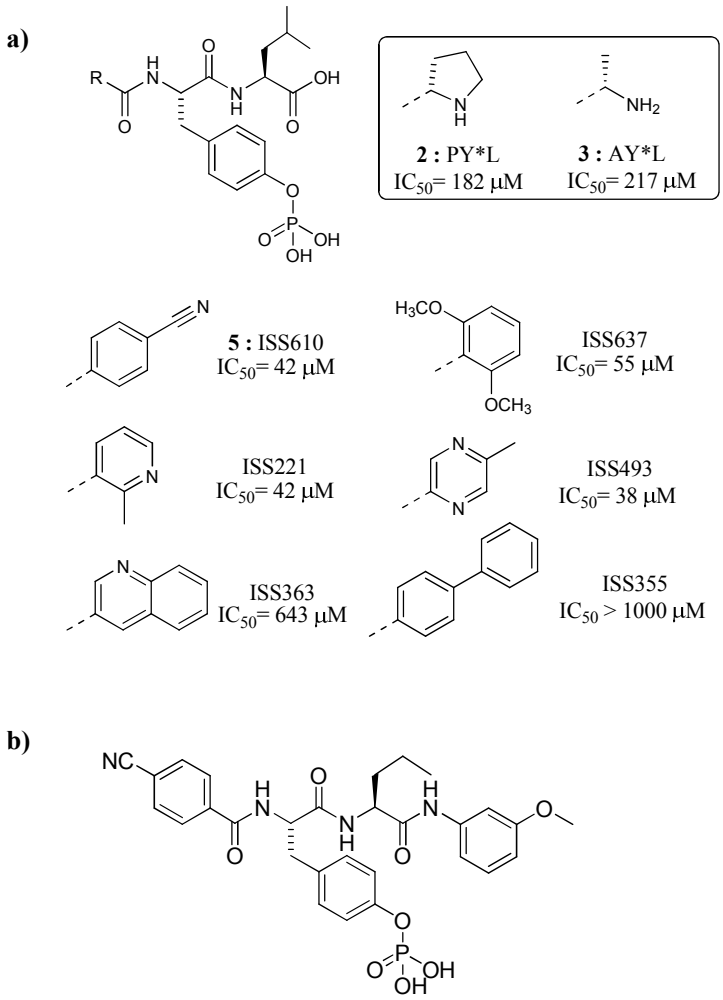

Figure 10. a) Structural modifications at the *N*-terminal proline of the tripeptide PY*L; **b**) Structure of **ISS840** (**6**).

A new library of approximately 50 compounds was synthesized, in order to rationalize the importance of the backbone and side chain interactions between compound **4** and the STAT3-SH2 domain. The phosphopeptide Ac-Y*LPQT-NH_2 (**7**, **Figure 11**) gave indication of a hydrophobic patch where Y* interacts in the surface of the SH2 domain. A SAR investigation was performed on derivative **7** and led to the identification of the peptidomimetic **8** (**Figure 11**), showing an IC_{50} value of 125 μM.

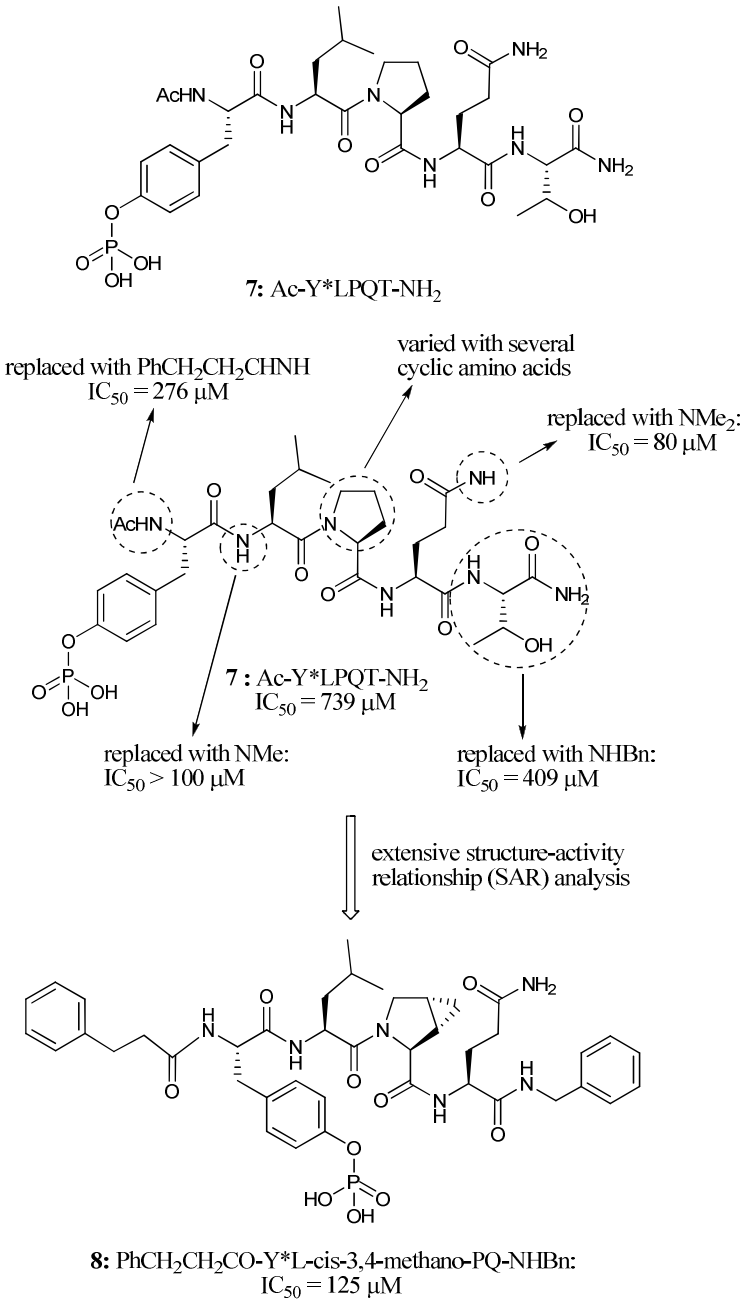

Figure 11. Structural modification and SAR study of peptidomimetics derived from the phosphopeptide **4**.

On the bases of molecular modeling experiments, new conformationally constrained macrocyclic peptidomimetic inhibitors were designed (**Figure 12**), with the aim to synthesize cyclic derivatives more resistant to proteases, and able to interact with the protein in an entropic favoured manner, as confirmed by their biological activity

determined in whole cell assays. The constrained analogue **9** (**Figure 12**, **a**) was prepared and found to exhibit a threefold improvement in STAT3 inhibition.

a)

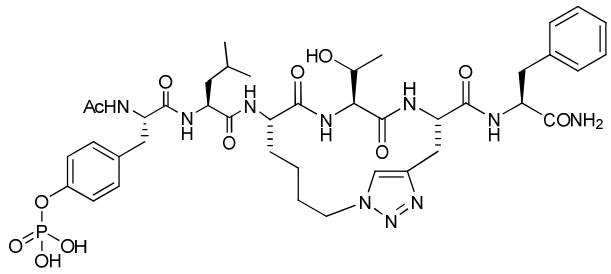

9

b)

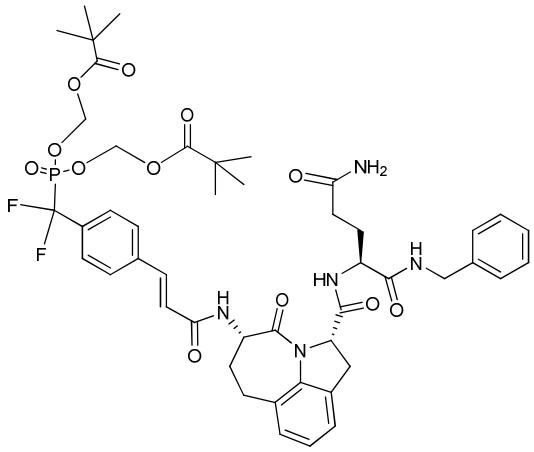

10: BP-PM6

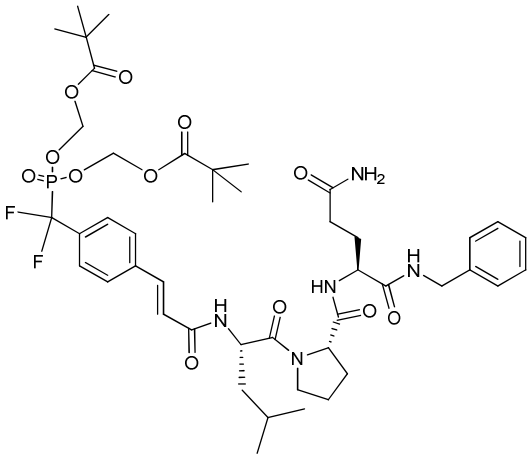

11: BP-PM279G

Figure 12. a) Example of the structure of a conformationally constrained macrocyclic peptidomimetic inhibitor; **b**) examples of permeable prodrugs (**10** and **11**) containing POM group.

To increase the membrane permeability, the pivaloyloxymethyl (POM) prodrug method has been applied; this approach was used for the preparation of two permeable prodrugs BP-PM6 (**10**, **Figure 12**, **b**) and BP-PM279G (**11**, **Figure 12**, **b**).

It was assumed that these pro-drugs entered into the cells after the POM cleavage by a carboxyesterase and then they bound the SH2 domain. This causes the separation of the pre-established STAT3 dimers, exposing the phosphotyrosines to the enzymatic cleavage and thus blocking the STAT3 activation. However, despite these efforts, the design of potent and cell-permeable STAT3 inhibitors remains a very challenging task.

Natural compounds

Among natural compounds with STAT3 inhibitory activity, Galiellalactone (**Figure 13**), a tetrahydro-isobenzofuranone isolated from the fermentation broth of the ascomycete strain A111-95, was identified. It was able to inhibit the IL-6-dependent JAK-STAT signaling cascade by the direct inhibition of STAT3 dimers binding to DNA, without inhibiting STAT3 tyrosine and serine phosphorylation.

The phenanthrenequinone derivatives, named tanshinones, were isolated from the roots of *Salvia miltiorrhiza* Bunge. Dried roots of this plant have commonly been used in traditional oriental medicine for the treatment of circulatory disorders, liver disease, coronary heart disease, hepatitis, and chronic renal failure. Two major tanshinones, Cryptotanshinone (**Figure 13**) and Tanshinone IIA, are well-known active components of this plant. Recently, Cryptotanshinone has been identified as a potent STAT3 inhibitor as it rapidly and selectively inhibits STAT3 Tyr705 phosphorylation in DU145 prostate cancer cells, but it does not inhibit the upstream tyrosine kinases.[154] To investigate the Cryptotanshinone inhibitory mechanism in DU145 cells, proteins upstream of STAT3 has been analyzed. Although the phosphorylation of JAK2 was inhibited by 7 μmol/L Cryptotanshinone at 24 h, the inhibition of STAT3 Tyr705 phosphorylation occurred within 30 minutes and the activity of the other proteins was not affected. These results suggest that inhibition of STAT3 phosphorylation is caused by a JAK2-independent mechanism, with suppression of JAK2 phosphorylation as a secondary effect of Cryptotanshinone treatment. Moreover, Cryptotanshinone inhibits phosphorylation of STAT3 selectively; it is unable to inhibit phosphorylation of STAT1 or STAT5. Other experiments have revealed the possibility that Cryptotanshinone might directly bind to STAT3 molecules. Cryptotanshinone was co-localized with STAT3 molecules in the cytoplasm, where it inhibited the formation of STAT3 dimers. Computational modeling studies have shown that cryptotanshinone could bind to the SH2 domain of STAT3. These results suggest that Cryptotanshinone is a potent anticancer agent targeting the activation STAT3 protein. The antitumor effects of Cryptotanshinone is also mediated by the suppression of the expression of STAT3-regulated target genes such as cyclin D1, survivin, and Bcl-xL, causing an accumulation of cells in the G_0-G_1 phase. In particular, the last effect could be attributed to the down-

regulation of cyclin D1 expression, as it is required for cell cycle progression from the G_1 phase to the S phase.

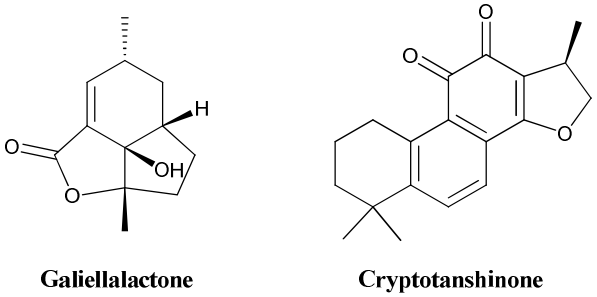

Galiellalactone **Cryptotanshinone**

Figure 13. Structures of natural compounds

Synthetic compounds

Among the small molecules that are able to inhibit STAT3 activity, several promising candidates have been identified through the screening of chemical libraries and computational studies. They include:

- *compounds that structurally mimic the peptidomimetic inhibitors*: a large number of these molecules, presenting substituted oxazole and thiazole scaffolds, disrupted the STAT3-DNA binding activity at low concentration;
- *compounds related to STA 21* (**Figure 14**):
  its mechanism of action seems to involve the binding to the SH2 domain and subsequently the blockage of STAT3 dimerization. The derivates, which exhibited *in vitro* significant anti-tumor activities, were obtained by simplifying the original moiety of STA-21 and by structure-based design;
- *porphyrine derivatives*
- *catechol derivatives*: docking studies highlighted the possibility that the catechol moiety may bind to the SH2 domain mimicking the tyrosine residue.
- *purine derivatives*
- *platinum-based compounds*: the effects of platinum complexes were explored on the STAT3 signaling pathway. Two platinum (IV) complexes, CPA-1 and CPA-7 (**Figure 14**), and one platinum (II) complex, CPA-3 (**Figure 14**), showed a selective inhibition of STAT3-DNA binding at low concentration.[25] Among them, CPA-7 was the most potent inhibitor (IC_{50} = 1.5 μM). Studies of the effects on cell proliferation has

revealed a strong inhibition of cells that only harbor persistently activated STAT3 but the exact mode of inhibition is still not completely known.

Another compound that belongs to this class of inhibitors is IS3295 (**Figure 14**) and it is selective for STAT3 over STAT1 and STAT5.

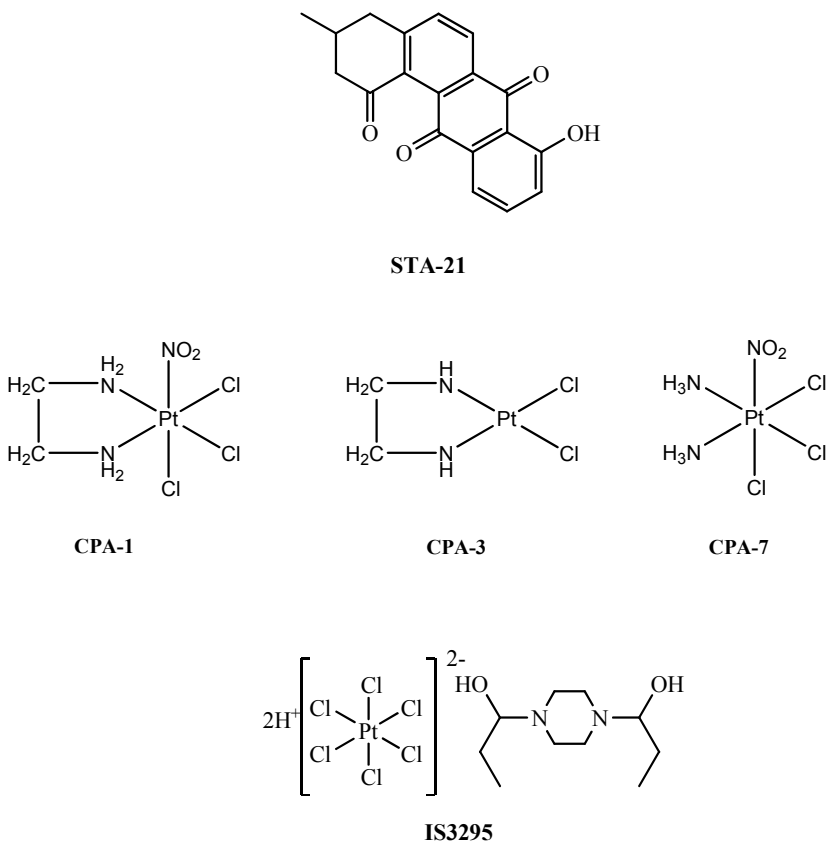

Figure 14. Stuctures of synthetic compounds

Oligonucleotides

Besides the SH2 domain, another potential target for the highly selective STAT3 inhibitors is the DBD domain, since it recognizes and binds DNA motifs in target genes. Decoy oligonucleotides (decoy ODNs), containing the TFs' DNA binding consensus sequences, selectively inhibit TFs by binding to the DBD . They can induce, *in vitro*, the death of tumour cells whose growth depends on TFs. This has notably been shown for several TFs, including NF-kB and STAT3. Because of the entrapment of activated

STAT3 dimers in the cytoplasm STAT3-decoy ODN efficiently induced cell death in mouse xenografts of a head and neck squamous cell carcinoma. One limitation of STAT3-decoy ODN is that despite the different functions of STAT1 and STAT3 in the cell, they recognize very similar DNA targets, with the result that STAT3-decoy ODN can inhibit both. The decoy ODNs do not need to enter the nucleus to exert their inhibitory effect, but new efforts must be done to solve the problem of the low membrane-permeability, caused by chemical and physical characteristics of oligonucleotides.

2.3.2 Indirect inhibitors

The indirect approach for STAT3 inhibition consists of blocking STAT3 upstream activators in the signal transduction pathway, leading to impairment of STAT3 function and, for certain types of cancer, induction of tumor-cell apoptosis. Several strategies to target STAT signaling have been developed, due to the acquired knowledge of the mechanism of constitutive STAT3 activation and its transcriptional activity from cell surface to the nucleus.

Among these approaches we can find a blockage of receptor-ligand interaction, inhibition of tyrosine or serine kinases, or an interruption of physiological protein modulators of STAT activity (e.g. SOCS, PIAS or phosphatases). However, these indirect strategies have some important limitations. Firstly, STAT3 can be activated by many different receptors and kinases and therefore, only in specific cases the inhibition of one receptor or kinase can block STAT3 phosphorylation. Additionally, it would be necessary to develop many different kinase inhibitors to treat all the possible disorders that present STAT3 activation, since in each case phosphorylation can be due to different kinases. Finally, these strategies lacks specificity of action, as they block multiple downstream signaling pathways in addition to STAT proteins, increasing the likelihood of undesirable toxicity. Therefore targeting the upstream regulators does not seem to be an optimal way to prevent STAT3 activation. A concise list of both natural and synthetic compounds is reported. It must be underlined that most of them have multiple targets and their spectrum of biological activities and effects is very wide and complex. Moreover the mechanisms of action in relation to STAT3 inhibition for some of these agents remain to be clearly defined. Among natural compounds, some examples of molecules which exert their effect on STAT3 pathway are: Epigallocatechin-3-

gallate (EGCG), Piceatannol, Curcumin, Plumbagin (**Figure 15**).

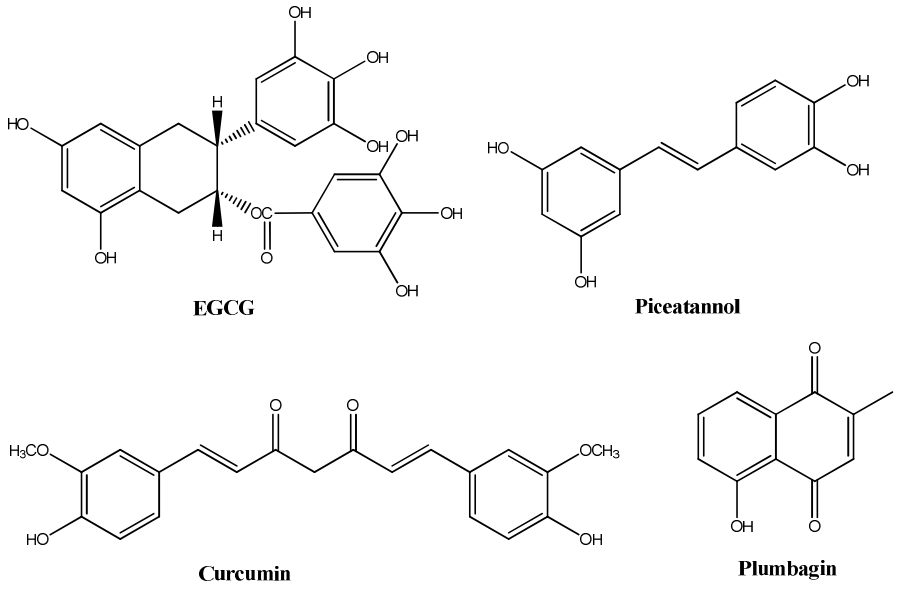

Figure 15. Structures of natural compounds

Among the synthetic compounds, a large number of molecules with different chemical structures has been found to play an important inhibitory role on STAT3 pathway, beyond various other primary effects on cells. [153] These derivatives can be classified as follows:

- *compounds endowed with JAK inhibition*: these molecules selectively bind a JAK protein implicated in STAT3 signaling pathway (*e.g.* FLLL31, NFD, Ruxolitinib (INCB018424) (**Figure 16**)).
- *Compounds interfering with STAT3 phosphorylation* (*e.g.* GO-Y030, CDDO-Me (**Figure 16**))
- *Patented compounds:* several patented compounds, belonging to different chemical classes, exhibited various mechanism of action. Among them, an oxadiazol ureidic derivative, AVS-0288 (**Figure 16**) was identified through a biological screening of a Korean chemical library. It was able to inhibit STAT3-dependent luciferase activity with an IC_{50} of 3 μM and suppress the growth of HCT-116 colon cancer cells (GI_{50} = 20 μM). However, its exact mechanism of action on STAT3 pathway has still not been elucidated yet.

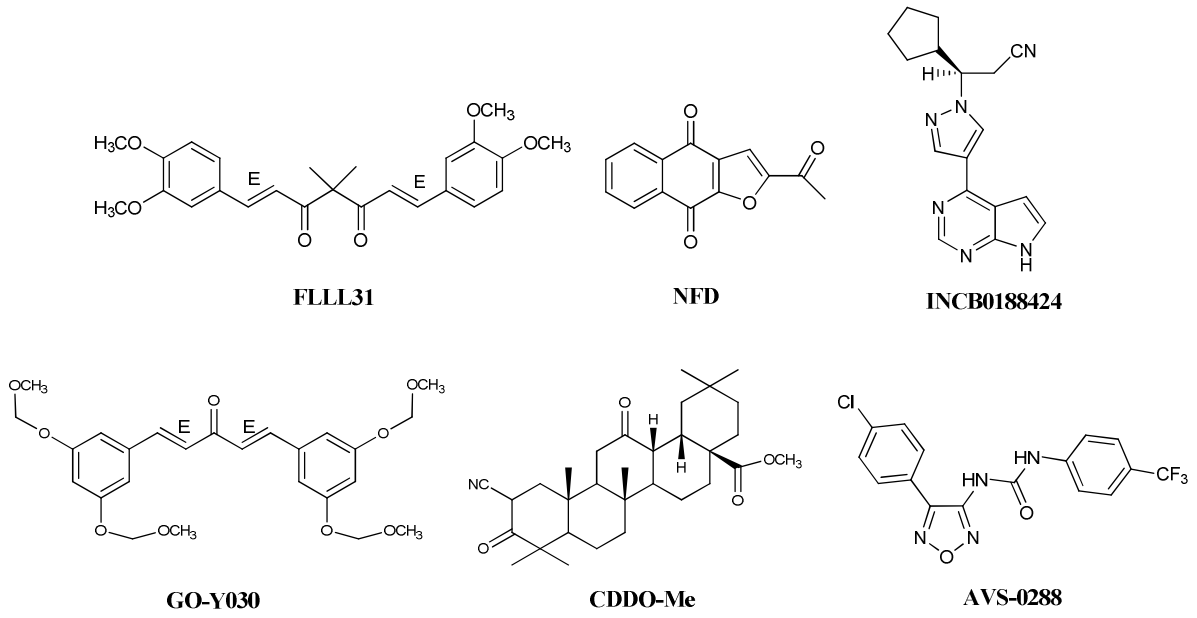

Figure 16. Structures of synthetic compounds

2.4 Conclusions and future perspectives

It has been 13 years since the original discovery of the association of constitutive STAT3 activation with malignant transformation.[155] Since then, a large number of studies have been undertaken for the validation of STAT3 as a cancer drug target, and substantial efforts have been poured into the discovery of novel STAT3 inhibitors. There is a large number of compounds with STAT3 inhibitory activity reported to date, which denotes an enhanced investigation in this field in recent years. Of these molecules, a few show good activity in terms of inhibition of STAT3 biological functions and the associated antitumor cell effects *in vitro*, as well as the suppression of tumor growth in mouse models of human tumors. However, these compounds are mostly at the experimental stage and not in a suitable form for clinical utility. Therefore the challenge is the discovery of new selective drug candidates, with high potency and *in vivo* activity.

In order to achieve this goal, a direct inhibitory approach should be preferred because the non-specific nature of the mechanism of action of indirect inhibitors could cause important adverse effects. Regarding the direct approach, much of the efforts has been directed at

disrupting the STAT3:STAT3 dimerization, which is a fundamental step in STAT3 activation. The slow progress of obtaining suitable STAT3 inhibitors for preclinical investigation and for clinical development could be attributed to the challenge of targeting protein-protein interactions (PPIs), given the large surface area of the target, and the chemistry of these interactions,[156] which are very different from those of more-established targets such as enzymes and G-protein-coupled receptors. Nonetheless, a number of successful examples have started to prove that it is possible to overcome these hurdles and develop PPI modulators as drugs.[157]

3. RESEARCH PROJECT

This thesis is focused on the discovery of new small molecules as potential STAT3 inhibitors, preferably endowed with a direct mechanism of action in order to avoid all the possible side effects typical of an indirect approach. This project began from the investigation of **AVS-0288**, a STAT3 inhibitor which was identified through a screening of a Korean chemical library[158] by Prof. Kwon research group, with whom our research group has been collaborating for several years. AVS-0288 showed an interesting dose-response profile of STAT3 inhibitory activity, but its exact mechanism of action had not been clarified yet. With the aim to identify the essential requirements for the development of novel lead compounds, several derivatives of AVS-0288 were design and synthesized: the 4-subtituted-3-amino-1,2,5-oxadiazole (**F1-F3**) (Chapter 3.1).

Subsequently, another different class of molecules were studied: the pyridazinone derivatives (**P1**-**P26**) (Chapter 3.2). They derived from the structure of the natural compound **Cryptotanshinone**, which had been discovered by Prof. Kwon research group as a direct STAT3 inhibitor.[154]

Furthermore, in order to combine the structural characteristics of the two series of molecules above, "chimera" compounds (**C1-C3**) (Chapter 3.3), with the support of conformational studies, were designed and synthesized.

Finally, another series of compounds more directly related to Cryptotanshinone was developed (**O1, O2**). These oxidised derivatives (Chapter 3.4) were characterized by the *ortho*-quinone moiety of Cryptotanshinone, since both molecular modeling studies and *in vitro* screening had suggested the importance of this structural feature for STAT3 inhibitory activity.

Synthetic procedures, conformational, crystallographic and docking studies, as well as biological studies performed, will be presented for each series of derivatives.

In detail, the conformational analysis was carried out by Dr. L. Legnani and Prof. L. Toma of the University of Pavia (Italy), the crystallographic studies were perfomed by Dr. F. Meneghetti of the University of Milan (Italy) and the docking studies by Dr. A. Pedretti of the University of Milan (Italy). Regarding the biological evaluation, the luciferase assay was performed by Prof. B-M. Kwon research group at the Korean Research Institute of Bioscience and Biotechnology (KRIBB) of Daejeon (South

Korea). I had the opportunity to spend six months of my PhD at KRIBB Institute, where, under the guidance of Prof. B-M. Kwon, I learned the basic molecular biologic techniques for the analysis of STAT3 inhibitors, thus contributing to the investigation on my compounds. Finally, the AlphaScreen-based assay was carried out by Prof. A.Asai research group of the University of Shizuoka (Japan).

3.1. The 1,2,5-oxadiazole derivatives

3.1.1 Project description

The oxadiazole ureidic derivative, AVS-0288, was identified through a screening of a Korean chemical library[158] as a potent STAT3 inhibitor. This screening was performed using the dual-luciferase assay,[159] a cell-based test able to identify inhibitors of the STAT3 pathway. A dose-dependent STAT3 inhibitory activity of AVS-0288 was detected and an IC_{50} of 2.5 μM was calculated after 24 h of treatment (**Figure 17**).

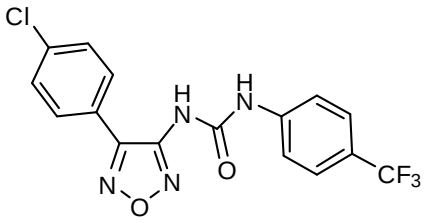

AVS-0288

a)

% Inhibition[a]	
2 μM	**5 μM**
31	82

[a]Values presented are the mean calculated from three experiments, which differ by less than 10%

b)

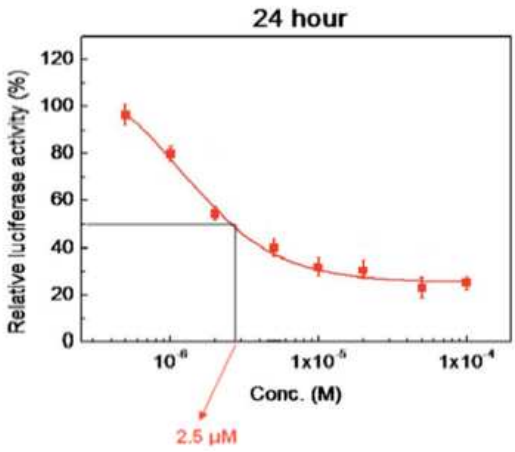

Figure 17. a) Inhibitory activity of AVS-0288 against STAT3 evaluated by dual-luciferase assay in HCT-116 colon cancer cells after 24 h of treatment; **b**) dose-dependent effect of AVS-0288 on STAT3 activity after incubation for 24 h.

On the basis of these promising results, a series of derivatives structurally related to AVS-0288 were designed and synthesized.[160, 161, 162] In detail, the central 1,2,5-oxadiazole ring was kept unchanged, whereas various substituents, characterized by different steric and electronics

features, were introduced at position 3 and 4. The performed structural modifications are summarized in **Chart I** and consist of: *i*) the replacement of the chlorophenyl moiety at position 4 of the heterocycle with groups which differed in size and polarity (R_3= CH_3, $COOCH_3$, CH_2OH, Ph); *ii*) the elimination of the trifluoromethyl group on the *N*-phenyl (R_1= H); *iii*) the subtitution of the urea with a carboxamido or a sulfonamido function (Y= CO, SO_2); *iv*) the insertion of a methylene between the group of item *iii* and the phenyl linked to it (*n* = 1).

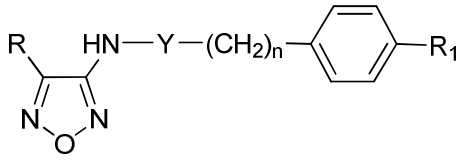

R= CH_3, $COOCH_3$, CH_2OH, C_6H_5, *p*Cl-C_6H_5
Y= NHCO, $NHSO_2$, NHCONH
n= 0, 1
R_1= H, CF_3

Chart I

3.1.2 Chemistry

3.1.2.1 Synthesis of key intermediates: 3-amino-1,2,5-oxadiazoles (1a-e)

Three series of 3,4-disubstituted-1,2,5-oxadiazole derivatives were synthesized: the ureido (**F1**), carboxamido (**F2**) and sulfonamido (**F3**) derivatives. They were prepared from the key intermediates (**1a-e**), which were prepared according to literature methods.[163, 164, 165] In detail, compound **1a** and **1d** were obtained through a one pot reaction starting from the appropriate β-keto esters: ethyl acetoacetate and ethyl benzoylacetate respectively. The key intermediate **1b** was derived from the Fisher esterification of **2**, which was in turn synthesized *via* a one pot reaction from ethyl cyanoacetate (**Scheme 1**). Compound **1c** was obtained by reduction with $LiAlH_4$ of **1b** (**Scheme 1**).

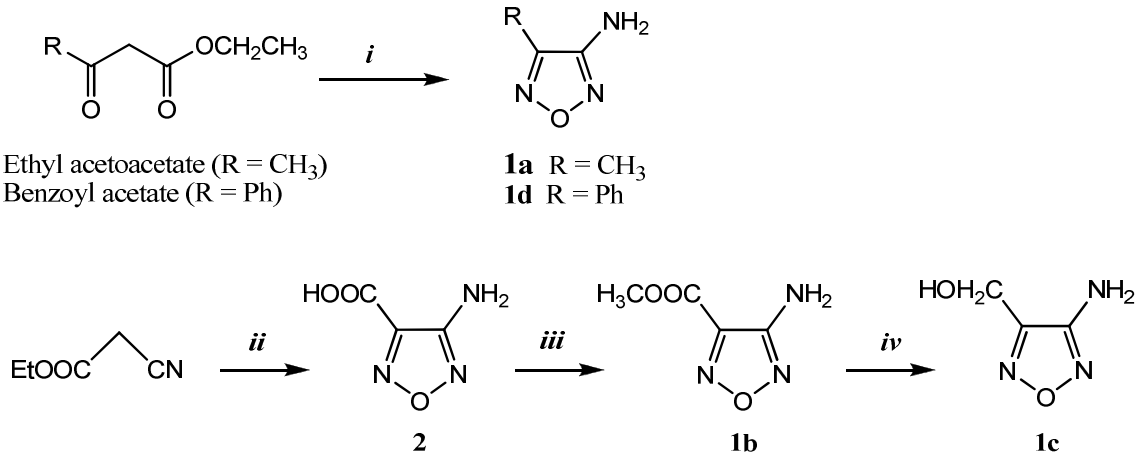

Scheme 1. *Reagents and conditions: i*) NaOH, $NaNO_2$, $HClO_4$ 20%, NaOH, $NH_2OH{\cdot}HCl$, urea; *ii)* 85% H_3PO_4, 25-30 °C, NaOH, KOH, $NH_2OH{\cdot}HCl$, 85-100 °C, HCl to pH=1; *iii*) CH_3OH, 96% H_2SO_4, reflux, 2 h; *iv)* $LiAlH_4$, dry THF, N_2, 2 h.

The key intermediate **1e** was synthesized following the five-step procedure depicted in **Scheme 2**. This synthesis was based on the construction of the 1,2,5-oxadiazole ring starting from the commercially available 4-chloro benzaldehyde, which was condensed with hydroxylamine hydrochloride to obtain the correspondent the aldoxime **3** which was readily converted to the hydroxyimidoyl chloride **4** using the chlorinating agent *N*-chlorosuccinimmide (NCS) in dimethylformamide. The substitution of the chlorine of **4** with a cyano group, performed with potassium cyanide, led to the intermediate **5**. This latter was then treated with an alkaline solution of hydroxylamine to afford the bis-oxime **6**, which was refluxed in basic conditions to carry out its cyclization and product **1e** was thus obtained. Since **1e** precipitated from the reaction mixture, it could be easily isolated by filtration.

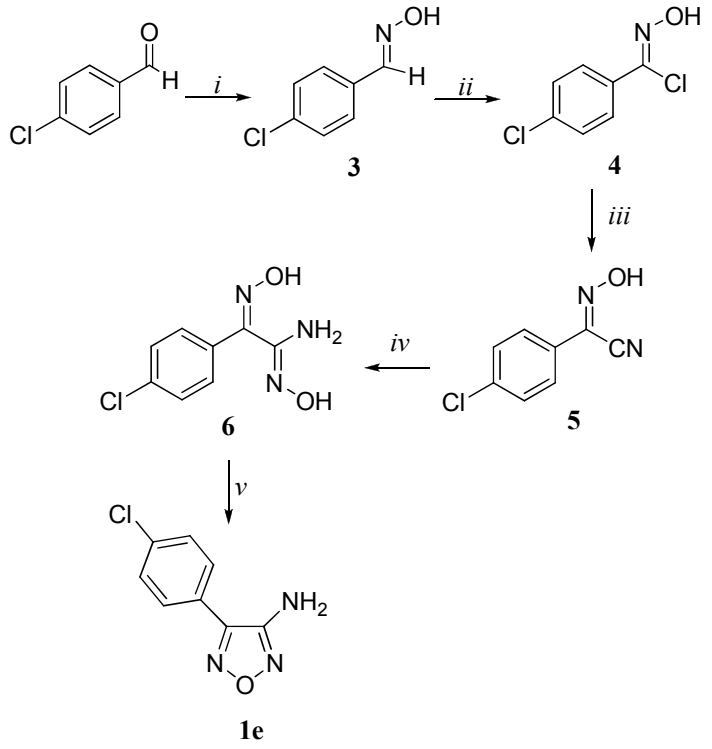

Scheme 2. *Reagents and conditions*: i) $NH_2OH{\cdot}HCl$, $NaHCO_3$, CH_3OH, reflux; ii) NCS, DMF, rt; iii) KCN, $(CH_3CH_2)_2O$, H_2O, 0 °C; iv) NH_2OH HCl, $NaHCO_3$, CH_3OH, reflux; v) 2N NaOH, reflux.

3.1.2.2 Synthesis of the 3-ureido (F1a-d), 3-amido (F2a-e) and 3–sulfonamido (F3a-e) 1,2,5-oxadiazoles

Key intermediates (**1a-e**) underwent coupling reactions with isocyanates with various chains length to afford the target compounds, which were divided in three main classes: ureido (**F1a-d**), amido (**F2a-e**) and sulfonamido derivatives (**F3a-e**).

The ureidic compounds (**F1a-d**) were obtained as shown in **Scheme 3**. The corresponding **1** was condensed with the required isocyanates, either in conventional conditions (for the obtainment of **F1a** and **F1aa**) or under microwave irradiation (for **F1b-d)**. Compound **F1aa** was also synthesized using microwave synthesizer at high temperature but in this case a mixture of other ureidic by-products was obtained.[166] The key intermediate **1c** had to be firstly protected at the alcoholic function by methyl chloroformate (compound **7**). The final deprotection of **8** (n = 0) and **9** (n = 1), using K_2CO_3 in methanol, gave the corresponding compounds **F1c** and **F1cc**.

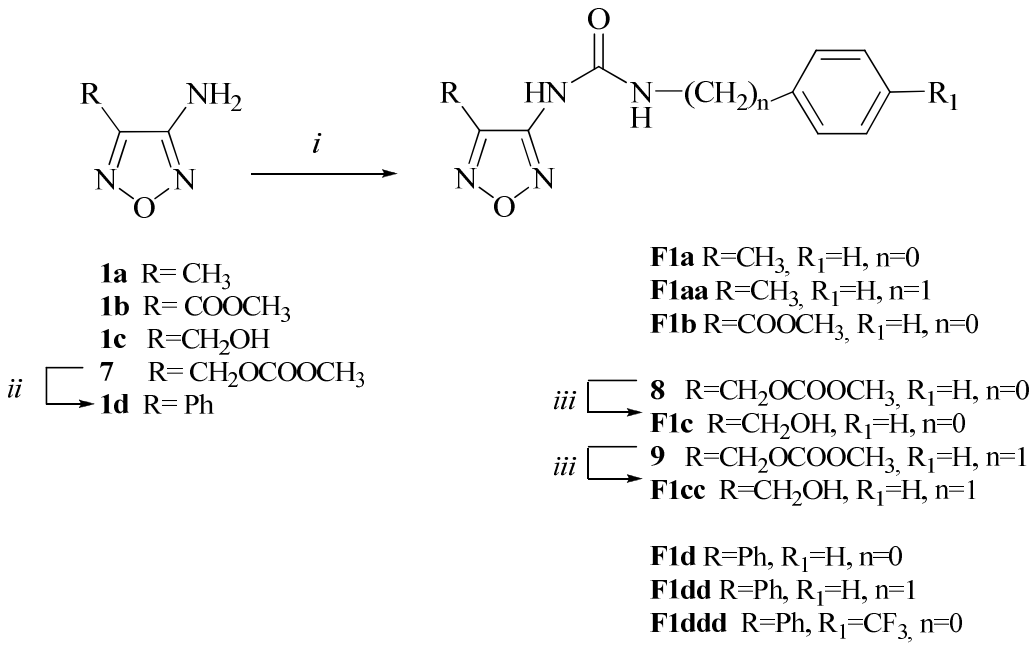

Scheme 3. *Reagents and conditions: i)* R_1-Ph-$(CH_2)_n$-NCO *ii)* CH_3OCOCl, TEA, THF, rt; *iii)* 1% K_2CO_3, CH_3OH, rt

The synthesis of the final styryl products (*E,Z*)-**F1g** and (*E,Z*)-**F1gg** started from the oxidation of the alcoholic function of the correspondent **F1c** and **F1cc** with Dess-Martin Periodinane in dry dichloromethane to give the cyclic hemiaminal **10** and **11**, respectively (**Scheme 4**). The aldehydic derivatives could not be isolated since they underwent a spontaneous cyclization forming **10** and **11**, obtained through the intramolecular reaction between the ureidic nitrogen and the aldehydic function. This is in agreement with the intramolecular ring closure originated when aldehydes bind to nitrogens able to give hemiaminals inside the stable medium-sized rings.[167] The equilibrium was completely shifted versus the cyclic form, and compounds **10** and **11** were the only products isolated, as established by ^{1}H NMR. The cyclic hemiaminals **10** and **11** underwent a Wittig reaction with benzyl triphenyl phosphonium chloride under basic conditions in tetrahydrofurane at reflux, yielding a 3:1 mixture of *E* and *Z* isomers of **F1g** and **F1gg** (**Scheme 4**). Isomers *E* and *Z* were easily separated by silica gel chromatography. The attribution of the *cis*/*trans* geometry about the styryl π-bond was determined by proton–proton coupling constants for the olefinic proton signals and confirmed by X-ray analysis.

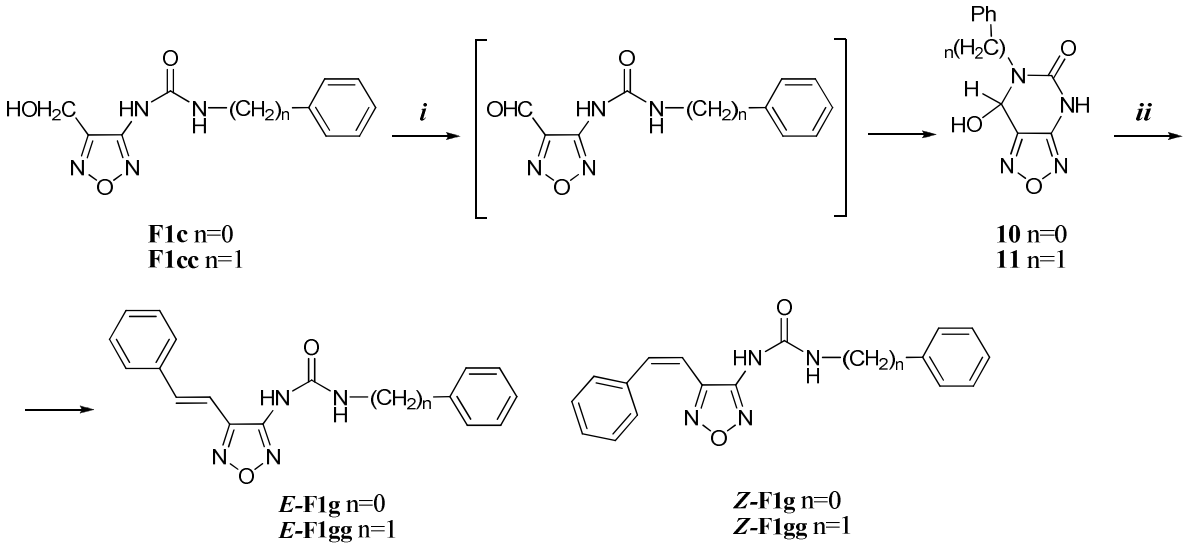

Scheme 4. *Reagents and conditions: i)* Dess-Martin Periodinane, dry CH_2Cl_2; *ii*) benzyl-triphenyl phosphonium chloride, K_2CO_3, 18 crown 6, THF, reflux, 1 h.

The amidic compounds (**F2a-e**) were prepared from the required intermediate **1** by reaction with a suitable acyl chloride in a proper medium. When necessary, the condensing agent EDAC was used (**Scheme 5**).

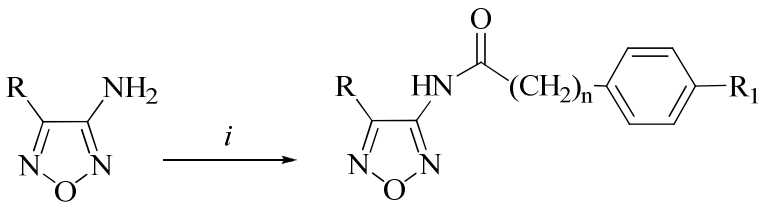

Scheme 5. *Reagents and conditions: i)* R_1-Ph-$(CH_2)_n$-COCl, $NaHCO_3$, THF, rt or R_1-Ph-$(CH_2)_n$-COCl, Py, toluene/diethyl ether, rt (EDAC in CH_2Cl_2 only for **F2b**)

Finally, the sulfonamidic compounds (**F3a-e**) were obtained by reaction of the appropriate **1** with the suitable sulfonyl chloride in pyridine (**Scheme 6**). The key intermediate **1c** had to be

firstly protected at the alcoholic function by methyl chloroformate (compound **7**) and the final deprotection of **12**, to obtain compound **F3c**, was performed with K_2CO_3 in methanol.

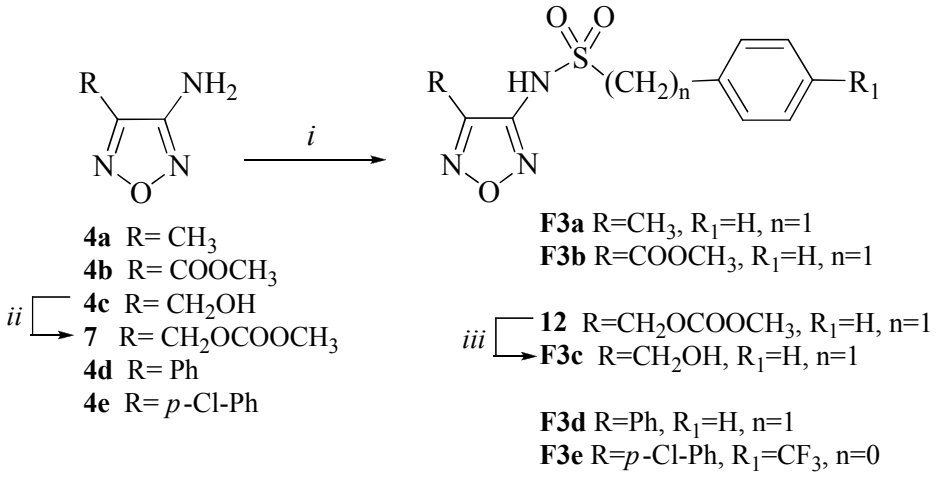

Scheme 6. *Reagents and conditions: i)* R_1-Ph-$(CH_2)_n$-SO_2Cl, Py, rt *ii)* CH_3OCOCl, TEA,THF, rt *iii)* 1% K_2CO_3, CH_3OH, rt

3.1.3 Pharmacological studies

3.1.3.1 High-throughput screening in drug discovery

A high-throughput screening (HTS) for early stage drug discovery has enabled researchers to screen more than a hundred thousand chemicals per day. Cell-free assay based on energy transfer, fluorescence polarization spectroscopy provide the sensitivity, ease and speed. Novel cell-based assays have been adapted for high-throughput screening, providing *in situ* analysis of a variety of biological targets. A number of assay systems have been developed and modified over the past few years to compensate the limitations on HTS; these assays can be divided into two groups: cell-free assays that measure the biological activity of a pure protein target *in vitro* and cell-based assays that investigate the activity of a target by monitoring a biological response of a cell. The advantage of these assay systems is that they both can be performed automatically in relatively small volumes, yield robust responses and are relatively stable to solvents and compounds used in drug screening.

The primary goal in cell-free assays is to simplify the steps required in setting up the assay and in detecting the activity. This goal has been met to a large extent by development of detection systems that do not require separation of the product of the reaction from the substrate, or other components of the assay mixture. Earlier approaches to such homogeneous assay formats relied on proximity-dependent energy transfer.

Cell-based assays are an increasingly attractive alternative to *in vitro* biochemical assays for HTS. These types of screening system have an ability to examine a specific cellular process. For instance, activation of a cell surface receptor can induce a change in the transcription pattern of a number of genes. This induced change in transcription can be readily captured by using enzymatic and proteomic techniques. It is the biggest merit of cell-based assay that a modulator regulating a target protein can be screened *in vivo* condition. Moreover, unexpected target proteins or modulators also can be detected on the screening process.

3.1.3.2 The cell-based luciferase assay system

Several types of screening system have been used for the evaluation of STAT3 activity in cell-based assays. For example, cell-based STAT3 (Tyr705) ELISA system and the luciferase assay system have been developed for high-throughput screening systems.[168] The luciferase assay, which is a rapid, convenient and sensitive method, has been used for signal transduction activity detection of epidermal growth factor displayed on phage.[169] Recently, the luciferase assay system has been commonly used in activity measurements of transcription factors such as STAT3, NF-κB and HSF1. Moreover, the assay system can be used for screening of modulators, such as siRNA and small molecules, targeting transcription factors in cultured human, mouse and rat cell lines. Since it is a cell-based assay, it can detect inhibitors with similar conditions to *in vivo*, unlike other screening methods such as virtual or *in vitro* screening systems. Furthermore, dual-luciferase assay systems using STAT3 sensitive reporter genes can screen a broad range of small-molecules inhibiting different points on JAK/STAT pathway (**Figure 18**).

For these reasons, the dual-luciferase assay system was used to screen the synthesized compounds to check their ability to inhibit STAT3 activation pathway in human cancer cells.

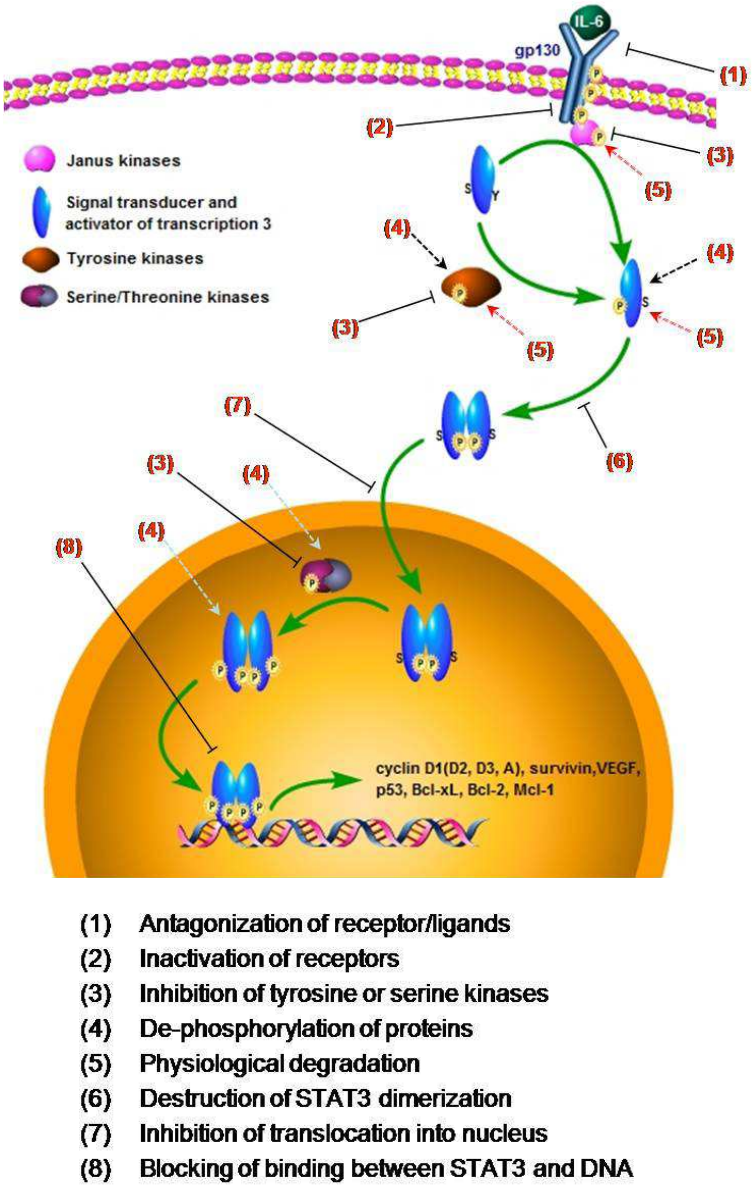

Figure 18. Scheme of predicted inhibition points on STAT3 activation pathway.[170]

The term "dual" refers to the simultaneous expression and measurement of two individual reporter enzymes within a single system. Three plasmids were used for dual-luciferase assay (**Figure 19**). The *pSTAT3-TA-Luc* has STAT3 binding sequences in its promoter region, and therefore the expression of firefly luciferase is regulated by STAT3 activity. On the contrary, the only *pTA-Luc* plasmid, which does not have the STAT3 binding sequence, was not able to bind STAT3 protein and therefore it was used for evaluation of basal luciferase expression in

cancer cells. The *pRL-TK*, which expresses *Renilla* luciferase, is driven by a constitutive promoter and it was used for normalization of firefly luciferase in each well.

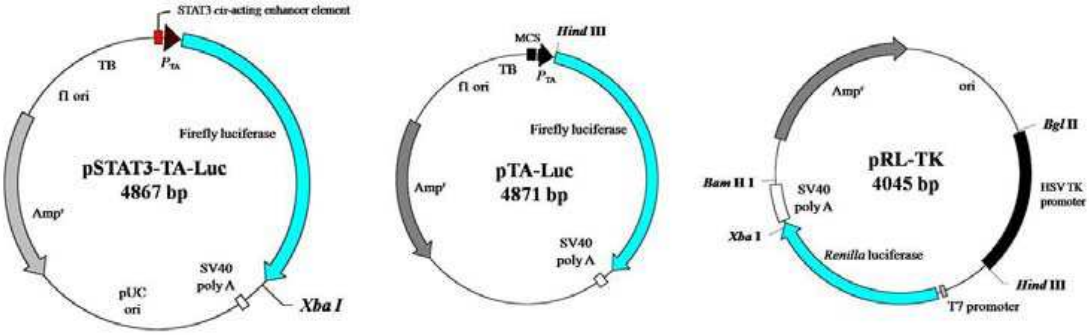

Figure 19. Reporter plasmids used for transient transfection. The *pSTAT3-TA-Luc* and *pRL-TK* were transiently transfected into host cells. The *pTA-Luc* was used for evaluation of basal activity of reporter gene.[170]

Cell line is an important factor for dual-luciferase assays because the activity of reporter genes reflecting STAT3 activity may vary at different cell lines. The primary concerns, when selecting a host cell line for the dual-luciferase assay using transient transfection, are its endogenous level of transcription factors, its transfection efficiency of reporter genes, and its biological relevance to transcription factor. HCT-116 cells were used for the biological assay performed on the synthesized compounds since these cells had all the features mentioned above. The dual-luciferase assay was carried by a modified manufacturer's protocol (see 'Chapter 6' for the experimental procedure).

3.1.3.3 Dual-luciferase assay results

The three series of 3,4-substituted-1,2,5-oxadiazoles were evaluated in the dual-luciferase assay to determine their ability to lower STAT3 activity. The compounds were tested at a concentration of 2 μM and the cells were incubated for 24 h.[160] The results, reported in **Table 6** as percentage inhibition, clearly indicate that none of the synthesized compounds had a better inhibitory activity than the parent compound AVS-0288.

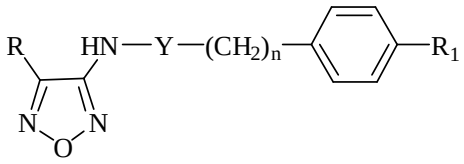

Compound	R	R_1	Y	n	% Inhibition[a] (2 µM)
F1a	CH_3	H	CONH	0	2
F1aa	CH_3	H	CONH	1	<1
F1b	$COOCH_3$	H	CONH	0	<1
F1c	CH_2OH	H	CONH	0	nt
F1cc	CH_2OH	H	CONH	1	<1
F1d	Ph	H	CONH	0	36
F1e	Ph	H	CONH	1	11
F1f	Ph	CF_3	CONH	0	<1
***E*-F1g**	PhCH=CH	H	CONH	0	<1
***Z*-F1g**	PhCH=CH	H	CONH	0	<1
***E*-F1gg**	PhCH=CH	H	CONH	1	16
***Z*-F1gg**	PhCH=CH	H	CONH	1	21
F2a	CH_3	H	CO	1	6
F2b	$COOCH_3$	H	CO	1	9
F2c	CH_2OH	H	CO	1	14
F2d	Ph	H	CO	1	11
F2e	*p*-Cl-Ph	CF_3	CO	0	<1
F3a	CH_3	H	SO_2	1	6
F3b	$COOCH_3$	H	SO_2	1	7
F3c	CH_2OH	H	SO_2	1	<1
F3d	Ph	H	SO_2	1	<1
F3e	*p*-Cl-Ph	CF_3	SO_2	0	<1
AVS-0288	*p*-Cl-Ph	CF_3	CONH	0	45

nt: not tested

[a]Inhibitory activity against STAT3 was evaluated by a dual-luciferase assay system in human colorectal carcinoma HCT-116 cells after 24 h treatment with the tested compounds. The values are the means of 3 experiments. The maximum deviation from the mean was less than 10%.

Table 6. Percentage inhibition of the synthesized oxadiazoles derivatives (**F1-F3**) evaluated with the dual-luciferase assay system.

3.1.3.4 AlphaScreen-based assay

In parallel, in order to investigate the ability of the synthesized compounds to bind STAT3 directly, an *in vitro* assay was performed. Previous studies have showen that AlphaScreen technology was capable of analyzing protein-protein or protein-peptide interactions,[171] and moreover it turned out to be a useful method to detect the interactions between the SH2 domain and the *p*Tyr-containing peptide.[172] In detail, the AlphaScreen-based assay is a bead-based non-radioactive assay system for detecting biomolecular interactions in a microlitre plate format. It allows the detection of phosphorylated proteins in cellular lysates in a highly sensitive, quantitive and user friendly assay. In this test, sandwich antibody complexes, which are only formed in the presence of analyte, are captured by AlphaScreen donor and acceptor beads, bringing them into close proximity. The excitation of the donor bead provokes the release of a singlet oxygen molecules that triggers a cascade of energy transfer in the acceptor bead, resulting in a fluorescent signal between 520 and 620 nm.

The synthesized compounds were tested in this assay system to evaluate their ability to inhibit the binding of SH2-containing proteins to their correspondent phosphopeptides, the physiological ligands.

3.1.3.5 AlphaScreen-based assay results

All the 3,4-substituted-1,2,5-oxadiazoles were tested in the AlphaScreen-based assay (Chapter 6) at a concentration of 50 μM and the results (**Table 7**) are expressed as percentage of inhibition of the interaction between SH2 domain and *p*Tyr-containing peptides. In particular, besides STAT3, other SH2-containing proteins, such as STAT1 and Gbr2 ("Growth factor receptor-bound protein 2"), having a high degree of sequence homology to STAT3 (78% and 65%, respectively), were also tested.

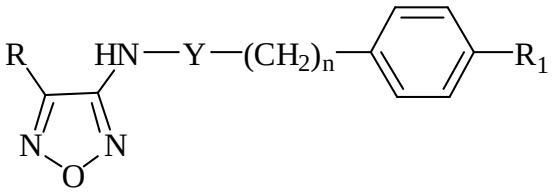

Compound	R	R_1	Y	n	% inhibition (50 μM)		
					STAT3	STAT1	Grb2[a]
F1a	CH_3	H	CONH	-	0.9	7.7	6.6
F1aa	CH_3	H	CONH	1	< 1	< 1	< 1
F1b	$COOCH_3$	H	CONH	-	6.8	2.2	< 1
F1c	CH_2OH	H	CONH	-	nt	nt	nt
F1cc	CH_2OH	H	CONH	1	< 1	0.2	< 1
F1d	Ph	H	CONH	-	< 1	4.9	8.2
F1e	Ph	H	CONH	1	< 1	11.6	11.0
F1f	Ph	CF_3	CONH	-	< 1	< 1	< 1
***E*-F1g**	PhCH=CH	H	CONH	-	nt	nt	nt
***Z*-F1g**	PhCH=CH	H	CONH	-	nt	nt	nt
***E*-F1gg**	PhCH=CH	H	CONH	1	< 1	10.6	6.6
***Z*-F1gg**	PhCH=CH	H	CONH	1	< 1	10.9	2.3
F2a	CH_3	H	CO	1	< 1	13.0	7.2
F2b	$COOCH_3$	H	CO	1	< 1	11.6	4.2
F2c	CH_2OH	H	CO	1	< 1	9.3	6.3
F2d	Ph	H	CO	1	< 1	11.8	2.2
F2e	*p*-Cl-Ph	CF_3	CO	-	36.5	61.5	10.7
F3a	CH_3	H	SO_2	1	22.9	7.8	< 1
F3b	$COOCH_3$	H	SO_2	1	44.0	23.8	2.1
F3c	CH_2OH	H	SO_2	1	< 1	5.9	3.6
F3d	Ph	H	SO_2	1	42.5	20.4	4.5
F3e	*p*-Cl-Ph	CF_3	SO_2	-	< 1	10.7	< 1

nt: not tested
[a] Growth factor receptor-bound protein 2

Table 7. Percentage inhibition of STAT3, STAT1 and Grb2 as determined in the AlphaScreen assay by **F1**, **F2** and **F3** compounds.

The results show interesting inhibitory activities *versus* STAT3 for a few derivatives: the carboxamido compound **F2e** had a percentage inhibition of 36.5%, while the sulfonamido derivatives **F3b** and **F3d** showed an inhibitory activity of 44% and 42.5%, respectively. As regards the selectivity of these compounds *versus* STAT3, **F2e** selectively antagonized STAT3-SH2 domain with respect to Grb2-SH2 domain (36.5% *versus* 10.7%), although it exhibited a higher affinity toward STAT1-SH2 domain (61.5% *versus* 36.5%). The other two sulfonamide derivatives selectively antagonized STAT3 with respect to Grb2 domain and only a low affinity was detected for STAT1-SH2 domain.

In light of these results, the compounds which showed positive trend in the AlphaScreen-based assay were re-tested in the dual-luciferase assay at a higher concentration (5 μM) than the previous one (2 μM). The results showed that only **F2e** exhibited an interesting percentage of inhibition (20%). Therefore a deeper biological investigation was performed on **F2e** and it turned out that its inhibitory activity in the AlphaScreen-based assay was dose-dependent (**Figure 20**) with calculated IC_{50} values of 17.7 μM for STAT3, 7.2 μM for STAT1 and higher than 100 μM for Grb2.

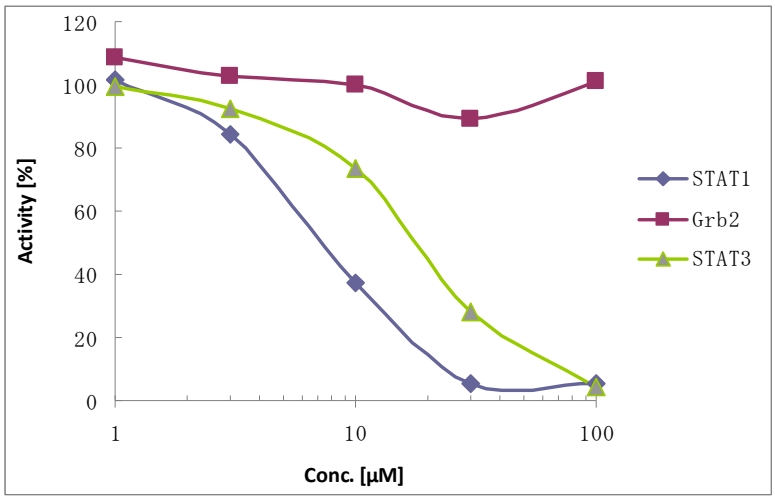

Figure 20. Dose-response curves of the inhibition of STAT3, STAT1, and Grb2 binding to *p*Tyr-containing peptides by compound **F2e** as determined by AlphaScreen-based assay (% of activity *versus* concentration expressed in logarithmic scale)

3.1.3.6 Anti-proliferative assay on compound F2e

The oxadiazoles derivatives, which had showed a positive results in the luciferase-based assay, were submitted to *National Cancer Institute* (NCI) in Bethesda, Maryland (USA) under the Developmental Therapeutic Program (DTP) which operates a two-stage anticancer compound screening course for the benefit of the general research community with the goal of identifying novel chemical leads and biological mechanisms. Among the compounds submitted for the screening, only the structures which were able to add diversity to the NCI small molecule compound collection were selected. In addition, the submission of compounds with drug-like properties utilizing the concept of privileged scaffold or structures based on computer-aided design were preferred.

The selected compounds were exposed, at a single dose of 10 μM,[173] to a panel of 58 human tumor cell lines, derived nine neoplastic cancer types (leukemia, lung, colon, CNS, melanoma, ovarian, renal, prostate, and breast cancers) (see 'Chapter 6' for the experimental procedure). In this preliminary screening, only compound **F2e** exhibited a significant growth inhibition value and thus, it was subjected to a complete analysis at five different doses for 48 h. The data are expressed as dose response parameters GI_{50}, TGI and LD_{50} referred to **F2e** molar concentration that produces 50% of growth inhibition, total growth inhibition and 50% of cytotoxicity, respectively (**Appendix I**). In this assay, **F2e** exhibited a good profile of inhibitory activity on the cell proliferation, with GI_{50} values ranging from 6.75×10^{-6} μM (renal cancer, TK10) to 5.46×10^{-7} μM (leukemia, HL60TB), and showed TGI values lower than 1.00×10^{-4} μM in most of the cell lines. The dose-response curves showing the activity of **F2e** on the panel/cell lines are represented in **Appendix II**. As expected, **F2e** inhibits the growth of the cell lines which are known to overexpress STAT3 (for instance HCT116, DU145, MDAMB-231), although several cell lines, as HL60TB (leukemia cells) and HOP-92 (non-small cells lung cancer) are the most sensitive.

3.1.4 X-Ray and conformational analysis of compound F2e[174]

The crystallographic structure of **F2e** is represented in **Figure 21**.

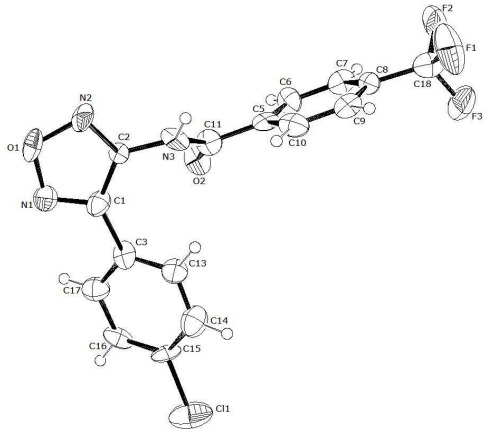

Figure 21. ORTEP[175] view of **F2e** and the relative arbitrary atom numbering scheme (thermal ellipsoids at 40% probability).

Bond lengths and angles assume the expected standard values. The overall conformation of the compound is defined by four torsional angles: N2-C2-N3-C11 (τ1) of -118(1)°, C2-N3-C11-C5 (τ2) of 175(1)°, N3-C11-C5-C6 (τ3) of -150(1)° and C2-C1-C3-C13 (τ4) of 22(1)°. The oxadiazole ring is rotated by 25(1)° and 88(1)° with respect to the chlorophenyl and trifluoromethyl-phenyl moieties, respectively. The latter two rings are perpendicular to each other, with a dihedral angle of 87(1)°. The analysis of the crystal packing has shown the important role played by the halogen atoms in connecting adjacent molecules, through Cπ-H…F, Cπ-H…Cl and C=O…F type contacts, influencing in this way the molecular conformation. The oxadiazole ring in the crystal gives rise to π interactions with the chloro-phenyl group of symmetry related molecules along the *b* axis, indicating the ability of the compound to interact through molecular stacking with a biological counterpart. The crystallographic structure represents only one of the accessible molecular conformations. Thus, in order to explore all its conformational space, a complete modeling study of **F2e** was carried out, considering all the degrees of conformational freedom that correspond to the above defined torsional angles (**Chart 2**) and, in particular, the arrangement of the amidic group with respect to the oxadiazole ring, described by the torsional angle τ1.

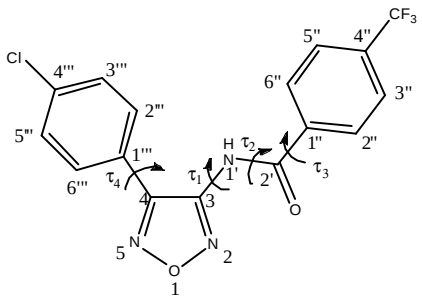

F2e

Chart 2

The geometry optimizations were performed at the B3LYP/6-311+G(d,p) level[176] and the energy of the optimized conformations was recalculated using a polarizable continuum solvent model (PCM)[177] to take into account the effect of water on the conformational population.

	E_{rel} vacuo (kcal/mol)	P vacuo (%)	E_{rel} water (kcal/mol)	P water (%)	τ_1 (°)	τ_2 (°)	τ_3 (°)	τ_4 (°)
A	2.10	1.9	0.00	40.9	22	-177	-154	43
B	2.49	1.0	0.17	30.6	0	177	-158	-48
C	0.00	65.0	0.28	25.5	-126	174	-159	34
D	0.42	32.1	1.53	3.0	-110	174	-156	-45

[a] τ_1 : N2-C3−N1'−C2'; τ_2 : C3−N1'−C2'−C1"; τ_3 : N1'−C2'− C1"− C2"; τ_4 : C3−C4−C1'"−C2'".

Table 8. Relative energies (kcal/mol), equilibrium percentages (%) in the gas phase and in water, and significant torsional angles[a] (°) of the located conformations of compound **F2e**.

Four minimum energy conformations were located and their geometrical descriptors (τ1-τ4), together with their gas-phase and water-solvated energies, and the corresponding percentage contributions to the overall population, are reported in **Table 8**. It is worth pointing out that a mirror image conformation exists for each described conformation; thus, the number of conformations accessible to the molecule is double with respect to those reported. Conformations **A** and **B** are very similar (**Figure 22**), as evidenced by their values of τ1, τ2, and τ3, the only difference being the orientation of the *p*-chlorophenyl ring (τ4). The same occurs for the couple **C** and **D**. The most stable conformation in water (**A**) accounts for 40.9

% of the overall population and, together with conformation **B**, less stable by 0.17 kcal/mol, represents 71.5 %, the remaining not negligible 28.5% being due to the *in vacuo* preferred conformations **C** and **D**.

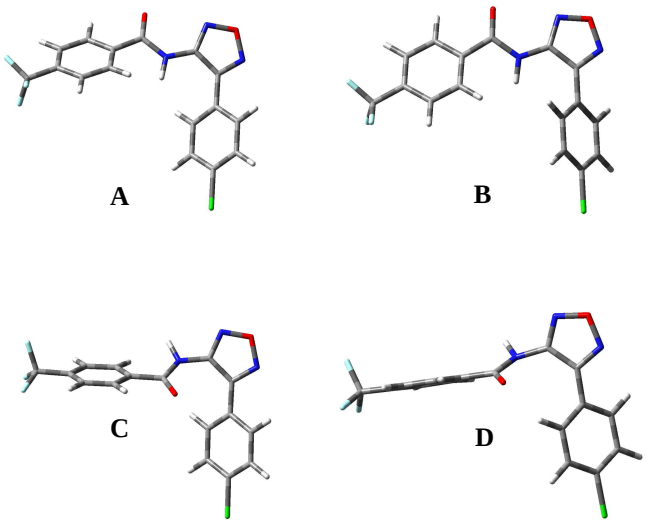

Figure 22. 3D plots of conformations **A**-**D** of compound **F2e**.

A comparison of conformations **A**-**D**, with the above described crystal structure of **F2e**, shows that it corresponds to **C**, which is the most stable conformation *in vacuo*. In fact, the two structures are characterized by about the same values of the torsional angles τ1-τ4 and the overlay of their heavy atoms produces an almost perfect super-imposition (**Figure 23**) with a rms difference value of 0.191 Å. By contrast, the comparison of the solid state structure with conformer **A** gives a rms difference value of 1.067 Å. The crystal structure and **A** orient their amide functionality in very different directions (**Figure 23**), as evidenced by the significantly different values of τ1: -118(1)° in the crystal *versus* 22° in **A**. The amide functionality usually represents a key moiety for anchoring a ligand at the binding site of the protein, and the ability of **F2e** to vary the orientation of the amide in different conditions is worthy of note. The orientation in the crystal is determined by packing interactions, as the molecules form chains through the hydrogen bond N3-H3…O2I (I at x, y-1, z), forcing in some way molecular bending, and favoring the conformation having the carbonyl oxygen pointing in the opposite direction with respect to the chlorophenyl group.

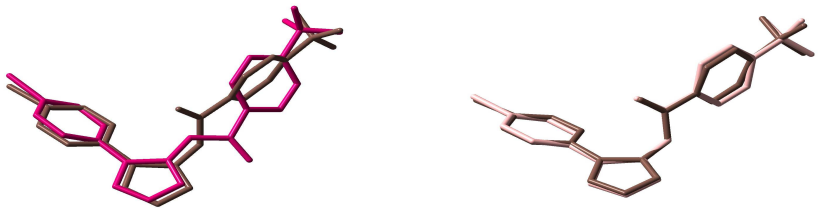

Figure 23. Superimposition of the crystal structure of compound **F2e** (brown) onto the **A** (magenta) and **C** (pink) conformers obtained through rms fitting of the heavy atoms. Hydrogen atoms are omitted for the sake of clarity.

3.1.5 Docking studies on compound F2e[174]

Docking studies were performed on **F2e** in order to clarify its interaction with the SH2 domain. In particular, considering the STAT3-MD77 complex and the conformational profile of the ligand, the best scored pose showed that the ligand assumes the most stable conformation **A**. The binding mode of **F2e** is comparable to that of phosphorylated Tyr-705, because it involves the same pocket in which *p*Tyr-705 is inserted when two subunits are assembled in the dimer. The phenyloxadiazole moiety of **F2e**, colored in cyan, occupies the same pocket (not shown) of *p*Tyr-705, colored in red (**Figure 24**).

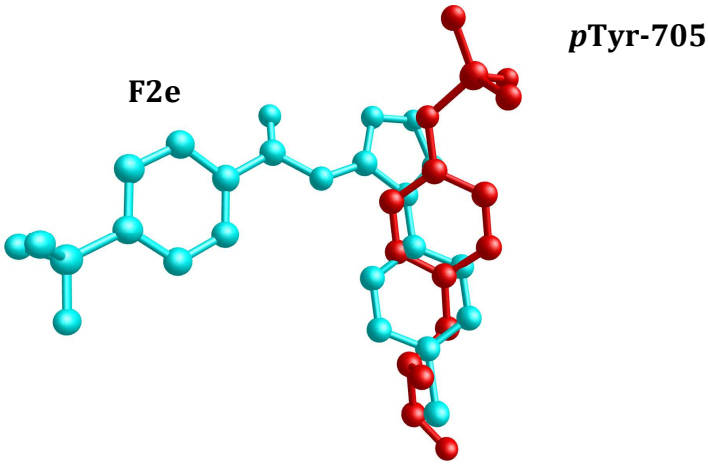

Figure 24. Comparison of **F2e** (cyan) in the docking pose with the *p*Tyr-705 (red) of the second subunit in the STAT3 dimer.

This pocket is placed on the protein surface and it is surrounded by hydrophilic and polar aminoacids to better interact with the negatively charged side chain of the phosphorylated tyrosine, mimed by the phenyloxadiazole moiety in the STAT3- **F2e** complex. As shown in **Figure 25**, the favored conformation **A** of **F2e** establishes many hydrogen bond interactions

within the binding pocket. In detail, they involve the trifluoromethyl group of the aromatic ring and the guanidine moiety of Arg-595 by three hydrogen bonds, the oxygen of the amidic group and the amine of side chain of Lys-591 by one hydrogen bond, the oxygen and the nitrogen atoms of the oxadiazole ring and the guanidine group of Arg-609 by two hydrogen bonds and finally the chlorine atom of the aromatic ring with one amidic hydrogen of Gln-635 side chain. Despite the presence of three aromatic rings in **F2e**, π-π interactions were not found in its complex with the macromolecule, due to the absence of aromatic amino acids in the binding pocket.

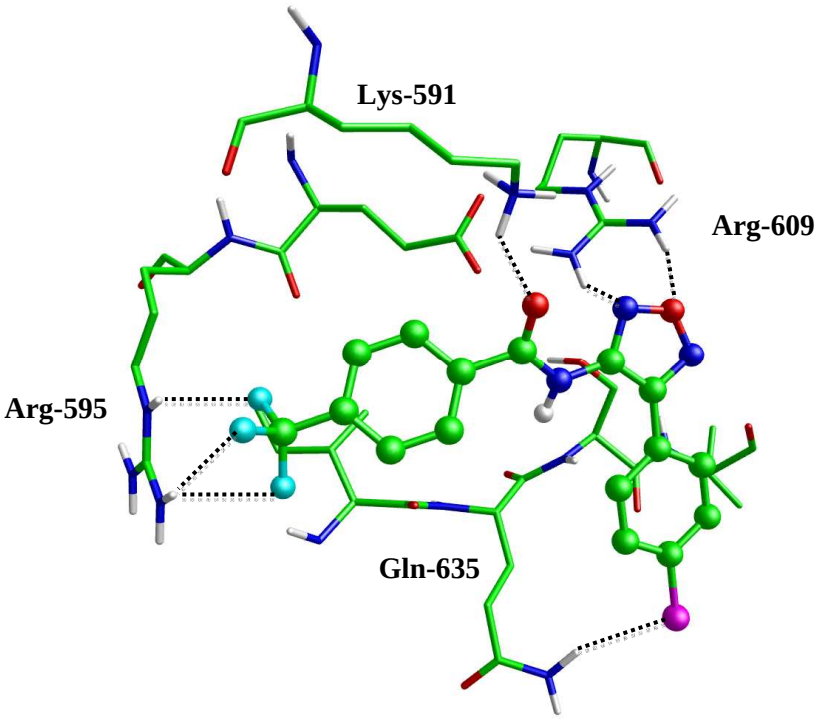

Figure 25. Main interactions between **F2e** and STAT3. The hydrogen bonds are shown as dotted lines.

Analyzing the other **F2e** complexes obtained by docking, it was possible to identify a pose in which the ligand assumes a conformation referable to the couple **C-D**, but its interaction energy is worse than all calculated complexes and the binding mode is much different if compared to the most stable one shown above. In particular, the *p*-trifluoromethylphenyl group is partially inserted in the *p*Tyr-705 pocket while, in the best complex, this pocket is occupied by the oxadiazole ring. Moreover, the *p*-trifluoromethyl is too far to reach the amino acids involved in the interaction with the phosphate. In this complex, the oxadiazole ring does

not mime the phosphate and stabilizes the complex through hydrogen bonds with Gln-635 and Lys-26. Finally, one of the poses of **F2e** corresponds to the mirror image of conformation **A**. It presents a different binding mode in which the *p*Tyr-705 pocket is not occupied, loosing the interaction with Arg-609, but keeping the weak hydrogen bonds between Arg-595 and trifluoromethyl group. It should be noted that the sulfonamido bioisoster (**F3e**) of **F2e**, which was found inactive both in the AlphaScreen and in the dual-luciferase assays, has a different conformational behavior with respect to our lead compound. In fact, none of the localized conformations of **F3e** show a relative arrangement of the aromatic groups similar to that displayed in the four geometries of **F2e**. Thus, the identification of its binding mode through docking calculations, seemed to be important to clarify the essential features for an efficient interaction with STAT3 (**Figure 26**).

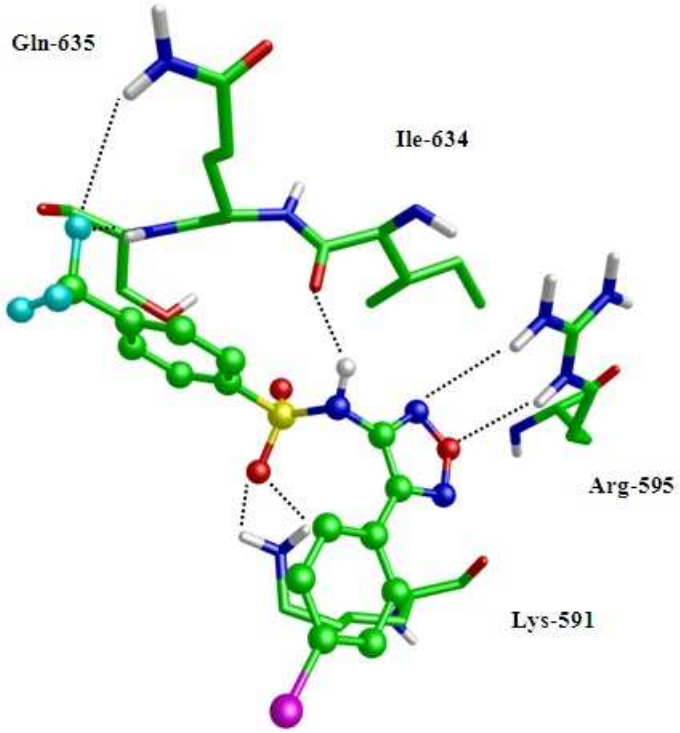

Figure 26. Main interactions between compound **F3e** and STAT3. The hydrogen bonds are shown as dotted lines.

Considering the STAT3-compound **F3e** complex, the pose and interacting conformation of the ligand are very different from those shown by **F2e**. In particular, compound **F3e** is unable to occupy the *p*Tyr-705 pocket and the oxadiazole ring interacts with Arg-595 instead of Arg-

609, which is the key residue involved in the **F2e** complex and in the formation of the salt bridge with the phosphate group when the protein dimerizes. Despite the different binding mode, the compound **F3e** complex is stabilized by an extended network of hydrogen bonds that involve: the oxygen and the nitrogen at position 5 of the oxadiazole ring and the guanidine group of Arg-609, one sulfonamide oxygen and the amine group of Lys-591, the sulfonamide hydrogen and the backbone oxygen of Ile-634, and finally the trifluoromethyl group of the aromatic ring with the amidic hydrogen of Gln-635 side chain. Analyzing the docked conformation of compound **F3e**, the two benzene rings are perpendicular and the angle between the planes, defined by the two rings, is 89°, significantly higher than the corresponding value of 28° found for **F2e**.

3.1.6 Conclusions

The ability to target the STAT3-SH2 domain of a series of 1,2,5 oxadiazole derivatives was evaluated in order to identify new direct inhibitors. One term (**F2e**) proved to be able to significantly interact with the SH2 domain: in the AlphaScreen binding assay, it showed an interesting dose response profile with an IC_{50} value of 17.7 μM. This result highlighted its potential as a protein-protein interaction inhibitor. In addition, **F2e** exhibited a significant activity (20% inhibition at 5 μM) in a dual-luciferase assay. To investigate the conformational behavior and the binding mode of **F2e**, modeling and docking studies were performed. The latter evidenced that in the best scored pose of the STAT3-**F2e** complex, **F2e** assumes the most stable conformation (calculated in water). It should be noted that the binding mode of **F2e** is comparable to that of *p*Tyr-705, when the latter is involved in the formation of STAT3 dimers. The computational data were supported by crystallographic studies. Finally, **F2e** displayed a significant growth inhibitory activity on a number of tumor cell lines. On light of these interesting results, **F2e** emerged as a lead for the development of a new series of derivatives, that is currently ongoing research in our group.

3.2 The pyridazinone derivatives

3.2.1 Project description

The phenanthrenequinone **Cryptotanshinone** (Chapter 2.3.1), isolated from the roots of *Salvia miltiorrhiza* Bunge, was a potent direct STAT3 inhibitor and found to induce apoptosis in human prostate cancer cell lines (DU145), by selectively inhibiting phosphorylation of STAT3 at a concentration of 7 μM.[154] This selectivity of action was due to its small effect on STAT3 serine 727 phosphorylation and to its inability to inhibit phosphorylation of the tyrosine residues of STAT1 and STAT5. Cryptotanshinone was also found to inhibit the phosphorylation of JAK2, but only after 4 h of treatment with the compound, whereas inhibition of STAT3 phosphorylation occured within 30 min after treatment. This result suggested that inhibition of STAT3 phosphorylation was caused by a JAK2-independent mechanism. Further studies showed that Cryptotanshinone was localized together with STAT3 proteins in the cytoplasm and could inhibit the formation of STAT3 dimers. This implied the possibility of a direct binding of Cryptotanshinone to the dimerization domain of STAT3.

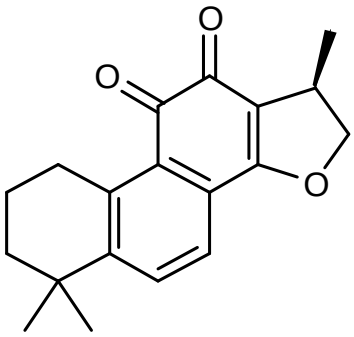

Cryptotanshinone

A conformational study of the reference compound Cryptotanshinone, and of a generic structure of benzo-cinnolinone compounds, which had been already investigated in our laboratories for other purposes,[178, 179] was performed. The result of these studies revealed a structural similarity between these compounds, and the superimposition of the preferred conformations of each molecule showed that the two compounds matched very well (Chapter 3.2.2). Therefore we designed and synthesized several new derivatives[180] based on the benzocinnolinnone structure, and a series of structural modifications (**Chart III**) were carried out in order to investigate their effects on STAT3 inhibition. In detail, the effects of modifications at the pyridazinone ring were first explored: at N-2 various kind of chains were inserted, differentiated on the basis of their length as well as the presence of esters, carboxylic acids or their bioisosteres, amines and amides. In addition, both saturated and unsaturated

derivatives of all the compounds at position 4 of the pyridazinone ring were obtained. Other structural variations were introduced at different positions of the aromatic ring, involving the insertion of substituents such as methoxy groups or halogens. Finally, we investigated the influence of the size of the central ring, synthesizing five-, six- and seven-membered ring compounds.

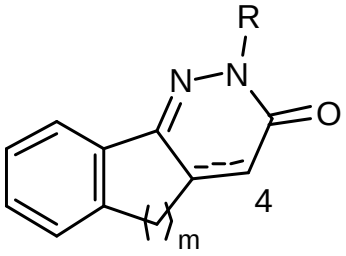

m = 1-3
R = -$(CH_2)_nCOOCH_2CH_3$; **n** = 1-6
-$(CH_2)_3COOH$
-$(CH_2)_3COONHCH_2CH_3$
-$(CH_2)_4NHCH_2CH_3$
-$(CH_2)_3OCOC(NH_2)CH_2Ph$

Chart III

3.2.2 Modeling studies

A conformational study of the reference compound Cryptotanshinone and of a general benzocinnolinone structure (**I**) was carried out. Particular attention was focused, for Cryptotanshinone, on the flexibility of the **A** and **C** rings, and, for (**I**), on the possible inversion of **C** ring.

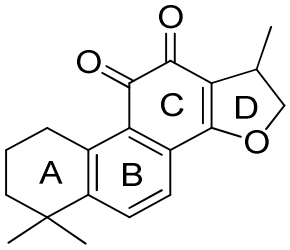

Cryptotanshinone

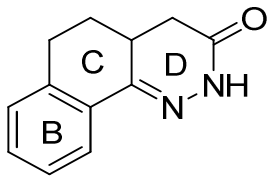

I

All calculations were carried out using the Gaussian03 program package.[181] The conformational space of the compounds was explored through optimizations at the B3LYP level with the 6-31G(d)[182] basis set, and the energy of the optimized conformations was re-calculated in water, at the same level as above, using a polarizable continuum solvent model (PCM)[177].

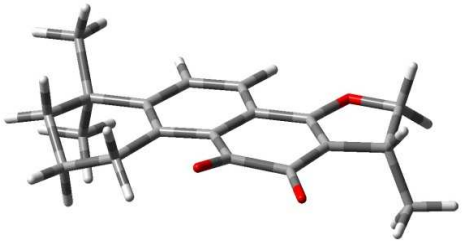

Cryptotanshinone

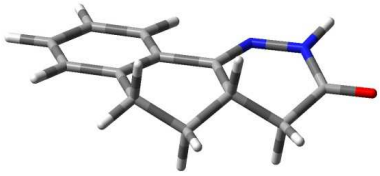

I

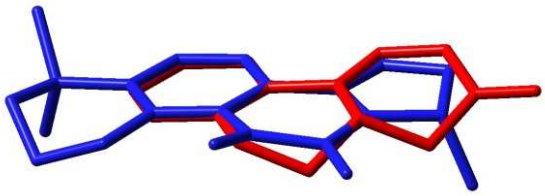

Cryptotanshinone *vs* **I**

Both molecules were found to be quite rigid and characterized by planarity, requisite thought important for the inhibitory activity.[160] In order to highlight analogies between the two structures, the preferred conformations of Cryptotanshinone (blue) and (**I**) (red) were superimposed through rms fitting of the atoms of the BCD tricyclic moiety. The overlap shows that the two compounds match very well.

3.2.3 Chemistry: the benzocinnolinones (P1-18)

3.2.3.1 Synthesis of:

4,4a,5,6-tetrahydrobenzo[h]cinnolin-3(2H)-one derivatives (P1a-c) and of 5,6-dihydrobenzo[h]cinnolin-3(2H)-one derivatives (P2a-c)

The final six-membered ring compounds (**P3-18**), *N*-2 substituted on the pyridazinone ring with different lateral chains, were prepared starting from common key intermediates: the saturated (**P1a-c**) and the unsaturated (**P2a**) derivatives (**Scheme 7**). The starting materials were either commercially available, as α-tetralone (for **P1a** and **P2a**), or they were prepared as shown in **Scheme 8**, such as 5,7-dimethoxy tetralone (for **P1b**) and 6-chloro-tetralone (for **P1c**). These starting materials underwent an aldol condensation with glyoxylic acid in basic conditions to give the unsaturated acids **13a-c**, which were reduced with zinc in acetic acid to afford the 1,2,3,4-tetrahydro-1-oxo-naphtalene-2-acetic acids **14a-c**. The reaction of **14a-c** with hydrazine hydrate in refluxing ethanol led to **P1a-c** in an overall yield of 57% for **P1a**, 60% for **P1b** and 42% for **P1c**. Oxidation of **P1a** to the unsaturated derivative **P2a** was accomplished using sodium *m*-nitrobenzensulfonic acid.

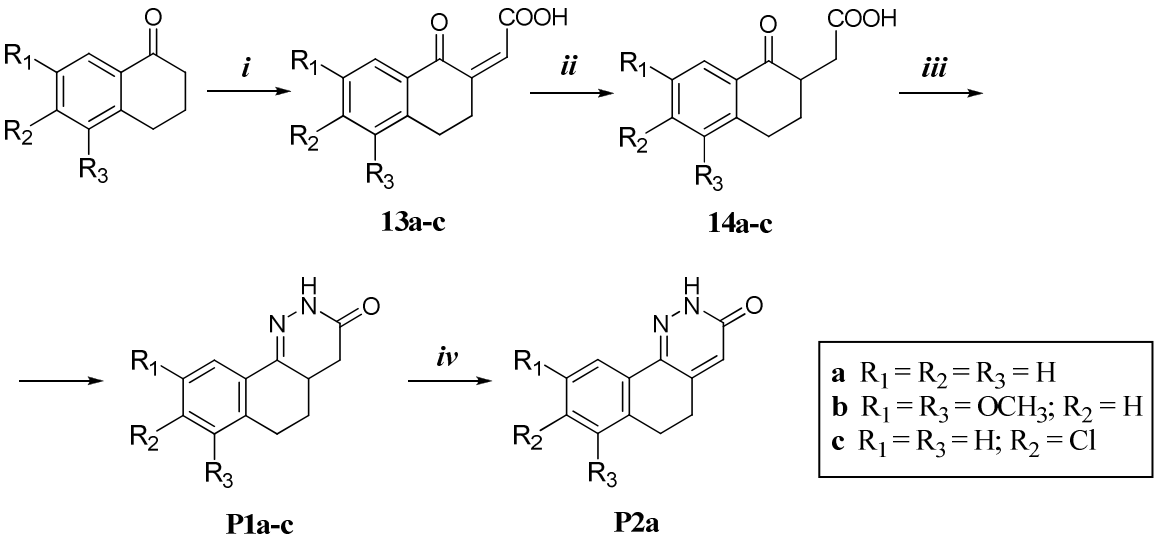

Scheme 7. *Reagent and conditions: i*) glioxylic acid, NaOH, H_2O, EtOH, reflux, 3 h; *ii*) Zn, CH_3COOH, H_2O, reflux, 40 min; *iii*) $NH_2NH_2 \cdot H_2O$, EtOH, reflux, 2 h; *iv*) sodium *m*-nitrobenzensulfonic acid, NaOH, H_2O, reflux, 1 h.

A)

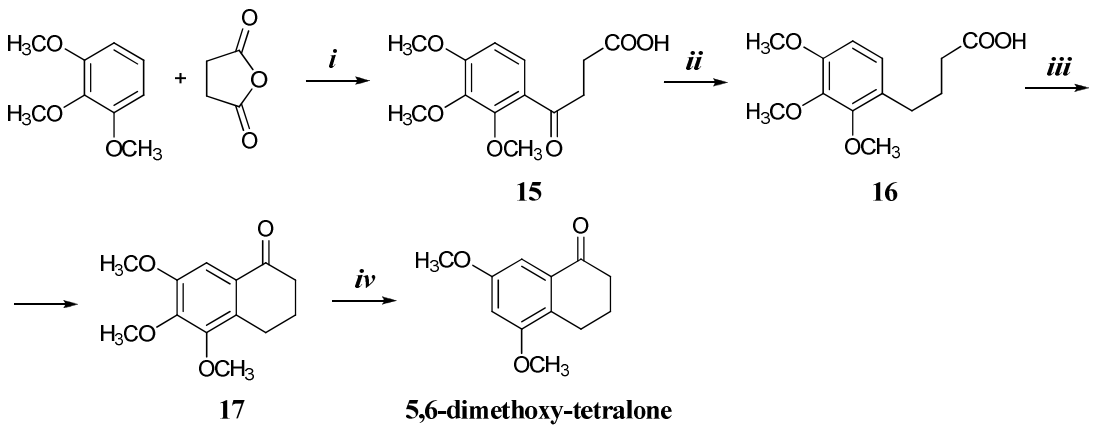

Reagents and conditions: i) $AlCl_3$, CH_2Cl_2, rt, 24 h; *ii*) Zn(Hg), HCl, reflux, 7 h; *iii*) PPA, 100 °C; *iv*) Na, THF, rt, 2.5 h.

B)

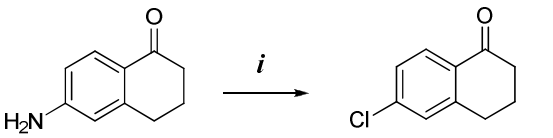

Reagents and conditions: i) $NaNO_2$, HCl, CuCl, t < 5°C, 1.5 h.

Scheme 8. A) Synthesis of the starting material 5,6-dimethoxy-tetralone ; **B)** Synthesis of the starting material 6-chloro-tetralone.

3.2.3.2 Synthesis of the 2-substituted-4,4a,5,6-tetrahydrobenzo[h]cinnolin-3-ones (P3-13)

The previously described key intermediates **P1a-c** and **P2a** were condensed with appropriate side chains to afford the final six-membered ring compounds (**P3-18**) (**Scheme 9** and **10**, respectively). They were divided in saturated (**P3-13**) and unsaturated (**P14-18**) derivatives.

Regarding the saturated derivatives (**P3-13**, **Scheme 9**), they were characterized by lateral chains which bore six different functional groups: ester, carboxylic acid, amide, amine, alkyl and an amino acidic moiety. For the synthesis of the ester derivatives (**P3a-P8a**), the starting

intermediate **P1a** was condensed with bromo esters with different chain lengths in the presence of sodium hydride as a base. The other two starting intermediates, **P1b** and **P1c**, were condensed only with 3-bromo butanoate to obtain compounds **P5b** and **P5c** respectively. Regarding the reaction of compound **P1b**, beyond the obtainment of the saturated ester **P5b**, there was also the formation of the unsaturated derivative **P15b**. A basic hydrolysis of the ester group was then performed on compounds **P4a** and **P5a** and this led to the formation of the corresponding acids **P4aa** and **P5aa**. Finally, **P5aa** was reacted with ethylamine in the presence of the coupling agent HATU and *N*-methyl-morpholine to afford the amido compound **P9a**. The amino derivatives **P10a** was synthesized with a two-step procedure starting from **P1a**. The latter was condensed with 1,4-dibromobutane to give the intermediate **18,** which underwent a nucleophilic substitution with ethylamine for the obtainment of the final compound **P10a**. The alkyl derivatives **P11a** and **P12a** were obtained through the coupling of **P1a** with bromoalkyl chains made up of four and five carbon atoms respectively. Also in these reactions, there was the simultaneous formation of the correspondent unsaturated alkyl derivatives **P17a** and **P18a**. The amino acidic derivative **P13a** was synthesized starting from compound **P1a** which was reacted with 3-chloro-1-propanol to give the alcoholic intermediate **19**. The latter was condensed with *N*-Boc-Phe–OH in the presence of the coupling agent HATU and *N*-methyl-morpholine to obtain compound **20**. Its Boc protecting group was hydrolysed with trifluoroacetic acid to afford the final product **P13a**.

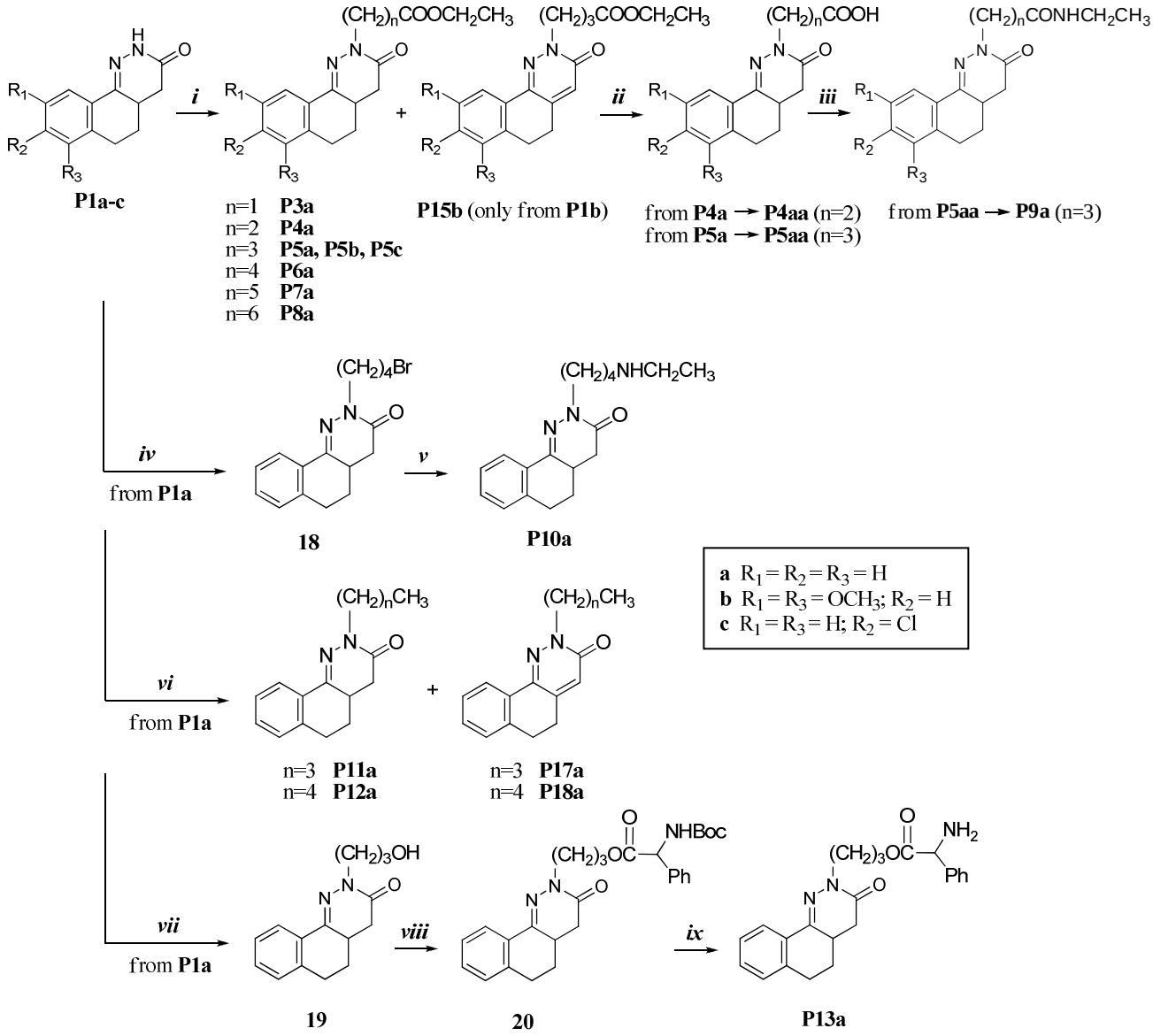

Scheme 9. *Reagent and conditions: i*) $Br(CH_2)_nCOOCH_2CH_3$, dry DMF, NaH, 70 °C, 15 h; *ii*) $NaOH/H_2O$, EtOH, reflux 2 h; *iii*) $EtNH_2$ 70% in water, HATU, *N*-methyl-morpholine, rt, 1.5 h; *iv*) $Br(CH_2)_4Br$, NaH, MW 60°C, 10 min; *v*) $EtNH_2$ 70% in water, Et_3N, DMF, 90-100 °C, 7h; *vi*) $Br(CH_2)_nCH_3$, NaH, DMF; *vii*) $Cl(CH_2)_3OH$, NaH, DMF, 60 °C, 4 h; *viii*) *N*-Boc-Phe-OH, HATU, *N*-methyl-morpholine, rt, 24 h; *ix*) trifluoroacetic acid, CH_2Cl_2.

3.2.3.3 Synthesis of 2-substituted-5,6-dihydrobenzo[h]cinnolin-3-ones (P14-18)

The unsaturated derivatives (**P14-18**) were characterized by side chains containing ester and carboxylic acid functionalities and by alkyl chains of different lengths. As depicted in **Scheme 10**, the ester derivatives (**P14a-P16a**) were obtained by condensing bromoester chains with the starting intermediate **P2a**, using potassium hydroxide as a base and tetra-*n*-butylammonium fluoride (TBAF) as a phase transfer catalyst. The synthesis of the unsaturated ester **P15b** is depicted in **Scheme 9**. The basic hydrolysis of the ester functionality of **P14a** and **P15a** led to formation of the carboxylic acids (**P14aa** and **P15aa**). The synthesis of other two unsaturated derivatives **P17a** and **P18a**, which bear an alkyl chain at N-2, is displayed in **Scheme 9**.

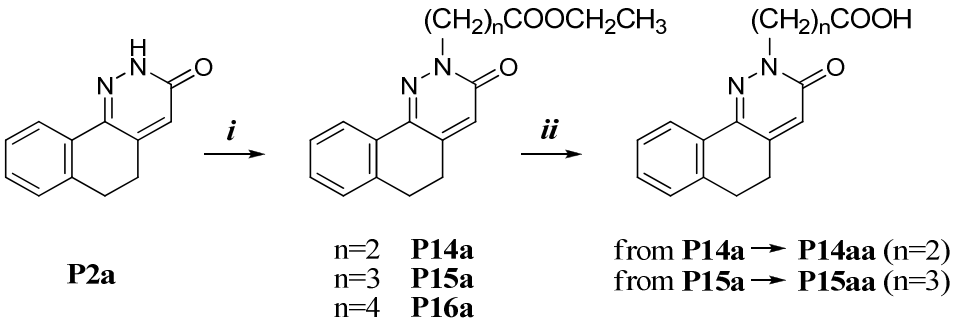

Scheme 10. *Reagent and conditions: i*) $Br(CH_2)_nCOOCH_2CH_3$, KOH, TBAF, toluene, 50 °C; *ii*) $NaOH/H_2O$, EtOH, reflux, 2 h.

3.2.4 Chemistry: the indeno-pyridazinones (P19-22) and the benzocyclohepta-pyridazinones (P23-26)

3.2.4.1 Synthesis of the 4,4a-dihydro-(5H)-indeno-[1,2-c]-pyridazin-3-one derivatives (P19- P22) and of the 2,4,4a,5,6,7-hexahydro-benzo[6,7] cyclohepta[1,2-c]pyridazin-3-one derivatives (P23- P26)

The synthesis of the five- and seven-membered ring compounds was accomplished by following a similar procedure to that employed for the six-membered ring compounds (**Scheme 11**).

Firstly, the key intermediates **P19** (m=1) and **P23** (m=3) were prepared starting from 1-indanone (for m=1) and 1-benzosuberone (for m=3). They underwent an aldol condensation with glyoxylic acid in basic environment to give intermediates **21** (m=1) and **23** (m=3). The following reduction of their double bond with zinc dust in acetic acid led to the intermediates **22** (m=1) and **24** (m=3), which cyclised in the presence of hydrazine monohydrate in ethanol to give the saturated **P19** (m=1) and **P23** (m=3). The unsaturated key intermediates were prepared in two different ways. For the five-membered ring derivatives, the cyclization with hydrazine monohydrate was performed on the unsaturated acid **21** to afford **P20**. For the seven-membered ring derivatives the insertion of the double bond was carried out only after the cyclization with hydrazine on compound **P23** to give the correspondent unsaturated derivative **P24.** This oxidation was performed using sodium *m*-nitrobenzensulfonic acid.

The saturated key interemediates (**P19**, **P23**) were condensed with ethyl bromobutanoate using NaH as a base to obtain the ester derivatives **P21** (m=1) and **P25** (m=3). The unsaturated intermediates (**P20**, **P24**) were reacted with the same bromoester chain but employing different conditions (potassium hydroxide as a base and tetra-*n*-butylammonium fluoride (TBAF) as a phase transfer catalyst) to obtain the final products **P22** (m=1) and **P26** (m=3).

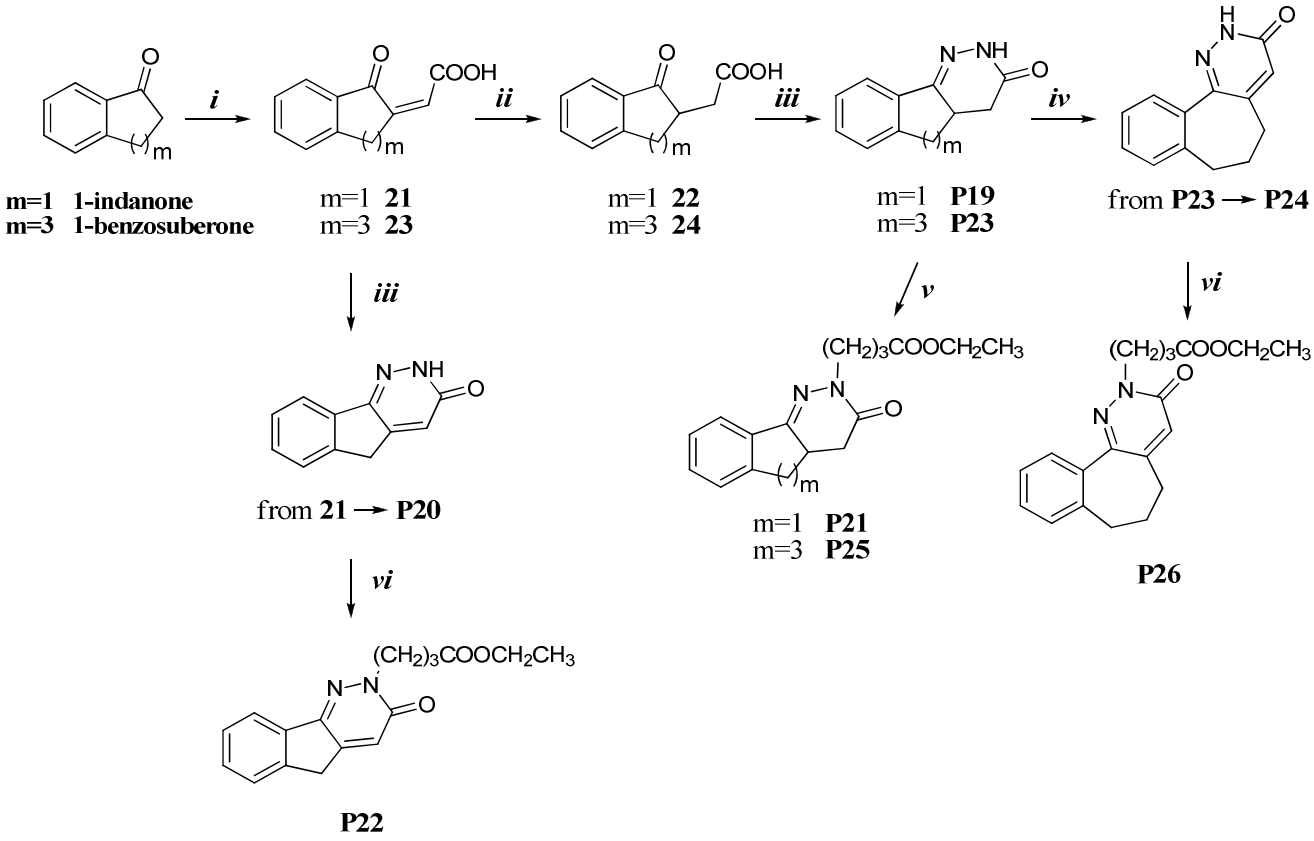

Scheme 11. *Reagents and conditions: i*) glioxylic acid, NaOH, H_2O, CH_3CH_2OH, reflux, 3 h; *ii*) Zn, CH_3COOH, H_2O, reflux, 40 min; *iii*) $NH_2NH_2 \cdot H_2O$, EtOH , reflux, 2 h; *iv*) sodium *m*-nitrobenzensulfonic acid, NaOH, H_2O, reflux, 1 h; *v*) $Br(CH_2)_3COOCH_2CH_3$, dry DMF, NaH, MW 70 °C, 20 min; *vi*) $Br(CH_2)_3COOCH_2CH_3$, KOH, TBAF, toluene, 50 °C.

3.2.5 Pharmacological studies

3.2.5.1 Dual-luciferase assay results

All the synthesized pyridazinones derivatives were evaluated in the dual-luciferase assay[159] system as a preliminary screening (see 'Chapter 3.1.3.2' for the description of this assay and 'Chapter 6' for the experimental procedure). In **Table 9** the inhibitory activities of the tested compounds are displayed. The values are reported as percentage of inhibition at 2 µM.

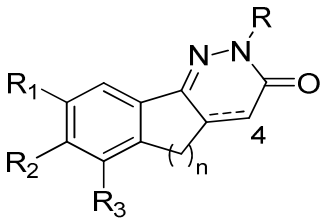

Compound	n	C at position 4	$R_1 = R_3$	R_2	R	% Inhibition[a] (2 μM)
P1a	2	CH_2	H	H	H	< 1
P1b	2	CH_2	OCH_3	H	H	nt
P1c	2	CH_2	H	Cl	H	nt
P2a	2	CH	H	H	H	< 1
P3a	2	CH_2	H	H	$-CH_2COOCH_2CH_3$	3
P4a	2	CH_2	H	H	$-(CH_2)_2COOCH_2CH_3$	30
P4aa	2	CH_2	H	H	$-(CH_2)_2COOH$	< 1
P5a	2	CH_2	H	H	$-(CH_2)_3COOCH_2CH_3$	46
P5aa	2	CH_2	H	H	$-(CH_2)_3COOH$	7
P5b	2	CH_2	OCH_3	H	$-(CH_2)_3COOCH_2CH_3$	23
P5c	2	CH_2	H	Cl	$-(CH_2)_3COOCH_2CH_3$	9
P6a	2	CH_2	H	H	$-(CH_2)_4COOCH_2CH_3$	21
P7a	2	CH_2	H	H	$-(CH_2)_5COOCH_2CH_3$	24
P8a	2	CH_2	H	H	$-(CH_2)_6COOCH_2CH_3$	22
P9a	2	CH_2	H	H	$-(CH_2)_3CONHCH_2CH_3$	16
P10a	2	CH_2	H	H	$-(CH_2)_4NHCH_2CH_3$	3
P11a	2	CH_2	H	H	$-(CH_2)_3CH_3$	< 1
P12a	2	CH_2	H	H	$-(CH_2)_4CH_3$	22
P13a	2	CH_2	H	H	$-(CH_2)_3OCOCH(CH_2Ph)NH_2$	< 1
P14a	2	CH	H	H	$-(CH_2)_2COOCH_2CH_3$	< 1
P14aa	2	CH	H	H	$-(CH_2)_2COOH$	nt
P15a	2	CH	H	H	$-(CH_2)_3COOCH_2CH_3$	< 1
P15aa	2	CH	H	H	$-(CH_2)_3COOH$	< 1
P15b	2	CH	OCH_3	H	$-(CH_2)_3COOCH_2CH_3$	29
P16a	2	CH	H	H	$-(CH_2)_4COOCH_2CH_3$	29
P17a	2	CH	H	H	$-(CH_2)_3CH_3$	1.31
P18a	2	CH	H	H	$-(CH_2)_4CH_3$	< 1
P19	1	CH_2	H	H	H	37
P20	1	CH	H	H	H	37
P21	1	CH_2	H	H	$-(CH_2)_3COOCH_2CH_3$	28

Compound	n	C at position 4	$R_1 = R_3$	R_2	R	% Inhibition[a] (2 μM)
P22	1	CH	H	H	$-(CH_2)_3COOCH_2CH_3$	< 1
P23	3	CH_2	H	H	H	30
P24	3	CH	H	H	H	< 1
P25	3	CH_2	H	H	$-(CH_2)_3COOCH_2CH_3$	< 1
P26	3	CH	H	H	$-(CH_2)_3COOCH_2CH_3$	15
Cryptotanshinone						25

nt: not tested

[a] Inhibitory activity against STAT3 was evaluated by a dual-luciferase assay system in human colorectal carcinoma HCT-116 cells after 24 h treatment with the tested compounds. The values are the means of 3 experiments. The maximum deviation from the mean was less than 10%.

Table 9. Percentage inhibition evaluated by dual-luciferase assay in human colorectal carcinoma HCT-116 cells at 2 μM concentration.

According to the obtained data, several compounds showed an interesting percentage inhibition, comparable of higher than the reference compound Cryptotanshinone. In particular, **P5a**, **P19** and **P20** were the most active compounds, with an inhibitory activity of 46%, 37% and 37% respectively.

Since a positive result in the dual-luciferase assay reflects the ability of the compound to block STAT3 activity at any level of its signaling pathway (**Figure 18**), a deeper investigation on the mechanism of action of the compounds was necessary. For this reason all of them were subjected to further biological studies.

3.2.5.2 AlphaScreen-based assay results

All the compounds, with particular attention to **P5a**, **P19** and **P20**, which showed the most interesting inhibitory activities, were tested with the AlphaScreen-based assay[172] (see 'Chapter 3.1.3.4' for the description of this assay and 'Chapter 6' for the experimental procedure) and the results (**Table 10**) were expressed as a measure of their ability to antagonize the interaction between STAT3-SH2 domain and its target *p*Tyr-containing peptide. In particular, besides STAT3, other SH2-containing proteins, such as STAT1 and

Gbr2, having a high degree of sequence homology to STAT3 (78% and 65%, respectively), were tested.

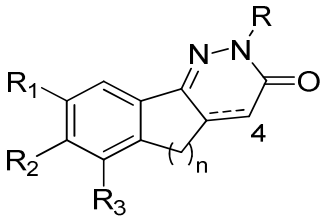

Compound	n	C at position 4	$R_1 = R_2$	R_3	R	% Inhibition (50 μM)		
						STAT3	STAT1	Grb2[a]
P1a	2	CH_2	H	H	H	< 1	< 1	< 1
P1b	2	CH_2	OCH_3	H	H	< 1	13.3	12.3
P1c	2	CH_2	H	Cl	H	< 1	13.9	5.0
P2a	2	CH	H	H	H	7.5	6.1	2.9
P3a	2	CH_2	H	H	$-CH_2COOCH_2CH_3$	< 1	7.2	2.9
P4a	2	CH_2	H	H	$-(CH_2)_2COOCH_2CH_3$	19.1	0.7	< 1
P4aa	2	CH_2	H	H	$-(CH_2)_2COOH$	< 1	< 1	< 1
P5a	2	CH_2	H	H	$-(CH_2)_3COOCH_2CH_3$	7.3	< 1	< 1
P5aa	2	CH_2	H	H	$-(CH_2)_3COOH$	5.6	4.5	< 1
P5b	2	CH_2	OCH_3	H	$-(CH_2)_3COOCH_2CH_3$	< 1	5.8	< 1
P5c	2	CH_2	H	Cl	$-(CH_2)_3COOCH_2CH_3$	< 1	9.1	2.0
P6a	2	CH_2	H	H	$-(CH_2)_4COOCH_2CH_3$	11.4	3.5	4.3
P7a	2	CH_2	H	H	$-(CH_2)_5COOCH_2CH_3$	7.7	6.7	5.5
P8a	2	CH_2	H	H	$-(CH_2)_6COOCH_2CH_3$	< 1	1.4	5.6
P9a	2	CH_2	H	H	$-(CH_2)_3CONHCH_2CH_3$	< 1	4.9	< 1
P10a	2	CH_2	H	H	$-(CH_2)_4NHCH_2CH_3$	< 1	< 1	< 1
P11a	2	CH_2	H	H	$-(CH_2)_3CH_3$	< 1	< 1	< 1
P12a	2	CH_2	H	H	$-(CH_2)_4CH_3$	18.9	< 1	< 1
P13a	2	CH_2	H	H	$-(CH_2)_3OCOCH(CH2Ph)NH_2$	< 1	15.9	7.5
P14a	2	CH	H	H	$-(CH_2)_2COOCH_2CH_3$	8.1	6.0	1.5
P14aa	2	CH	H	H	$-(CH_2)_2COOH$	nt	nt	nt
P15a	2	CH	H	H	$-(CH_2)_3COOCH_2CH_3$	10.4	5.4	6.4
P15aa	2	CH	H	H	$-(CH_2)_3COOH$	12.5	5.5	< 1
P15b	2	CH	OCH_3	H	$-(CH_2)_3COOCH_2CH_3$	< 1	< 1	< 1
P16a	2	CH	H	H	$-(CH_2)_4COOCH_2CH_3$	2.7	2.7	< 1

Compound	n	C at position 4	$R_1 = R_2$	R_3	R	% Inhibition (50 μM)		
						STAT3	STAT1	Grb2[a]
P17a	2	CH	H	H	$-(CH_2)_3CH_3$	4.2	7.1	2.2
P18a	2	CH	H	H	$-(CH_2)_4CH_3$	6.2	< 1	< 1
P19	1	CH_2	H	H	H	< 1	12.9	3.2
P20	1	CH	H	H	H	< 1	9.8	5.2
P21	1	CH_2	H	H	$-(CH_2)_3COOCH_2CH_3$	1.3	13.3	6
P22	1	CH	H	H	$-(CH_2)_3COOCH_2CH_3$	< 1	9.5	< 1
P23	3	CH_2	H	H	H	5.8	5.8	2.1
P24	3	CH	H	H	H	nt	nt	nt
P25	3	CH_2	H	H	$-(CH_2)_3COOCH_2CH_3$	< 1	7.2	5.4
P26	3	CH	H	H	$-(CH_2)_3COOCH_2CH_3$	< 1	8.2	1.0
Cryptotanshinone						11.2	40.3	34.7

nt: not tested

[a] **Grb2**: Growth factor receptor-bound protein 2

Table 10. Percentage inhibition of STAT3, STAT1 and Grb2 as determined in the AlphaScreen assay by **P1-26** compounds.

None of the molecules was able to antagonize the interaction between the SH2-STAT3 domain and its target *p*Tyr-containing peptide. However, a binding of the compounds with different portions of the SH2 domain or with any other part of STAT3 protein is still probable. Further investigations (*i.e.* Western blotting, ELISA, etc.) will be carried out to assess this possibility and to give an explanation of the positive results we obtained in the dual-luciferase assay.

3.2.5.3 Anti-proliferative assay

In order to evaluate the anti-proliferative activity of the synthesized pyridazinone derivatives, cell proliferation assays were performed by NCI (Bethesda, USA) under the Developmental Therapeutic 20 Program (DTP) to determine its effect on tumor cells growth[173] ('Chapter 3.1.3.6' for the description of this assay and 'Chapter 6' for the experimental procedure). The

compounds were tested at a concentration of 10 μM**.** All the derivatives turned out to be mostly inactive. For instance, the table reported in **Appendix II** displays the data for compounds which showed slight inhibition in some cell lines: *e.g*. compound **P1a** had a growth inhibitory activity of 36% on EKVX cell line (non-small-cell lung carcinoma), compound **P5a** had a discrete inhibition on SR cell line (leukemia cell line) and compound **P19** a 19% of growth inhibition on UO-31 cell line (renal cancer cell line).

3.2.6 Conclusions

In the preliminary dual-luciferase assay screening, the synthesized pyridazinone derivatives exerted promising percentage inhibition of STAT3 activity. In order to clarify these interesting results, and to understand the mechanism of action of the compounds, a deeper biological investigation was carried out. The molecules were firstly tested in the *in vitro* AlphaScreen-based assay, but none antagonized the interaction between the SH2-STAT3 domain and its target *p*Tyr-containing peptide. However, binding of the compounds with different portions of the SH2 domain, or with any other part of STAT3 protein, is still probable. The molecules were also submitted to an anti-proliferative assay but did not exert any remarkable effect on cell proliferation. Therefore, the dual-luciferase assay was repeated on the compounds with the most interesting activities, considering a wide range of concentrations (from 1 to 50 μM, data not shown). The obtained data revealed a non-dose dependent profile of inhibitory activity of the tested compounds and thus, we could assume that the noteworthy percentage inhibition at 2 μM previously obtained in the dual-luciferase assay was not significant for the STAT3 inhibition.

3.3 The "chimera" compounds

3.3.1 Project description

In parallel with the execution of the AlphaScreen-based assay on the previously synthesized compounds (the 1,2,5-oxadiazoles and the pyridazinones), a different approach for the design of new derivatives was carried out. The aim was to combine the structural characteristics of the different series of molecules, explored in this project, which had showed an ability to inhibit STAT3 activity in the dual-luciferase assay. Therefore, the following structures were considered:

- the oxadiazole ureido derivative **AVS 0288** (Chapter 3.1.1)

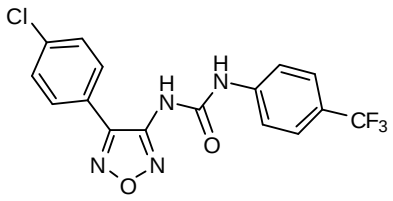

- the natural compound **Cryptotanshinone** (Chapter 3.2.1)

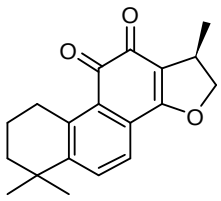

- **P5a**, the pyridazinone compound with the best inhibitory activity among all the previously synthesized pyridazinone derivatives (% inhibition at 2 µM = 46%). (Chapter 3.2.5.1)

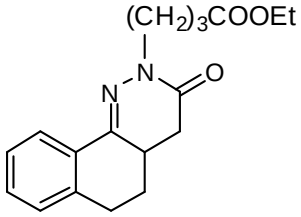

Conformational studies on the selected compounds were performed and the preferred conformations turned out to have a planar arrangement. This feature was supposed to be an important requisite for STAT3 inhibitory activity, as it was observed in our previous studies.[160] The superimposition of their conformations led to the design of two new compounds: **C2** and **C4**. The first is characterized by the benzocinnolinone moiety of **P5a**, which resembled the tricyclic system of Cryptotanshinone, and a lateral chain, which mimicked the one on **AVS-0288**. Moreover this new structure can be considered a cyclic analogue of **AVS-0288**, as it can be seen overlapping the oxadiazole ring of **AVS-0288** with the pyridazinone ring of the new planned compound (Chapter 3.3.2).

On the contrary, the chimera **C4** is constituted by a pyridazinone ring, substituted at position 3 and 4 with the same groups which are present in **AVS-0288**: a *p*-chloro-phenyl group and a *p*-trifluoromethylphenyl urea. This structure clearly resembled **AVS-0288** if the pyridazinone ring is overlapped to the oxadiazole ring and moreover, it can be considered analogues of **C2**. However, to date, only compound **C3**, which has a phenyl ring instead of a p-chloro-phenyl ring as a substituent, has been synthesized, whereas the synthesis of compound **C4** is still in progress.

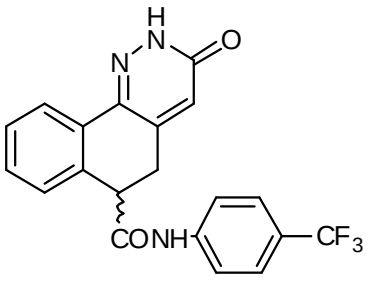

C2

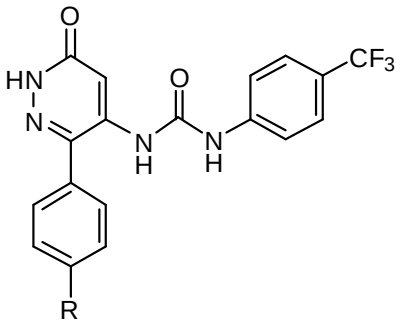

C3 R = H
C4 R = Cl

3.3.2 Molecular modeling

A modeling study of **Cryptotanshinone**, a potent STAT3 inhibitor,[154] and the previously synthesized pyridazinone compound **P5a**, was performed using the Gaussian09 program package.[181] All the calculations were carried out at the b3lyp/6-311+G(d,p) level. The solvent effects were determined by single-point calculations, at the same level as above, on the gas-phase optimized geometries, using a self-consistent reaction field (SCRF) method, based on the polarizable continuum model (PCM). Particular attention focused on the tricyclic portion

of the two molecules, and in detail, on the flexibility of the **A** and **C** rings in the case of **Cryptotanshinone**, and on the possible inversion of the **C** ring in the case of **P5a**. Both molecules were found to be quite rigid and characterized by planarity.

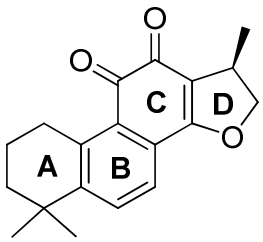

Cryptotanshinone

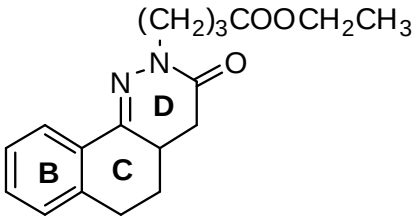

P5a

In **Figure 27** are shown the located conformations of **Cryptotanshinone** and **P5a** together with their corresponding energy values in water.

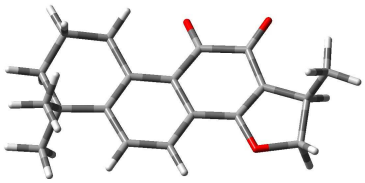

Cryptotanshinone A

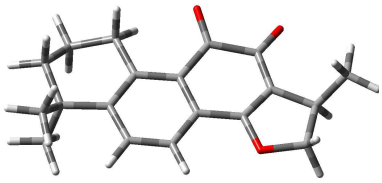

CryptotanshinoneB
0.14 kcal/mol

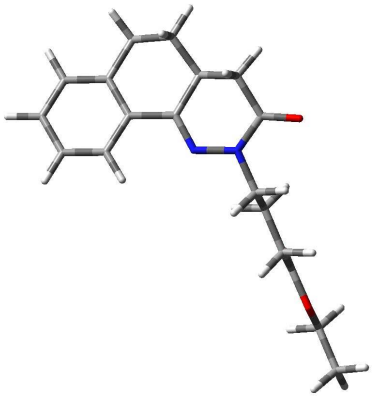

P5a A
0.00 kcal/mol

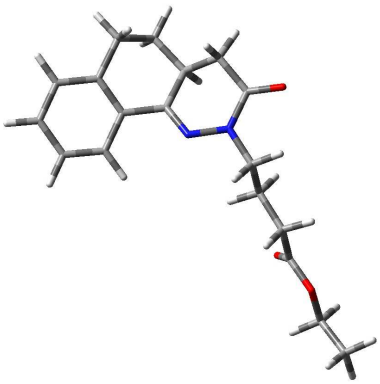

P5a B
2.59 kcal/mol

Figure 27. 3D plots of the located conformations of **Cryptotanshinone** and **P5a** together with their corresponding energy values in water.

In a recent paper,[160] the conformational space of the oxadiazole ureido **AVS-0288** was completely explored. All its degrees of conformational freedom were considered with particular attention to the different arrangements of the ureido moiety (*trans*/*trans*, **TT**; *trans*/*cis*, **TC**; *cis*/*trans*, **CT**; and *cis*/*cis*, **CC**). In water the **TT** arrangement resulted largely preferred (92.2%).

On the basis of this data, the possible analogies between the three structures of the selected compounds were investigated. In **Figure 28a** the preferred conformations of the three compounds are reported and the related portions are highlighted in green. These conformation were superimposed and the corresponding overlay is shown in **Figure 28b**.

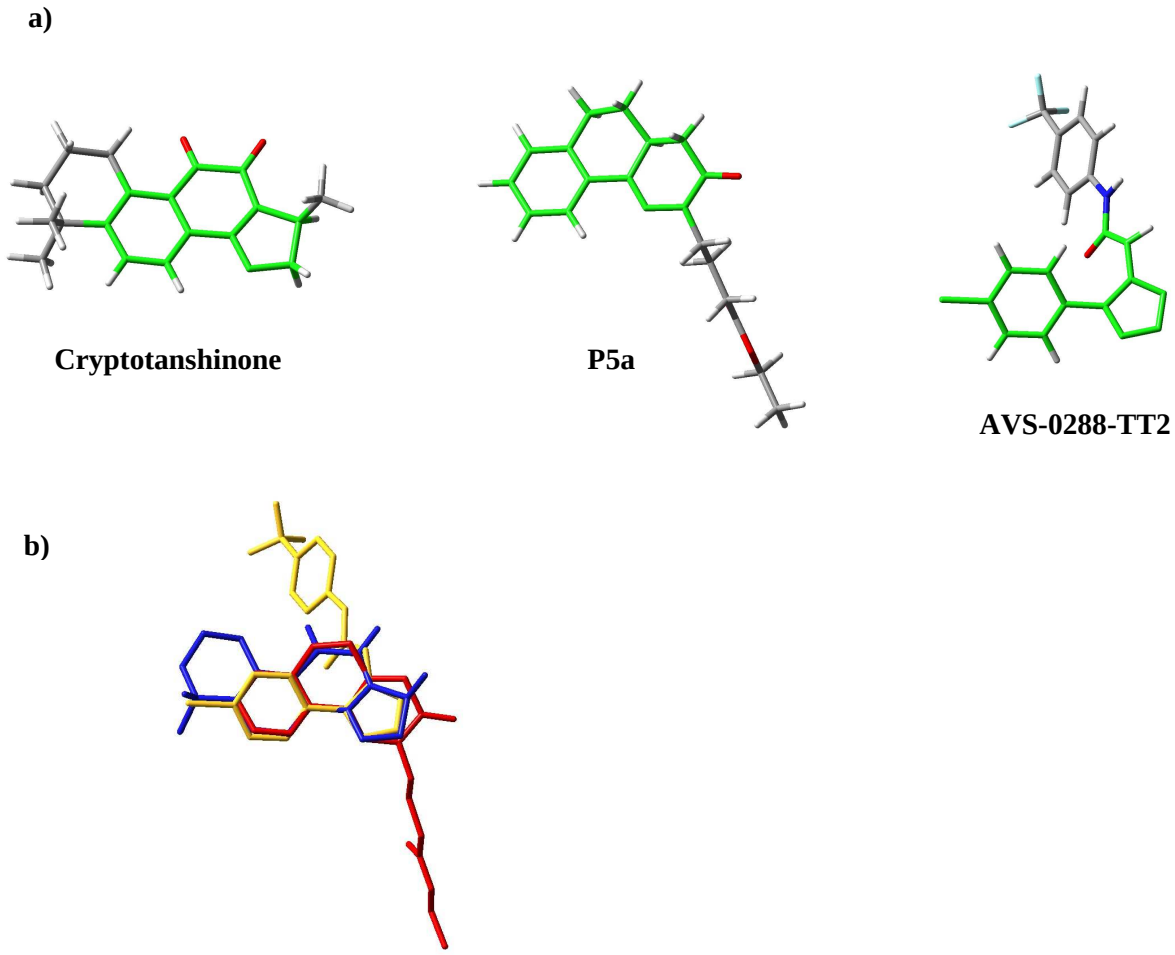

Figure 28. a) Preferred conformations of **Cryptotanshinone**, **P5a** and **AVS-0288** with the tricyclic moiety highlighted in green; **b**) Overlay of the preferred conformations of **Cryptotanshinone** (blue), **P5a** (red), and **AVS-0288** (yellow) through RMS fitting of the tricyclic moiety.

Looking at the evident similarity between the three compounds, the chimera **C2** was designed and modeled. Finally, the preferred conformation of **C2** was overlapped to the conformation **TT2** of **AVS-0288**. As can be seen in **Figure 29**, there is a nice overlap of the two structures: in particular the trifluoromethylphenyl groups occupy the same spatial region, such as the amidic groups and the oxadiazole and pyridazinone rings, suggesting a good analogy between compounds.

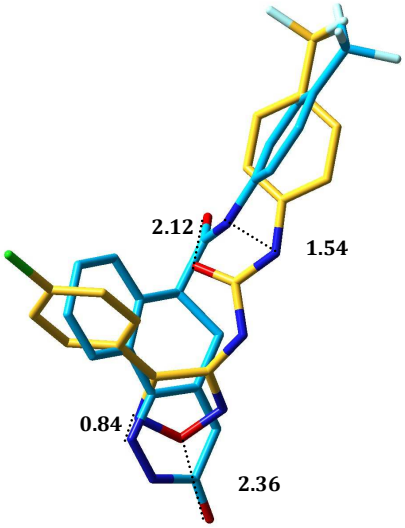

Figure 29. Overlay of the preferred conformation of compound **C2** (light blue), and **TT2** conformation of **AVS-0288** (yellow) with the distances between the heteroatoms of the two molecules shown through dotted line and the corresponding values in Å.

Also the preferred conformation of the chimera **C3** was overlapped to the conformation **TT2** of **AVS-0288** (**Figure 30**), highlighting the good analogy between the two molecules.

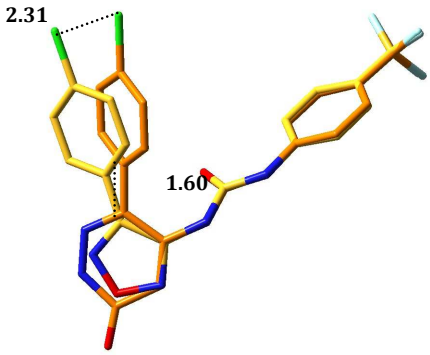

Figure 30. Overlay of the preferred conformation of compound **C3** (orange), and **TT2** conformation of **AVS-0288** (yellow) with the distances between the heteroatoms of the two molecules shown through dotted line and the corresponding values in Å.

Finally, the overlap of **Cryptotanshinone**, **P5a** and **C3** was performed (**Figure 31**).

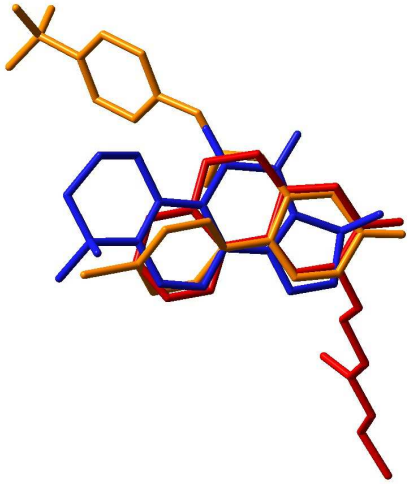

Figure 31. Overlay of the preferred conformations of **Cryptotanshinone** (blue), **P5a** (red), and **C3** (orange) through RMS fitting of the tricyclic moiety.

3.3.3 Chemistry

3.3.3.1 Synthesis of 3-oxo-N-(4-(trifluoromethyl)phenyl)-2,3,4,4a,5,6-hexahydrobenzo [h]cinnoline-6-carboxamides (C1a, b) and 3-oxo-N-(4-(trifluoromethyl)phenyl)-2,3,5,6-tetrahydrobenzo[h]cinnoline-6-carboxamide (C2)

The synthesis of compounds **C1a, b** and **C2** is shown in **Scheme 12**. The commercially available α-phenylglutaric anhydride was cyclised with polyphosphoric acid to obtain the racemic compound **25**. The carboxylic group of **25** was condensed with 4-(trifluoromethyl)aniline to obtain the amide **26**. This reaction was performed with the coupling agent TBTU (*O*-(Benzotriazol-1-yl)-*N*,*N*,*N*',*N*'-tetramethyluronium tetrafluoroborate) in the presence of *N*-methylmorpholine (pH = 7) at room temperature for 24 h. The aldol condensation between compound **26** and glyoxylic acid, followed by dehydration, led to the α/β-unsaturated acid **27**. The reduction of the double bond of **7**, by means of zinc in acetic acid gave compound **28** as a mixture of two couples of diastereoisomers. After the cyclization of **28** with hydrazine monohydrate in ethanol at reflux to obtain **C1a-b**, the separation of the obtained couple of diasteroisomers was performed by means of flash chromatography. Their relative configuration was assigned with the support of

NMR studies (NOESY experiment). The introduction of a double bond in the pyridazinone ring of compounds **C1a** and **C1b** was carried out with sodium 3-nitrobenzenesulfonate in alkaline acqueous solution and led to the final racemic compound **C2**. Only one of the two diastereoisomers (**C1a**) led to compound **C2** while the other one **C1b** didn't react. This is probably due to the fact that the hydrogen atoms of the two stereogenic centers have to be located in axial position (*S,S* or *R,R*) to allow the dehydrogenation, as shown in **Figure 32**.

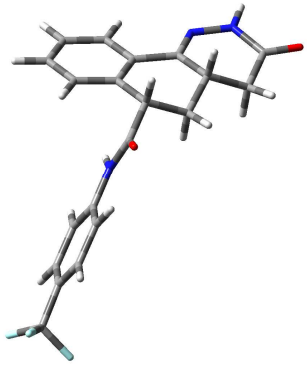

Figure 32. Structure of compound **C1a**

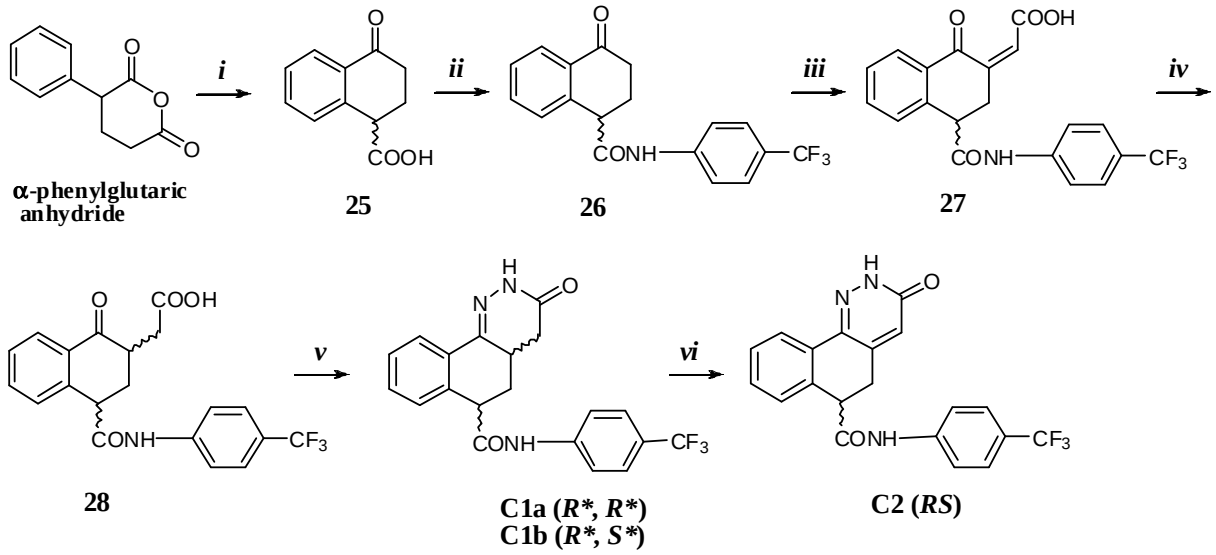

Scheme 12. *Reagents and conditions:* ***i***) PPA, 100/110 °C, 30 min; ***ii***) 4-(trifluoromethyl)aniline, CH_2Cl_2, TBTU, N-methylmorpholine up to pH=7, rt, 24 h; ***iii***) CHO-COOH, NaOH, H_2O, CH_3CH_2OH, rt, 1 h; ***iv***) Zn, CH_3COOH, H_2O, rt, 20 min; ***v***) NH_2NH_2 H_2O, CH_3CH_2OH, reflux, 2 h; (f) sodium 3-nitrobenzenesulfonate, NaOH, H_2O, reflux, 30 min.

3.3.3.2 Synthesis of 1-(6-oxo-3-phenyl-1,6-dihydropyridazin-4yl)-3-(4-(trifluoromethyl) phenyl)urea (C3)

The general synthetic strategy followed for the preparation of the 5-substituted pyridazinone **C3** is outlined in **Scheme 13**. The commercially available starting material 3-benzoyl propionic acid underwent a hydroxymethylation with formaldehyde and potassium carbonate in water and the subsequent cyclization in acidic conditions led to the β-benzoyl-γ-butyrolactone **29**.[183] The treatment of **29** with a large excess of hydrazine hydrate gave 5-hydroxymethyl-6-phenyl-4,5-dihydro-3(2H)-pyridazinone **30,** which was firstly protected at the alcoholic function with acetic anhydride and then dehydrogenated to the correspondent aromatic derivative **32** with activated manganese dioxide. The removal of the protecting group of **32**, followed by oxidation of the alcohol with activated manganese dioxide led to intermediate **34**. This underwent a further oxidation to carboxylic acid **35** by means of silver oxide.[184] The conversion of **35** into the urea **C3** was accomplished in moderate yield (20%) by Curtius rearrangement with DPPA in toluene, then followed by addition of trifluoromethylphenyl aniline.

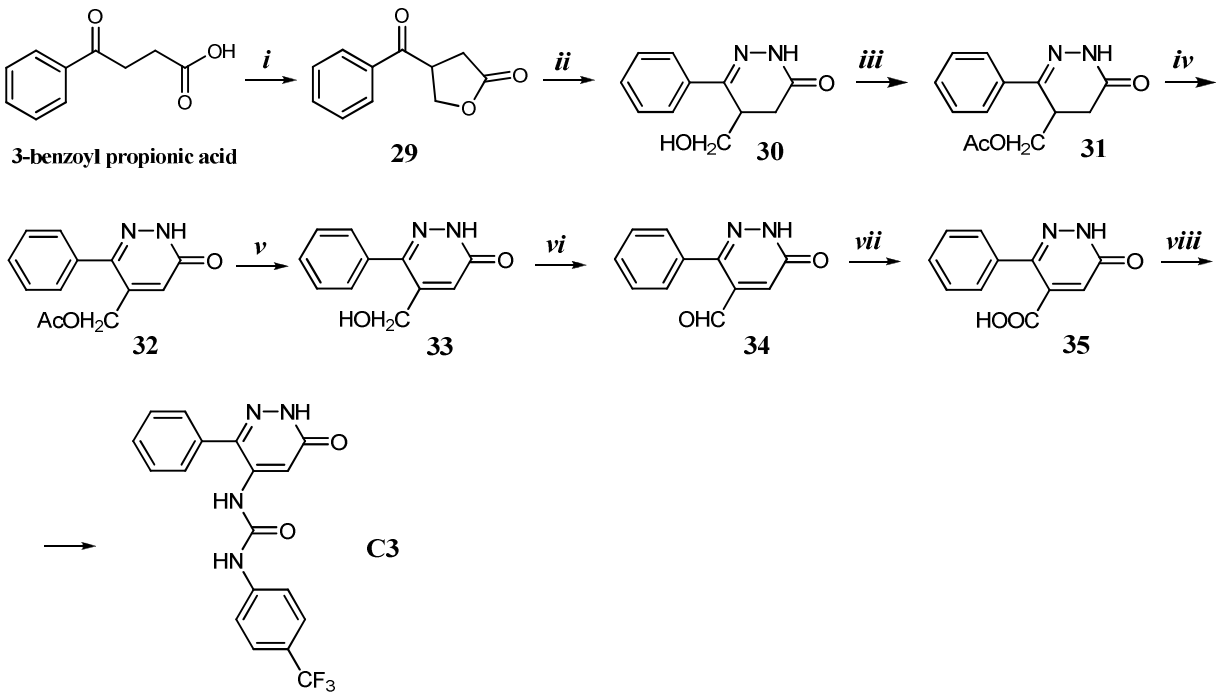

Scheme 13. *Reagents and conditions:* ***i***) 1. HCHO 37%, NaOH 2N, HCl conc, rt; ***ii***) NH_2NH_2, CH_3CH_2OH, reflux; ***iii***) Ac_2O, Py, rt; ***iv***) MnO_2, $CHCl_3$, reflux; ***v***) HCl 2N, reflux; ***vi***) MnO_2, THF, rt; ***vii***) Ag_2O; ***viii***) *a*. DPPA, Et_3N, toluene, 80 °C; *b*. *p*-trifluoromethyl aniline, THF, reflux

3.3.4 Pharmacological studies

3.3.4.1 Dual-luciferase assay results

The chimera compounds **C1a,b** and **C2** were evaluated in the dual-luciferase assay[159] system as a preliminary screening (see 'Chapter 3.1.3.2' for the description of this assay and 'Chapter 6' for the experimental procedure). In **Table 11** the inhibitory activities of the tested compounds are displayed. The values are reported as percentage of inhibition evaluated at 10 µM and 50 µM. The inhibitory activity of the tested molecules is compared with the reference compounds **Cryptotanshinone** and **AVS-0288**.

Compound	% Inhibition[a] (2 μM)	
	10 μM	**50 μM**
C1a	7	67
C1b	14	< 1
C2	13	82
Cryptotanshinone	78	85
AVS-0288	70	75

[a] The values are the means of 3 experiments. The maximum deviation from the mean was less than 10%.

Table 11. Percentage inhibition of the chimera compounds (**C1a, b** and **C2**) evaluated with the dual-luciferase assay system.

According to the obtained data, compound **C2** is the most active compound: the results indicate that at the concentration of 50 μM it shows equivalent activity to the references. Despite the inhibitory values of derivative **C1a** is lower than **C2**, it still has an interesting inhibitory profile. Both molecules **C1a** and **C2** show a dose-dependent inhibition activity.

3.3.4.2 AlphaScreen-based assay results

To date only the chimeras **C1a**, **b** and **C2** have been evaluated in biological assays. In particular, they were submitted to the *in vitro* AlphaScreen-based assay.[172] ('Chapter 3.1.3.4' for the description of this assay and 'Chapter 6' for the experimental procedure). In **Table 12** the results are presented as percentages of inhibition of the interaction between STAT3-SH2 domain and its target *p*Tyr-containing peptide. In particular, besides STAT3, other SH2-containing proteins, such as STAT1 and Gbr2, having a high degree of sequence homology to STAT3 (78% and 65%, respectively), were tested.

Compound	% Inhibition (50 μM)		
	STAT3	STAT1	Grb2[a]
C1a	< 1	9.1	< 1
C1b	< 1	6.8	< 1
C2	< 1	10.3	< 1

[a] **Grb2**: Growth factor receptor-bound protein 2

Table 12. % inhibition of STAT3, STAT1 and Grb2 as determined by AlphaScreen assay by **C1a**, **C1b** and **C2**.

According to these results, all these molecules didn't antagonize *p*Tyr-SH2 interaction. Anyway, a binding of the compounds with different portions of the SH2 domain or with any other part of STAT3 protein is still probable.

3.3.5 Future perspectives

Regarding the racemic chimera **C2**, the separation of the two enantiomers will performed by chiral chromatography. Moreover, the synthesis of the chimera **C4** will be completed. All the synthesized compounds will be submitted to a complete biological study, starting from the dual-luciferase assay in order to check their inhibitory properties on STAT3 pathway.

3.4 The oxidized compounds

3.4.1 Project description

This section of the project was focused on the natural compound **Cryptotanshinone**[154] with the aim to design and the synthesize analogues more directly related to it. Preliminary modeling studies, performed by our research group, had suggested the importance of the *ortho*-quinone moiety of **Cryptotanshinone** in the interaction with STAT3. To support this hypothesis, commercially available compounds (**ST1-6**, **Table 13**) were selected on the basis of their similarity with **Cryptotanshinone**, and tested by the AlphaScreen-based assay.[172] This allowed the evaluation of the binding of small molecules to a specific portion of STAT3-SH2 domain, and the results obtained confirmed the positive influence of the *ortho*-quinone moiety in the interaction with STAT3. According to the data (**Table 13**), the *1,2-naftoquinone* was the most active compound among the tested ones; the introduction of bulky substituents on this molecule reduced its activity. Moreover, despite the activity of derivatives **ST2-ST5** being lower than **ST1**, they still had interesting inhibitory values. Only **ST6**, *dibenzothiophene sulfone,* characterized by a five-membered central core with a sulfone moiety, was inactive.

Structure	Chemical name	% inhibition (50 μM)		
		STAT3	STAT1	Grb2[a]
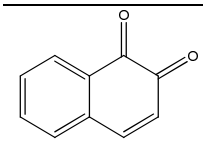 ST1	*1,2-naphtoquinone*	81,5	99,0	52,2
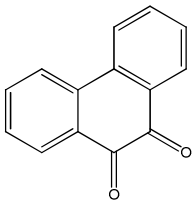 ST2	*phenantrene quinone*	54,5	31,6	40,9
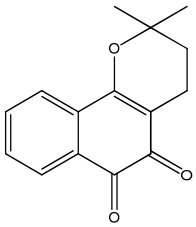 ST3	*β-lapachone*	22,6	20,2	17,2
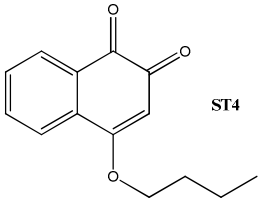 ST4	*4-butoxy-1,2-naphtoquinone*	21,8	26,9	28,0
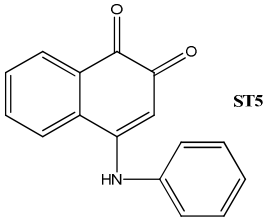 ST5	*phenylanilino-1,2-naphtoquinone*	52,5	42,8	48,7
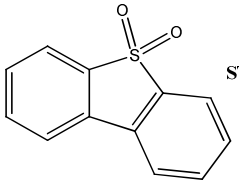 ST6	*dibenzothiophene sulfone*	-14,0	0,3	-9,4

[a] **Grb2**: Growth factor receptor-bound protein 2

Table 13. % inhibition of STAT3, STAT1 and Grb2 of compounds **ST1-ST6** as determined by AlphaScreen assay.

In light of these results, a series of compounds, derived from a simplification of the Cryptotanshinone structure, were synthesized, characterised by the presence of only two rings and by the *ortho*-quinone moiety (**Figure 33**).

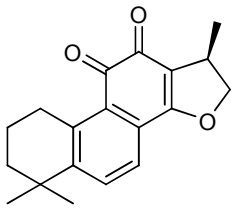

Cryptotanshinone

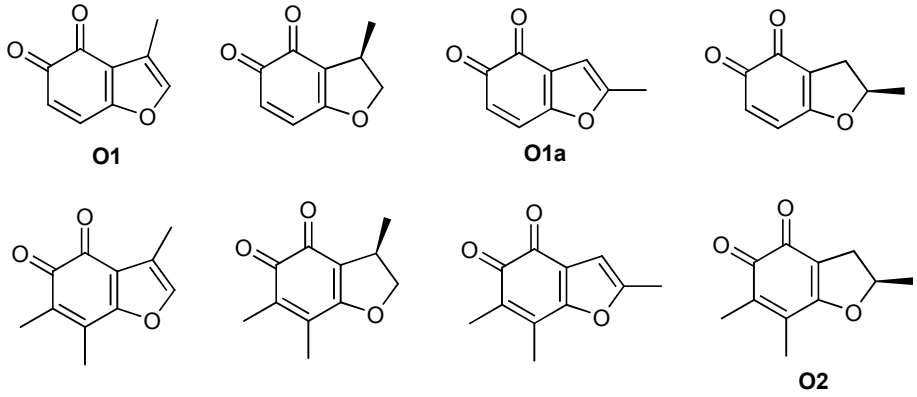

Figure 33. Designed simplified analogues of **Cryptotanshinone**.

Among the planned derivatives, compounds **O1** and **O1a**, along with **O2**, were already known in the literature.[185] However, upon synthesis product **O1** was found to be unstable at room temperature,[186] whilst **O1a** could not be isolated, due to its volatility and high reactivity.[187] No such problems arose with the synthesis of **O2**. Since product **O1** is most directly related to Cryptotanshinone, molecular docking studies have been performed on product **O2** (Chapter 3.4.3) to predict its potential binding to the STAT3-SH2 domain.

3.4.2 Molecular docking studies

Molecular modeling studies were carried out in order to verify if the synthesized products (*R*)-**O2**, (*S*)-**O2**, and the intermediate (*R*)-**41**, (*S*)-**41** (as a control) (**Figure 34**), could interact with

STAT3. Molecular docking calculations were performed to evaluate the binding affinity of these compounds with the STAT3-SH2 domain and to compare the results to those obtained in the previous computational studies. STAT3 structure, co-crystallized with a DNA fragment, was downloaded from the Protein Data Bank[188] (PDB ID 1BG1[189]) and was dimerized applying the transformation matrix as reported in the PDB file. The model was completed adding the hydrogens in two steps: 1) to STAT3, applying the algorithm for proteins; 2) to DNA, applying the algorithm for nucleic acids. In both cases, we used the features included in the VEGA ZZ package.[190] Atom charges (Gasteiger – Marsili method[191]) and potentials (CHARMM 22 for proteins[192] and nucleic acids [193]) were assigned to the obtained structure. Finally, the model was optimized through a conjugate gradients minimization (30.000 steps) in order to reduce the high-energy sterical interactions. In order to preserve the experimental data, atom constraints were applied to protein and DNA backbones. This step was carried out by NAMD 2.8[194] integrated in the VEGA ZZ graphic environment. In order to perform the molecular docking studies, all considered compounds were built by ISIS/Draw and automatically converted to 3D by VEGA ZZ. For chiral molecules that in the considered set include only one chiral center, both stereoisomers were built and docked as two different chemical entities.

Finally, a semi-empirical calculation was performed to optimize the structures (Mopac 2009,[195] PM6 PRECISE keywords) which were included in a SQLite database, in order to convert them in a suitable file format readable by GriDock, the in-home made structure-based virtual screening system. This software, especially designed to run on HPC and GRID hardware, is a front-end to the well knownAutoDock 4 package.[196] More in detail, GriDock is able to extract each molecule from a database and to perform a docking calculation running AutoDock 4. Before runningGriDock, the grid maps required to evaluate docking score were calculated, selecting the atoms included in a sphere of 12 Å radius centred on the phosphorylated Tyr-705 (PTR-705 in the PDB file), which is known to play a pivotal role in the STAT3 dimerization and activation. This phase was carried out by AutoGrid 4 interfaced to VEGA ZZ. All considered potential STAT3 ligands were docked by GriDock/AutoDock using the genetic-algorithm search and generating 20 possible solutions for each molecule. Previous computational studies showed that at least two binding pockets are present in the SH2 domain: the phosphotyrosine binding site (*PTR-pocket*) involved in the dimerization

process and Cryptotanshinone pocket (*CRY-pocket*) that is close to the previous one, but isn't directly involved in the protein-protein interaction. For this reason, for each ligand, two poses were chosen for each binding site on the basis of the binding energy and the quality of the ligand-protein interactions. All complexes were minimized by NAMD (conjugate gradients, 10.000 steps), keeping the atoms fixed outside from the spheroid defined by a layer of 12Å thickness around the ligand. For each optimized complex, some docking scores were calculated in order to obtain more reliable and comparable results: non-bond R^6-R^{12}Lennard-Johnes interaction energy calculated by both CHARMM 22 and CVFF[197] force fields, electrostatic energy calculated by classical Coulomb equation and distance-dependent equation in which the distance between two charges is considered as square value, binding energy calculated by AutoDock 4, molecular lipophilicity potential interaction scores (MLPInS)[198] to evaluate the hydrophobic interactions.

3.4.3 Docking results

In order to estimate inhibitory activity, the docking results of the proposed molecules (**O2** and **41**) were compared to **Cryptotanshinone** and **F2e** (**Figure 34**), whose STAT3 inhibitory activity had previously been evaluated by experimental assays.

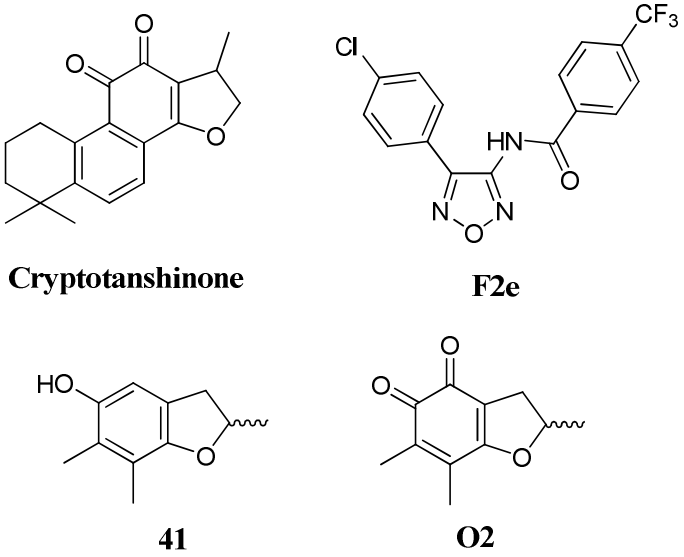

Figure 34. Structures of **Cryptotanshinone** and compounds **F2e**, **3**, **O2**.

In previous docking studies (Chapter 3.1.5), **F2e** was found to bind the PTR-pocket, and thus was suitable to analyze the complexes in which this binding site is involved. Since this site must interact with the large chain bound to the phosphorylated tyrosine of the second subunit, to perform the protein dimerization, its cavity is placed on the surface and it is surrounded by hydrophilic and polar amino acids. For this reason, the scores taking into account the hydrophobic interactions were discarded because they were unable to describe such kinds of interactions. In **Table 14**, the non-bonding interaction energies are shown.

Compound	CHARMM	Elect	ElectDD	AutoDock
F2d	-28,55	-18,69	-10,48	-6,07
(*S*)-**O2**	-22,80	-5,16	-7,31	-5,08
(*R*)-**O2**	-17,77	-42,34	-11,40	-4,20
(*S*)-**41**	-18,51	-12,66	-7,88	-3,65
(*R*)-**41**	-19,90	-2,93	-2,60	-3,23

Table 14. Docking scores obtained considering the PTR-pocket as target. *CHARMM* is the interaction energy calculated by CHARMM force field, *Elect* and *ElectDD* are the electrostatic energies calculated by Coulomb equation. ElectDD includes the distance-dependent dielectric constant. *AutoDock* is the interaction energy calculated by AutoDock software using a modified version of AMBER force field. The data are sorted by increasing AutoDock energy.

Classifying the molecules by their different energies, **F2e** is always ranked first, with the exception of the electrostatic interaction energy, but this behaviour can be explained considering that these scores do not take into account the discontinued dielectric, which is typical of a protein. Sorting the compounds by their AutoDock score, recalculated after the final minimization, the score difference between product (*S*)-**O2** and **F2e** is approximately 1 kcal/mol, meaning that the former could be less active than the latter. Arranging by CHARMM energy, product (*S*)-**O2** always shows a good score. Finally, the CVFF energy gives very similar results and thus this data has been omitted in **Table 14**.

Figure 35 shows the main interactions between (*S*)-**O2** and PTR-pocket amino acids; the ligand is placed in the same small pocket in which *p*Tyr-705 is inserted when two subunits are assembled in the dimer. The main interactions involve both the oxygens of carbonyl groups

and the guanidine group of Arg-609 by two hydrogen bonds, even if the interaction with Lys-591, which played a pivotal role to bond *p*Tyr-705, is missing.

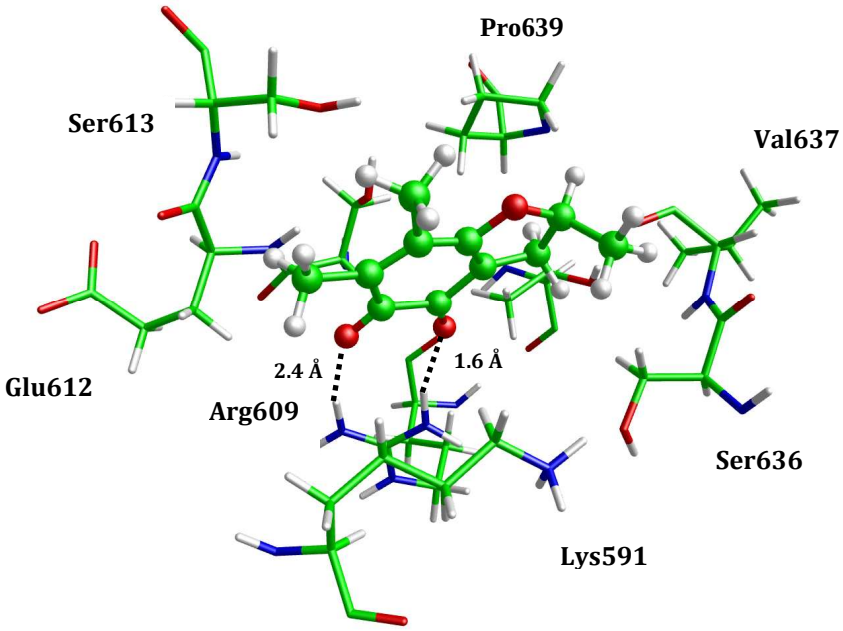

Figure 35. Main interactions between product (*S*)-**O2** and PTR-pocket.

Analyzing the docking results related to the *CRY-pocket*, Cryptotanshinone obtains the best score only with the AutoDock interaction energy, whereas, products (*S*)-**O2** and (*R*)-**O2** have better scores than Cryptotanshinone (**Table 15**).

Compound	MLPInS	MLPInS2	MLPIns3	MLPInSF	CHARMM	AutoDock
Cryptotanshinone	5,05	0,89	0,17	1,74	-7,74	-5,42
(*R*)-**O2**	-9,79	-1,22	-0,18	-1,53	-19,92	-4,76
(*S*)-**O2**	-9,04	-1,05	-0,14	-0,95	-17,76	-3,83
(*S*)-**41**	9,64	1,29	0,20	1,70	-18,20	-3,61
(*R*)-**41**	9,02	1,27	0,21	1,70	-19,11	-3,16

Table 15. Docking scores obtained considering the CRY-pocket as a target. *MLPIns* are the molecular lipophilicity potential interaction scores, *CHARMM* is the interaction energy calculated by CHARMM force field, *AutoDock* is the interaction energy calculated by AutoDock software using modified version of AMBER force field. The data are sorted by increasing AutoDock energy. The electrostatic energies are omitted to make the table more readable.

For this binding site, the MLPInS scores were considered because the pocket was lined by a number of hydrophobic amino acids, and these scores could evaluate the hydrophobic interactions that the others were unable to do. Sorting these results by MLPInS scores, products (*S*)-**O2** and (*R*)-**O2** showed good results. However, a comparison of (*R*)-**O2** and **Cryptotanshinone** found that the ligand poses are not fully overlapped (**Figure 36**); this could be due to the different position of the methyl group on the furane ring (2 instead of 3).

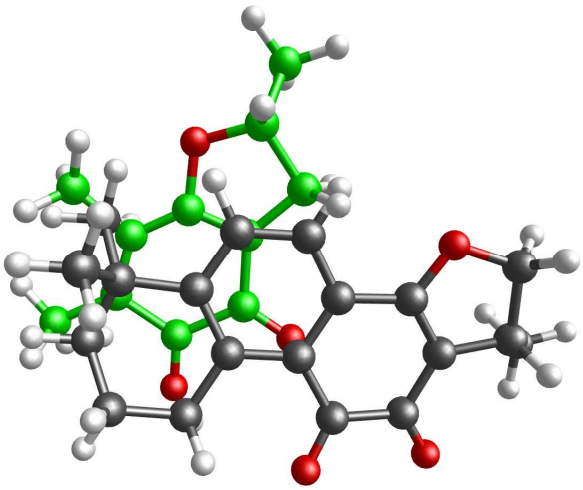

Figure 36. Product (*R*)-**41** (green carbons) and **Cryptotanshinone** (gray carbons) poses in *CRY-pocket*.

3.4.4 Chemistry

3.4.4.1 Synthesis of 3-methylbenzofuran-4,5-dione (O1) [199]

The synthesis of 3-methylbenzofuran-4,5-dione (**O1**) started from the condensation of *p*-benzoquinone with *N*-propenylmorpholine **36**, prepared *in situ* from morpholine and propionaldehyde.[200] The obtained dihydrobenzofuran **37** underwent firstly an acid hydrolysis of its hemiaminal functionality, and then an oxidation on the phenol ring with IBX, to afford the final 3-methylbenzofuran-4,5-dione (**O1**) (**Scheme 14**).

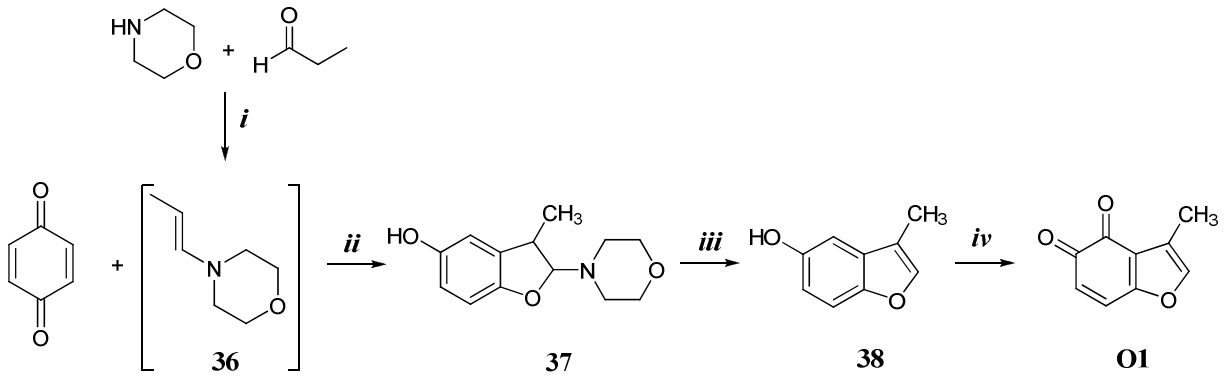

Scheme 14. Reagents and conditions: ***i***) toluene, rt, 18 h; ***ii***) toluene, 0°C, 25 h; ***iii***) HCl 5N, THF, reflux; ***iv***) IBX, CH_2Cl_2, rt.

3.4.4.2 Synthesis of (*RS*)-2,6,7-trimethyl-2,3-dihydrobenzofuran-4,5,-dione ((*R*)-O2, (*S*)-O2)

(*RS*)-2,6,7-trimethyl-2,3-dihydrobenzofuran-4,5,-dione ((*RS*)-**O2)** were obtained starting from the commercially available 2,3-dimethylhydroquinone. It was treated with allyl iodide and potassium carbonate in acetone to obtain a mixture of 4-(allyloxy)2,3-dimethylphenol **39** (the monoallyl ether) and 1,4-bis(allyloxy)-2,3-dimethylbenzene (the diallyl ether), which were separated by flash chromatography. A solution of the monoallyl ether **39** in decalin was heated at 220 °C under pressure (using an autoclave), obtaining a 5-allyl-2,3-dimethylbenzene-1,4-diol **40** *via* Claysen rearrangement. Intermediate **40** the underwent a

cyclization to the dihydrobenzofurane **41**, which was finally oxidized with IBX to afford a racemic mixture of compound **O2**. (**Scheme 15**)

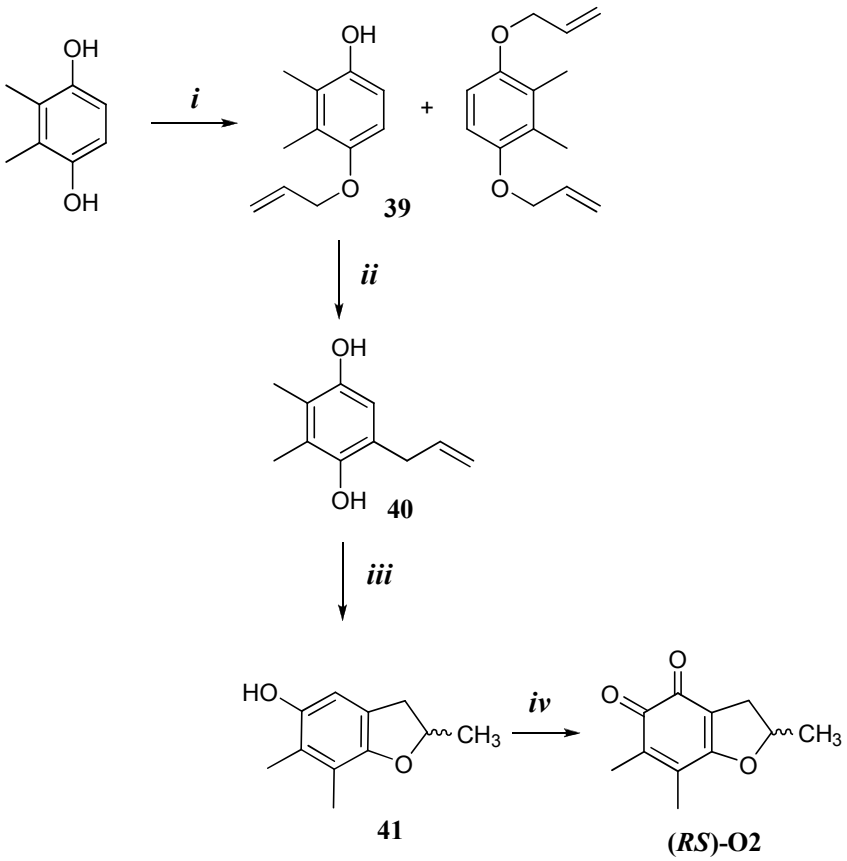

Scheme 15. *Reagents and conditions:* ***i***) allyl iodide, K_2CO_3, acetone, reflux; ***ii***) decaline, 200 °C, autoclave; ***iii***) *p*-toluensulfonic acid, toluene, MW; ***iv***) IBX, CH_2Cl_2, rt.

3.4.5 Future perspectives

Due to synthetic problems during the preparation of the designed compounds (**Figure 33**), their synthesis has not been completed to date. Therefore, new synthetic pathways will be developed in order to obtain the desired molecules. Moreover, as compound **O2** is a racemic mixture, a separation of its enantiomers, using chiral chromatography will be performed, and these will be submitted for biological testing.

However, according to the docking results on the synthesized products, the racemic mixture of compound **O2** turned out to have a potential inhibitory activity on the STAT3 pathway, as

it was able to interact with two different portions of the SH2 domain: *i*) phosphotyrosine binding site (*PTR-pocket*), which is directly involved in dimerization process; *ii*) Cryptotanshinone pocket (*CRY-pocket*), close to the previous one but not directly involved in dimerization. In order to verify the hypotheses pointed out in the docking studies, biological assays will be performed on all the synthesized compounds. In particular, they will be tested using the *in vitro* AlphaScreen-based assay to check their ability to inhibit STAT3 dimerization through the interaction with the STAT3-SH2 domain.

4. FINAL REMARKS

In this research project, various classes of derivatives have been investigated in order to identify lead compounds to further develop as STAT3 inhibitors. Starting from the structure of molecules, known in literature for their ability to inhibit STAT3 activity, several derivatives, by the support of molecular modeling and docking studies, were designed and synthesized. Three main series of molecules were developed: the oxadiazoles, the pyridazinones and the *ortho*-quinone compounds. Their biological investigation lead to the identification of the oxadiazole derivative **F2e**, which resembled the structure of its parent compound **AVS-0288** but showed a very different, yet promising, biological profile. **F2e** was found to inhibit STAT3 activity in cancer cells, acting through a direct mechanism: its binding to the SH2-domain of STAT3 protein was proven by *in vitro* binding test. Moreover, anti-proliferative assays on a panel of 58 cancer cell lines showed its significant growth inhibitory activity. Therefore, **F2e** presents the suitable features to become a lead compound for the future development of new derivatives.

5. EXPERIMENTAL SECTION: CHEMISTRY

5.1 Materials and Methods

All the reagents including solvents were purchased from Sigma-Aldrich and were used without any further purification. All reactions involving air-sensitive reagents were performed under nitrogen atmosphere and anhydrous solvents were used when necessary. The Biotage-Initiator microwave synthesizer was used. The course of the reaction was monitored by thin layer chromatography (TLC) analysis on aluminium-backed Silica Gel 60 plates (0.2 mm, Merck) and were visualized under a UV lamp operating at wavelengths of 254 and 365 nm. Visualisation was aided by opportune staining reagents. Intermediates and final compounds were purified by flash chromatography using Merck Silica Gel 60 (70-230 mesh). Melting points were determined in open capillary tubes on a Büchi Melting Point B-540. The purity of final compounds were determinated by HPLC analysis and were ≥95%. ^{1}H and ^{13}C NMR spectra were recorded at room temperature on a Varian 300 MHz Oxford instrument. $CDCl_3$, CD_3OD, acetone-d_6 and DMSO-d_6 were used as deuterated solvents for all spectra run. Chemical shifts are expressed in ppm from tetramethylsilane resonance in the indicated solvent (TMS: 0.0 ppm) and coupling constants (J-values) are given in Hertz (Hz). ^{1}H NMR data are reported in the following order: ppm, multiplicity (s, singlet; d, doublet; t, triplet; q, quartet; m, multiplet; br, broad), and number of protons.

5.2 Experimental procedures: the oxadiazoles (F1-F3)

5.2.1 Synthesis of the key intermediates: the 3-amino-1,2,5-oxadiazole derivatives (1a-e)

3-amino-4-methyl-1,2,5-oxadiazole (1a)[163]

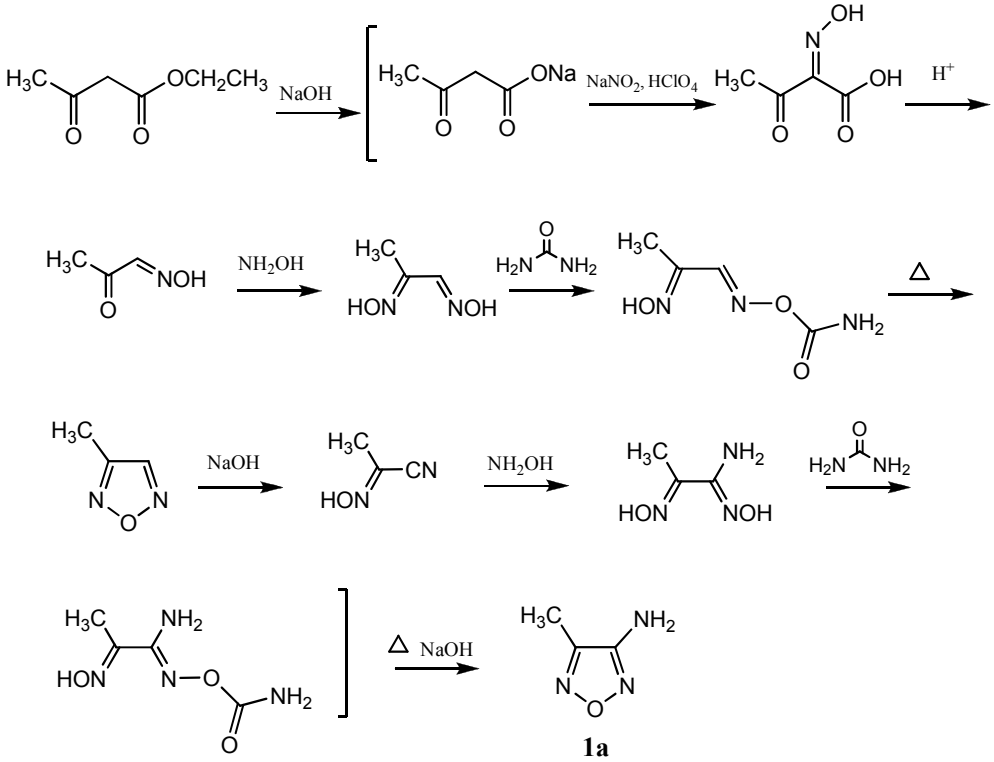

Ethyl acetoacetate (5 g, 38.4 mmol) was added at 10 °C to a solution of NaOH (1.75 g, 43.8 mmol) in water (14.7 mL). The resulting emulsion was stirred for 12 h and $NaNO_2$ (2.9 g, 41.8 mmol) was added. Then 20% $HClO_4$ (5.3 mL, 85.6 mmol) was slowly added dropwise at 10 to 15 °C. The reaction mixture was warmed to room temperature and stirred for 14 h. Sodium hydroxide (4.9 x 10^{-2} g, 1.23 mmol) followed by a solution of $NH_2OH{\cdot}HCl$ (8.2 g, 118.15 mmol) in water (14.7 mL) were added dropwise. After half the solution of $NH_2OH{\cdot}HCl$ was added, a solution of NaOH (5.32 g, 132.9 mmol) in water (9.8 mL) was simultaneously added dropwise keeping the temperature under 30 °C. Then the mixture was heated to 95 °C for 1.5 to 2 h and urea (1.98 g, 33 mmol) was added in one portion. The

resulting reaction mixture was refluxed for 3 h and then cooled. The product was extracted with dichloromethane (3 x 30 mL). The combined extracts were washed with water (1 x 30 mL), 5% sodium carbonate (1 x 30 mL), brine (1 x 30 mL) and the dried with anhydrous Na_2SO_4. The solvent was removed **1a** (0.76 g, 7.7 mmol) was obtained.

- White solid
- Yield: 20%
- TLC (petroleum ether/ethyl acetate 7:3) Rf = 0.27
- M.p. 72-73°C
- ^{1}H NMR ($CDCl_3$) 2.30 (s, 3H, CH_3), 4.10 (br s, 2H, NH_2, exchangeable with D_2O)

3-amino-1,2,5-oxadiazole-4-carboxylic acid (2)[164]

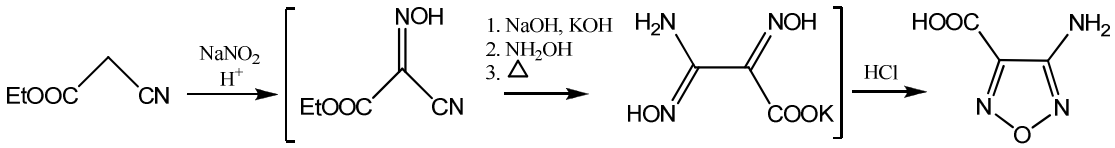

2

To a stirred emulsion of ethyl cyanoacetate (5 g, 44.2 mmol) and sodium nitrite (3.1 g, 44.2 mmol) in a mixture of ethanol (3.1 mL) and water (35.4 mL), 85% H_3PO_4 (1.8 mL) was added dropwise at 25-30 °C. After 1 h, the mixture was cooled to 10 °C, stirred for a further 12 h and treated with sodium hydroxide (4 x 1.8 g, 176.8 mmol) and potassium hydroxide (2 x 2.5 g, 88.4 mmol). To the resulting emulsion $NH_2OH{\cdot}HCl$ (12.3 g, 176.8 mmol) was slowly added at room temperature. The mixture was heated to 95-100 °C for 2 h and a yellow solution was obtained, which was then cooled to room temperature and quenched with concentrated HCl to pH = 1. Precipitation occurred on cooling to 0-5 °C for 6 h and the precipitate was collected by filtration and dried. The filtrate was extracted with diethyl ether (3 x 20 mL) and the combined organic extracts were evaporated under reduced pressure. The residue was collected with the previously obtained precipitate. Compound **2** was obtained as a white solid (4 g, 30.9 mmol).

- Yield: 70%
- TLC (dichloromethane/methanol 8.2) Rf = 0.33
- M.p. 214-215 °C

- ^{1}H NMR (DMSO-d_6): 6.31 (s, 2H, NH_2, exchangeable with D_2O) 9.1 (br s, 1H, OH, exchangeable with D_2O). ^{13}C NMR (DMSO-d_6): 140.4 (*C*-CO_2H), 156.8 (*C*-NH_2), 160.5 (*C*=O).

Ethyl 3-amino-1,2,5-oxadiazole-4-carboxylate (1b)

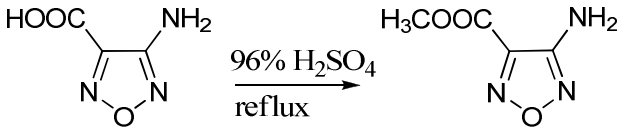

2 **1b**

Compound **2** (4 g, 30.9 mmol) was suspended in methanol (8 mL) and 96% H_2SO_4 (1 mL) was added dropwise. The obtained solution was refluxed for 2 h. Then, the solvent was removed, the residue was diluted with dichloromethane (50 mL) and washed with water (1 x 20 mL) and 0.1 M NaOH (1 x 20 mL). The organic layer was dried over anhydrous Na_2SO_4 and concentrated *in vacuo* to give a solid which was recrystallized from chloroform (1:9) to give ester **1b** (4.1 g, 28.7 mmol).

- White solid
- Yield: 93%
- TLC (petroleum ether/ethyl acetate 7:3) Rf = 0.55
- M.p. 120-122 °C
- ^{1}H NMR ($CDCl_3$) 4.0 (s, 3H, CH_3), 5.0 (s, 2H, NH_2, exchangeable with D_2O).

3-amino-4-hydroxymethyl-1,2,5-oxadiazole (1c)

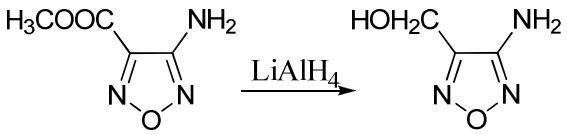

1b **1c**

To a stirred suspension of $LiAlH_4$ (1.60 g, 42 mmol) in dry tetrahydrofurane (5 mL) at 0 °C under nitrogen atmosphere, a solution of **1b** (1.20 g, 8.4 mmol) in dry tetrahydrofurane (2 mL) was added dropwise. The suspension was then stirred at room temperature for 2 h. The reaction was quenched by slowly adding cold water (3 mL) and basified with acqueous 2 N NaOH (2 mL) to pH = 10-11. The mixture was then filtered and the precipitated aluminium

salts washed with ethyl acetate (3 x 3 mL). The filtrate was dried with Na_2SO_4 and concentrated under reduced pressure to afford the expected compound **1c** as a thick yellow oil which was used without any further purification in the next step.

- Quantitaitve yield
- TLC (petroleum ether/ethyl acetate 1:1) Rf = 0.5
- ^{1}H NMR (CD_3OD) 4.85 (s, 2H, CH_2).

(4-amino-1,2,5-oxadiazole-3-yl)methyl-methyl-carbonate (7)

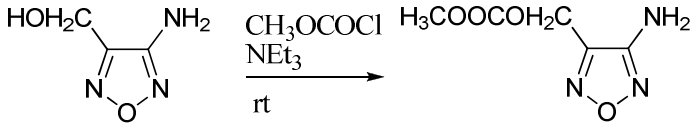

1c **7**

To a stirred solution of **1c** (0.1 g, 0.87 mmol) in tetrahydrofurane (2 mL) and triethylamine (0.18 mL, 1.3 mmol) at 0 °C was added methyl chloroformate (0.11 mL, 1.3 mmol) dropwise and a yellow solid precipitated. The resulting mixture was stirred at rt for 12 h. The reaction was diluted with water (2 mL) and extracted with ethyl acetate (3 × 2 mL). The organic layers were collected, dried over Na_2SO_4, and evaporated under reduced pressure. The residue was then purified by flash chromatography (eluent: petroleum ether/ethyl acetate 7:3) to afford the compound **7** as a yellow/orange oil (0.141 g, 0.82 mmol).

- Yield: 94%.
- TLC (petroleum ether/ethyl acetate 7:3) Rf = 0.3
- ^{1}H NMR ($CDCl_3$) 3.80 (s, 3H, OCH_3), 4.70 (br s, 2H, NH_2), 5.25 (s, 2H, CH_2O).

3-amino-4-phenyl-1,2,5-oxadiazole (1d)[165]

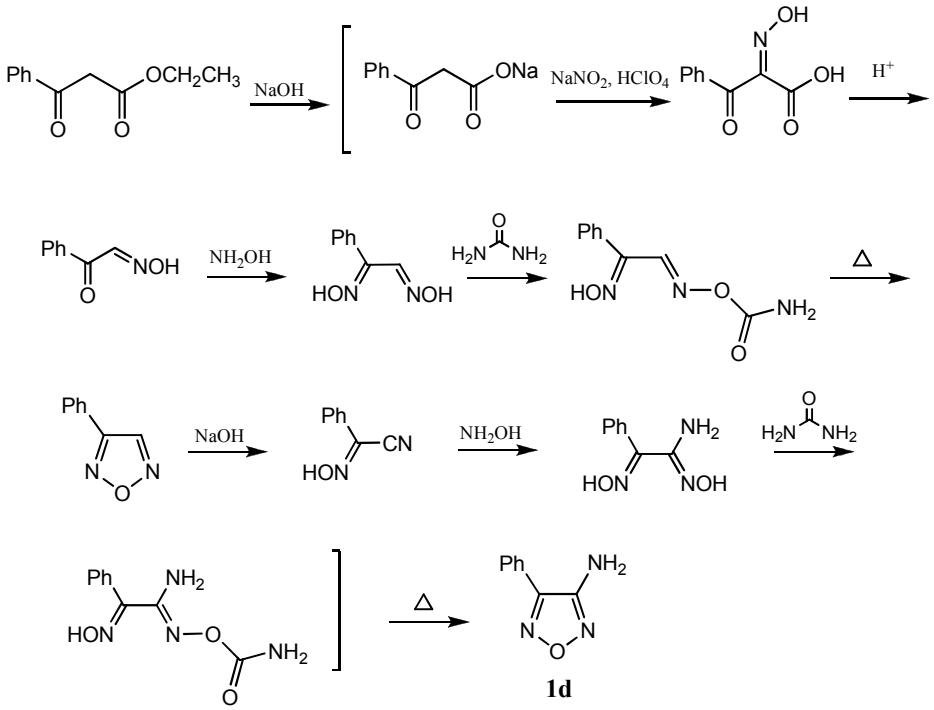

Ethyl benzoylacetate (5 g, 26 mmol) was added at 0 °C to a solution of NaOH (1.14 g, 28.6 mmol) in water (13 mL) and the resulting mixture was stirred for 12 h. Sodium nitrite (2.15 g, 31.2 mmol) was added and then 20% $HClO_4$ (3.7 mL, 59.8 mmol) was slowly added dropwise at temperature < 10 °C. After the addition of the acid was completed, the reaction mixture was warmed to room temperature and left for 14 h. Then a solution of $NH_2OH \cdot HCl$ (7.23 g, 104 mmol) in water (13 mL) was added dropwise with vigorous stirring. After half the solution of $NH_2OH \cdot HCl$ was added, a solution of NaOH (4.68 g, 117 mmol) in water (13 mL) was simultaneously added dropwise at a temperature lower than 30 °C. Then the mixture was heated to 95 °C for 2 h and urea (1.56 g, 26 mmol) was added in one portion. The resulting mixture was refluxed for 3 h and cooled. The white precipitate was filtered off, washed with water and dried. The obtained solid was purified by flash chromatography (petroleum ether/ethyl acetate 7:3) to afford **1d** as a white solid (1.42 g, 8.84 mmol).

- Yield: 34%
- TLC (petroleum ether/ethyl acetate 7:3) Rf = 0.45
- M.p. 99.5-100.5 °C
- ^1H NMR ($CDCl_3$) 4.20 (br s, 2H, NH_2, exchangeable with D_2O), 7.55 (m, 3H), 7.75 (m, 2H).

4-chloro benzaldehyde oxime (3)

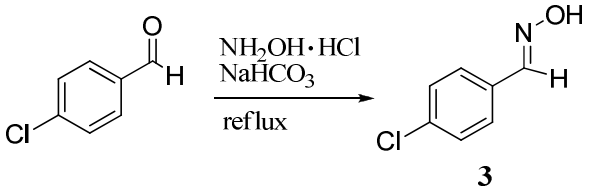

3

To 4-chloro benzaldehyde (5 g, 35.6 mmol) in methanol (100 mL) were added $NH_2OH \cdot HCl$ (3 g, 47.7 mmol) and $NaHCO_3$ (3.6 g, 42.7 mmol). The mixture was refluxed under stirring for 2 h, subsequently water (100 mL) was added and the solvent was evaporated under vacuum. The aqueous phase was extracted with ethyl acetate (3 x 30 mL), the organic solvent dried over Na_2SO_4 and evaporated under reduced pressure to obtain the oxime intermediate **3** as a white solid (5.43 g, 34.9 mmol).

- Yield: 98%
- TLC (petroleum ether/ethyl acetate 7:3) Rf = 0.60
- ^1H NMR ($CDCl_3$) 7.42-7.47 (d, 2H, J= 9.6 Hz, ArH), 7.50-7.56 (d, 2H, J= 9.6 Hz, ArH), 8.10 (s, 1H, CH), 10.00 (s, 1H, NH).

4-chloro benzoyl chloride oxime (4)

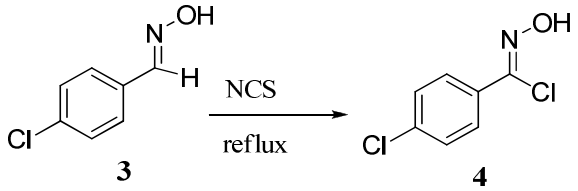

3 **4**

The intermediate **3** (5.45 g, 35 mmol) and NCS (4.67 g, 35 mmol) were dissolved in dimethylformamide (150 mL) and the solution was stirred for 12 h at rt. After addition of water (100 mL) to the reaction mixture, the aqueous solution was extracted by ethyl acetate (3 x 50 mL). The organic phases were collected, dried over Na_2SO_4 and evaporated under vacuum to give a yellow oil of crude hydroxylimino derivative **4** that was directly used without further purification in the next reaction.

- TLC (petroleum ether/ethyl acetate 9:1) Rf = 0.60

2-(4-chlorophenyl)-2-(hydroxyimino)acetonitrile (5)

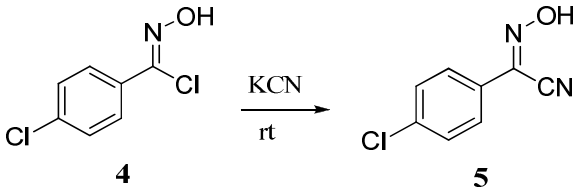

4 **5**

The derivative **4** (6.65 g, 35 mmol) was dissolved in diethyl ether (100 mL) and cooled at 0°C. A solution of KCN (4.56 g, 70 mmol) dissolved in water (100 mL) was added and the reaction mixture was stirred at rt for 5 h, subsequently water (30 mL) was added and the aqueous phase was extracted by ethyl acetate (3 x 30 mL). The organic solvent was dried over Na_2SO_4 and evaporated under reduced pressure. The residue was purified by flash chromatography (eluent: petroleum ether/ethyl acetate 9:1) to obtain **5** as a light yellow solid (5.67 g, 31.5 mmol).

- Yield: 90%
- TLC (petroleum ether/ethyl acetate 8:2) Rf = 0.50
- ^{1}H NMR ($CDCl_3$) 7.55-7.63 (d, 2H, J= 9.6 Hz, ArH), 7.65-7.73 (d, 2H, J= 9.6 Hz, ArH), 8.95 (br s, 1H, OH).

2-(4-chlorophenyl)-*N'*-hydroxy-2-(hydroxyimino)acetamidine (6)

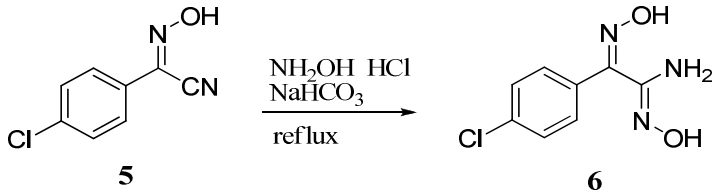

5 **6**

To the intermediate **5** (5.69 g, 31.5 mmol) in methanol (150 mL) were added $NH_2OH{\cdot}HCl$ (3.27 g, 47 mmol) and $NaHCO_3$ (3.95 g, 47 mmol). The mixture was refluxed under stirring for 12 h. After addition of water (100 mL), the solvent was removed under vacuum. The aqueous phase was extracted by ethyl acetate (3 x 30 mL), the organic solvent dried over Na_2SO_4 and evaporated under reduced pressure to give the crude acetamidine intermediate **6** that was directly used without further purification in the next reaction.

- TLC (petroleum ether/ethyl acetate 6:4) Rf = 0.30

4-(4-chlorophenyl)-1,2,5-oxadiazol-3-amine (1e)

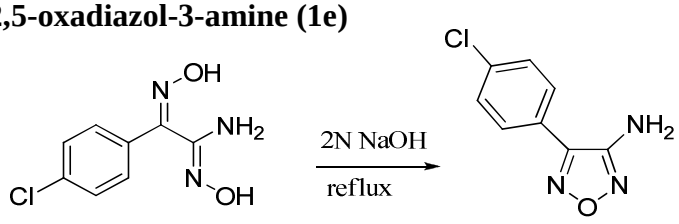

6 **1e**

The derivative **6** (6.72 g, 31.5 mmol) was dissolved in 2 N NaOH (100 mL) and the solution was refluxed under stirring for 12 h. The mixture was cooled to rt and the formed precipitate was collected by filtration and washed with water. Compound **1e** was obtained as a white crystalline solid (2.7 g, 13.8 mmol).

- Yield: 44%
- TLC (petroleum ether/ethyl acetate 7:3) Rf = 0.6
- ^{1}H NMR ($CDCl_3$) 4.20 (br s, 2H, NH_2), 7.50-7.55 (d, 2H, J=9.6 Hz, ArH), 7.62-7.67 (d, 2H, J=9.6 Hz, ArH).

5.2.2 Synthesis of the 4-substituted 1,2,5-oxadiazol-3-yl ureido derivatives (F1a-f)

1-(4-methyl-1,2,5-oxadiazol-3-yl)-3-phenylurea (F1a)

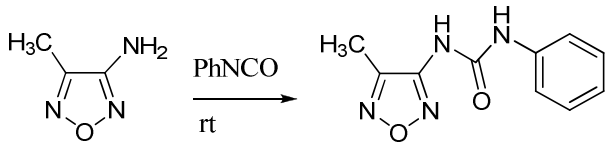

1a **F1a**

3-amino-4-methyl-1,2,5-oxadiazole **1a** (5 x 10^{-2} g, 0.50 mmol) was solubilized in tetrahydrofurane and phenyl isocyanate (8.1 x 10^{-2} g, 0.68 mmol) was added. The mixture was stirred at rt for 24 h. The reaction mixture was evaporated and purified with flash chromatography on silica gel eluting with petroleum ether/ethyl acetate 7:3 to give **F1a** as white solid (6.55 x 10^{-2} g, 0.3 mmol).

- Yield: 60%
- TLC (petroleum ether/ethyl acetate 7:3) Rf = 0.3

- ^{1}H NMR ($CDCl_3$) 2.35 (s, 3H, CH_3), 7.20-7.60 (m, 5H, ArH), 8.95 (br s, 1H, NH), 9.40 (br s, 1H, NH).

Synthesis of 1-(4-methyl-1,2,5-oxadiazol-3-yl)-3-benzylurea (F1aa)

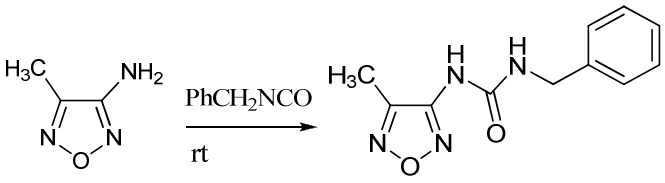

1a **F1aa**

3-amino-4-methyl-1,2,5-oxadiazole (**1a**) (50 mg, 0.50 mmol) was mixed with benzyl isocyanate (101 mg, 0.76 mmol) in neat conditions. The mixture was stirred at rt for 2 days. The reaction mixture was purified with flash chromatography on silica gel eluting with cyclohexane/ethyl acetate/methanol 6:3.8:0.2 to give **F1aa** (9.4×10^{-2} g, 0.40 mmol).

- White solid
- Yield: 80%
- ^{1}H NMR ($CDCl_3$) 2.35 (s, 3H, CH_3), 4.55 (d, 2H, CH_2), 7.20-7.40 (m, 5H, ArH), 7.90 (br s, 1H, NH), 9.90 (br s, 1H, NH).

General procedure A for the synthesis of the 4-substituted-1,2,5-oxadiazol-3-yl ureido derivatives (F1b-f) under microwave irradiation.

To a solution of the appropriate 3-amino-1,2,5-oxadiazole (0.50 mmol) in toluene (1.5 mL), the suitable isocyanate (0.60 mmol) was added at rt. The reaction mixture was irradiated in a microwave synthesizer at 300 Watts at a temperature of 90 °C for 20 min. Purification conditions are specified in the description of each product.

Methyl 4-(3-phenylureido)-1,2,5-oxadiazole-3-carboxylate (F1b)

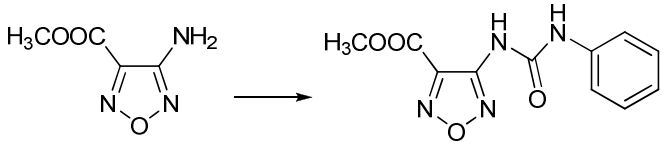

1b **F1b**

General procedure A was followed to prepare the final compound **F1b** from intermediate **1b**. Purification by flash chromatography (petroleum ether/ethyl acetate 8:2) gave **F1b** as a white solid.

- Yield: 60%
- TLC (petroleum ether/ethyl acetate 1:1) Rf = 0.4
- M.p. 200-201 °C
- ^{1}H NMR ($CDCl_3$) 4.0 (s, 3H,OCH_3), 6.45 (s, 2H, NH), 7.30-7.40 (m, 5H, ArH).

(4-(3-benzylureido)-1,2,5-oxadiazol-3-yl)methyl methyl carbonate (8)[166]

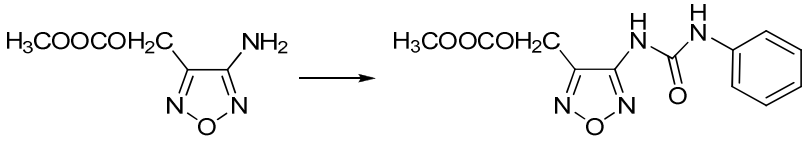

7 **8**

General procedure A was followed to prepare the final compound **8** from intermediate **7**. After the cooling of the vial, a white jelly-like solid began to precipitate. The solid **8** was filtrated and washed with toluene.

- Yield: 35%
- TLC (petroleum ether/ethyl acetate 7:3) Rf = 0.3
- ^{1}H NMR ($CDCl_3$) 3.80 (s, 3H, OCH_3), 5.40 (d, 2H, CH_2O), 7.20 (d, 2H, ArH), 7.40 (t, 2H, ArH), 7.60 (t, 2H, ArH), 8.60 (s, 1H, NH), 9.20 (s, 1H, NH).

(4-(3-phenylureido)-1,2,5-oxadiazol-3-yl)methyl methyl carbonate (9)[166]

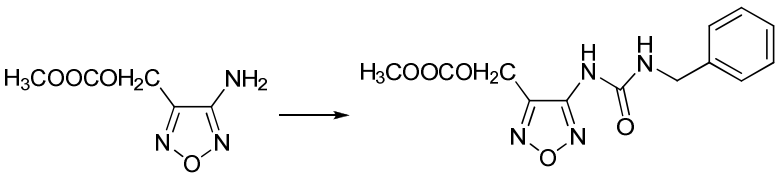

7 **9**

General procedure A was followed to prepare the final compound **9** from intermediate **7**. After the cooling of the vial, a white jelly-like solid began to precipitate. The solid **9** was filtrated and washed with toluene.

- Yield: 31%
- TLC (petroleum ether/ethyl acetate 7:3) Rf = 0.3

- ^{1}H NMR ($CDCl_3$) 3.80 (s, 3H, OCH_3), 5.40 (d, 2H, CH_2O), 7.20 (d, 2H, ArH), 7.40 (t, 2H, ArH), 7.60 (t, 2H, ArH), 8.60 (s, 1H, NH), 9.20 (s, 1H, NH).

Synthesis of 1-phenyl-3-3(4-phenyl-1,2,5-oxadiazol-3-yl)urea (F1d)

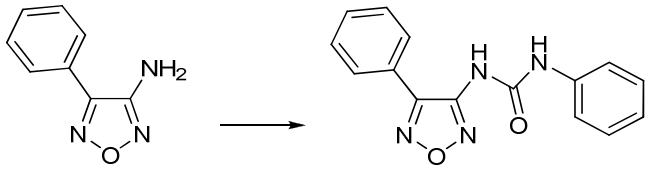

1d **F1d**

General procedure A was followed to prepare the final compound **F1d** from intermediate **1d**. Purification by flash chromatography (eluent: dichloromethane/petroleum ether/ethyl acetate 7:2.5:0.5) gave **F1d** as a white solid.

- Yield: 86%
- M.p. 151-152 °C
- TLC (petroleum ether/ethyl acetate 7:3) Rf = 0.3
- ^{1}H NMR ($CDCl_3$) 6.85 (br s, 1H, NH), 7.20-7.60 (m, 10H, ArH), 9.35 (br s, 1H, NH).

1-benzyl-3-(4-phenyl-1,2,5-oxadiazol-3-yl)urea (F1dd)

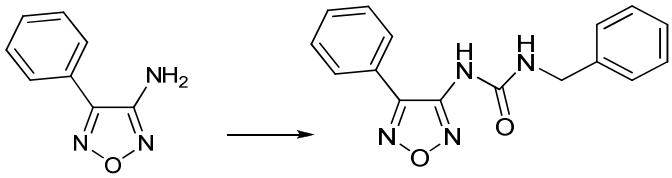

1d **F1dd**

General procedure A was followed to prepare the final compound **F1dd** from intermediate **1d**. Purification by flash chromatography (eluent: petroleum ether/ethyl acetate 7.5:2.5) gave **F1dd** as a yellowish solid.

- Yield: 20%
- M.p. 154-155 °C
- TLC (petroleum ether/ethyl acetate 7:3) Rf = 0.3
- ^{1}H NMR ($CDCl_3$) 4.55 (d, 2H, CH_2), 7.10 (br s, 1H, NH), 7.25-7.65 (10H, m, ArH), 7.75 (br s, 1H, NH).

Synthesis of 1-phenyl-3-3(4-phenyl-1,2,5-oxadiazol-3-yl)urea (F1ddd)

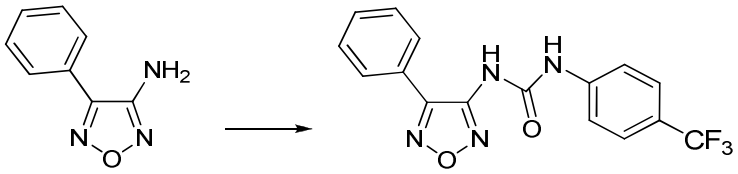

1d **F1ddd**

General procedure A was followed to prepare the final compound **F1d** from intermediate **1d**. Purification by flash chromatography (eluent: dichloromethane/petroleum ether/ethyl acetate 7:2.5:0.5) gave **F1ddd** as a white solid.

- Yield: 70%
- TLC (petroleum ether/ethyl acetate 7:3) Rf = 0.35
- ^{1}H NMR ($CDCl_3$) 6.85 (br s, 1H, NH), 7.30-7.70 (m, 9H, ArH), 9.35 (br s, 1H, NH).

General procedure B for the deprotection of the carbonate protecting group to obtain the products F1c and F1cc.[166]

The appropriate carbonate (0.21 mmol) was dissolved in 1% solution of K_2CO_3 in methanol (2 mL) and the resulting solution was stirred at reflux for 2 h. After completion of the reaction, methanol was removed in vacuo. The residue was diluted with ethyl acetate (3 mL) and washed with water (2 x 1 mL). The organic phase was dried with Na_2SO_4 and evaporated to obtain the final alcohol.

1-(4-(hydroxymethyl)-1,2,5-oxadiazol-3-yl)-3-phenylurea (F1c)

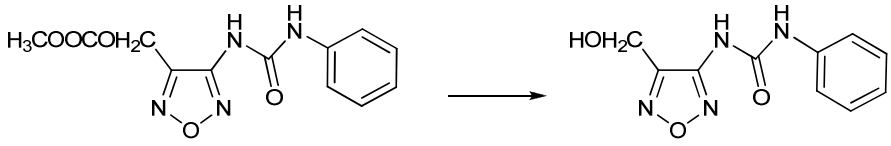

8 **F1c**

General procedure B was followed to prepare the final compound **F1c** (white solid) from intermediate **8**.

- Quantitative yield.
- TLC (petroleum ether/ethyl acetate 6:4) Rf = 0.3

- ^{1}H NMR (CD_3OD) 4.85 (d, 2H, CH_2), 7.10 (d, 1H, ArH), 7.30 (t, 2H, ArH), 7.50 (t, 2H, ArH).

1-(4-(hydroxymethyl)-1,2,5-oxadiazol-3-yl)-3-benzylurea (F1cc)

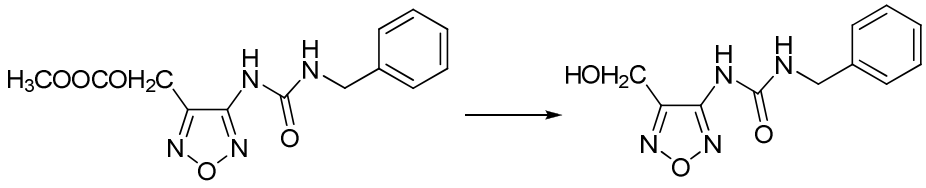

9 **F1cc**

General procedure B was followed to prepare the final compound **F1cc** (white solid) from intermediate **9**.

- Quantitative yield.
- M.p. 159.3-162 °C
- TLC (petroleum ether/ethyl acetate 6:4) Rf = 0.3
- ^{1}H NMR ($CDCl_3$) 4.55 (d, 2H, CH_2), 4.80 (s, 2H, CH_2), 7.25-7.40 (m, 5H, ArH), 8.10 (s, 1H, NH), 10.30 (s, 1H, NH).

General procedure C for the synthesis of the cyclic hemiaminals 10 and 11[166]

To an ice-cold solution of the suitable alcohol (0.20 mmol) in dry dichloromethane (1.5 mL), Dess-Martin Periodinane (0.31 mmol) was added in one portion. The reaction was stirred at 0 °C for 30 min and then at rt for 24 h. The reaction was quenched at 0 °C by stirring with a saturated aqueous solutions of $Na_2S_2O_3$ (1 mL) and of $NaHCO_3$ (1 mL) for 10 min, to destroy any unreacted Dess-Martin reagent. The organic phase was then separated, dried over Na_2SO_4 and concentrated in vacuo. The crude product was purified by flash chromatography (eluent: petroleum ether/ethyl acetate 6:4) to give the cyclic hemiaminal.

6-phenyl-7-hydroxy-6,7-dihydro-[1,2,5]oxadiazol-[3,4-d]-pyrimidin-5(4H)-one (10)

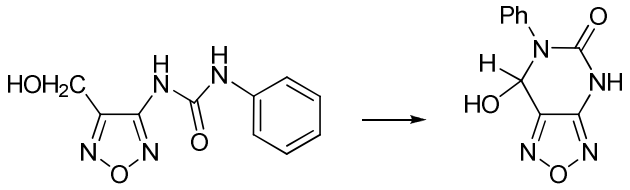

F1c **10**

General procedure C was followed to prepare the final compound **10** (light yellow solid) from intermediate **F1c**.

- Yield: 80%
- TLC (petroleum ether/ethyl acetate 1:1) Rf = 0.7
- M.p. 182-184 °C
- ^{1}H NMR ($CDCl_3$) 6.35 (d, 1H, CH), 7.30-7.50 (m, 5H, ArH), 7.55 (d, 1H, OH), 11.40 (s, 1H, NH).

6-benzyl-7-hydroxy-6,7-dihydro-[1,2,5]oxadiazol-[3,4-d]-pyrimidin-5(4H)-one (11).

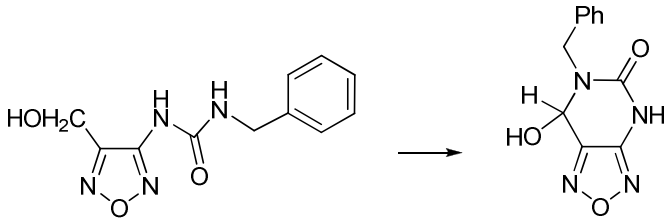

F1cc **11**

General procedure C was followed to prepare the final compound **11** (light yellow solid) from intermediate **F1cc**.

- Yield 85%
- TLC (petroleum ether/ethyl acetate 1:1) Rf = 0.7
- M.p. 194-196 °C
- ^{1}H NMR (DMSO-d_6) 4.40 (d, 1H, J=15 Hz, CH_2), 4.90 (d, 1H, J=15 Hz, CH_2), 6.10 (d, 1H, J=9 Hz, CH, collapses to a singlet on D_2O exchange), 7.20-7.30 (m, 5H, ArH), 7.40 (d, 1H, J=9 Hz, -OH, exchangeable with D_2O), 11.3 (s, 1H, -NH-, exchangeable with D_2O); ^{13}C NMR (DMSO-d_6) 40.80 (CH_2), 70.35 (CH-OH), 120.80 (CH_{aro}), 120.85 (2 x CH_{aro}), 120.90 (2 x CH_{aro}), 130.80 (C^q), 140.40 (CH^q_{aro}), 150.05 (C^q), 150.10 (C=O).

General procedure D for the synthesis of the styryl derivatives (*E*/*Z*-F1g and *E*/*Z*-F1gg)[166]

A mixture of the required cyclic hemiaminal (0.20 mmol), benzyltriphenylphosphonium chloride (0.23 mmol), K_2CO_3 (0.43 mmol), 18-crown-6 (catalytic quantity), and tetrahudrofurane (2 mL) as a solvent was stirred at reflux for 1 h. The solvent was evaporated in vacuo, the residue was treated with brine and extracted with ethyl acetate (3 x 1 mL). The organic layer was dried over Na_2SO_4 and evaporated *in vacuo*. The products were purified by flash chromatography (eluent: petroleum ether/ethyl acetate 7:3).

1-phenyl-3-(4-styryl-1,2,5-oxadiazol-3-yl)urea (*E,Z*-F1g)

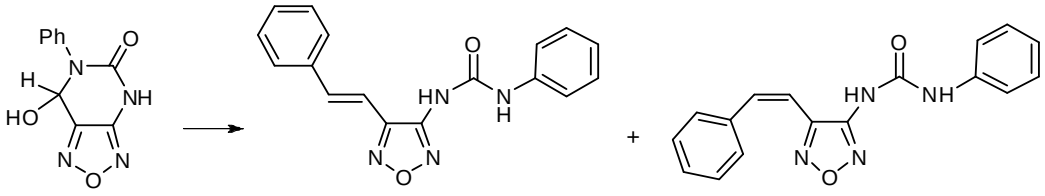

10 *E*-**F1g** *Z*-**F1g**

General procedure D was followed to prepare the final compound *E,Z*-**F1g** from intermediate **10**.

Derivative *E*-**F1g** (yellow solid)

- Yield: 55%
- TLC (cyclohexane/ethyl acetate 6:4) Rf = 0.7
- M.p. 201-203 °C
- ^{1}H NMR ($CDCl_3$) 7.03 (d, 1H, J= 15.1 Hz, CH), 7.10-7.57 (m, 10H, ArH), 7.61 (d, 1H, J= 15.1 Hz, CH), 8.70 (br s, 1H, NH), 9.45 (br s, 1H, NH);

Derivative *Z*-**F1g** (yellow solid)

- Yield: 25%
- TLC (cyclohexane/ethyl acetate 6:4) Rf = 0.5
- M.p. 173-175 °C
- ^{1}H NMR ($CDCl_3$) 6.51 (d, 1H, J= 12.1 Hz, CH), 7.03 (br s, 1H, NH), 7.19 (d, 1H, J= 12.1 Hz, CH), 7.10-7.50 (m, 10H, ArH), 9.17 (br s, 1H, NH).

1-benzyl-3-(4-styryl-1,2,5-oxadiazol-3-yl)urea (*E,Z*-F1gg).

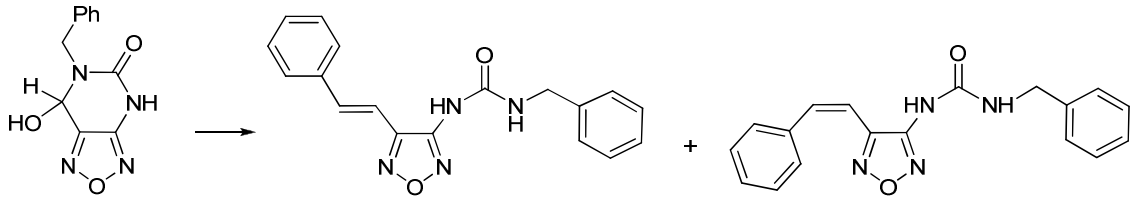

11 ***E*-F1gg** ***Z*-F1gg**

General procedure D was followed to prepare the final compound *E,Z*-**F1gg** from intermediate **11**.

Derivative *E*-**F1gg** (pale yellow solid)

- Yield: 50%
- TLC (cyclohexane/ethyl acetate 6:4) Rf = 0.7
- M.p. 192-194 °C
- ^{1}H NMR ($CDCl_3$) 4.59 (d, 2H, J=5.7 Hz, CH_2), 7.20 (d, 1H, J= 15.5 Hz, CH), 7.20-7.67 (m, 10H, ArH), 7.60 (d, 1H, J= 15.5 Hz, CH), 7.98 (t, 1H, J=5.7 Hz, NH), 9.96 (br s, 1H, NH);

Derivative *Z*-**F1gg** (yellow solid)

- Yield: 19%
- TLC (cyclohexane/ethyl acetate 6:4) Rf = 0.5
- M.p. 170-172 °C
- ^{1}H NMR ($CDCl_3$) 4.48 (d, 2H, J=5.7 Hz, CH_2), 6.44 (d, 1H, J= 12.2 Hz, CH), 7.11 (d, 1H, J= 12.2 Hz, CH), 7.20-7.40 (m, 10H, ArH), 7.58 (t, 1H, J=5.7 Hz, NH), 9.60 (s, 1H, NH).

5.2.3 Synthesis of the 4-substituted 1,2,5-oxadiazol-3-yl amido derivatives (F2a-e)

Method 1 (F2a, c). To a solution of the suitable amine **1a**, **c** (0.51 mmol) in dry tetrahydrofurane (2 mL) cooled at 0 °C, phenyl acetyl chloride (0.070 mL, 0.53 mmol) in dry tetrahydrofurane (0.5 mL) was added dropwise. $NaHCO_3$ (0.53 mmol) was then added and the resulting mixture was stirred at room temperature for 3 h. The reaction was monitored by

TLC until completion, then quenched with distilled water (2 mL) and extracted with ethyl acetate (3 × 1 mL). The combined organic layers were dried with Na_2SO_4, filtrated and concentrated under vacuum.

Method 2 (F2d, e). A solution of the suitable amine **1d, e** (0.31 mmol) in dry toluene (0.6 mL) and diethyl ether (0.2 mL) was cooled to 0 °C with an ice/water bath and treated with pyridine (0.03 mL). Phenyl acetyl chloride (0.05 mL, 0.33 mmol) was then added dropwise. The mixture was stirred for 30 min at 0 °C and then for 5 h at rt. The solvent was removed under vacuum and the crude product was purified by flash chromatography.

N-(4-methyl-1,2,5-oxadiazol-3-yl)-2-phenylacetamide (F2a)

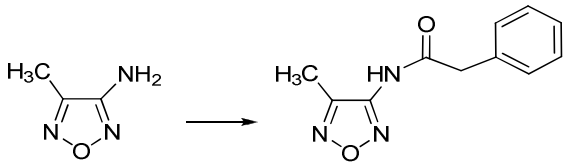

1a **F2a**

Method 1 was followed for the synthesis of **F2a** starting from **1a**. Purification with flash chromatography (eluent: petroleum ether/ethyl acetate 8:2) was performed as to obtain **F2a** as a white solid.

- Yield: 90%
- TLC (petroleum ether/ethyl acetate 8:2) Rf = 0.35
- M.p. 135.7-137 °C
- ^{1}H NMR ($CDCl_3$) 2.40 (s, 3H, CH_3), 3.80 (s, 2H, CH_2), 7.30-7.50 (m, 5H, ArH), 8.50 (br s, 1H, NH).

4-(2-phenylacetamido)-1,2,5-oxadiazole-3-methylcarboxylate (F2b)

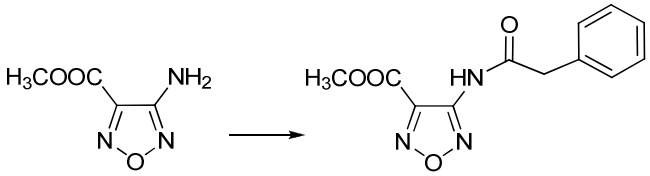

1b **F2b**

To a solution of **1b** (5 x 10^{-2} g, 0.35 mmol) in dichloromethane (1 mL), phenyl acetyl chloride (0.049 mL, 0.42 mmol) and EDAC (8.05 x 10^{-2} mg, 0.42 mmol) were added. The solution

was brought to pH 7 with 2 drops of *N*-methylmorfoline and stirred for 24 h at rt. Then solvent was removed under vacuum, the residue diluted with dichloromethane (4 mL) and washed respectively with: 1N HCl (3 × 1 mL), saturated solution of $NaHCO_3$ (3 × 1 mL), water (2 × 1 mL) and brine (2 × 1 mL). The solvent was dried with Na_2SO_4 and evaporated. The crude product was purified by flash chromatography (eluent: petroleum ether/ethyl acetate 8:2) to obtain the white solid **F2b** (6 x 10^{-2} mg, 0.23 mmol).

- Yield: 66%
- TLC (petroleum ether/ethyl acetate 8:2) Rf = 0.4
- M.p. 98-99°C
- ^{1}H NMR ($CDCl_3$) 3.90 (2 H, s, CH_2), 3.95 (3 H, s, OCH_3), 7.35-7.50 (5 H, m, ArH), 8.80 (1 H, br s, NH).

N-(4-(hydroxymethyl)-1,2,5-oxadiazol-3-yl)-2-phenylacetiamide (F2c)

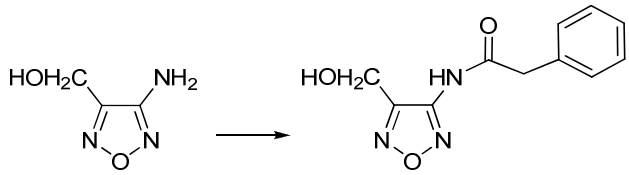

1c **F2c**

Method 1 was followed for the synthesis of **F2c** starting from **1c**. Purification with flash chromatography (eluent: petroleum ether/ethyl acetate 7.5:3.5) was performed as to obtain **F2c** as a white solid.

- Yield: 22%
- TLC (petroleum ether/ethyl acetate 7.5:3.5) Rf = 0.35
- M.p. 133-134°C
- ^{1}H NMR ($CDCl_3$) 3.20 (1 H, br s, NH), 3.85 (2 H, s, CH_2), 4.80 (2 H, s, OCH_2), 7.30-7.50 (5 H, m, ArH), 8.10 (1 H, br s, OH).

2-phenyl-N-(4-phenyl-1,2,5-oxadiazol-3-yl)acetamide (F2d)

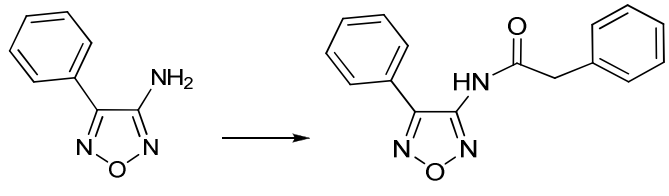

1d **F2d**

Method 2 was followed for the synthesis of **F2d** starting from **1d**. Purification with flash chromatography (eluent: petroleum ether/ethyl acetate 9:1) was performed as to obtain **F2d** as a white solid.

- Yield: 58%
- TLC (petroleum ether/ethyl acetate 9:1) Rf = 0.4
- M.p. 97-98.5°C
- ^{1}H NMR ($CDCl_3$) 1.55 (1 H, br s, NH), 3.85 (2 H, s, CH_2), 7.30-7.50 (10 H, m, ArH).

N-(4-(4-chlorophenyl)-1,2,5-oxadiazol-3-yl)-4-(trifluoromethyl)benzamide (F2e)

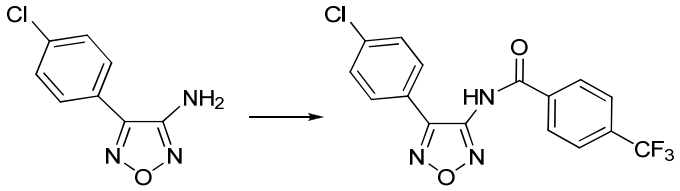

1e **F2e**

Method 2 was followed for the synthesis of **F2e** starting from **1e**. Purification with flash chromatography (eluent: petroleum ether/ethyl acetate 9:1) was performed as to obtain **F2e** as a white solid.

- Yield: 50%
- TLC (petroleum ether/ethyl acetate 9:1) Rf = 0.4
- M.p. 111-114°C
- ^{1}H NMR (acetone-d_6) 7.54-7.59 (d, 2H, ArH), 7.85-7.89 (m, 2H, ArH), 7.93 (d, 2H, J=8.1 Hz, ArH), 8.25 (d, 2H, J=8.1 Hz, ArH)
- ^{13}C NMR (acetone-d_6) 124.9, 125.9, 126.0, 128.3, 128.51, 133.5, 133.9, 136.4, 136.5, 150.04, 151.0, 165.4
- Cell proliferation assay: see **Appendix I**

5.2.4 Synthesis of the 4-substituted 1,2,5-oxadiazol-3-yl sulfonamido derivatives (F3a-e)

General procedure E for the synthesis of the 4-substituted 1,2,5-oxadiazol-3yl sulfonamido derivatives (F3a-e). To a solution of the corresponding 3-amino-1,2,5-

oxadiazole (0.50 mmol) in pyridine (2 mL), the suitable benzyl sulfonyl chloride (1 mmol) was added portionwise at rt. The reaction mixture was monitored by TLC until completion, then evaporated to dryness and the residue treated with 2 N HCl (6 mL) until pH = 1. The resulting mixture was stirred at rt for 1 h, the precipitated filtered and washed with 2 N HCl and dried.

N-(4-methyl-1,2,5-oxadiazol-3-yl)-1-phenylmethanesulfonamide (F3a)

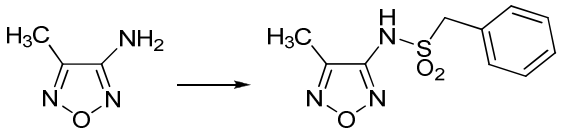

1a **F3a**

General procedure E was followed to prepare compound **F3a** starting from **1a**. Purification by flash chromatography (eluent: dichloromethane/methanol 9.5:0.5) was performed to obtain compound **F3a** as a brown solid.

- Yield: 40%
- TLC (dichloromethane/methanol 9.5:0.5) Rf = 0.3
- M.p. 168-169.2 °C
- ^{1}H NMR (CD_3OD_3) 2.25 (s, 3H, CH_3), 4.65 (s, 2H, CH_2), 7.35-7.45 (m, 5H, ArH).

4-(phenylmethylsulfonamido)-1.2.5-oxadiazole-3-methylcarboxylate (F3b)

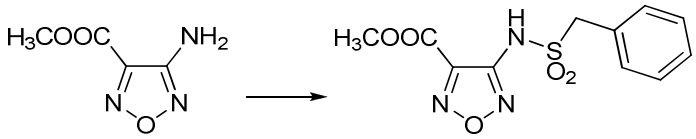

1b **F3b**

General procedure E was followed to prepare compound **F3b** starting from **1b**. Purification by flash chromatography (eluent: dichloromethane/methanol 9.5:0.5) was performed to obtain compound **F3b** as a brown solid.

- Yield 50%
- TLC (dichloromethane/methanol 9.5:0.5) Rf = 0.3
- M.p. 121-122.5 °C

- ^{1}H NMR ($CDCl_3$) 1.60 (br s, 1H, NH), 4.00 (s, 3H, OCH_3), 4.70 (s, 2H, CH_2), 7.35-7.45 (m, 5H, ArH).

(4-phenylmethylsulfonamido-1,2,5-oxadiazole-3-yl)methyl-methyl-carbonate (12)

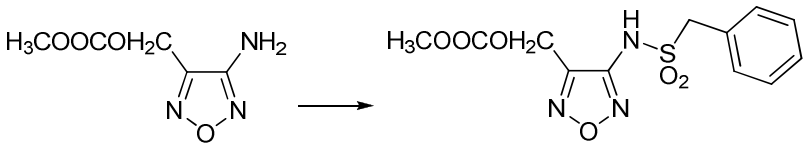

7 **12**

General procedure E was followed to prepare compound **12** starting from **7**. Purification by flash chromatography (eluent: dichloromethane/methanol 9.5:0.5) was performed to obtain compound **12** as a dark green solid.

- Yield: 50%
- TLC (dichloromethane/methanol 9.5:0.5) Rf = 0.35
- ^{1}H NMR ($CDCl_3$) 3.70 (s, 3H, CH_3), 4.50 (s, 2H, CH_2), 5.15 (s, 2H, CH_2O), 7.20-7.40 (m, 5H, ArH).

N-(4-(hydroxymethyl)-1,2,5-oxadiazol-3-yl)-1-phenylmethylsulfonamido (F3c)

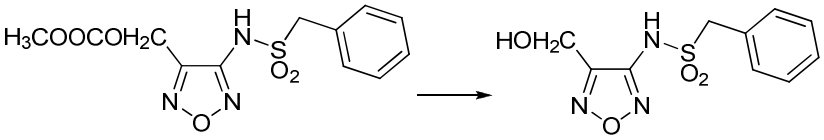

12 **F3c**

General Procedure B was followed for the synthesis of **F3c** from **12** as a brown solid.

- Quantitative yield.
- TLC (dichloromethane/methanol 9:1) Rf = 0.4
- M.p. 130-132 °C
- ^{1}H NMR ($CDCl_3$) 3.65 (br s, 1H, OH), 4.00 (br s, 1H, NH), 4.45 (s, 2H, CH_2), 4.55 (s, 2H, CH_2OH), 7.20-7.30 (m, 5H, ArH).

N-(4-phenyl-1,2,5-oxadiazol-3-yl)-1-phenylmethanesulfonamide (F3d)

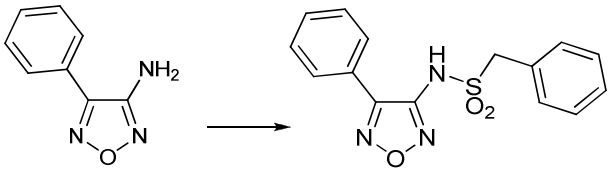

1d **F3d**

General procedure E was followed to prepare compound **F3d** starting from **1d**. Purification by flash chromatography (eluent: dichloromethane/methanol 9.5:0.5) was performed to obtain compound **F3d** as a brown solid.

- Yield: 59%
- TLC (dichloromethane/methanol 9.5:0.5) Rf = 0.35
- M.p. 121-123 °C
- ^{1}H NMR ($CDCl_3$) 4.75 (s, 2H, CH_2), 7.25 (br s, 1H, NH), 7.30-7.65 (m, 10H, ArH).

N-(4-(4-chlorophenyl)-1,2,5-oxadiazol-3-yl)-4-(trifluoromethyl)benzenesulfonamide (F3e)

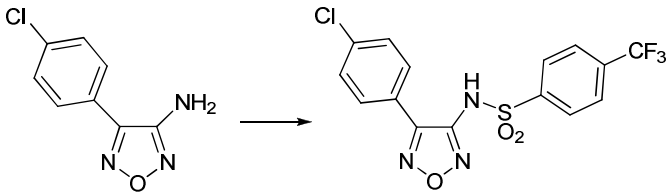

1e **F3e**

General procedure E was followed to prepare compound **F3e** starting from **1e**. Purification by flash chromatography (eluent: dichloromethane/methanol 9.5:0.5) was performed to obtain compound **F3e** as a dark green solid.

- Yield: 20%
- TLC (dichloromethane/methanol 9.5:0.5) Rf = 0.3
- M.p. 129-130.4 °C
- ^{1}H NMR ($CDCl_3$) 7.15 (br s, 1H, NH), 7.35 (d, 2H, ArH), 7.55 (d, 2H, ArH), 7.75 (d, 2H, ArH), 7.95 (d, 2H, ArH).

5.3 Experimental procedures: the pyridazinone derivatives

5.3.1 Synthesis of the six-membered ring compounds (P1-18)

General procedure F for the synthesis of 1-oxo-3,4-dihydronaphthalene-2(1H)-ylidene) acetic acids (13a-c)

To a mixture of the appropriate tetralones (20.5 mmol) and glyoxylic acid (6.08 g, 82.1 mmol) in 29 mL of water, a solution of NaOH (102 mmol) in water (49 mL) and of ethanol (25 mL) was added dropwise at a temperature between 10 ˚C and 15 ˚C. The solution was stirred at room temperature for 1 h and then refluxed for 3 h. The solution was cooled to room temperature and acidified with 6 N HCl until pH = 2. The precipitated solid was filtered, washed with water and dried to give the final unsaturated acids which were used in the next reaction without further purification.

1-oxo-3,4-dihydronaphthalene-2(1H)-ylidene) acetic acid (13a)

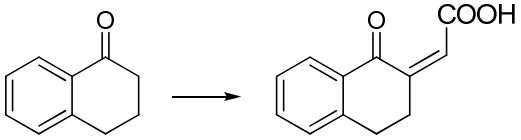

α-teralone **13a**

General procedure F was followed for the synthesis of **13a** from α-tetralone.

- White solid
- Yield: 55%
- TLC (dichloromethane/methanol 8:2) Rf = 0.3
- ^{1}H NMR ($CDCl_3$) 2.95 (t, 2H, CH_2), 3.09 (t, 2H, CH_2), 6.39 (s, 1H, CH=C), 7.46-7.73 (m, 4H, ArH), 11 (br s, 1H, COOH)

5,7-dimethoxy-1-oxo-3,4-dihydronaphthalene-2(1H)-ylidene) acetic acid (13b)

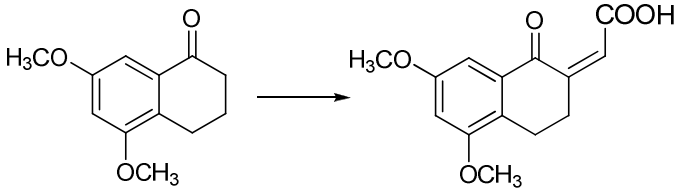

5,7-dimethoxy tetralone **13b**

General procedure F was followed for the synthesis of **13b** from 5,7-dimethoxy tetralone.

- Bright yellow solid
- Yield: 70%
- TLC (dichloromethane/methanol 9:1) Rf = 0.3
- ^{1}H NMR ($CDCl_3$) 2.90 (t, 2H, J=5.4 Hz, CH_2), 3.40 (t, 2H, J=5.4 Hz, CH_2), 3.85 (s, 1H, CH_3), 3.87 (s, 1H, CH_3), 6.65 (s, 1H, CH=C), 6.85 (s, 1H, ArH), 7.20 (s, 1H, ArH)

6-chloro-1-oxo-3,4-dihydronaphthalene-2(1H)-ylidene) acetic acid (13c)

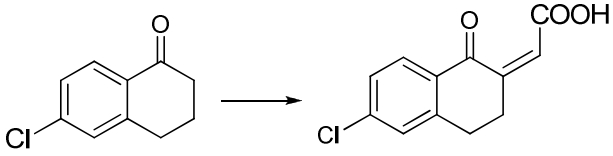

6-chloro-tetralone **13c**

General procedure F was followed for the synthesis of **13a** from 6-chloro-tetralone.

- Yellow oil
- Yield: 73%
- TLC (dichloromethane/methanol 9:1) Rf = 0.4
- ^{1}H NMR ($CDCl_3$) 3.0 (t, 2H, J=5.4 Hz, CH_2), 3.45 (t, 2H, J=5.4 Hz, CH_2), 6.90 (s, 1H, CH=C), 7.30 (s, 1H, ArH), 7.35 (d, 2H, J=10.7 Hz, ArH), 8.05 (d, 1H, J=10.7 Hz, ArH)

General procedure G for the synthesis of 2-(1-oxo-1,2,3,4-tetrahydronaphthalen-2-yl)acetic acids (14a-c)

The suitable unsaturated acid (11.4 mmol) was solubilized in a mixture of 39 mL of acetic acid and 14 mL of water. Zinc dust (0.85 g, 13 mmol) was then added and the suspension was stirred at reflux for 40 min. The suspension was then filtered to remove the zinc dust and

extracted with ethyl acetate (3 x 10 mL). The organic layer was dried over anhydrous sodium sulfate and evaporated under reduced pressure. The final saturated acid was used in the following reaction without further purification.

2-(1-oxo-1,2,3,4-tetrahydronaphthalen-2-yl)acetic acids (14a)

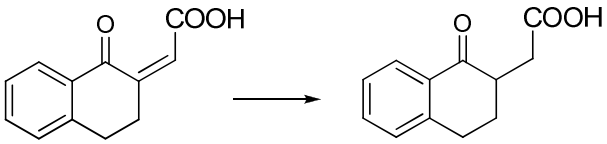

13a **14a**

General procedure G was followed for the synthesis of **14a** from **13a**.

- Red solid
- Quantitative yield
- TLC (dichloromethane/methanol 9:1) Rf = 0.4
- ^{1}H NMR (CD_3OD) 1.91-2.60 (m, 1H, CH), 2.21-2.30 (m, 1H, CH), 2.42-2.52 (m, 1H, CH), 2.82-2.92 (m, 1H, CH), 2.94-3.05 (m, 1H, CH), 3.08-3.20 (m, 1H, CH), 3.44-3.53 (m, 1H, CH) 7.25-8.0 (m, 4H, ArH)

5,7-dimethoxy-2-(1-oxo-1,2,3,4-tetrahydronaphthalen-2-yl)acetic acids (14b)

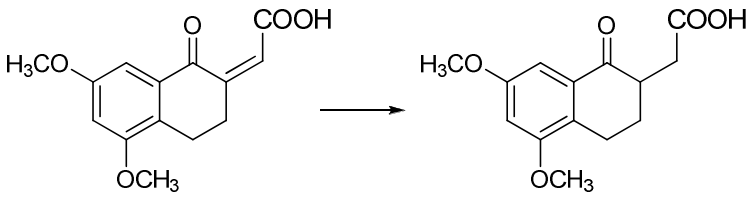

13b **14b**

General procedure G was followed for the synthesis of **14b** from **13b**.

- Red solid
- Quantitative yield
- TLC (dichloromethane/methanol 9:1) Rf = 0.6

6-chloro-2-(1-oxo-1,2,3,4-tetrahydronaphthalen-2-yl)acetic acids (14c)

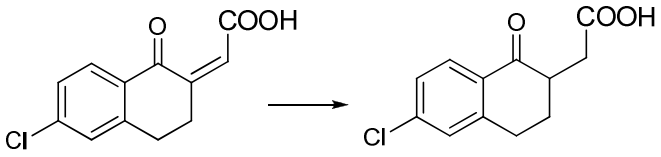

13c **14c**

General procedure G was followed for the synthesis of **14c** from **13c**.

- Yellow/orange solid
- Quantitative yield
- TLC (dichloromethane/methanol 9:1) Rf = 0.7
- ^{1}H NMR ($CDCl_3$) 1.90-2.10 (m, 1H, CH), 2.20-2.30 (m, 1H, CH), 2.40-2.60 (m, 1H, CH), 2.80-3.10 (m, 4H, CH_2), 7.25 (m, 2H, ArH), 7.95 (d, 1H, ArH)

General procedure H for the synthesis of 4,4a,5,6-tetrahydrobenzo[h]cinnolin-3(2H)-ones (P1a-c)

The suitable acid (11.26 mmol) was dissolved in ethanol (3 mL) and hydrazine monohydrate was added (13.6 mmol). The solution was stirred at reflux for 3 h. The final benzocinnolinones precipitated in the reaction mixture. They were filtered, washed with ethanol and dried.

4,4a,5,6-tetrahydrobenzo[h]cinnolin-3(2H)-one (P1a)

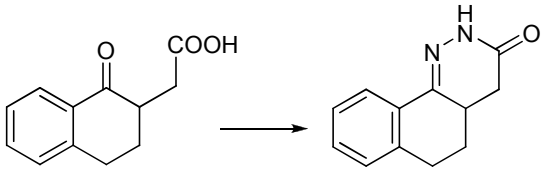

14a **P1a**

General procedure H was followed for the synthesis of **P1a** from **14a**.

- Light yellow solid
- Yield: 81%
- TLC (dichloromethane/methanol 95:5) Rf = 0.5
- M.p. 200 °C [95]

- ^{1}H NMR (CD_3OD) 1.41 (m, 1H, CH), 1.7-1.5 (m, 2H, CH_2), 2.3-2.1 (m, 2H, CH_2), 2.85-2.75 (t, 2H, CH_2), 7.0 (br s, 1H, NH), 7.30-7.78 (m, 4H, ArH)
- Cell proliferation assay (**Appendix III**)

5,7-dimethoxy-4,4a,5,6-tetrahydrobenzo[h]cinnolin-3(2H)-one (P1b)

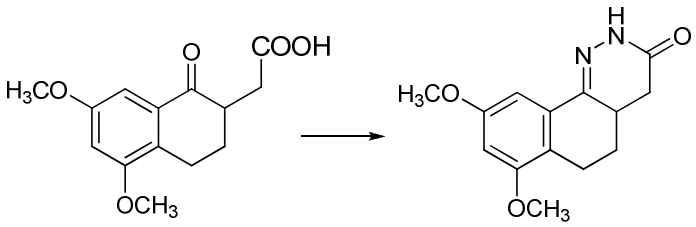

14b **P1b**

General procedure H was followed for the synthesis of **P1b** from **14b**.

- Grey solid
- Yield: 72%
- TLC (dichloromethane/methanol 95:5) Rf = 0.7
- ^{1}H NMR ($CDCl_3$) 2.10-2.45 (m, 2H, CH), 2.65-2.85 (m, 2H, CH_2), 3.10-3.20 (m, 2H, CH_2), 3.85 (s, 3H, CH_3), 3.87 (s, 3H, CH_3), 6.45 (s, 1H, ArH), 7.20 (s, 1H, ArH), 8.45 (br s, 1H, NH)

6-chloro-4,4a,5,6-tetrahydrobenzo[h]cinnolin-3(2H)-one (P1c)

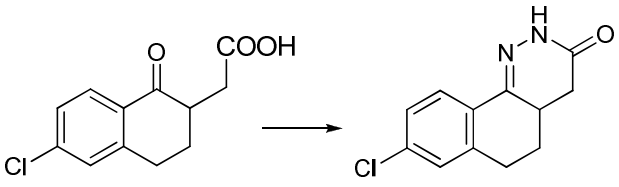

14c **P1c**

General procedure H was followed for the synthesis of **P1c** from **14c**.

- Light brown solid
- Yield: 60%
- TLC (dichloromethane/methanol 95:5) Rf = 0.5
- ^{1}H NMR ($CDCl_3$) 1.60 (m, 1H, CH), 2.20-2.35 (m, 2H, CH_2), 2.60-2.75 (m, 2H, CH_2), 2.80-2.95 (m, 2H, CH_2), 7.20 (m, 2H, ArH), 7.95-8.05 (m, 1H, ArH), 8.45 (br s, 1H, NH)

5,6-dihydrobenzo[h]cinnolin-3(2H)-one (P2a)

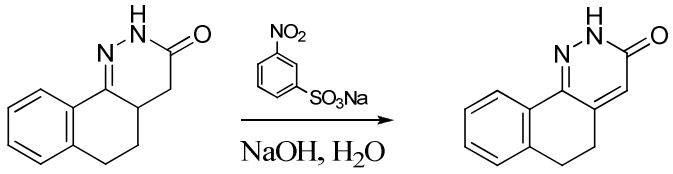

P1a **P2a**

A mixture of compound **P1a** (0.1 g, 0.50 mmol), sodium *m*-nitro-benzenesulfonate (0.112 g, 0.50 mmol), NaOH (8 x 10^{-2} g, 2 mmol) in water (2 mL) was refluxed for 30 min. After cooling, compound **P2a** was extracted with ethyl acetate (3 x 1 mL). The organic layer was dried over anhydrous Na_2SO_4, filtered and the solvent was evaporated under reduced pressure. The obtained residue was purified by flash chromatography (eluent: dichloromethane/methanol 9.7:0.3).

- Yellow solid
- Yield: 90%
- TLC (dichloromethane/methanol 95:5) Rf = 0.4
- ^{1}H NMR ($CDCl_3$) 2.90 (m, 4H, CH_2), 6.80 (s, 1H, CH), 7.20-7.40 (m, 3H, ArH), 8.0-8.10 (m, 1H, ArH), 10.45 (br s, 1H, NH)

General procedure I for the synthesis of ethyl 2-(3-oxo-4,4a,5,6-tetrahydrobenzo[h] cinnolin-2(3H)-yl)esters (P3-8a, P5b, P5c) and of ethyl-7,9-dimethoxy-2-(3-oxo-5,6-dihydrobenzo[h] cinnolin-2(3H)-yl)butanoate (P15b)

To a solution of the required benzocinnolinone derivative (0.25 mmol) in dry dimethylformamide (2 mL), NaH (7.2 x 10^{-3} g, 0.3 mmol) and the $Br(CH_2)_nCOOCH_2CH_3$ (0.3 mmol) were added. The mixture was stirred at 70 ˚C for 15 h. It was then evaporated under reduced pressure to remove the solvent and extracted with ethyl acetate (3 x 2 mL). The organic layers were collected, dried over Na_2SO_4, and evaporated under reduced pressure. Upon purification by flash chromatography thick oils of the final products were obtained.

Ethyl 2-(3-oxo-4,4a,5,6-tetrahydrobenzo[h]cinnolin-2(3H)-yl)acetate (P3a)

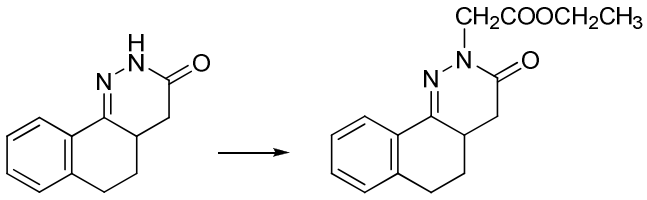

P1a **P3a**

General procedure I was followed for the synthesis of **P3a** from **P1a**.

- Light yellow oil
- Yield: 71%
- TLC (dichloromethane/methanol 95:5) Rf = 0.6
- ^{1}H NMR ($CDCl_3$) 1.29 (t, 3H, CH_3), 1.41 (dq, 1H, CH), 1.7-1.5 (dd, 2H, CH_2), 2.3-2.1 (dd, 2H, CH_2), 2.85-2.75 (dd, 2H, CH_2), 4.13 (q, 2H, CH_2), 4.16 (d, 2H, CH_2), 7.30-7.78 (m, 4H, ArH)

Ethyl 3-(3-oxo-4,4a,5,6-tetrahydrobenzo[h]cinnolin-2(3H)-yl)propanoate (P4a)

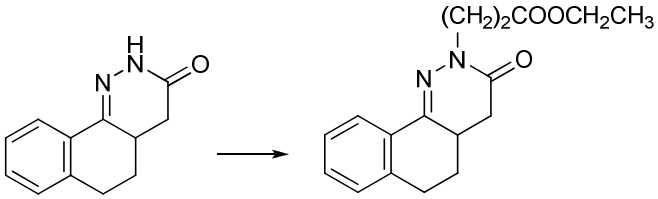

P1a **P4a**

General procedure I was followed for the synthesis of **P4a** from **P1a**.

- Light yellow oil
- Yield: 61%
- TLC (dichloromethane/methanol 95:5) Rf = 0.75
- ^{1}H NMR ($CDCl_3$) 1.29 (t, 3H,CH_3), 1.41 (dq, 1H, CH), 1.7-1.5 (dd, 2H, CH_2), 2.3-2.1 (dd, 2H, CH_2), 2.65 (d, 2H, CH_2), 2.85-2.75 (d, 2H, CH_2), 3.59 (dd, 2H, CH_2), 4.13 (dq, 2H, CH_2), 7.30-7.78 (m, 4H, ArH)
- Cell proliferation assay (**Appendix III**)

Ethyl 4-(3-oxo-4,4a,5,6-tetrahydrobenzo[h]cinnolin-2(3H)-yl)butanoate (P5a)

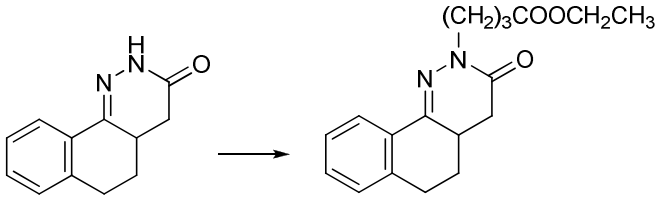

P1a **P5a**

General procedure I was followed for the synthesis of **P5a** from **P1a**.

- Light yellow oil
- Yield: 60%
- TLC (dichloromethane/methanol 95:5) Rf = 0.73
- ^{1}H NMR ($CDCl_3$) 1.29 (t, 3H,CH_3), 1.41 (dq, 1H, CH), 1.7-1.5 (dd, 2H, CH_2), 2.04 (d, 2H, CH_2), 2.3-2.1 (dd, 2H, CH_2), 2.47 (d, 2H,CH_2), 2.85-2.75 (dd, 2H, CH_2), 3.20 (q, 2H, CH_2), 4.13 (dq, 2H, CH_2), 7.30-7.78 (m, 4H, ArH)
- Cell proliferation assay (**Appendix III**)

Ethyl-7,9-dimethoxy-4-(3-oxo-4,4a,5,6-tetrahydrobenzo[h]cinnolin-2(3H)-yl)butanoate (P5b) and ethyl-7,9-dimethoxy-2-(3-oxo-5,6-dihydrobenzo[h]cinnolin-2(3H)-yl)butanoate (P15b)

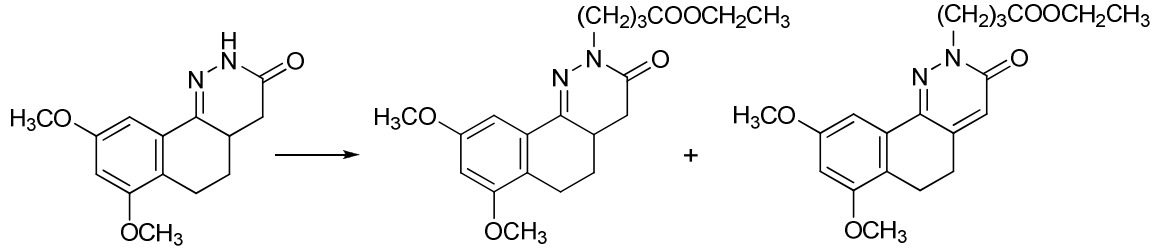

P1b **P5b** **P15b**

General procedure I was followed for the synthesis of **P5b** and **P15b** from **P1b**.

Compound **P5b**:

- Yellow solid
- Yield: 56%
- TLC (dichloromethane/methanol 95:5) Rf = 0.7

- ^{1}H NMR ($CDCl_3$) 1.25 (t, 3H, CH_3), 1.45 (m, 1H, CH), 2.0-2.40 (m, 6H, CH_2), 2.60-2.80 (m, 2H, CH_2), 3.15 (m, 2H, CH_2), 3.81 (s, 3H, CH_3), 3.85 (s, 3H, CH_3), 3.95 (m, 2H, CH_2), 4.15 (q, 2H, CH_2), 6.45 (s, 1H, ArH), 7.25 (s, 1H, ArH)

Compound **P15b**:

- Yellow solid
- Yield: 20%
- TLC (dichloromethane/methanol 95:5) Rf = 0.6
- ^{1}H NMR ($CDCl_3$) 1.25 (t, 3H, CH_3), 2.20-2.25 (m, 2H, CH_2), 2.35-2.45 (m, 2H, CH_2), 2.75-2.85 (m, 4H, CH_2), 3.85 (s, 3H, CH_3), 3.89 (s, 3H, CH_3), 4.15 (q, 2H, CH_2), 4.30 (t, 2H, CH_2), 6.50 (s, 1H, ArH), 6.80 (s, 1H, CH), 7.20 (s, 1H, ArH)

Ethyl-8-chloro-4-(3-oxo-4,4a,5,6-tetrahydrobenzo[h]cinnolin-2(3H)-yl)butanoate (P5c)

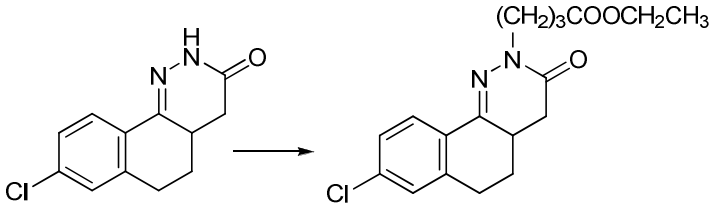

P1c **P5c**

General procedure I was followed for the synthesis of **P5c** from **P1c**

- Yellow solid
- Yield: 60%
- TLC (dichloromethane/methanol 95:5) Rf = 0.75
- ^{1}H NMR ($CDCl_3$) 1.25 (t, 3H, CH_3), 1.50 (m, 1H, CH), 2.20-2.40 (m, 6H, CH_2), 2.60-2.95 (m, 4H, CH_2), 3.80-4.0 (m, 2H, CH_2), 4.10 (q, 2H, CH_2), 7.10-7.25 (m, 3H, ArH), 8.05 (d, 1H, ArH)

Ethyl 5-(3-oxo-4,4a,5,6-tetrahydrobenzo[h]cinnolin-2(3H)-yl)pentanoate (P6a)

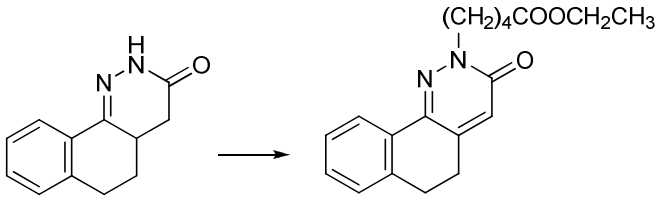

P1a **P6a**

General procedure I was followed for the synthesis of **P6a** from **P1a**.

- Yellow oil
- Yield: 50%
- TLC (dichloromethane/methanol 95:5) Rf = 0.65
- ^{1}H NMR ($CDCl_3$) 1.29 (t, 3H,CH_3), 1.41 (dq, 1H, CH), 1.52 (d, 2H, CH_2), 1.64 (d, 2H, CH_2), 1.7-1.5 (dd, 2H, CH_2), 2.3-2.1 (dd, 2H, CH_2), 2.32 (d, 2H,CH_2), 2.85-2.75 (dd, 2H, CH_2), 3.20 (q, 2H, CH_2), 4.13 (dq, 2H, CH_2), 7.30-7.78 (m, 4H, ArH)

Ethyl 6-(3-oxo-4,4a,5,6-tetrahydrobenzo[h]cinnolin-2(3H)-yl)hexanoate (P7a)

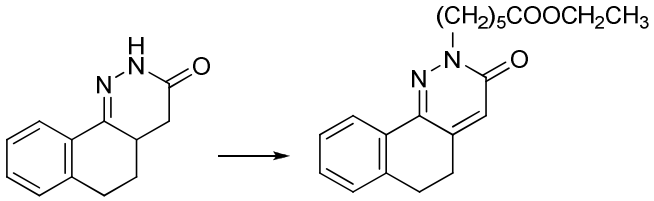

P1a **P7a**

General procedure I was followed for the synthesis of **P7a** from **P1a**.

- Yellow oil
- Yield: 70%
- TLC (dichloromethane/methanol 95:5) Rf = 0.82
- ^{1}H NMR ($CDCl_3$) 1.29 (t, 5H, CH_3, CH_2), 1.41 (dq, 1H, CH), 1.52 (t, 2H, CH_2), 1.64 (t, 2H, CH_2), 1.7-1.5 (dd, 2H, CH_2), 2.3-2.1 (dd, 2H, CH_2), 2.32 (dd, 2H,CH_2), 2.85-2.75 (dd, 2H, CH_2), 3.20 (t, 2H, CH_2), 4.13 (dq, 2H, CH_2), 7.30-7.78 (m, 4H, ArH)

Ethyl 7-(3-oxo-4,4a,5,6-tetrahydrobenzo[h]cinnolin-2(3H)-yl)heptanoate (P8a)

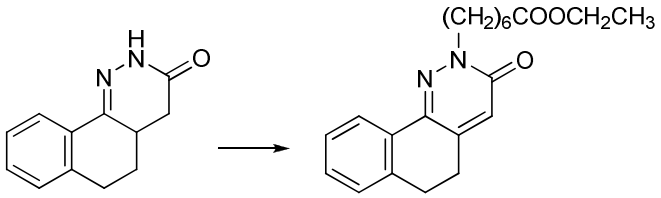

P1a **P8a**

General procedure I was followed for the synthesis of **P8a** from **P1a**.

- Yellow oil
- Yield: 70%
- TLC (dichloromethane/methanol 95:5) Rf = 0.8
- ^{1}H NMR ($CDCl_3$) 1.29 (m, 7H, CH_3, CH_2, CH_2), 1.41 (dq, 1H, CH), 1.52 (d, 2H, CH_2), 1.64 (d, 2H, CH_2), 1.7-1.5 (dd, 2H, CH_2), 2.3-2.1 (dd, 2H, CH_2), 2.32 (d, 2H,CH_2), 2.85-2.75 (dd, 2H, CH_2), 3.20 (t, 2H, CH_2), 4.13 (dq, 2H, CH_2), 7.30-7.78 (m, 4H, ArH)

General procedure J for the synthesis of 4-(3-oxo-4,4a,5,6-tetrahydrobenzo[h]cinnolin-2(3H)-yl)carboxilic acids (P4aa, P5aa)

The required ester (0.464 mmol) was dissolved in ethanol (5 mL) and an aqueous solution of 1 N NaOH (3 mL) was added. The solution was stirred at reflux for 2 h. Then the solvent was removed under reduced pressure and the residue was diluted with water (5 mL) and extracted with ethyl acetate (1 x 2 mL). The aqueous layer was acidified with 6 N HCl (1 mL) and extracted with ethyl acetate (3 x 2 mL). The organic layer was dried over Na_2SO_4 anhydrous and evaporated under reduced pressure.

4-(3-oxo-4,4a,5,6-tetrahydrobenzo[h]cinnolin-2(3H)-yl)propanoic acid (P4aa)

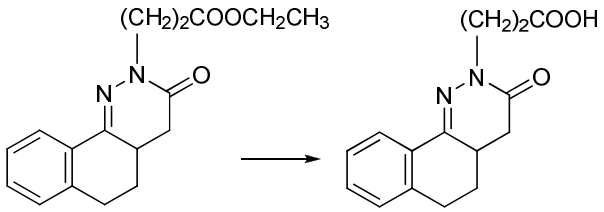

P4a **P4aa**

General procedure J was followed for the synthesis of **P4aa** from **P4a**.

- Yellow solid
- Yield: 97%
- TLC (dichloromethane/methanol 9:1) Rf = 0.40
- ^{1}H NMR ($CDCl_3$) 1.41 (dq, 1H,CH), 1.7-1.5 (t, 2H, CH_2), 1.92 (d, 2H, CH_2) , 2.3-2.1 (t, 2H, CH_2), 2.3 (d, 2H, CH_2), 2.85-2.75 (dd, 2H, CH_2) 3.20 (d, 2H, CH_2), 7.30-7.78 (m, 4H, ArH), 11 (s, 1H, OH)

4-(3-oxo-4,4a,5,6-tetrahydrobenzo[h]cinnolin-2(3H)-yl)butanoic acid (P5aa)

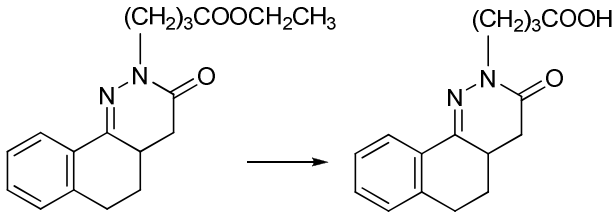

P5a **P5aa**

General procedure J was followed for the synthesis of **P5aa** from **P5a**.

- Yellow solid
- Yield: 97%
- TLC (dichloromethane/methanol 9:1) Rf = 0.50
- ^{1}H NMR ($CDCl_3$) 1.55-1.70 (m, 1H, CH), 2.0-2.50 (m, 6H, CH_2), 2.70-3.0 (m, 4H, CH_2), 3.90-4.0 (m, 2H, CH_2), 7.15-7.35 (m, 3H, ArH), 8.15 (d, 1H, ArH)
- Cell proliferation assay (**Appendix III**)

N-ethyl-4-(3-oxo-4,4a,5,6-tetrahydrobenzo[h]cinnolin-2(3H)-yl)butanamide (P9a)

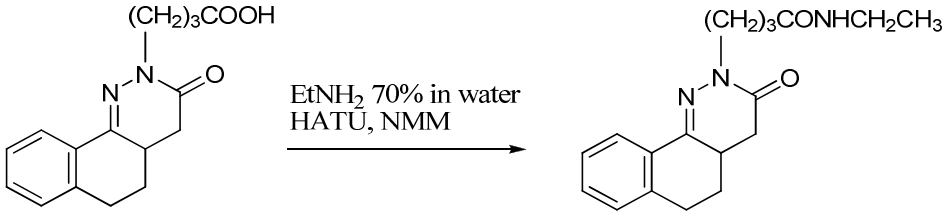

P5aa **P9a**

To a solution of compound **P5aa** (3.7×10^{-2} g, 0.13 mmol) in dichloromethane (3 mL), the coupling agent HATU (7.41×10^{-2} g, 0.20 mmol), ethylamine (0.02 mL, 0.35 mmol) and *N*-

methyl morpholine (until ph =7) were added. The mixture was stirred at room temperature for 1 h and then washed with 1 N HCl solution (2 x 1 mL), with saturated $NaHCO_3$ solution (2 x 1 mL) and finally with brine (2 x 1 mL). The organic layer was separated, dried over anhydrous Na_2SO_4 and evaporated under reduced pressure to obtain **P9b**.

- Pale pink solid
- Yield: 83%
- TLC (dichloromethane/methanol 9:1) Rf = 0.65
- ^{1}H NMR ($CDCl_3$) 1.04 (m, 3H, CH_3), 1.41 (dq,1H, CH), 1.7-1.5 (dd, 2H, CH_2), 1.93 (m, 2H, CH_2), 2.3-2.1 (dd, 2H, CH_2), 2.34 (dd, 2H, CH_2), 2.85-2.75 (m, 2H, CH_2), 3.11 (t, 2H, CH_2), 3.20 (dq, 2H, CH_2), 7.30-7.78 (m, 4H, ArH), 8.03 (br s, 1H, NH)

2-(4-bromobutyl)-4,4a,5,6-tetrahydrobenzo[h]cinnolin-3(2H)-one (18)

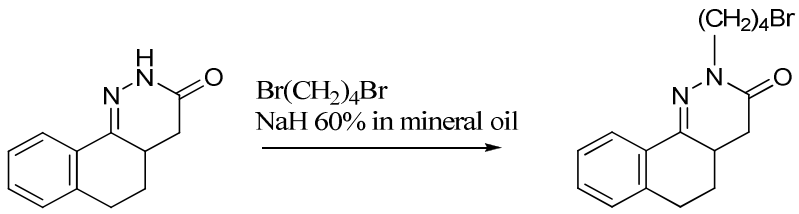

P1a **18**

To a solution of **P1a** (5 x10^{-2} mg, 0.25 mmol) in dry dimethylformamide, NaH (7.2 x 10^{-3} g, 0.3 mmol) and $Br(CH_2)_4Br$ (0.036 mL, 0.3 mmol) were added. The mixture was irradiated for 10 min at 60 ˚C in a microwave synthesizer. The solution was evaporated under reduced pressure to remove dimethylformamide and extracted with ethyl acetate (3 x 2 mL). The organic layer was separated, dried over anhydrous Na_2SO_4, and evaporated under reduced pressure. Upon purification by flash chromatography (eluent: petroleum ether/ethyl acetate 7:3) compound **18** was obtained.

- White solid
- Yield: 64%
- TLC (dichloromethane/methanol 95:5) Rf = 0.73
- ^{1}H NMR ($CDCl_3$) 1.41 (dq, 1H, CH), 1.52 (d, 2H, CH_2), 1.7-1.5 (dd, 2H, CH_2), 1.82 (d, 2H, CH_2), 2.3-2.1 (dd, 2H, CH_2), 2.85-2.75 (m, 2H, CH_2), 3.20 (dq, 2H, CH_2), 3.51 (t, 2H, CH_2), 7.30-7.78 (m, 4H, ArH)

2-(4-(ethylamino)butyl)-4,4a,5,6-tetrahydrobenzo[h]cinnolin-3(2H)-one (P10a)

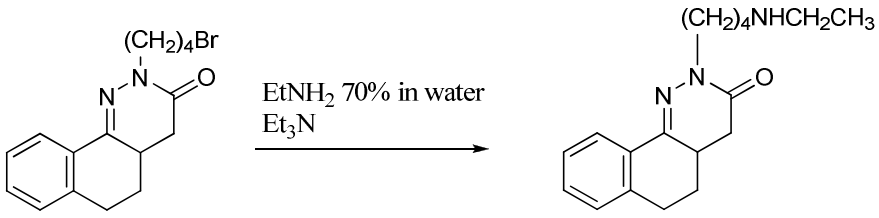

18 **P10a**

To a solution of compound **18** (4.6 x 10^{-2} g, 0.14 mmol) in dimethylformamide (2 mL), ethylamine (0.011 mL, 0.17 mmol) and triethylamine (0.024 mL, 0.17 mmol) were added and the mixture was stirred at 50 °C for 7 h. The solvent was removed under reduced pressure and the residue diluted with water (2 mL) and extracted with ethyl acetate (3 x 1 mL). The organic layer was dried over anhydrous Na_2SO_4 and evaporated under reduced pressure. Upon purification by flash chromatography (eluent: dichloromethane/methanol 9:1) **P10a** was obtained.

- Yellow oil
- Yield: 50%
- TLC (dichloromethane/methanol 9:1) Rf = 0.17
- ^{1}H NMR ($CDCl_3$) 1.02 (t, 3H, CH_3), 1.38 (m, 2H, CH_2), 1.41 (dq, 1H, CH), 1.52 (dd, 2H, CH_2), 1.7-1.5 (dd, 2H, CH_2), 2.0 (br s, 1H, NH), 2.3-2.1 (dd, 2H, CH_2), 2.55 (d, 2H, CH_2), 2.59 (d, 2H, CH_2), 2.85-2.75 (dd, 2H, CH_2), 3.20 (dq, 2H, CH_2), 7.30-7.78 (m, 4H, ArH)

Genral procedure K for the synthesis of 2-alkyl-4,4a,5,6-tetrahydrobenzo[h]cinnolin-3[2H]-ones (P11a, P12a)

To a solution of **P1a** (0.25 mmol) in dry dimethylformamide (2 mL), NaH 60% in mineral oil (1.2 x 10^{-2} g, 0.3 mmol) and $Br(CH_2)_nCH_3$ (0,3 mmol) were added and the mixture was stirred at 80 ˚C for 15 h. The solvent was evaporated under reduced pressure and the residue was extracted with ethyl acetate (3 x 2 mL). The organic layers were collected, dried over anhydrous Na_2SO_4, and evaporated under reduced pressure. Upon purification by flash chromatography (eluent: petroleum ether/ethyl acetate 8:2) the final products were obtained as yellow oils.

2-butyl-4,4a,5,6-tetrahydrobenzo[h]cinnolin-3[2H]-ones (P11a) and 2-butyl-4,4a,5,6-tetrahydrobenzo[h]cinnolin-3[2H]-ones (P17a)

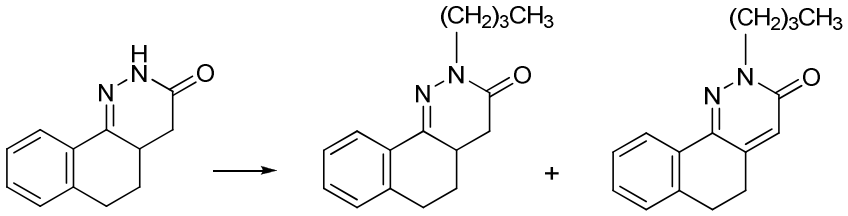

P1a **P11a** **P17a**

General procedure K was followed for the synthesis of **P11a** and **P17a** from **P1a**.

Compound **P11a**:

- Yellow oil
- Yield: 75%
- TLC (petroleum ether/ethyl acetate 8:2) Rf = 0.70
- ^{1}H NMR ($CDCl_3$) 0.95 (t, 3H, CH_3), 1.30-1.45 (m, 2H, CH_2), 1.50-1.75 (m, 5H, CH), 2.15-2.30 (m, 2H, CH_2), 2.60-3.95 (m, 4H, CH_2), 3.75-4.0 (m, 2H, CH_2), 7.15-7.35 (m, 3H, ArH), 8.15 (d, 1H, ArH)

Compound **P17a**:

- Yellow oil
- Yield: 25%
- TLC (petroleum ether/ethyl acetate 8:2) Rf = 0.60
- ^{1}H NMR ($CDCl_3$) 0.95 (t, 3H, CH_3), 1.30-1.45 (m, 2H, CH_2), 1.80-1.95 (m, 2H, CH), 2.80-3.0 (m, 4H, CH_2), 4.20-4.30 (m, 2H, CH_2), 6.75 (s, 1H, CH), 7.15-7.35 (m, 3H, ArH), 8.15 (d, 1H, ArH)

2-pentyl-4,4a,5,6-tetrahydrobenzo[h]cinnolin-3[2H]-ones (P12a) and

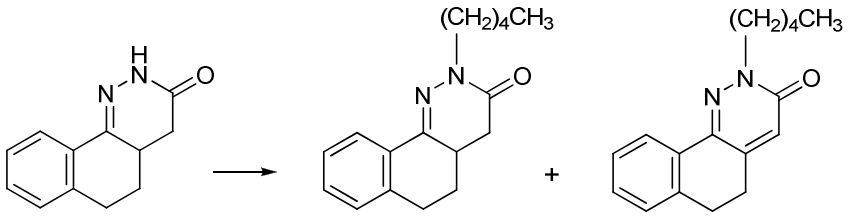

P1a **P12a** **P18a**

General procedure K was followed for the synthesis of **P12a** and **P18a** from **P1a**.

Compound **P12a**:

- Yellow oil
- Yield: 80%
- TLC (petroleum ether/ethyl acetate 8:2) Rf = 0.70
- ^{1}H NMR ($CDCl_3$) 0.95 (t, 3H, CH_3), 1.20-1.35 (m, 4H, CH_2), 1.50-1.80 (m, 4H, CH), 2.15-2.30 (m, 2H, CH_2), 2.60-3.95 (m, 4H, CH_2), 3.75-4.0 (m, 2H, CH_2), 7.15-7.35 (m, 3H, ArH), 8.15 (d, 1H, ArH)

Compound **P18a**:

- Yellow oil
- Yield: 80%
- TLC (petroleum ether/ethyl acetate 8:2) Rf = 0.60
- ^{1}H NMR ($CDCl_3$) 0.95 (t, 3H, CH_3), 1.30-1.50 (m, 4H, CH_2), 1.80-1.95 (m, 2H, CH), 2.80-3.0 (m, 4H, CH_2), 4.20-4.25 (m, 2H, CH_2), 6.75 (s, 1H, CH), 7.15-7.35 (m, 3H, ArH), 8.15 (d, 1H, ArH)

2-(3-hydroxypropyl)-4,4a,5,6-tetrahydrobenzo[h]cinnolin-3(2H)-one (19)

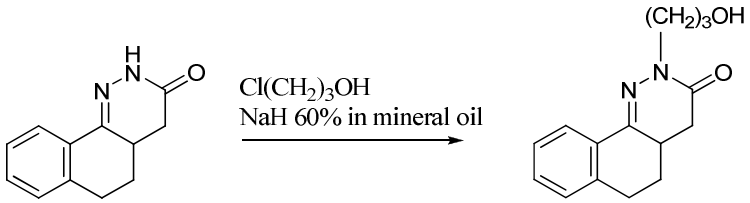

P1a **19**

A mixture of **P1a** (5.7×10^{-2} g, 0.28 mmol) in dimethylformamide (2 mL) and NaH 60% in mineral oil (1.34×10^{-2} g, 0.56 mmol) was stirred for 15 min. Then $Cl(CH_2)_3OH$ (0.025 mL, 0.30 mmol) was added and the mixture was stirred for further 4 h at 60 ˚C. The solvent was removed under reduced pressure, the residue was diluted with water (2 mL) and extracted with ethyl acetate (3 x 1 mL). The organic layer was dried over anhydrous Na_2SO_4 and evaporated under reduced pressure. Upon purification by flash chromatography (eluent: petroleum ether/ethyl acetate 1:1) **19** was obtained.

- Light yellow oil
- Yield: 53%

- TLC (dichloromethane/methanol 95:5) Rf = 0.49
- ^{1}H NMR ($CDCl_3$) 1.41 (dq, 1H, CH), 1.7-1.5 (m, 2H, CH_2), 1.75 (d, 2H, CH_2), 2.3-2.1 (dd, 2H, CH_2), 2.85-2.75 (dd, 2H, CH_2), 3.20 (t, 2H, CH_2), 3.50 (dq, 2H, CH_2), 3.65 (s, 1H, OH), 7.30-7.78 (m, 4H, ArH)

3-(3-oxo-4,4a,5,6-tetrahydrobenzo[h]cinnolin-2(3H)-yl)propyl 2-(tert-butoxycarbonyl amino)-3-phenylpropanoate (20)

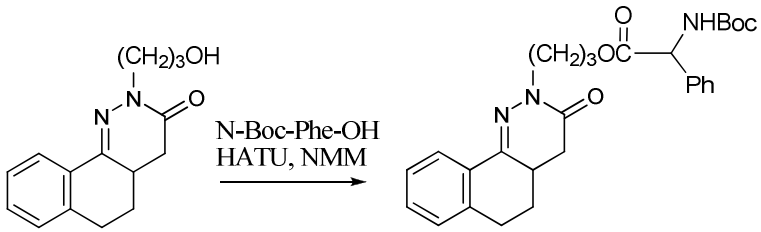

19 **20**

To a solution of **19** (4 x 10^{-2} g, 0.15 mmol) in dichloromethane (3 mL) *N*-Boc-Phe-OH (1.1 x 10^{-2} g, 0.40 mmol) and the coupling agent HATU (8.8 x 10^{-2} g, 0.23 mmol) were added. The solution was brought to pH = 7 with drops of *N*-methylmorpholine. It was stirred at room temperature for 24 h. The solvent was removed under reduced pressure, the residue diluted with dichloromethane (3 mL) and washed respectively with: 1 N HCl (3 × 1 mL), saturated solution of $NaHCO_3$ (3 × 1 mL) and brine (2 × 1 mL). The solvent was dried with Na_2SO_4 and evaporated. The crude product was purified by flash chromatography (eluent: dichloromethane/ethyl acetate 85:15) to obtain compound **20**.

- Yellow oil
- Yield: 33%
- TLC (dichloromethane/ethyl acetate 75:25) Rf = 0.38
- ^{1}H NMR ($CDCl_3$) 1.38 (m, 9H, $3CH_3$), 1.41 (dq, 1H, CH), 1.7-1.5 (t, 2H, CH_2), 1.84 (d, 2H, CH_2), 2.3-2.1 (dd, 2H, CH_2), 2.85-2.75 (dd, 2H, CH_2), 3.20 (dq, 2H, CH_2), 3.23-2.98 (dd, 2H, CH_2), 4.08 (t, 2H, CH_2), 4.68 (dq, 1H, CH), 7.27-7.40 (m, 5H, ArH), 7.30-7.78 (m, 4H, ArH), 8.03 (br s, 1H, NH)

3-(3-oxo-4,4a,5,6-tetrahydrobenzo[h]cinnolin-2(3H)-yl)propyl 2-amino-2-hydroxyacetate (P13a)

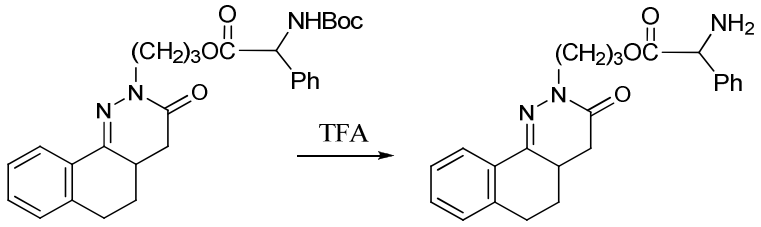

20 **P13a**

Compound **20** (3 x 10^{-2} g, 0.06 mmol) was dissolved in dichloromethane (3 mL) and the solution was cooled to 0 ˚C with an ice bath. Trifluoroacetic acid (0.05 mL, 0.71 mmol) was slowly added and the solution was stirred at room temperature for 3 h. The reaction was monitored by TLC until completion. The mixture was cooled to 0 ˚C and treated with a slolution of 0.5 N NaOH (1 mL) and extracted with dichloromethane (3 x 1.5 mL). The organic layer was dried over anhydrous Na_2SO_4 and evaporated under reduced pressure. Upon purification by flash chromatography (eluent: dichloromethane/ethyl acetate /methanol 6:3.5:0.5) **P13a** was obtained.

- Yellow oil
- Yield: 50%
- TLC (dichloromethane/methanol 9:1) Rf = 0.59
- ^{1}H NMR ($CDCl_3$) 1.41 (dq, 1H, CH), 1.7-1.5 (m, 2H, CH_2), 1.84 (d, 2H, CH_2), 2.3-2.1 (dd, 2H, CH_2), 2.85-2.75 (dd, 2H, CH_2), 3.20 (t, 2H, CH_2N), 3.65 (dq, 1H, OH), 4.08 (m, 2H, CH_2O), 5.11 (br s, 2H, NH_2), 5.19 (s, 1H, COCH), 7.30-7.78 (m, 4H, ArH)

General procedure L for the synthesis of ethyl 2-(3-oxo-5,6-dihydrobenzo[h]cinnolin-2(3H)-yl)esters (P14-P16a)

The required pyridazinone (0.25 mmol) was suspended in toluene (1.5 mL) and KOH (0.33 mmol), TBAF · $3H_2O$ (0.025 mmol) and the corresponding bromoalkyl ester (0.33 mmol) were added. The mixture was heated at 50 °C for 3 h. The mixture was then extracted with ethyl acetate (3 x 1mL) and the collected organic layer was washed with acqueous 5% NaOH (1 x 2mL) and with acqueous 5% HCl. The organic phase was dried over over anhydrous

Na_2SO_4 and evaporated under reduced pressure. Purification with flash chromatography was performed to obtain the final esters derivative.

Ethyl 2-(3-oxo-5,6-dihydrobenzo[h]cinnolin-2(3H)-yl)propanoate (P14a)

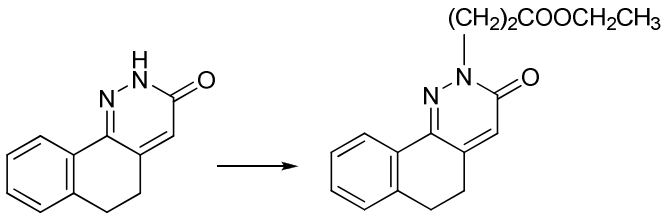

P2a **P14a**

General procedure L was followed for the synthesis of **P14a** from **P2a**. A purification of the crude product with flash chromatography (eluent: dichloromethane/ethyl acetate 6:4) was performed.

- Yellow oil
- Quantitative yield
- TLC (dichloromethane/methanol 95:5) Rf = 0.60
- ^{1}H NMR ($CDCl_3$) 1.25 (t, 3H, CH_3), 1.50-1.65 (m, 2H, CH_2), 2.80-3.0 (m, 4H, CH_2), 4.15 (q, 2H, CH_2), 4.25-4.30 (t, 2H, CH_2), 6.75 (s, 1H, CH), 7.20-7.40 (m, 3H, ArH), 8.0-8.10 (m, 1H, ArH)

Ethyl 2-(3-oxo-5,6-dihydrobenzo[h]cinnolin-2(3H)-yl)butanoate (P15a)

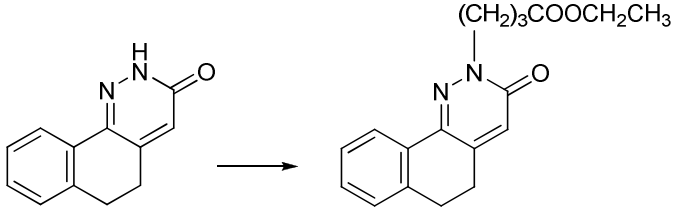

P2a **P15a**

General procedure L was followed for the synthesis of **P15a** from **P2a**. A purification with flash chromatography (eluent: dichloromethane/ethyl acetate 6:4) was performed.

- Yellow oil
- Quantitative yield
- TLC (dichloromethane/methanol 95:5) Rf = 0.70

- ^{1}H NMR ($CDCl_3$) 1.25 (t, 3H, CH_3), 2.15-2.27 (m, 2H, CH_2), 2.38-2.48 (m, 2H, CH_2), 2.80-2.95 (m, 4H, CH_2), 4.10 (q, 2H, CH_2), 4.25-4.32 (t, 2H, CH_2), 6.75 (s, 1H, CH), 7.20-7.40 (m, 3H, ArH), 8.0-8.10 (m, 1H, ArH)

Ethyl 2-(3-oxo-5,6-dihydrobenzo[h]cinnolin-2(3H)-yl)pentanoate (P16a)

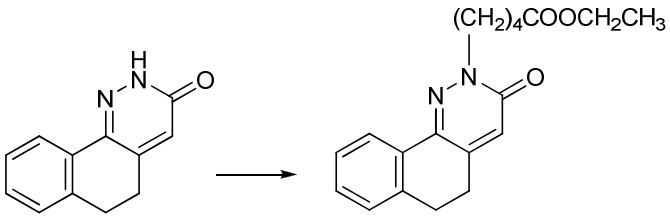

P2a **P16a**

General procedure L was followed for the synthesis of **P16a** from **P2a**. A purification with flash chromatography (eluent: dichloromethane/ethyl acetate 6:4) was performed.

- Yellow oil
- Quantitative yield
- TLC (dichloromethane/methanol 9:1) Rf = 0.75
- ^{1}H NMR ($CDCl_3$) 1.25 (t, 3H, CH_3), 2.15-2.27 (m, 2H, CH_2), 2.38-2.48 (m, 2H, CH_2), 2.80-2.95 (m, 4H, CH_2), 4.10 (q, 2H, CH_2), 4.25-4.32 (t, 2H, CH_2), 6.75 (s, 1H, CH), 7.20-7.40 (m, 3H, ArH), 8.0-8.10 (m, 1H, ArH)

4-(3-oxo-5,6-dihydrobenzo[h]cinnolin-2(3H)-yl)carboxilic acids (P14aa, P15aa)

4-(3-oxo-5,6-dihydrobenzo[h]cinnolin-2(3H)-yl)propanoic acid (P14aa)

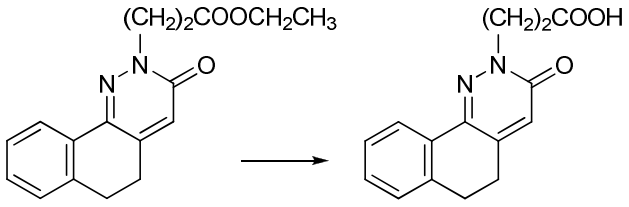

P14a **P14aa**

General procedure J was followed for the synthesis of **P14aa** from **P14a**.

- Yellow solid
- Quantitative yield
- TLC (dichloromethane/methanol 9:1) Rf = 0.50

- ^{1}H NMR ($CDCl_3$) 1.50-1.65 (m, 2H, CH_2), 2.80-3.0 (m, 4H, CH_2), 4.25-4.30 (t, 2H, CH_2), 6.75 (s, 1H, CH), 7.20-7.40 (m, 3H, ArH), 8.0-8.10 (m, 1H, ArH)

4-(3-oxo-5,6-dihydrobenzo[h]cinnolin-2(3H)-yl)butanoic acid (P15aa)

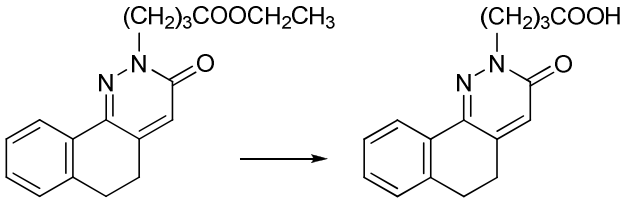

P15a **P15aa**

General procedure J was followed for the synthesis of **P15aa** from **P15a**.

- Yellow solid
- Quantitative yield
- TLC (dichloromethane/methanol 9:1) Rf = 0.60
- ^{1}H NMR ($CDCl_3$) 2.15-2.27 (m, 2H, CH_2), 2.38-2.48 (m, 2H, CH_2), 2.80-2.95 (m, 4H, CH_2), 4.25-4.32 (t, 2H, CH_2), 6.75 (s, 1H, CH), 7.20-7.40 (m, 3H, ArH), 8.0-8.10 (m, 1H, ArH)

5.3.2 Synthesis of the five- and seven-membered ring compounds (P19-26)

Synthesis of the unsaturated carboxylic acid 21 and 23

2-(1-oxo-1H-inden-2(3H)-ylidene)acetic acid (21)

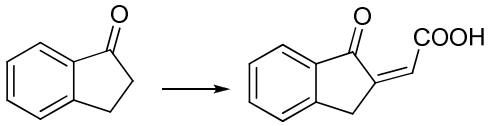

1-indanone **21**

General procedure F was followed for the synthesis of **21 from 1-indanone.** In this case the reaction mixture was stirred at rt for 2 h.

- Light yellow solid
- Yield: 64%
- TLC (dichloromethane/methanol 9:1) Rf = 0.32
- ^{1}H NMR ($CDCl_3$) 3.68 (d,2H, CH_2), 6.32 (dd, 1H, CH=C), 7.45-7.66 (m, 4H, ArH), 11.0 (br s, 1H, COOH)

2-(5-oxo-8,9-dihydro-5H-benzo[7]annulen-6(7H)-ylidene)acetic acid (23)

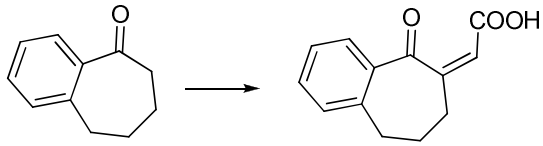

1-benzosuberone **23**

General procedure F was followed for the synthesis of **37** from 1-benzosuberone. In this case the reaction mixture was stirred at rt for 4 h.

- White solid
- Quantitative yield
- TLC (dichloromethane/methanol 9:1) Rf = 0.33
- ^{1}H NMR ($CDCl_3$) 1.66 (d, 2H, CH_2), 1.96 (d, 2H, CH_2), 2.85 (d, 2H, CH_2), 6.39 (dd, 1H, CH=C), 7.46-7.73 (m, 4H, ArH), 11.0 (br s, 1H, COOH)

Synthesis of the saturated carboxylic acid 22 and 24

2-(1-oxo-2,3-dihydro-1H-inden-2-yl)acetic acid (22)

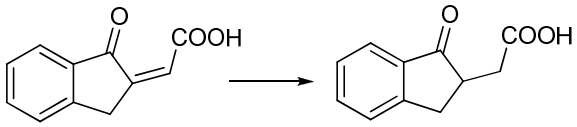

21 **22**

General procedure G was followed for the synthesis of **22** from **21**.

- Yellow solid
- Yield: 95%
- TLC (dichloromethane/methanol 9:1) Rf = 0.5
- ^{1}H NMR ($CDCl_3$) 2.71-2.46 (dd, 2H, CH_2), 2.83-2.58 (dt, 2H,CH_2), 3.70 (q, 1H, CH), 7.35-7.92 (m, 4H, ArH), 11.0 (br s, 1H, COOH)

2-(5-oxo-6,7,8,9-tetrahydro-5H-benzo[7]annulen-6-yl)acetic acid (24)

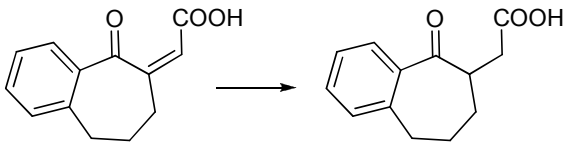

23 **24**

General procedure G was followed for the synthesis of **24** from **23**.

- Yellow/orange oil
- Quantitative yield
- TLC (dichloromethane/methanol 9:1) Rf = 0.61
- ^{1}H NMR ($CDCl_3$) 1.56-1.31 (m, 2H, CH_2), 1.90-1.80 (m, 2H, CH_2), 2.71-2.46 (dd, 2H, CH_2), 2.88-2.84 (dd, 2H,CH_2), 3.31 (q, 1H, CH), 7.35-7.92 (m, 4H, ArH), 11.0 (br s, 1H, COOH)

Synthesis of the pyridazinones P19 and P23

4a,5-dihydro-2H-indeno[1,2-c]pyridazin-3(4H)-one (P19)

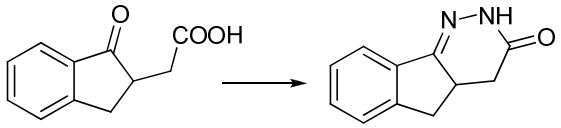

22 **P19**

General procedure H was followed for the synthesis of **P19** from **22**.

- white crystalline solid

- Yield: 79%
- TLC (dichloromethane/methanol 95:5) Rf = 0.48
- ^{1}H NMR ($CDCl_3$) 2.29 (t, 1H, CH), 2.3-2.1 (dd, 2H, CH_2), 2.7-2.4 (dd, 2H,CH_2), 7.0 (br s, 1H, NH), 7.30-7.78 (m, 4H, ArH)
- Cell proliferation assay (**Appendix III**)

2,4,4a,5,6,7,-hexahydro-3H-benzo[6,7]-cyclohepta[1,2-c]pyridazin-3-one (P23)

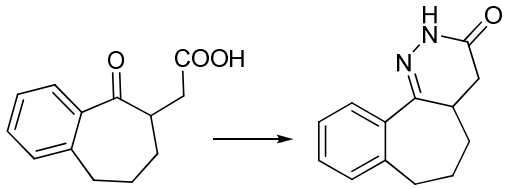

24 **P23**

General procedure H was followed for the synthesis of **P23** from **24**.

- white crystalline solid
- Yield: 75%
- TLC (dichloromethane/methanol 95:5) Rf = 0.57
- M.p. 187˚C [95]
- ^{1}H NMR ($CDCl_3$) 1.41 (m, 1H, CH), 1.4-1.2 (dd, 2H, CH_2), 1.90-1.80 (dd, 2H, CH_2), 2.3-2.1 (dd, 2H, CH_2), 2.88-2.84 (m, 2H,CH_2), 7 .0 (br s, 1H, NH), 7.30-7.78 (m, 4H, ArH)
- Cell proliferation assay (**Appendix III**)

2H-indeno[1,2-c]pyridazin-3(5H)-one (P20)

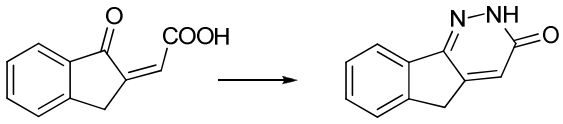

21 **P20**

General procedure H was followed for the synthesis of **P20** from **21**. In this case, the product needed a purification with flash chromatography (eluent: dichloromethane/ethyl acetate/methanol 8:1.8:0.2).

- Yellow solid
- Yield: 57%
- TLC (dichloromethane/methanol 9:1) Rf = 0.50
- ^{1}H NMR ($CDCl_3$) 3.95 (s, 2H, CH_2), 7.0 (s, 1H, CH), 7.40-7.55 (m, 3H, ArH), 7.80-7.90 (m, 1H, ArH)

2,5,6,7-tetrahydro-3H-benzo[6,7]-cyclohepta[1,2-c]pyridazin-3-one (P24)

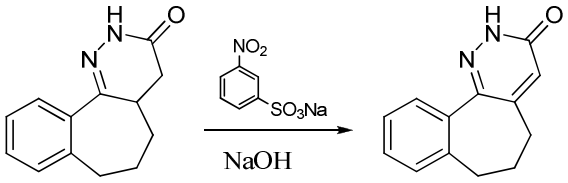

P23 **P24**

The procedure for the synthesis of compound **P24**, starting from **P23**, was the same to that used for the synthesis of compound **P2a**.

- Light yellow solid
- Yield: 75%
- TLC (dichloromethane/methanol 9:1) Rf = 0.50
- ^{1}H NMR ($CDCl_3$) 2.10-2.20 (m, 2H, CH_2), 2.40-2.50 (m, 2H, CH_2), 2.60-2.70 (m, 2H, CH_2), 6.85 (s, 1H, CH), 7.20-7.25 (m, 2H, ArH), 7.35-7.40 (m, 2H, ArH), 7.50-7.55 (m, 1H, ArH)

Synthesis of the saturated esters P21 and P25

Ethyl 4-(3-oxo-3,4,4a,5-tetrahydro-2H-indeno[1,2-c]pyridazin-2-yl)butanoate (P21)

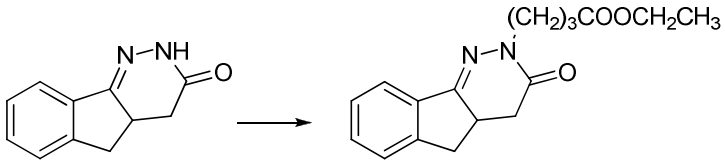

P19 **P21**

General procedure I was followed for the synthesis of **P21** from **P19**.

- Yellow oil
- Yield: 55%
- TLC (dichloromethane/methanol 95:5) Rf = 0.75
- ^{1}H NMR ($CDCl_3$) 1.29 (t, 3H, CH_3), 2.0-2.10 (m, 2H, CH_2), 2.25-2.40 (m, 3H, CH, CH_2), 2.65-2.80 (m, 1H, CH_2), 2.85-2.95 (m, 1H, CH_2), 3.0-3.20 (m, 1H, CH_2), 3.35-45 (m, 1H, CH), 3.75-3.90 (m, 1H, CH), 3.95-4-15 (m, 3H, CH, CH_2), 7.30-7.45 (m, 3H, ArH), 7.70-7.80 (m, 1H, ArH)
- Cell proliferation assay (**Appendix III**)

Ethyl-4-(3-oxo-2,5,6,7-hexahydro-3H-benzo[6,7]-cyclohepta[1,2-c]pyridazin-3-yl) butanoate (P25)

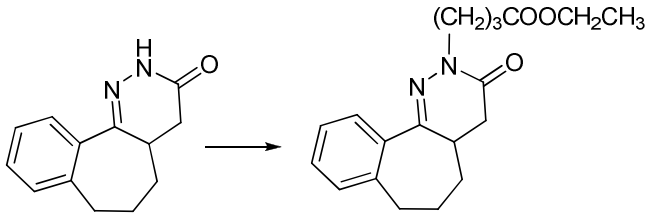

P23 **P25**

General procedure I was followed for the synthesis of **P25** from **P23**.

- Yellow oil
- Yield: 33%
- TLC (dichloromethane/methanol 95:5) Rf = 0.77
- ^{1}H NMR ($CDCl_3$) 1.29 (t, 3H, CH_3), 1.4-1.2 (m, 2H, CH_2), 1.41 (m, 1H, CH), 1.90-1.80 (m, 2H, CH_2), 2.04 (q, 2H, CH_2), 2.3-2.1 (dd, 2H, CH_2), 2.47 (dd, 2H, CH_2CO), 2.88-2.84 (dd, 2H,CH_2), 3.20 (t, 2H, CH_2N), 4.13 (t, 2H, CH_2O), 7.30-7.78 (m, 4H, ArH)

Synthesis of the unsaturated esters P22 and P26

Ethyl 4-(3-oxo-3,5-dihydro-2H-indeno[1,2-c]pyridazin-2-yl)butanoate (P22)

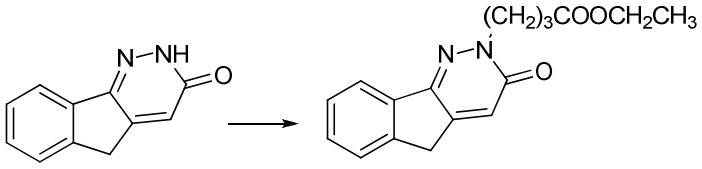

P20 **P22**

General procedure L was followed for the synthesis of **P22** from **P20**. A purification with flash chromatography (eluent: dichloromethane/ethyl acetate 6:4) was performed.

- Yellow oil
- Yield: 68%
- TLC (dichloromethane/methanol 95:5) Rf = 0.80
- ^{1}H NMR ($CDCl_3$) 1.25 (t, 3H, CH_3), 2.15-2.25 (m, 2H, CH_2), 2.35-2.45 (m, 2H, CH_2), 3.90 (s, 2H, CH_2), 4.05-4.15 (q, 2H, CH_2), 4.25-4.35 (m, 2H, CH_2), 6.95 (s, 1H, CH), 7.40-7.50 (m, 3H, ArH), 7.80-7.90 (m, 1H, ArH)

Ethyl-4-(3-oxo-2,5,6,7-tetrahydro-3H-benzo[6,7]-cyclohepta[1,2-c]pyridazin-3-yl) butanoate (P26)

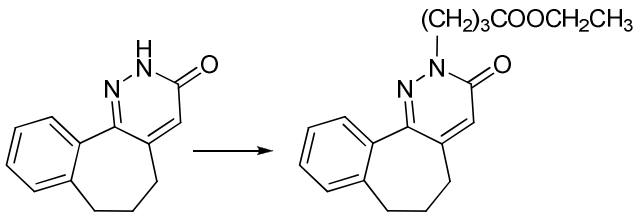

P24 **P26**

General procedure L was followed for the synthesis of **P26** from **P24**. A purification with flash chromatography (eluent: petroleum ether/ethyl acetate 7:3) was performed.

- Yellow oil
- Yield: 68%
- TLC (dichloromethane/methanol 95:5) Rf = 0.80
- ^{1}H NMR ($CDCl_3$) 1.25 (t, 3H, CH_3), 2.05-2.25 (m, 4H, CH_2), 2.35-2.45 (m, 4H, CH_2), 2.80-2.90 (m, 2H, CH_2), 4.05-4.15 (q, 2H, CH_2), 4.25-4.35 (m, 2H, CH_2), 6.80 (s, 1H, CH), 7.20-7.30 (m, 1H, ArH), 7.30-7.40 (m, 2H, ArH), 7.50-7.60 (m, 1H, ArH)

5.4 Experimental procedures: the chimera compounds

5.4.1 Synthesis of the chimera compounds C1a,b and C2

4-oxo-1,2,3,4-tetrahydronaphthalene-1-carboxylic acid (25)[201]

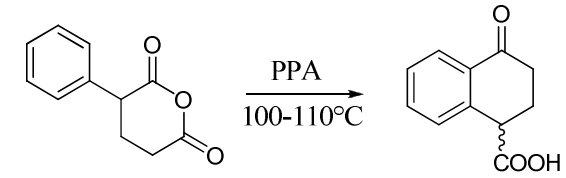

α-phenylglutaric anhydride **25**

A mixture of α-phenylglutaric anhydride (0.5 g, 2.69 mmol) and 2 g of polyphosphoric acid was heated to 100-110 °C and kept at that temperature for 15 min. Another 1 g of polyphosphoric acid was added and the mixture was heated for 15 min at the same temperature. The solution appeared as a dense brown oil. The mixture was cooled with an ice bath, treated with water and extracted with ethyl acetate (3 x 2 mL). In order to purify the reaction mixture from the unreacted starting material, the organic phase was firstly treated with 1 N NaOH (2 mL) and then the collected alkaline aqueous solution, which contained the sodium salt of compound **25**, was acidified with 6 N HCl (1 mL) and extracted with ethyl acetate (3 x 1 mL). The organic layer was dried over anhydrous Na_2SO_4 and evaporated under reduced pressure to afford **25**.

- Brown oil
- Yield: 90%
- TLC (dichloromethane/methanol 9:1) Rf = 0.5
- ^{1}H NMR ($CDCl_3$) 2.25-2.40 (m, 1H, CH_2-2), 2.45-2.55 (m, 1H, CH_2-2), 2.55-2.70 (dt, 1H, CH_2-3), 2.85-2.95 (m, 1H, CH_2-3), 3.96 (t, 1H, CH-1), 7.30-7.40 (m, 2H, ArH), 7.40-7.55 (m, 1H, ArH), 8.05 (d, 1H, ArH), 11.15 (s, 1H, OH, exchangeable with D_2O)

4-oxo-N-(4-(trifluoromethyl)phenyl)-1,2,3,4-tetrahydronaphthalene-1-carboxamide (26)

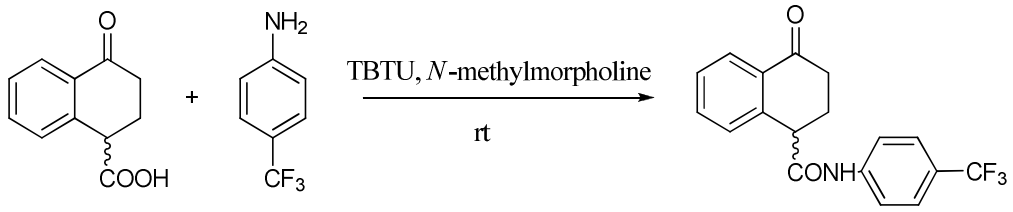

25 **26**

To a solution of compound **25** (0.2 g, 1.05 mmol) in dichloromethane (6 mL) the coupling agent TBTU (0.46 g, 1.42 mmol), *N*-methylmorpholine (up to pH=7) and 4-(trifluoromethyl)aniline (0.4 mL, 3.21 mmol) were added. The resulting mixture was stirred at room temperature for 24 h. The product was extracted with dichloromethane (3 x 2 mL). The organic layer was washed first with 1 N HCl (1 x 2 mL), then with a saturated solution of sodium hydrogencarbonate (1 x 2 mL) to neutralize the excess of TBTU and finally with brine (1 x 2 mL). The organic phase was dried over anhydrous Na_2SO_4, filtered and concentrated in *vacuo* to provide a yellow solid. The residue was purified by flash chromatography (eluent: cyclohexane/ethyl acetate 7:3) to afford the intermediate **26**.

- White solid
- Yield: 62%
- TLC (petroleum ether/ethyl acetate 7:3) Rf = 0.3 (Compound **26** was visualized by dipping TLC plates into a solution of phosphomolybdic acid in ethanol)
- ^{1}H NMR ($CDCl_3$) 2.35-2.45 (m, 1H, CH_2-2), 2.60-2.85 (m, 3H, [1H, CH_2-2; 2H, CH_2-3]), 3.90-3.95 (t, 1H, CH-1), 7.1-7.6 (m, 7H, ArH), 8.11 (dd, 1H, ArH)

(Z)-2-(1-oxo-4-(4-(trifluoromethyl)phenylcarbamoyl)-3,4-dihydronaphthalen-2(1H)-ylidene)acetic acid (27)

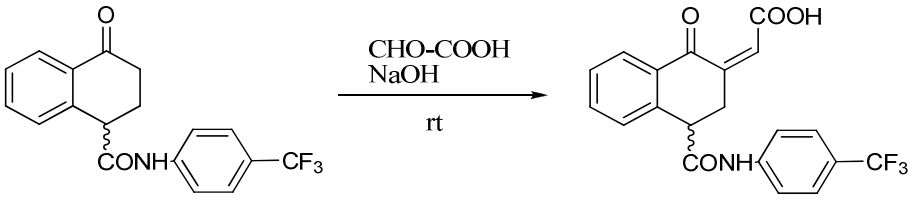

26 **27**

A solution of NaOH (0.26 g, 6.53 mmol) in water (3.1 mL) and ethanol (1.63 mL) was added dropwise to an ice-cooled solution (0 °C) of compound **26** (0.44 g, 1.33 mmol) and glyoxylic

acid (0.49 g, 5.27 mmol) in water (1.8 mL). This solution was stirred at room temperature for 1 h and then ethanol was removed under reduced pressure. The obtained acqueous mixture was acidified with 6 N HCl and the precipitate was filtered, washed with 6 N HCl (1 x 1 mL) and dried to give a yellow residue. The crude solid was purified by flash chromatography (eluent: dichloromethane/methanol 9:1 with 0.02 mL of acetic acid) to provide compound **27**.

- White solid
- Yield: 47%
- TLC (dichloromethane/methanol 9:1 with 0.02 mL of acetic acid) Rf = 0.4
- ^{1}H NMR (CD_3OD) 3.10-3.20 (m, 1H, CH_2-3), 4.10-4.25 (m, 2H, [1H, CH_2-3; 1H, CH-4]), 6.90 (d, 1H, CH-9), 7.40 -7.80 (m, 7H, ArH), 8.11 (dd, 1H, ArH)
- ^{19}F NMR (CD_3OD) 64 (s, 3F, CF_3)

2-(1-oxo-4-(4-(trifluoromethyl)phenylcarbamoyl)-1,2,3,4-tetrahydronaphthalen-2-yl)acetic acid (28)

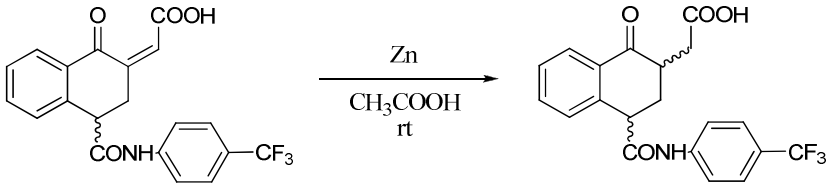

27 **28**

A mixture of compound **27** (0.173 g, 0.44 mmol) and zinc dust (0.34 g, 0.52 mmol) in acetic acid (4.95 mL) and water (1.24 mL) was heated at 60 °C for 20 min. Since the amount of zinc was minimal, it was not necessary to filter the suspension to remove the excess of zinc, whereas the acetic acid was removed under reduced pressure. Compound **28** was extracted with ethyl acetate (3 x 2 mL) and the organic layer was dried over anhydrous Na_2SO_4, filtered and the solvent was evaporated.

- Light yellow solid
- Yield: 91%
- TLC (dichloromethane/methanol 9:1) Rf = 0.4 (Compound **8** was visualized by dipping TLC plates into a solution of phosphomolybdic acid in ethanol)
- ^{1}H NMR (CD_3OD) 2.30 (dd, 1H, CH_2-9), 2.40-2.60 (m, 2H, CH_2-3), 2.95 (dd, 1H, CH-2), 3.05-3.20 (m, 1H, CH_2-9), 4.30 (dd, 1H, CH-4), 7.25-8.11 (m, 8H, ArH)

3-oxo-N-(4-(trifluoromethyl)phenyl)-2,3,4,4a,5,6-hexahydrobenzo[h]cinnoline-6-carboxamide (C1a, C1b)

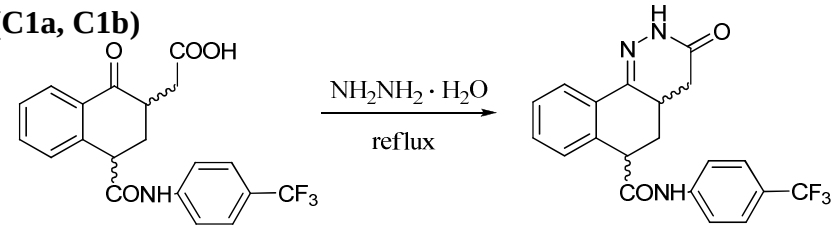

28

C1a (R*,R*)
C1b (R*, S*)

To a solution of compound **28** (0.15 g, 0.38 mmol) in ethanol, hydrazine monohydrate (0.09 mL, 1.93 mmol) was added dropwise and the obtained yellow solution was refluxed for 2 h. After evaporation of the solvent, the reaction mixture was extracted with ethyl acetate (5 x 1 mL). The organic layer was dried over anhydrous Na_2SO_4, filtrated and the solvent was evaporated under reduced pressure. The two diastereoisomers **C1a** and **C1b** was separated by flash chromatography (eluent: dichloromethane/methanol 9.8:0.2).

- Total yield: 64% (diastereomeric excess **C1a**:**C1b** = 8:2)

Compound **C1a:**

- Yellow solid
- TLC (dichloromethane/methanol 9:1) Rf = 0.53 (Compounds **C1a** was visualized also with iodine)
- Melting point: 230.2-232.4 °C
- ^{1}H NMR (CD_3OD) 1.80-2.00 (m, 2H, CH_2-6), 2.00-2.15 (m, 1H) 2.40-2.50 (m, 2H), 2.65-2.75 (m, 1H), 4.05-4.10 (m, 1H), 7.20-7.30 (m, 3H, ArH), 7.50-7.55 (m, 2H, ArH), 7.70-7.75 (m, 2H, ArH), 8.05-8.10 (m, 1H, ArH);

Compound **C1b**

- White solid
- TLC (dichloromethane/methanol 9:1) Rf = 0.48 (Compounds **C1b** was visualized also with iodine)
- ^{1}H NMR (DMSO) 1.80-2.00 (m, 1H) 2.20-2.40 (m, 2H), 2.40-2.45 (m, 1H), 2.85-3.00 (m, 1H), 3.90-4.00 (m, 1H), 7.15-7.20 (m, 1H, ArH), 7.30 (d, 2H, ArH), 7.75 (d, 2H, ArH), 7.90 (d, 2H, ArH), 8.05 (d, 1H, ArH)

3-oxo-N-(4-(trifluoromethyl)phenyl)-2,3,5,6-tetrahydrobenzo[h]cinnoline-6-carboxamide (C2)

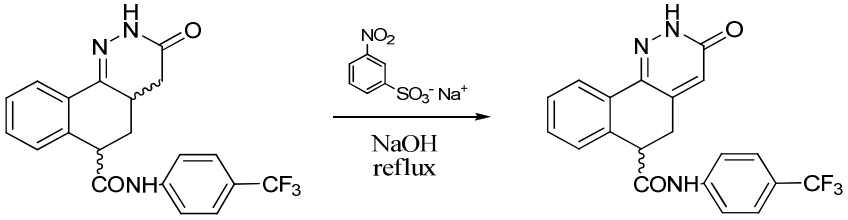

C1a **C2**

A mixture of compound **C1a** (5 x 10^{-2} g, 0.13 mmol), sodium *m*-nitro-benzenesulfonate (2.9 x 10^{-2} g, 0.13 mmol), NaOH (2.1 x 10^{-2} g, 0.52 mmol) in water (1 mL) was refluxed for 30 min. After cooling, the reaction mixture was extracted with ethyl acetate (3 x 1 mL) and the organic layer was dried over anhydrous Na_2SO_4, filtrated and the solvent was evaporated under reduced pressure. The obtained residue was purified by flash chromatography (eluent: dichloromethane/methanol 9.7:0.3) to afford **C2**.

- Yellow solid
- Yield: 85%.
- TLC (dichloromethane/methanol 9:1) Rf = 0.4
- ^{1}H NMR (CD_3OD) 3.25 (t, 1H, CH_2), 4.15 (t, 1H, CH_2), 4.30 (t, 1H, CH), 6.85 (s, 1H, CH),7.40-7.55 (m, 3H, ArH), 7.60 (d, 2H, ArH), 7.65 (d, 2H, ArH), 8.15-8.25 (m, 1H, ArH)

5.4.2 Synthesis of the chimera compound C3

β-benzoyl-γ-butyrolactone (29)[183]

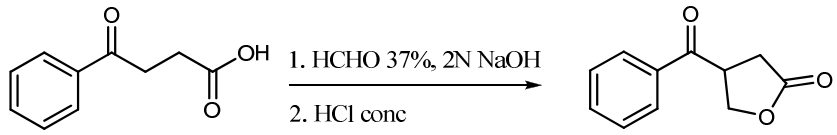

3-benzoyl propionic acid **29**

Formaldehyde 37% (0.25 mL, 3.08 mmol) was added to a stirred solution of 3-benzoyl propionic acid (0.5 g, 2.81 mmol) in a solution 0.5 N NaOH (6.2 mL, 3.1 mmol) (molar ratio of 3-benzoyl propionic acid/CH_2O/NaOH = 1.0 : 1.1 : 1.1). After 1 h at room temperature, the mixture was acidified with concentrated hydrochloric acid (~ 0.31 mL) and stirred for additional 12 h. The mixture was extracted with ethyl acetate (3 x 5 mL) and the combined organic layers were dried over anhydrous Na_2SO_4 and concentrated *in vacuo*. The crude was purified by flash chromatography (eluent: petroleum ether/ethyl acetate 7:3) to obtain intermediate **29**.

- Transparent oil
- Yield: 69%
- TLC (dichloromethane/methanol 9:1) Rf = 0.8
- ^{1}H NMR ($CDCl_3$) 2.75-3.05 (m, 2H, CH_2), 4.35-4.50 (m, 2H, CH_2), 4.60-4.65 (m, 1H, CH), 7.50-7.95 (m, 5H, ArH).

5-hydroxymethyl-6-phenyl-4,5-dihydro-3(2H)-pyridazinone (30)[184]

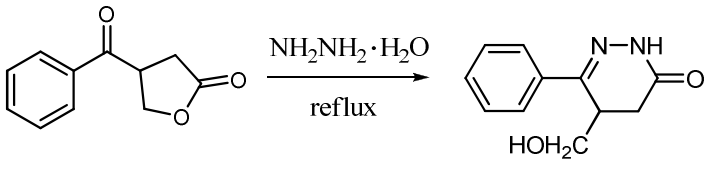

29 **30**

To a solution of compound **29** (5 x 10^{-2} g, 0.26 mmol) in ethanol (2 mL), hydrazine monohydrate (0.037 mL, 0.78 mmol) was added and the mixture was refluxed for 1.5 h. The solvent was then removed *in vacuo* and the residue was extracted with ethyl acetate (5 x 3

mL). The organic layer was dried over anhydrous Na_2SO_4, evaporated and the crude was directly used without purification in the next reaction.

- Pale yellow solid
- Yield: 67%
- TLC (dichloromethane/methanol 95:5) Rf = 0.3
- ^{1}H NMR ($CDCl_3$) 2.65-2.95 (m, 2H, CH_2), 3.25-3.55 (m, 1H, CH), 3.70-3.90 (m, 2H, CH_2), 7.20-7.80 (m, 5H, ArH), 8.50 (br s, 1H, NH, exchangeable with D_2O).

6-phenyl-5-hydroxymethyl-4,5-dihydro-3(2H)-pyridazinone acetate (31)

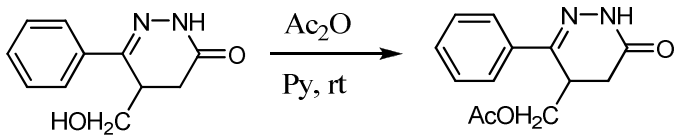

30 **31**

To a solution of **30** (5 x 10^{-2} g, 0.25 mmol) in pyridine (2 mL), acetic anhydride (0.045 mL, 0.48 mmol) was added and the mixture was stirred at rt for 4 h. The pyridine was then removed under reduced pressure and the residue was extracted with ethyl acetate (5 x 3 mL). The organic layer was dried over anhydrous Na_2SO_4, evaporated and the crude was purified by flash chromatography (eluent cyclohexane/ethyl acetate 3:7) to afford intermediate **31**.

- Pale yellow solid
- Yield: 98%
- TLC (dichloromethane/methanol 95:5) Rf = 0.5
- ^{1}H NMR ($CDCl_3$) 2.0 (s, 3H, CH_3), 2.70-2.80 (m, 2H, CH_2), 3.60-3.70 (m, 1H, CH), 4.0-4.10 (m, 1H, CH), 4.30-4.40 (m, 1H, CH), 7.40-7.85 (m, 5H, ArH), 8.80 (br s, 1H, NH, exchangeable with D_2O).

6-phenyl-5-hydroxymethyl-3(2H)-pyridazinone acetate (32)

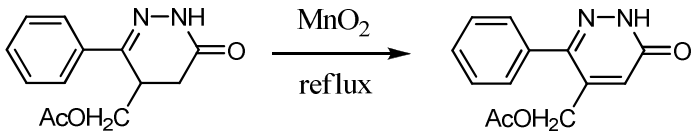

31 **32**

A mixture of **31** (5 x 10^{-2} g, 0.20 mmol) and activated manganese dioxide (0.184 g, 2.1 mmol) in dry dichloromethane (2 mL) was refluxed for 24 h. After cooling, the oxidant was removed by filtration through Celite and the manganese dioxide was washed with dichloromethane. The obtained filtrate was concentrated to give a solid residue, which was purified by flash chromatography (eluent: dichloromethane/ethyl acetate 8:2).

- White solid
- Yield: 60%
- TLC (dichloromethane/methanol 95:5) Rf = 0.4
- ^{1}H NMR ($CDCl_3$) 2.15 (s, 3H, CH_3), 4.9 (s, 2H, CH_2), 7.05 (s, 1H, CH), 7.38-7.49 (m, 5H, ArH), 11.13 (br s, 1H, NH, exchangeable with D_2O).

6-phenyl-5-hydroxymethyl-3(2H)-pyridazinone (33)

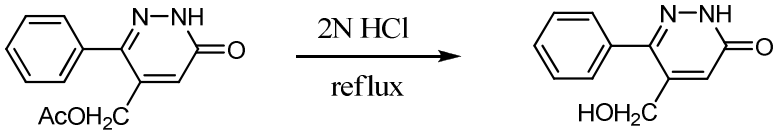

32 **33**

A solution of **32** (5 x 10^{-2} g, 0.20 mmol) in ethanol (3 mL) was treated with 2N HCl (1 mL) and the mixture was heated to reflux for 4 h. After cooling, the solvent was removed *in vacuo* and the residue extracted with with ethyl acetate (4 x 3 mL). The organic layer was dried over anhydrous Na_2SO_4 and concentrated *in vacuo* to obtain intermediate **33** as white solid.

- Quantitative yield
- TLC (dichloromethane/methanol 9:1) Rf = 0.3
- ^{1}H NMR (CD_3OD) 4.38 (s, 2H, CH_2), 7.2 (s, 1H, CH), 7.05 (s, 1H, CH), 7.43-7.50 (m, 5H, ArH).

6-phenyl-5-formyl-3(2H)-pyridazinone (34)

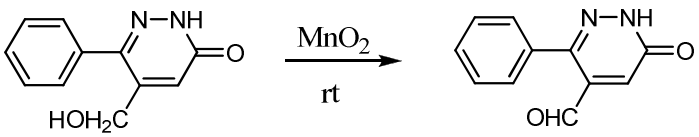

33 **34**

A solution of **33** (5 x 10^{-2} g, 0.25 mmol) in dry tetrahydrofurane (2 mL) was stirred with activated manganese dioxide (0.27 g, 2.5 mmol) for 48 h at rt. The suspension was filtered through Celite and the manganese dioxide was washed with tetrahydrofurane. The obtained filtrate was concentrated to give a solid residue, which was purified by flash chromatography (eluent: dichloromethane/methanol 95:5).

- Yellow solid
- Yield: 81%
- TLC (dichloromethane/methanol 95:5) Rf = 0.3
- ^{1}H NMR ($CDCl_3$) 7.43 (s, 1H, CH), 7.45-7.55 (m, 5H, ArH), 9.92 (s, 1H, CHO).

6-phenyl-5-carboxy-3(2H)-pyridazinone (35)

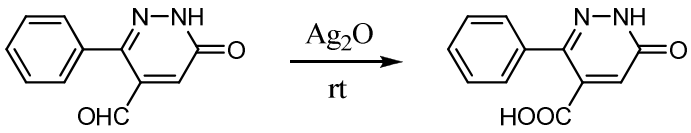

34 **35**

A solution of aldehyde **34** (5 x 10^{-2} g, 0.25 mg) and silver nitrate (0.212 g, 1.25 mmol) in ethanol (0.5 mL) and water (0.6 mL) was stirred rapidly under nitrogen atmosphere. A 10% NaOH solution was added until the pH of the reaction mixture reached 12. The resulting black suspension was stirred at room temperature for 15 h and then filtered. The filtrate was concentrated under reduced pressure, then acidified with 6N HCl, extracted with diethyl ether (3 x 2 mL), dried over anhydrous Na_2SO_4 and concentrated *in vacuo*. The obtained crude was purified with flash chromatography (dichloromethane/methanol 9:1) to give intermediate **35**.

- Yellow solid
- Yield: 60%
- TLC (dichloromethane/methanol 9:1) Rf = 0.2
- ^{1}H NMR (DMSO) 7.15 (s, 1H, COOH), 7.46 (s, 5H, ArH).

1-(6-oxo-3-phenyl-1,6-dihydropyridazin-4yl)-3-(4-(trifluoromethyl) phenyl)urea (C3)

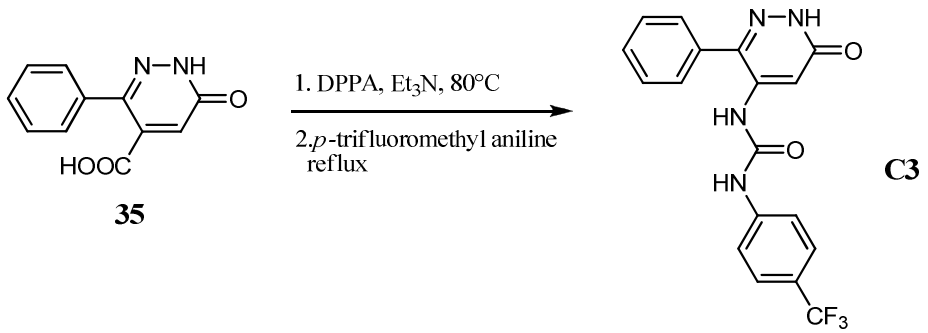

35 **C3**

The carboxylic acid **35** (5 x 10^{-2} g, 0.23 mmol) was suspended in a mixture of dry toluene (8 mL) and dry tetrahydrofurane (8 mL) under nitrogen atmosphere, and DPPA (0.078 mL, 0.36 mmol) was added. Triethylamine (0.032 mL, 3.6 mmol) was then added dropwise and the mixture stirred at room temperature for 30 min. The solution was heated at 80 °C for 2 h and then *p*-trifluoromethyl aniline (0.036 mL, 0.29 mmol) in THF (3 mL) was added together with triethylamine (0.032 mL, 3.6 mmol). The mixture was stirred at 80 °C overnight and then was diluted with 10 mL of water and extracted with ethylacetate (3 x 10 mL). The organic phase was then extracted with 1 M HCl (1 x 10 mL). The organic layer was dried over anhydrous Na_2SO_4 and concentrated *in vacuo* to obtain the chimera **C3**.

- White solid
- Yield: 20%
- TLC (dichloromethane/methanol 95:5) Rf = 0.4
- ^{1}H NMR (CD_3OD) 7.50-7.60 (m, 10H, ArH), 7.85 (s, 1H, CH).
- ^{13}C NMR (CD_3OD) 110, 118, 126, 129, 130, 133, 142, 143, 152, 164

5.5 Experimental procedures: the oxidized compounds

5.5.1 Synthesis of the *ortho*-quinone derivative O1

3-methyl-2-morpholino-2,3-dihydrobenzofuran-5-ol (36)[199, 200]

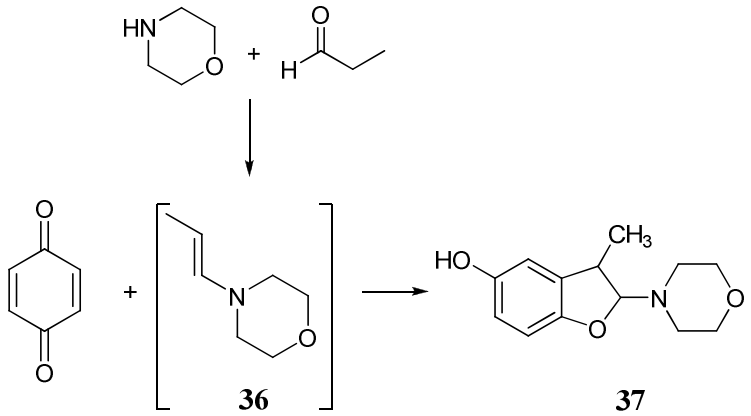

To a solution of propionaldehyde (0.174 g, 3 mmol) in toluene (4 mL), morpholine (0.26 g, 3 mmol) was added dropwise and the mixture was stirred at room temperature for 18 h until the consumption of the starting material (the reaction was monitored by ^{1}H NMR).

The mixture was cooled to 0 °C and a solution of *p*-benzoquinone (150 mg, 3 mmol) in toluene (1 mL) was added. The mixture was stirred at 0 °C for 2.5 h and then it was concentrated *in vacuo* to obtain the crude product (dark red solid) used without further purifications.

3-methylbenzofuran-5-ol (38)

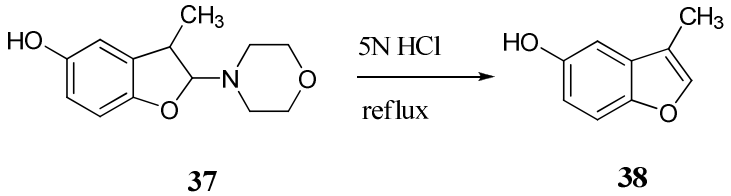

A solution of **37** (5 x 10^{-2} g, 0.21 mmol) in tetrahydrofuran (1 mL) was acidified with 3 mL of 5N HCl and it was refluxed for 2 h. The mixture was then extracted with diethyl ether (3 x 2 mL), dried over anhydrous Na_2SO_4 and the solvent was evaporated under reduced pressure.

The obtained crude was purified by flash chromatography (eluent: ciclohexane/ethyl acetate 8:2 → 7:3 → 6:4).

- Yield over two steps: 3%
- TLC (ciclohexane/ethyl acetate 7:3) Rf = 0.53
- ^{1}H NMR ($CDCl_3$) 2.2 (s, 3H, CH_3), 5.2 (s, 1H, OH), 6.8-6.9 (m, 1H, ArH), 6.9 (s, 1H, ArH), 7.25-7.35 (m, 1H, ArH), 7.4 (s, 1H, CH)

3-methylbenzofuran-4,5-dione (O1)

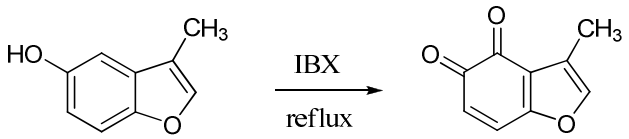

38 **O1**

IBX 45 wt. % (0.21 g, 0.34 mmol) was added to a solution of **38** (5 x 10^{-2} g, 0.34 mmol) in dichloromethane (1.5 mL) and the resulting mixture was stirred at room temperature for 24 h. The reaction was then diluted with water (2 mL) and extracted with dichloromethane (3 x 2 mL). The combined organic layers were washed with brine, dried over Na_2SO_4 and evaporated *in vacuo*.

- Purple solid
- Yield: 3.6%
- TLC (cyclohexane/ethyl acetate 7:3) Rf = 0.2
- ^{1}H NMR ($CDCl_3$) 2.0 (s, 3H, CH_3), 7.25 (s, 1H, ArH),7.5 (d, 1H, ArH), 8.07 (d, 1H, CH).

5.5.2 Synthesis of the *ortho*-quinone derivatives (*RS*)-O2

4-(allyloxy)-2,3-dimethylphenol (39)

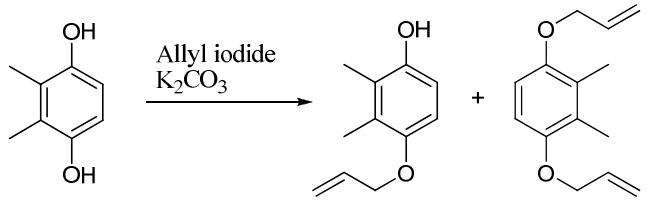

39

Allyl iodide (1 mL, 10.91 mmol) and potassium carbonate (2 g, 14.05 mmol) were added to a solution of 2,3-dimethyl hydroxyl hydroquinone (1 g, 7.24 mmol) in acetone (4 mL). The resulting mixture was stirred under reflux for 18 h. Then the solvent was removed *in vacuo* and the remaining residue was poured into water and extracted with diethyl ether. Flash chromatography (eluent: ciclohexane/ethylacetate 95:5 → 8:2) of the crude product gave two products: the desired monoallyl ether **39** and its correspondent diallylether.

- Yield (monoallyl ether **39**): 30%
- TLC (ciclohexane/ethyl acetate 8:2) $Rf_{\text{monoallyl ether } \mathbf{39}} = 0.38$; $Rf_{\text{diallyl ether}} = 0.76$
- ^1H NMR (monoallyl ether **39**) ($CDCl_3$) 2.18 (s, 3H, CH_3), 2.2 (s, 3H, CH_3), 4.45 (d, 2H, CH_2), 5.2 (dd, 1H, CH), 5.4 (dd, 1H, CH), 6.1 (m, 1H, CH), 6.6 (d, 2H, ArH).

5-allyl-2,3-dimethylbenzene-1,4-diol (40)

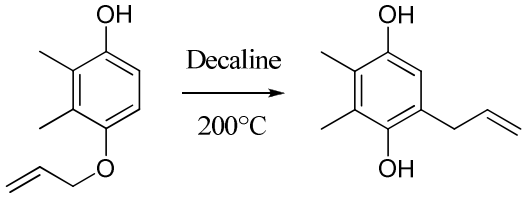

39 **40**

A solution of monoallyl ether **39** (0.2 g, 1.12 mmol) in decalin (1 mL) is heated to 220 ºC for 7 h in autoclave and then cooled to room temperature. A light grey solid product was separated by filtration and washed with *n*-hexane. The precipitation could be enhanced by leaving the autoclave in freezer overnight. The crude product was purified by flash chromatography (eluent: cyclohexane/ethyl acetate 95:5 → 9:1 → 8:2).

- Yield: 92%

- TLC (ciclohexane/ethylacetate 8:2) Rf = 0.28
- ^{1}H NMR ($CDCl_3$) 2.14 (s, 3H, CH_3), 2.16 (s, 3H, CH_3), 3.25 (d, 2H, CH_2), 4.20 (s, 1H, OH), 4.50 (s, 1H, OH), 5.09 (s, 1H, CH_2), 5.10 (d, 1H, CH_2), 5.85-6.0 (m, 1H, CH), 6.40 (s, 1H, ArH).

2,6,7-trimethyl-2,3-dihydrobenzofuran-5-ol (41)

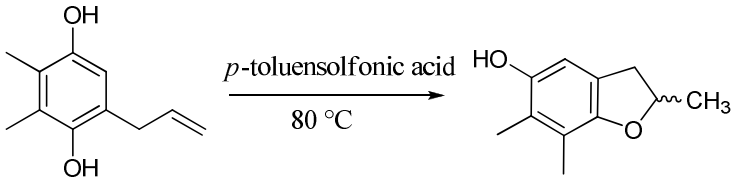

40 **41**

p-toluenesulfonic acid (0.36 g, 2.1 mmol) was added to a solution of **40** (0.2 g, 1.12 mmol) in toluene (1.5 mL) and the reaction mixture was heated at 80 °C for 8 h. To the mixture, cooled to room temperature, a solution of saturated $NaHCO_3$ (3 mL) was added and it was extracted with ethyl acetate (3 x 2 mL). The organic layer was dried over anhydrous Na_2SO_4 and evaporated *in vacuo*. Purification of the obtained crude solid was carried out by flash chromatography (eluent: cyclohexane/ethyl acetate 8:2) to afford compound **41**.

- White solid
- Yield: 99%
- TLC (cyclohexane/ethyl acetate 8:2) Rf = 0.5
- ^{1}H NMR ($CDCl_3$) 1.47 (s, 3H, CH_3), 2.01 (s, 3H, CH_3), 2.03 (s, 3H, CH_3), 2.7 (dd, 1H, CH_2), 3.1 (dd, 1H, CH_2), 4.8-5.1 (m, 1H, CH), 6.4 (s, 1H, ArH).

2,6,7-trimethyl-2,3-dihydrobenzofuran-4,5-dione (O2)

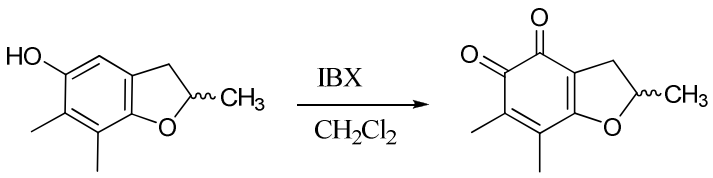

41 **O2**

IBX 45% wt. (0.18 g, 0.29 mmol) was added to a solution of **41** (5 x 10^{-2} g, 0.28 mmol) in dichloromethane (1 mL). The resulting mixture was stirred at room temperature for 24 h. The

reaction was then diluted with water (2 mL) and extracted with dichloromethane (3 x 2 mL). The combined organic layers were washed with brine, dried over anhydrous Na_2SO_4 and evaporated *in vacuo*. The crude product was purified by gradient flash chromatography (ciclohexane/ethyl acetate 8:2 → 7:3).

- Red solid
- Yield: 3.6%
- TLC (cyclohexane/ethyl acetate 8:2) Rf = 0.2
- ^{1}H NMR ($CDCl_3$) 1.45 (s, 3H, CH_3), 1.9 (s, 3H, CH_3), 2.0 (s, 3H, CH_3), 2.6 (dd, 1H, CH_2), 3.2 (dd, 1H, CH_2), 5.0-5.15 (m, 1H, CH).
- ^{13}C NMR ($CDCl_3$) 30, 128, 129, 130, 134, 172.

6. EXPERIMENTAL SECTION: BIOLOGY

6.1 Dual luciferase assay[159]

Cell culture. The cancer cell lines were obtained from American Type Culture Collection. Human colon cancer cells (HTC-116) were maintained in RPMI 1640 (Gibco/BRL). Human colon cancer cell line (HCT-116) was maintained in McCoy's 5A (Gibco/BRL). All culture media were supplemented with 10% heat-inactivated fetal bovine serum (Gibco/BRL). Cell cultures were maintained at 37 °C under a humidified atmosphere of 5% CO_2 in an incubator.
Transient transfection and dual-luciferase assays. HCT-116 cells were seeded at a density of $10x10^5$ cells in 100 mm^2 culture plate. On the following day, the cells were co-transfected with *pSTAT3-TA-Luc* carrying firefly luciferase gene, which is dependently expressed by STAT3 activity, and *pRL-TK* carrying Renilla luciferase gene, which is independently expressed by STAT3 activity. *Renilla* luciferase activity was determined to calibrate transfection efficiency and cytotoxicity of chemicals. Beetle *luciferin* and *coelenterazine* were used as substrates for the two enzymes, respectively. The transfection was carried out using *TransFectin* (*Bio-Rad*). After 5 h of transfection, the cells were trypsinized and seeded onto sterilized black bottom 96-well plates at a density of 1×10^4 cells per well. On the following day, cells were treated with the tested compounds at different concentration and incubated for 24 h. *Firefly* and *Renilla* luciferase activity was measured using a dual-light reporter gene assay kit (*Promega*). Renilla luciferase activity was determined to calibrate transfection efficiency and cytotoxicity of chemicals. Relative STAT3 activity was calculated by dividing the firefly luciferase activity with Renilla luciferase activity in each transfection experiment. The values of STAT3 inhibitory activity were the means of 3 experiments and the maximum deviation from the mean was less than 10%.

As shown in **Figure 37**, the activities of *Firefly* and *Renilla* luciferases are measured sequentially from a single sample. Measurement of the luminescent signal from the two luciferase reporter enzymes was performed immediately following preparation of lysates with passive lysis buffer. Both *Renilla* and firefly luciferase exhibit glow-type reaction kinetics

when each specific substrates are added to lysates. The firefly luciferase reporter is measured first by adding *Luciferase Assay Reagent II* (*LAR II*) to generate a stabilized luminescent signal. After quantifying the firefly luminescence, this reaction is quenched, and the *Renilla* luciferase reaction is simultaneously initiated by adding *Stop & Glo Reagent* to the same tube. The *Stop & Glo Reagent* also produces a stabilized signal from the *Renilla* luciferase, which decays slowly over the course of the measurement. Both of luminescence was measured by Wallac Victor™ 2 luminometer (Perkin-Elmer, Inc., Wellesley, MA).

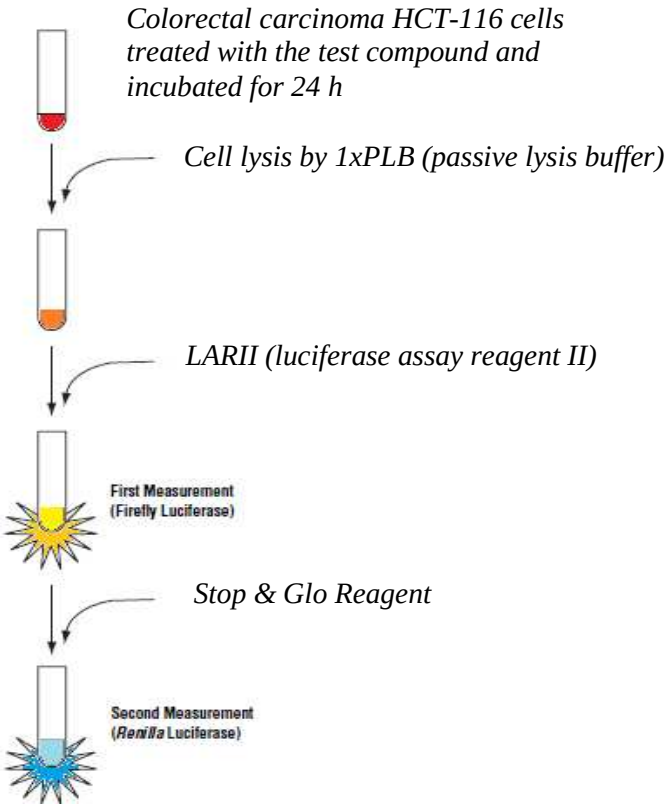

Figure 37. Dual-luciferase report assay.

6.2 AlphaScreen-based assay protocol

The AlphaScreen-based assay was performed in a final reaction volume of 25 µL of the assay buffer containing 10 mM HEPES-NaOH (pH=7.4), 50 mM NaCl, 1 mM EDTA (pH = 8.0), 0,1% NP-40, and 10 ng/µL BSA, in a 96-well microtiter plate at 25 °C. Phospho-Tyr (*p*Tyr) peptide probes used in this study were 5-carboxyfluorescein (FITC)-GpYLPQTV for STAT3, FITC-GpYDKPHVL for STAT1 and FITC-PSpYVNVQN for Grb2. Firstly, 75 nM of each SH2-conteining protein was incubated with a test compound for 15 min. Each protein sample was then incubated for 90 min with 50 nM of its corresponding FITC-pTyr peptide, and mixed with streptavidin-coated donor beads and anti-FITC acceptor beads simultaneously before detection at 570 nm using EnVision Xcite (PerkinElmer).

6.3 Cell proliferation assays

The anti-proliferative assay was performed according to the US NCI protocol.[173] The human tumor cancer cell lines of the screening panel were grown in RPM 1640 medium containing 5% fetal bovine serum and 2 mM L-glutamine. Cells were inoculated into 96-well microtiter plates in 100 µL of complete medium at densities ranging from 5000 to 40.000 50 cells/well. The microtiter plates containing the cells were incubated for 24 h at 37 °C, 5% CO_2, 95% air and 100% relative humidity prior to addition of the experimental drug. This latter was solubilized in dimethyl sulfoxide at 400-fold the desired final maximum test concentration and stored frozen prior to use. At the time of drug addition, an aliquot of frozen concentrate was thawed and diluted twice to the desired final maximum test concentration with complete medium containing 50 µg/mL gentamicin. Additional four, 10-fold serial dilutions were made to provide a total of five drug concentrations plus control. Aliquots of 100 µL of these different drug dilutions were added to the appropriate microtiter wells already containing 100 µL of medium, resulting in the required final drug concentrations. Following the addition of the compound, the plates were incubated for an additional 48 h at 37 °C, 5% CO_2, 95% air, and 100% relative humidity. Cells were fixed by the gentle addition of 50 µL of cold 50% (w/v) trichloroacetic acid (TCA) and incubated for 60 min at 4 °C. After washing with tap water and air drying, Sulforhodamine B (SRB) 70 solution (100 µL) at 0.4% (w/v) in 1%

acetic acid was added to each well, and plates were incubated for 10 min at room temperature. After removing the unbound dye by washing with 1% acetic acid, the bound stain was subsequently solubilized with 10 mM Trizma base and the absorbance was measured on a microplate reader. Dose response parameters (GI_{50}, TGI, LD_{50}) were calculated as reported in the NCI protocol.[173]

7 . Appendix

Appendix I

Mean optical densities, percent growth, GI_{50}, TGI and LC_{50} of **F2e** evaluated on a panel of 58 human tumor cell lines (data obtained from NCI).

			Log10 Concentration												
	Time		Mean Optical Densities					Percent Growth							
Panel/Cell Line	Zero	Ctrl	-8.0	-7.0	-6.0	-5.0	-4.0	-8.0	-7.0	-6.0	-5.0	-4.0	GI50	TGI	LC50
Leukemia															
CCRF-CEM	0.516	1.667	1.641	1.583	1.052	0.520	0.453	98	93	47	.	-12	8.42E-7	1.07E-5	> 1.00E-4
HL-60(TB)	0.896	2.698	2.551	2.597	1.512	0.530	0.508	92	94	34	-41	-43	5.46E-7	2.85E-6	> 1.00E-4
MOLT-4	0.792	2.313	2.252	2.182	1.856	0.638	0.518	96	91	70	-20	-35	1.67E-6	6.05E-6	> 1.00E-4
RPMI-8226	0.882	2.526	2.422	2.319	1.725	0.747	0.667	94	87	51	-15	-24	1.05E-6	5.89E-6	> 1.00E-4
SR	0.482	1.949	1.759	1.826	1.815	0.497	0.306	87	92	91	1	-37	2.85E-6	1.06E-5	> 1.00E-4
Non-Small Cell Lung Cancer															
A549/ATCC	0.323	1.791	1.764	1.647	1.506	0.391	0.373	98	90	81	5	3	2.53E-6	> 1.00E-4	> 1.00E-4
EKVX	0.795	1.899	1.953	1.846	1.816	0.935	0.705	105	95	92	13	-11	3.40E-6	3.36E-5	> 1.00E-4
HOP-62	0.453	1.182	1.134	1.122	1.176	0.425	0.357	93	92	99	-6	-21	2.93E-6	8.74E-6	> 1.00E-4
HOP-92	1.283	1.815	1.760	1.751	1.506	0.922	0.816	90	88	42	-28	-36	6.68E-7	3.96E-6	> 1.00E-4
NCI-H226	0.762	1.666	1.635	1.656	1.570	0.682	0.724	97	99	89	-10	-5	2.48E-6	7.85E-6	> 1.00E-4
NCI-H23	0.591	2.066	1.962	1.919	1.656	0.544	0.562	93	90	72	-8	-5	1.89E-6	7.94E-6	> 1.00E-4
NCI-H322M	0.790	1.913	1.716	1.706	1.507	0.888	0.808	82	82	64	9	2	1.78E-6	> 1.00E-4	> 1.00E-4
NCI-H460	0.250	2.519	2.561	2.629	1.071	0.212	0.378	102	105	36	-15	6	6.29E-7	.	> 1.00E-4
NCI-H522	0.827	2.251	2.107	2.076	1.959	0.713	0.700	90	88	79	-14	-15	2.07E-6	7.12E-6	> 1.00E-4
Colon Cancer															
COLO 205	0.318	1.053	1.078	1.039	1.116	0.373	0.045	103	98	109	7	-86	3.80E-6	1.20E-5	4.13E-5
HCC-2998	0.405	1.471	1.416	1.407	1.379	0.592	0.529	95	94	91	17	12	3.63E-6	> 1.00E-4	> 1.00E-4
HCT-116	0.169	1.368	1.324	1.308	1.091	0.164	0.211	96	95	77	-3	3	2.17E-6	.	> 1.00E-4
HCT-15	0.462	2.285	2.193	2.239	2.342	0.564	0.501	95	97	103	6	2	3.50E-6	> 1.00E-4	> 1.00E-4
HT29	0.187	1.162	1.160	1.122	1.167	0.201	0.221	100	96	100	1	3	3.23E-6	> 1.00E-4	> 1.00E-4
KM12	0.437	2.310	2.302	2.220	2.168	0.534	0.557	100	95	92	5	6	3.06E-6	> 1.00E-4	> 1.00E-4
SW-620	0.255	1.810	1.808	1.745	1.574	0.374	0.568	100	96	85	8	20	2.82E-6	> 1.00E-4	> 1.00E-4
CNS Cancer															
SF-268	0.430	1.384	1.302	1.328	1.052	0.487	0.533	91	94	65	6	11	1.81E-6	> 1.00E-4	> 1.00E-4
SF-295	0.662	2.396	2.298	2.223	1.545	0.409	0.291	94	90	51	-38	-56	1.02E-6	3.72E-6	4.54E-5
SF-539	0.870	2.107	2.043	2.045	2.172	0.965	0.652	95	95	105	8	-25	3.68E-6	1.71E-5	> 1.00E-4
SNB-19	0.506	1.630	1.640	1.661	1.570	0.622	0.586	101	103	95	10	7	3.38E-6	> 1.00E-4	> 1.00E-4
SNB-75	1.084	1.617	1.520	1.595	1.459	0.978	0.777	82	96	70	-10	-28	1.79E-6	7.54E-6	> 1.00E-4
U251	0.270	1.413	1.330	1.336	1.100	0.339	0.298	93	93	73	6	2	2.19E-6	> 1.00E-4	> 1.00E-4
Melanoma															
LOX IMVI	0.169	1.395	1.361	1.332	0.748	0.293	0.164	97	95	47	10	-3	8.72E-7	5.70E-5	> 1.00E-4
MALME-3M	0.631	1.351	1.245	1.277	1.066	0.654	0.592	85	90	60	3	-6	1.52E-6	2.18E-5	> 1.00E-4
M14	0.367	1.353	1.315	1.317	1.049	0.438	0.436	96	96	69	7	7	2.04E-6	> 1.00E-4	> 1.00E-4
MDA-MB-435	0.391	1.878	1.808	1.755	1.477	0.446	0.540	95	92	73	4	10	2.15E-6	> 1.00E-4	> 1.00E-4
SK-MEL-2	0.684	1.261	1.219	1.222	1.214	0.426	0.364	93	93	92	-38	-47	2.10E-6	5.11E-6	> 1.00E-4
SK-MEL-28	0.519	1.283	1.295	1.252	1.223	0.710	0.660	102	96	92	25	18	4.25E-6	> 1.00E-4	> 1.00E-4
UACC-257	0.760	1.961	1.921	1.877	1.686	0.733	0.702	97	93	77	-4	-8	2.17E-6	9.02E-6	> 1.00E-4
UACC-62	0.695	2.450	2.392	2.372	2.128	0.583	0.686	97	96	82	-16	-1	2.11E-6	6.83E-6	> 1.00E-4
Ovarian Cancer															
IGROV1	0.623	2.102	2.103	2.061	2.100	1.005	0.935	100	97	100	26	21	4.72E-6	> 1.00E-4	> 1.00E-4
OVCAR-3	0.475	1.523	1.480	1.461	1.315	0.432	0.468	96	94	80	-9	-2	2.18E-6	7.90E-6	> 1.00E-4
OVCAR-4	0.576	1.062	1.051	1.058	0.996	0.277	0.462	98	99	86	-52	-20	1.83E-6	4.21E-6	.
OVCAR-5	0.565	1.219	1.167	1.162	1.227	0.669	0.564	92	91	101	16	.	3.98E-6	9.63E-5	> 1.00E-4
OVCAR-8	0.349	1.880	1.838	1.872	1.635	0.497	0.445	97	99	84	10	6	2.87E-6	> 1.00E-4	> 1.00E-4
NCI/ADR-RES	0.504	1.865	1.923	1.861	1.727	0.484	0.527	104	100	90	-4	2	2.66E-6	.	> 1.00E-4
SK-OV-3	0.507	1.026	1.027	1.012	1.057	0.435	0.394	100	97	106	-14	-22	2.92E-6	7.60E-6	> 1.00E-4
Renal Cancer															
786-0	0.638	2.146	2.132	2.121	1.928	0.421	0.421	99	98	86	-34	-34	1.98E-6	5.19E-6	> 1.00E-4
A498	1.240	2.029	1.895	1.810	1.822	0.915	0.893	83	72	74	-26	-28	1.73E-6	5.46E-6	> 1.00E-4
ACHN	0.491	1.697	1.690	1.597	1.752	0.459	0.429	99	92	105	-7	-13	3.10E-6	8.74E-6	> 1.00E-4
CAKI-1	0.731	1.927	1.893	1.894	1.605	0.659	0.682	97	97	73	-10	-7	1.90E-6	7.59E-6	> 1.00E-4
RXF 393	0.695	1.084	1.102	1.107	1.043	0.523	0.441	104	106	89	-25	-37	2.21E-6	6.07E-6	> 1.00E-4
SN12C	0.595	2.074	2.078	2.026	1.931	0.629	0.648	100	97	90	2	4	2.87E-6	> 1.00E-4	> 1.00E-4
TK-10	0.640	1.377	1.307	1.290	1.332	0.942	0.715	91	88	94	41	10	6.75E-6	> 1.00E-4	> 1.00E-4
UO-31	0.572	1.715	1.499	1.487	1.468	0.601	0.626	81	80	78	2	5	2.37E-6	> 1.00E-4	> 1.00E-4
Prostate Cancer															
PC-3	0.600	2.183	2.110	2.096	1.527	0.582	0.565	95	94	59	-3	-6	1.38E-6	8.91E-6	> 1.00E-4
DU-145	0.402	1.476	1.483	1.509	1.390	0.558	0.507	101	103	92	15	10	3.48E-6	> 1.00E-4	> 1.00E-4
Breast Cancer															
MCF7	0.309	1.543	1.537	1.507	1.536	0.279	0.235	100	97	99	-10	-24	2.84E-6	8.15E-6	> 1.00E-4
MDA-MB-231/ATCC	0.623	1.414	1.402	1.383	1.425	0.537	0.447	99	96	101	-14	-28	2.79E-6	7.59E-6	> 1.00E-4
HS 578T	0.765	1.761	1.697	1.686	1.518	0.886	0.933	94	92	76	12	17	2.53E-6	> 1.00E-4	> 1.00E-4
BT-549	0.793	1.708	1.633	1.660	1.546	0.708	0.619	92	95	82	-11	-22	2.22E-6	7.66E-6	> 1.00E-4
T-47D	0.610	1.424	1.427	1.392	1.384	0.643	0.631	100	96	95	4	3	3.13E-6	> 1.00E-4	> 1.00E-4
MDA-MB-468	0.514	0.863	0.862	0.850	0.816	0.574	0.398	100	96	87	17	-23	3.36E-6	2.70E-5	> 1.00E-4

Appendix II

Dose-response curves showing the percentage growth inhibition of compound **F2e** in panel/cell lines (data obtained from NCI *in vitro* disease oriented tumor cell screen).

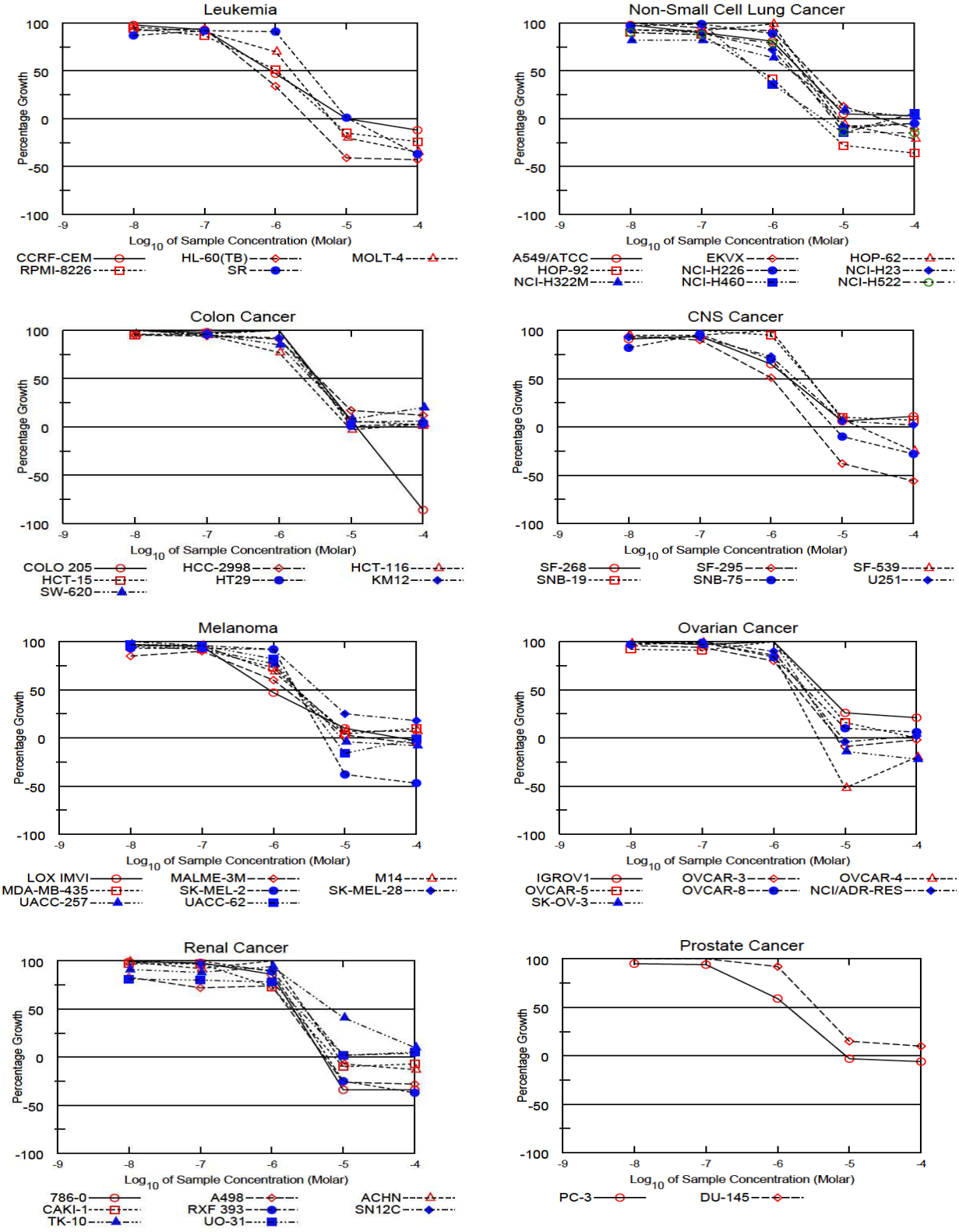

Appendix III

Growth inhibitory % of pyridazinone compounds (**P1a**, **P4a**, **P5a**, **P5aa**, **P19**, **P21**, **P23**) evaluated by cell proliferation assay against a panel of 58 cell lines at a single dose of 10 µM.

	Growth inhibition %						
	P1a	**P4a**	**P5a**	**P5aa**	**P19**	**P21**	**P23**
LEUKEMIA							
CCRF-CEM	n.a.	13.76	n.a.	7.49	n.a.	8.2	8.2
HL-60(TB)	5.5	3.68	n.a.	6.86	2.14	4.71	n.a.
K-562	2.52	n.t.	10.73	1.74	2.87	7.68	n.a.
MOLT-4	1.76	9.03	14.7	n.a	n.a.	5,1	n.a.
RPMI-8226	0.7	n.a.	n.a.	n.a	n.a.	n.a.	12.3
SR	11.84	20.07	22.2	4.57	7.26	9.98	1.47
NON-SMALL CELL LUNG CANCER							
A549/ATCC	n.a.	0.84	7.92	n.a	0.82	1,24	n.a.
EKVX	36.08	9.32	3.62	2.41	19.93	n.a.	4.93
HOP62	n.a.	n.a.	n.a.	n.a	n.a.	n.a.	1.05
HOP92	5.17	1.62	0.22	14.32	12.06	n.a.	n.a.
NCI H226	n.a.	n.a.	n.a.	n.a	n.a.	n.a.	n.a.
NCI H23	n.a.	n.a.	n.a.	n.a	n.a.	n.a.	n.a.
NCI H322M	n.a.	n.a.	n.a.	n.a	n.a.	n.a.	n.a.
NCI H460	n.a.	n.a.	n.a.	n.a	n.a.	n.a.	n.a.
NCI H522	17.4	n.a.	10.7	2.54	3.97	n.a.	6.37
COLON CANCER							
COLO 205	n.a.	n.a.	n.a.	n.a	n.a.	n.a.	n.a.
HCC 2998	n.a.	n.a.	n.a.	2.13	n.a.	n.a.	n.a.
HCT 116	n.a.	n.a.	n.a.	1.58	n.a.	n.a.	n.a.
HCT 15	2.64	n.a.	n.a.	n.a	n.a.	n.a.	n.a.
HT29	3.17	n.a.	4.15	n.a	n.a.	n.a.	n.a.
KM12	n.a.	n.a.	n.a.	n.a	n.a.	n.a.	n.a.
SW620	n.a.	n.a.	n.a.	n.a	n.a.	0.59	n.a.
CNS CANCER							
SF 268	0.09	n.a.	n.a.	n.a	n.a.	n.a.	n.a.
SF 295	n.a.	11.23	8.9	6.85	1.78	n.a.	n.a.
SF 539	2.27	0.85	n.a.	n.a	1.51	n.a.	0.04
SNB 19	n.a.	n.a.	n.a.	1,2	n.a.	n.a.	n.a.
SNB 75	5.55	n.a.	3.55	4.99	n.a.	4.17	4.86
U251	2.05	5.00	n.a.	5.17	n.a.	n.a.	1.72
MELANOMA							
LOX IMVI	n.a.	n.a.	n.a.	n.a	n.a.	n.a.	n.a.

MALNE 3M	n.a.	10.17	n.a.	n.a	1.7	n.a.	n.a.
M14	1.91	n.a.	n.a.	1.19	n.a.	n.a.	n.a.
MDA-MB-435	n.a.	0.95	n.a.	n.a	n.a.	0.18	n.a.
SK MEL 2	n.a.	n.a.	n.a.	n.a	12.31	n.a.	n.a.
SK MEL 28	n.a.	n.a.	n.a.	n.a	n.a.	n.a.	n.a.
SK MEL 5	n.a.	n.a.	n.a.	n.a	n.a.	n.a.	n.a.
UACC-257	2.68	n.a.	1.12	2.95	4.16	0.66	n.a.
UACC-62	n.a.	n.a.	n.a.	1.48	n.a.	n.a.	n.a.
OVARIAN CANCER							
IGROV 1	n.a.	n.a.	n.a.	n.a	n.a.	n.a.	n.a.
OVCAR 3	n.a.	n.a.	n.a.	n.a	n.a.	n.a.	n.a.
OVCAR 4	n.a.	2.65	1.12	n.a	n.a.	n.a.	n.a.
OVCAR 5	5.23	n.a.	n.a.	5.39	n.a.	n.a.	2.69
OVCAR 8	n.a.	n.a.	n.a.	n.a	n.a.	n.a.	n.a.
NCI/ADR-RES	n.a.	n.a.	n.a.	n.a	n.a.	n.a.	n.a.
SK-OV-3	n.a.	n.a.	n.a.	n.a	n.a.	n.a.	0.13
RENAL CANCER							
786-0	10.19	16.89	12.96	2.77	n.a.	1.24	1.32
A498	2.54	n.a.	11.93	n.a	n.a.	1.42	2.08
ACHN	2.59	n.a.	n.a.	4.35	n.a.	n.a.	n.a.
CAKI-1	n.a.	6.94	3.82	1.5	3.22	n.a.	n.a.
SN 12C	n.a.	n.a.	n.a.	4.64	n.a.	n.a.	n.a.
TK-10	4.36	5.51	0,97	n.a	11.99	n.a.	0,3
UO-31	14.44	1.01	6.55	7.34	19.05	n.a.	11,87
PROSTATE CANCER							
PC 3	4,14	n.a.	1,77	6,42	n.a.	n.a.	n.a.
DU 145	n.a.	n.a.	n.a.	n.a	n.a.	n.a.	n.a.
BREAST CANCER							
MCF7	0.94	2.96	9.82	5.64	n.a.	8	n.a.
MDA-MB-231/ATCC	n.a.	n.a.	n.a.	1,85	n.a.	n.a.	n.a.
HS 578T	n.a.	n.a.	9,48	n.a	n.a.	14.12	n.a.
BT 549	n.a.	n.a.	n.a.	n.a	n.a.	n.a.	n.a.
T-47D	n.a.	n.a.	n.a.	n.a	0.84	n.a.	n.a.
MDA-MB-468	n.a.	n.a.	n.a.	n.a	n.a.	n.a.	6.64

n.a. not active

7. References

1. Darnell Jr JE, Kerr IM, Stark GR. Jak-STAT pathways and transcriptional activation in response to IFNs and other extracellular signaling proteins. *Science* (**1994**) 264, 1415-1421.
2. Shindler C, Darnell JE Jr. Transcriptional responses to polypeptide ligands: the JAK-STAT pathway. *Annu. Rev. Biochem.* (**1995**) 64, 621-652.
3. Leaman DW, Leung S, Li X, Stark GR. Regulation of STAT-dependent pathways by growth factors and cytokines. *FASEB J.* (**1996**) 10, 1578-1588.
4. Darnell Jr JE. STATs and gene regulation. *Science* (**1997**) 277, 1630-1635.
5. Zhong Z, Wen Z, Darnell Jr JE. Stat3 and Stat4: members of the family of signal transducers and activators of transcription. *Natl Acad Sci USA* (**1994**) 91, 4806-4810.
6. Heim MH. The Jak–STAT pathway: specific signal transduction from the cell membrane to the nucleus. *Europ. J. Clin. Invest.* (**1996**) 26(1), 1-12.
7. Zhang X, Darnell JE Jr. Functional importance of Stat3 tetramerization in activation of the α2-macroglobulin gene. *J. Biol. Chem.* (**2001**) 276(36), 33576-33581.
8. Strehlow I, Schindler C. Amino-terminal Signal Transducer and Activator of Transcription (STAT) domains regulate nuclear translocation and STAT deactivation. *J. Biol. Chem.* (**1998**) 273(43), 28049-28056.
9. Murphy TL, Geissal ED, Farrar JD, Murphy KM. Role of the Stat4 N Domain in Receptor Proximal Tyrosine Phosphorylation *Mol. Cell. Biol.* (**2000**) 20(19), 7121-7131.
10. Schindler C, Levy DE, Decker T. JAK–STAT signaling: from interferons to cytokines. *J. Biol. Chem.* (**2007**) 282, 20059–20063.
11. McBride KM, Reich NC. The ins and outs of STAT1 nuclear transport. *Sci STKE* (**2003**) 2003, RE13.
12. Becker S, Groner B, Muller CW. Three-dimensional structure of the Stat3beta homodimer bound to DNA. *Nature* (**1998**) 394, 145-151.
13. Bhattacharya S, Schindler C. Regulation of Stat3 nuclear export. *J Clin Invest* (**2003**) 111, 553-559.
14. Gupta P, Blazar BR, Gupta K, Verfaillie CM. Human CD34(+) bone marrow cells regulate stromal production of interleukin-6 and granulocyte colonystimulating factor and increase the colony-stimulating activity of stroma. *Blood* (**1998**) 91,3724-3733.
15. Shuai K, Horvath CM, Huang LH, Qureshi SA, Cowburn D, Darnell Jr JE. Interferon activation of the transcription factor Stat91 involves dimerization through SH2-phosphotyrosyl peptide interactions. *Cell* (**1994**), 76, 821-828.
16. Mertens C, Zhong M, Krishnaraj R, Zou W, Chen X, Darnell Jr JE. Dephosphorylation of phosphotyrosine on STAT1 dimers requires extensive spatial reorientation of the monomers facilitated by the N-terminal domain. *Genes Dev* (**2006**) 20, 3372–3381.
17. Mao X, Ren Z, Parker GN, Sondermann H, Pastorello MA, Wang W, McMurray JS, Demeler B, Darnell Jr JE, Chen X. Structural bases of unphosphorylated STAT1 association and receptor binding. *Mol Cell* (**2005**)

17, 761-771.

18. Park C, Lecomte MJ, Schindler C. Murine Stat2 is uncharacteristically divergent. *Nucleic Acids Res* (**1999**) 27, 4191-4199.
19. Ramsauer K, Farlik M, Zupkovitz G, Seiser C, Kroger A, Hauser H, Decker T. Distinct modes of action applied by transcription factors STAT1 and IRF1 to initiate transcription of the IFN-{gamma}-inducible gbp2 gene. *Proc Natl Acad Sci U S A* (**2007**) 104, 2849-2854.
20. Wen Z, Darnell Jr JE. Mapping of Stat3 serine phosphorylation to a single residue (727) and evidence that serine phosphorylation has no influence on DNA binding of Stat1 and Stat3. *Nucleic Acids Res.* (**1997**) *25*, 2062-2067.
21. Wang D, Moriggl R, Stravopodis D, Carpino N, Marine JC, Teglund S, Feng J, Ihle JN. A small amphipathic alpha-helical region is required for transcriptional activities and proteasome-dependent turnover of the tyrosine phosphorylated Stat5. *Embo J* (**2000**) 19, 392-399.
22. Tanaka T, Soriano MA, Grusby MJ. SLIM is a nuclear ubiquitin E3 ligase that negatively regulates STAT signaling. *Immunity* (**2005**) 22, 729-736.
23. Levy DE, Darnell JE Jr. Stats: transcriptional control and biological impact. *Nat Rev Mol Cell Biol* (**2002**) 3(9), 651-662.
24. Maritano D, Sugrue ML, Tininini S, Dewilde S, Strobl B, Fu X, Murray-Tait V, Chiarle R, Poli V. The STAT3 isoforms alpha and beta have unique and specific functions. *Nat Immunol* (**2004**) 5, 401-409.
25. Ivanov VN, Bhoumik A, Krasilnikov M, Raz R, Owen-Schaub LB, Levy D, Horvath CM, Ronai Z. Cooperation between STAT3 and c-jun suppresses Fas transcription. *Mol Cell* (**2001**) 7, 517-528.
26. C. Schindler, C. Plumlee. Inteferons pen the JAK-STAT pathway. *Semin Cell Dev Biol* (**2008**) 19(4), 311-318.
27. Yoo JY, Huso DL, Nathans D, Desiderio S. Specific ablation of Stat3beta distorts the pattern of Stat3 responsive gene expression and impairs recovery from endotoxic shock. *Cell* (**2002**) 108, 331-344.
28. Akira S. Functional Roles of STAT Family Proteins: Lessons from Knockout Mice. *Stem Cells* (**1999**) 17(3), 138-146
29. Yu H., Jove R. STATs signaling pathway. *Nat Rev Cancer* (**2004**) 4, 97-105.
30. Bach EA, Tanner JW, Marsters S, Ashkenazi A, Aguet M, Shaw AS, Schreiber RD. Ligand-induced assembly and activation of the gamma interferon receptor in intact cells. *Mol Cell Biol* (**1996**) 16, 3214-3221.
31. Shuai K, Stark GR, Kerr IM, Darnell Jr JE. A single phosphotyrosine residue of Stat91 required for gene activation by interferon-gamma. *Science* (**1993**) 261(5129), 1744-1746.
32. Vignais ML, Sadowski HB, Watling D, Rogers NC, Gilman M. Platelet-derived growth factor induces phosphorylation of multiple JAK family kinases and STAT proteins. *Mol Cell Biol* (**1996**) 16, 1759-1769.
33. Novak U, Harpur AG, Paradiso L, Kanagasundaram V, Jaworowski A, Wilks AF, Hamilton JA. Colony-stimulating factor 1-induced STAT1 and STAT3 activation is accompanied by phosphorylation of Tyk2 in macrophages and Tyk2 and JAK1 in fibroblasts. *Blood* (**1995**) 86, 2948-2956.

34. Marrero MB, Schieffer B, Paxton WG, Heerdt L, Berk BC, Delafontaine P, Bernstein KE. Direct stimulation of Jak/STAT pathway by the angiotensin II AT1 receptor. *Nature* (**1995**) 373, 247-250.
35. Guillet-Deniau I, Burnol A-F, Girard J. Identification and localization of a skeletal muscle serotonin 5-HT2A receptor coupled to the Jak/STAT pathway. *J. Biol. Chem.* (**1997**) 272, 14825-14829.
36. Welte T, Leitenberg D, Dittel BN et al. STAT5 interaction with the T cell receptor complex and stimulation of T cell proliferation. *Science* (**1999**) 283,222-225.
37. Karras JG, Wang Z, Huo L, Frank DA, Rothstein TL. Induction of STAT protein signaling through the CD40 receptor in B lymphocytes: distinct STAT activation following surface Ig and CD40 receptor engagement. *J Immunol* (**1997**) 159, 4350-4355.
38. Horvath CM. STAT proteins and transcriptional responses to extracellular signals. *Trends Biochem Sci* (**2000**) 25, 496-502.
39. Pellegrini S, Dusanter-Fourt I, The structure, regulation and function of the Janus Kinases (JAKs) and the Signal Transducers and Activators of Transcription (STATs). *Europ J Biochem* (**1997**) 248(3), 615-633.
40. Kunihiro Yamaoka PS, Pesu M, Holt VET, Silvennoinen O, O'Shea JJ. The Janus kinases (Jaks). *Genome Biol.* (**2004**) *5*(12), 253-258.
41. Imada K, Leonard WJ. The Jak-STAT pathway. *Mol Immunol* (**2000**) 37(1-2), 1-11.
42. Lacronique V, Boureux A, Della Valle V, Poirel H, Quang CT, Mauchauffé M, Berthou C, Lessard M, Berger R, Ghysdael J, Bernard OA. A TEL-JAK2 Fusion Protein with Constitutive Kinase Activity in Human Leukemia. *Science* (**1997**) 278(5341), 1309-1312.
43. Goldfarb DS, Corbett AH, Mason DA, Harreman MT, Adam SA. Importin alpha: a multipurpose nuclear-transport receptor. *Trends Cell Biol* (**2004**) 14(9), 505-514.
44. Toshihiro Sekimoto KN, Tachibana T, Hirano T, Yoneda Y. Interferon-gamma-dependent nuclear import of Stat1 is mediated by the GTPase activity of Ran/TC4. *J. Biol. Chem.* (**1996**) 271(49), 31017-31020.
45. Pemberton LF, BM Paschal.. Mechanisms of receptor-mediated nuclear import and nuclear export. *Traffic* (**2005**) 6(3), 187-198.
46. Melen K, Kinnunen L, Julkunen I. Arginine/lysine-rich structural element is involved in interferon induced nuclear import of STATs. *J. Biol. Chem.* (**2001**) 276, 16447-16455.
47. McBride, KM, Banninger G, McDonald C, Reich NC. Regulated nuclear import of the STAT1 transcription factor by direct binding of importin-alpha. *Embo J* (**2002**) 21, 1754-1763.
48. Ma J, Zhang T, Novotny-Diermayr V, Tan AL, Cao X. A novel sequence in the coiled-coil domain of Stat3 essential for its nuclear translocation. *J. Biol. Chem.* (**2003**) 278, 29252-29260.
49. Ma J, Cao X. Regulation of Stat3 nuclear import by importin alpha5 and importin alpha7 via two different functional sequence elements. *Cell Signal* (**2006**) 18, 1117-1126.
50. Ushijima R, Sakaguchi N, Kano A, Maruyama A, Miyamoto Y, Sekimoto T, Yoneda Y, Ogino K, Tachibana T. Extracellular signal-dependent nuclear import of STAT3 is mediated by various importin alphas. Biochem *Biophys Res Commun* (**2005**) 330, 880-886.
51. Liu L, McBride KM, Reich NC. STAT3 nuclear import is independent of tyrosine phosphorylation and

mediated by importin-alpha3. *Proc Natl Acad Sci U S A* (**2005**) 102, 8150-8155.

52. Marg A, Shan Y, Meyer T, Meissner T, Brandenburg M, Vinkemeier U. Nucleocytoplasmic shuttling by nucleoporins Nup153 and Nup214 and CRM1-dependent nuclear export control the subcellular distribution of latent Stat1. *J Cell Biol* (**2004**) 165, 823-833.
53. McBride KM, Banninger G, McDonald C, Reich NC. Regulated nuclear import of the STAT1 transcription factor by direct binding of importin-alpha. *Embo J*. (**2002**) 21, 1754-1763.
54. Begitt A, Meyer T, Van Rossum T, Nucleocytoplasmic translocation of Stat1 is regulated by a leucine-rich export signal in the coiled-coil domain. *Proc Natl Acad Sci U S A*. (**2000**) 97, 10418-10423.
55. Meyer T, Marg A, Lemke P, Wiesner B, Vinkemeier U. DNA binding controls inactivation and nuclear accumulation of the transcription factor Stat1. *Genes Dev*. (**2003**) 17, 1992-2005.
56. Zhong Z, Wen Z, Darnell Jr JE. Stat3: a Stat family member activated by tyrosine phosporylation in response to epidermal growth factor and interleukine-6. *Science* (**1994**) 264, 95-98.
57. Yamamoto K, Quelle FW, Thierfelder WE, Kreider BL, Gilbert DJ, Jenkins NA, Copeland NG, Silvennoinen O, Ihle JN. Stat4, a novel gamma interferon activation site-binding protein expressed in early myeloid differentiation. *Mol Cell Biol.* (**1994**) 14(7), 4342-4349.
58. Horvath CM, Wen Z, Darnell Jr JE. A STAT protein domain that determines DNA sequence recognition suggests a novel DNA-binding domain. *Genes Dev* (**1995**) 9(8), 984-994.
59 Sadowshi HB, Shuai K, Darnell Jr JE, Gilman MZ. A common nuclear signal transduction pathway activated by growth factor and cytokine receptors. *Science* (**1993**) 261(5129), 1739-1744
60. Ungureanu D, Saharinen P, Junttila I, Hilton DJ, Silvennoinen O. Regulation of Jak2 through the ubiquitin-proteasome pathway involves phosphorylation of Jak2 on Y1007 and interaction with SOCS-1. *Mol Cell Biol*. (**2002**) 22, 3316-26.
61. Kim T.K, Maniatis T. Regulation of interferon-gamma-activated STAT1 by the ubiquitin-proteasome pathway. *Science* (**1996**) 273, 1717-1719.
62. Ulane CM, Rodriguez JJ, Parisien JP, Horvath CM. STAT3 ubiquitylation and degradation by mumps virus suppress cytokine and oncogene signaling. *J Virol*. (**2003**) 77, 6385-6393.
63. Shuai K, Liu B. Regulation of JAK-STAT signaling in the immune system. *Nat Rev Immunol* (**2003**) 3, 900-911.
64. Jiao H, Berrada K, Yang W, Tabrizi M, Platanias LC, Yi T. Direct association with and dephosphorylation of Jak2 kinase by the SH2-domaincontaining protein tyrosine phosphatase SHP-1. *Mol Cell Biol*. (**1996**) 16, 6985-6992.
65. Chen X, Vinkemeier U, Zhao Y, Jeruzalmi D, Darnell Jr JE, Kuriyan J. Crystal structure of a tyrosine phosphorylated STAT-1 dimer bound to DNA. *Cell* (**1998**) 93, 827-839.
66. Aoki N, Matsuda T. A cytosolic protein-tyrosinephosphatase PTP1B specifically dephosphorylates and deactivates prolactin-activated STAT5a and STAT5b. *J. Biol.Chem.* (**2000**) 275, 39718-39726.
67. Ten Hoeve J, De Jesus I, Barra-Sanchez M, Fu Y, Zhu W, Tremblay M, David M, Shuai K. Identification of a nuclear Stat1 protein tyrosine phosphatase. *Mol. Cell. Biol.* (**2002**) 22, 5662-5668.

68. Wu TR, Hong YK, Wang XD, Ling MY, Dragoi AM, Chung AS, Campbell AG, Han ZY, Feng GS, Chin YE. SHP-2 is a dual-specificity phosphatase involved in Stat1 dephosphorylation at both tyrosine and serine residues in nuclei. *J. Biol. Chem.* (**2002**) 277, 47572-47580.

69. Krebs DL, Hilton DJ. SOCS: physiological suppressors of cytokine signaling. *J Cell Sci*. (**2000**) 113, 2813-2819.

70. Zhang JG, Farley A, Nicholson SE, Willson TA, Zugaro LM, Simpson RJ, Moritz RL, Cary D, Richardson R, Hausmann G, Kile BJ, Kent SB, Alexander WS, Metcalf D, Hilton DJ, Nicola NA, Baca M. The conserved SOCS box motif in suppressors of cytokine signaling binds to elongins B and C and may couple bound proteins to proteasomal degradation. *Proc Natl Acad Sci U S A*. (**1999**) 96, 2071-2076.

71. Matsumoto A, Masuhara M, Mitsui K, Yokouchi M, Ohtsubo M, Misawa H, Miyajima A, Yoshimura A. CIS, a cytokine inducible SH2 protein, is a target of the JAK-STAT5 pathway and modulates STAT5 activation. *Blood* (**1997**) 89, 3148-3154.

72. Nicholson SE, Willson TA, Farley A, Starr R, Zhang JG, Baca M, Alexander WS, Metcalf D, Hilton DJ, Nicola NA. Mutational analyses of the SOCS proteins suggest a dual domain requirement but distinct mechanisms for inhibition of LIF and IL-6 signal transduction. *Embo J*. (**1999**) 18, 375-385.

73. Verdier F, Chretien S, Muller O, Varlet P, Yoshimura A, Gisselbrecht S, Lacombe C, Mayeux P. Proteasomes regulate erythropoietin receptor and signal transducer and activator of transcription 5 (STAT5) activation. Possible involvement of the ubiquitinated Cis protein. *J Biol Chem*. (**1998**) 273, 28185-28190.

74. Shuai K. Modulation of STAT signaling by STAT-interacting proteins. *Oncogene* (**2000**) 19, 2638-2644.

75. Liu B, Liao J, Rao X, Kushner SA, Chung CD, Chang DD, Shuai K. Inhibition of Stat1-mediated gene activation by PIAS1. *Proc. Natl Acad. Sci. USA* (**1998**) 95, 10626-10631.

76. Chung CD, Liao J, Liu B, Rao X, Jay P, Berta P, Shuai K. Specific inhibition of Stat3 signal transduction by PIAS3. *Science* (**1997**) 278, 1803-1805

77. Arora T, Liu B, He H, Kim J, Murphy TL, Murphy KM, Modlin RL, Shuai K. PIASx is a transcriptional co-repressor of signal transducer and activator of transcription 4. *J. Biol. Chem.* (**2003**) 278, 21327-21330.

78. Liao J, Fu Y, Shuai K. Distinct roles of the NH2- and COOH-terminal domains of the protein inhibitor of activated signal transducer and activator of transcription (STAT)1 (PIAS1) in cytokine-induced PIAS1–Stat1 interaction. *Proc. Natl Acad. Sci. USA* (**2000**) 97, 5267-5272.

79. Liu B, Gross M, Ten Hoeve J, Shuai K. A transcriptional co-repressor of Stat1 with an essential LXXLL signature motif. *Proc. Natl Acad. Sci. USA* (**2001**) 98, 3203-3207-

80. Tussie-Luna MI, Bayarsaihan D, Seto E, Ruddle FH, Roy AL. Physical and functional interactions of histone deacetylase 3 with TFII-I family proteins and PIASx. *Proc. Natl Acad. Sci. USA* (**2002**) 99, 12807-12812.

81. Long J, Matsuura I, He D, Wang G, Shuai K, Liu F. Repression of Smad transcriptional activity by PIASy. *Proc. Natl Acad. Sci. USA* (**2003**) 100, 9791-9796.

82. Johnson ES, Gupta AA. An E3-like factor that promotes SUMO conjugation to the yeast septins. *Cell* (**2001**) 106, 735-744.

83. Durbin JE, Hackenmiller R, Simon MC, Levy DE. Targeted disruption of the mouse Stat1 gene results in compromised innate immunity to viral disease. *Cell*. (**1996**) 84, 443-450.

84. Meraz MA, White JM, Sheehan KC, Bach EA, Rodig SJ, Dighe AS, Kaplan DH, Riley JK, Greenlund AC, Campbell D, Carver-Moore K, DuBois RN, Clark R, Aguet M, Schreiber RD. Targeted disruption of the Stat1 gene in mice reveals unexpected physiologic specificity in the JAK-STAT signaling pathway. *Cell*. (**1996**) 84, 431-442.

85 Dupuis S, Dargemont C, Fieschi C, Thomassin N, Rosenzweig S, Harris J, Holland SM, Schreiber RD, Casanova JL. Impairment of mycobacterial but not viral immunity by a germline human STAT1 mutation. *Science*. (**2001**) 293, 300-303.

86. Shankaran V, Ikeda H, Bruce AT, White JM, Swanson PE, Old LJ, Schreiber RD. IFNgamma and lymphocytes prevent primary tumour development and shape tumour immunogenicity. *Nature* (**2001**) 410, 1107-1111.

87. Park C, Li S, Cha E, Schindler C. Immune response in Stat2 knockout mice. *Immunity* (**2000**) 13, 795-804.

88. Kaplan MH, Sun YL, Hoey T, Grusby MJ. Impaired IL-12 responses and enhanced development of Th2 cells in Stat4-deficient mice. *Nature* (**1996**) 382, 174-177.

89. Chitnis T, Najafian N, Benou C, Salama AD, Grusby MJ, Sayegh MH, Khoury SJ. Effect of targeted disruption of STAT4 and STAT6 on the induction of experimental autoimmune encephalomyelitis. *J Clin Invest* (**2001**) 108,739-747.

90. Rogge L, D'Ambrosio D, Biffi M, Penna G, Minetti LJ, Presky DH, Adorini L, Sinigaglia F. The role of Stat4 in species-specific regulation of Th cell development by type I IFNs. *J Immunol* (**1998**) 161, 6567-6574.

91. Farrar JD, Smith JD, Murphy TL, Leung S, Stark GR, Murphy KM. Selective loss of type I interferon-induced STAT4 activation caused by aminisatellite insertion in mouse Stat2. *Nat Immunol* (**2000**) 1, 65-69.

92. Azam M, Lee C, Strehlow I, Schindler C. Functionally distinct isoforms of STAT5 are generated by protein processing. *Immunity*. (**1997**) 6, 691-701.

93. Mui AL, Wakao H, O'Farrell AM, Harada N, Miyajima A. Interleukin-3,granulocyte-macrophage colony stimulating factor and interleukin-5 transduce signals through two STAT5 homologs. *Embo J*. (**1995**) 14, 1166-1175.

94. Teglund S, McKay C, Schuetz E, Van Deursen JM, Stravopodis D, Wang D, Brown M, Bodner S, Grosveld G, Ihle JN. Stat5a and Stat5b proteinshave essential and nonessential, or redundant, roles in cytokine responses. *Cell* (**1998**) 93, 841-850.

95. Kisseleva T, Bhattacharya S, Braunstein J, Schindler CW. Signaling through the JAK/STAT pathway, recent advances and future challenges. *Gene*. (**2002**) 285, 1-24.

96. Kaplan MH, Schindler U, Smiley ST, Grusby MJ. Stat6 is required for mediating responses to IL-4 and for development of Th2 cells. *Immunity* (**1996**) 4, 313-319.

97. Shimoda K, Van Deursen J, Sangster MY, Sarawar SR, Carson RT, Tripp RA, Chu C, Quelle FW, Nosaka T, Vignali DA, Doherty PC, Grosveld G, Paul WE, Ihle JN. Lack of IL-4-induced Th2 response and IgE class switching in mice with disrupted Stat6 gene. *Nature* (**1996**) 380, 630-633.

98. Takeda K, Tanaka T, Shi W, Matsumoto M, Minami M, Kashiwamura S, Nakanishi K, Yoshida N, Kishimoto T, Akira S. Essential role of Stat6 in IL-4 signaling. *Nature* (1996) 380, 627-630.

99. Chitnis T, Najafian N, Benou C, Salama AD, Grusby MJ, Sayegh MH, Khoury SJ. Effect of targeted disruption of STAT4 and STAT6 on the induction of experimental autoimmune encephalomyelitis. *J Clin Invest* (**2001**) 108, 739-747.

100. Lentsch AB, Kato A, Davis B, Wang W, Chao C, Edwards MJ. STAT4 and STAT6 regulate systemic inflammation and protect against lethal endotoxemia. *J Clin Invest* (**2001**) 108, 1475-1482.

101 .Wegenka UM, Buschmann J, Lutticken C, Heinrich PC, Horn F. Acutephase response factor, a nuclear factor binding to acute-phase response elements, is rapidly activated by interleukin-6 at the posttranslational level. *Mol Cell Biol* (**1993**) 13, 276-288.

102. Akira S, Nishio Y, Inoue M, Wang XJ, Wei S, Matsusaka T, Yoshida K, Sudo T, Naruto M, Kishimoto T. Molecular cloning of APRF, a novel IFNstimulated gene factor 3 p91-related transcription factor involved in the gp130-mediated signaling pathway. *Cell* (**1994**) 77, 63-71.

103. Hirano T, Ishihara K, Hibi M. Roles of STAT3 in mediating the cell growth, differentiation and survival signals relayed through the IL-6 family of cytokine receptors. *Oncogene* (**2000**) 19, 2548-2556.

104. Minami M, Inoue M, Wei S, Takeda K, Matsumoto M, Kishimoto T, Akira S. STAT3 activation is a critical step in gp130-mediated terminal differentiation and growth arrest of a myeloid cell line. *Proc Natl Acad Sci USA* (**1996**) 93, 3963-3966.

105. Fukada T, Ohtani T, Yoshida Y, Shirogane T, Nishida K, Nakajima K, Hibi M, Hirano T. STAT3 orchestrates contradictory signals in cytokine-induced G1 to S cell-cycle transition. *Embo J* (**1998**) 17, 6670-6677.

106. Ihara S, Nakajima K, Fukada T, Hibi M, Nagata S, Hirano T, Fukui Y. Dual control of neurite outgrowth by STAT3 and MAP kinase in PC12 cells stimulated with interleukin-6. *Embo J* (**1997**) 16, 5345-5352.

107. Boeuf H, Hauss C, Graeve FD, Baran N, Kedinger C. Leukemia inhibitory factor-dependent transcriptional activation in embryonic stem cells. *J Cell Biol* (**1997**) 138, 1207-1217.

108. Niwa H, Burdon T, Chambers I, Smith A. Self-renewal of pluripotent embryonic stem cells is mediated via activation of STAT3. *Genes Dev*. (**1998**) 12, 2048-2060.

109. Raz R, Lee CK, Cannizzaro LA, D'Eustachio P, Levy DE. Essential role of STAT3 for embryonic stem cell pluripotency. *Proc Natl Acad Sci U S A*. (**1999**) 96, 2846-51.

110. Matsuda T, Nakamura T, Nakao K, Arai T, Katsuki M, Heike T, Yokota T. STAT3 activation is sufficient to maintain an undifferentiated state of mouse embryonic stem cells. *Embo J* (**1999**) 18, 4261-4269.

111. Takeda K, Noguchi K, Shi W, Tanaka T, Matsumoto M, Yoshida N, Kishimoto T, Akira S. Targeted disruption of the mouse Stat3 gene leads to early embryonic lethality. *Proc Natl Acad Sci U S A* (**1997**) 94, 3801-3804.

112. Takeda K, Kaisho T, Yoshida N, Takeda J, Kishimoto T, Akira S. Stat3 activation is responsible for IL-6-dependent T cell proliferation through preventing apoptosis: generation and characterization of T cell-specific Stat3-deficient mice. *J Immunol* (**1998**) 161, 4652-4660.

113. Takeda K, Clausen BE, Kaisho T, Tsujimura T, Terada N, Forster I, Akira S. Enhanced Th1 activity and development of chronic enterocolitis in mice devoid of Stat3 in macrophages and neutrophils. *Immunity* (**1999**) 10, 39-49.

114. Riley JK, Takeda K, Akira S, Schreiber RD. Interleukin-10 receptor signaling through the JAK-STAT pathway. Requirement for two distinct receptorderived signals for anti-inflammatory action. *J Biol Chem* (**1999**) 274, 16513-16521.

115. Chapman RS, Lourenco PC, Tonner E, Flint DJ, Selbert S, Takeda K, Akira S, Clarke AR, Watson CJ. Suppression of epithelial apoptosis and delayed mammary gland involution in mice with a conditional knockout of Stat3. *Genes Dev* (**1999**) 13, 2604-2616.

116. Sano S, Itami S, Takeda K, Tarutani M, Yamaguchi Y, Miura H, Yoshikawa K, Akira S, Takeda J. Keratinocyte-specific ablation of Stat3 exhibits impaired skin remodeling, but does not affect skin morphogenesis. *Embo J* (**1999**) 18, 4657-4668.

117. Alonzi T, Middleton G, Wyatt S, Buchman V, Betz UA, Muller W, Musiani P, Poli V, Davies AM. Role of STAT3 and PI 3-kinase/Akt in mediating the survival actions of cytokines on sensory neurons. *Mol Cell Neurosci* (**2001**) 18, 270-282.

118. Schweizer U, Gunnersen J, Karch C, Wiese S, Holtmann B, Takeda K, Akira S, Sendtner M. Conditional gene ablation of Stat3 reveals differential signaling requirements for survival of motoneurons during development and after nerve injury in the adult. *J Cell Biol* (**2002**) 156, 287-297.

119. Jacoby JJ, Kalinowski A, Liu MG, Zhang SS, Gao Q, Chai GX, Ji L, Iwamoto Y, Li E, Schneider M, Russell KS, Fu XY. Cardiomyocyte-restricted knockout of STAT3 results in higher sensitivity to inflammation, cardiac fibrosis, and heart failure with advanced age. *Proc Natl Acad Sci U S A* (**2003**) 100, 12929-12934.

120. Alonzi T, Maritano D, Gorgoni B, Rizzuto G, Libert C, Poli V. Essential role of STAT3 in the control of the acute-phase response as revealed by inducible gene inactivation [correction of activation] in the liver. *Mol Cell Biol* (**2001**) 21, 1621-1632.

121. Yoo JY, Huso DL, Nathans D, Desiderio S. Specific ablation of Stat3beta distorts the pattern of Stat3-responsive gene expression and impairs recovery from endotoxic shock. *Cell*. (**2002**) 108, 331-344.

122. Darnell JE Jr. Validating Stat3 in cancer therapy. *Nature Medicine* (**2005**) 11, 595-596.

123. Chan KS, Sano S, Kiguchi K, Anders J, Komazawa N, Takeda J, Di Giovanni J. Disruption of Stat3 reveals a critical role in both the initiation and the promotion stages of epithelial carcinogenesis. *J. Clin. Invest.* (**2004**) 114, 720-728.

124. R. Chiarle, Simmons WJ, Cai H, Dhall G, Zamo A, Raz R, Karras JG, Levy DE, Inghirami G. Stat3 is required for ALK-mediated lymphomagenesis and provides a possible therapeutic target. *Nat. Med.* (**2005**) 11(6), 623-629

125. Yoshikawa H, Matsubara K, Qian GS, Jackson P, Groopman JD, Manning JE, Harris CC, Herman JG. SOCS-1, a negative regulator of the JAK/STAT pathway, is silenced by methylation in human hepatocellular carcinoma and shows growth-suppression activity. *Nat. Genet.* (**2001**) 28(1), 29-35.

126. He B, You L, Uematsu K, Zang K, Xu Z, Lee AY, Costello JF, McCormick F, Jablons DM. SOCS-3 is frequently silenced by hypermethylation and suppresses cell growth in human lung cancer. *Proc. Natl. Acad. Sci. USA* (**2003**) 100(24), 14133-14138.

127. Zhang Q, Raghunath PN, Xue L, Majewski M, Carpentieri DF, Odum N, Morris S, Skorski T, Wasik MA. Multilevel Dysregulation of STAT3 Activation in Anaplastic Lymphoma Kinase-Positive T/Null-Cell Lymphoma. *J. Immunol.* (**2002**) 168, 466-474.

128. Buettner R, Mora LB, Jove R. Activated STAT Signaling in Human Tumors Provides Novel Molecular Targets for Therapeutic Intervention. *Clin Cancer Res* (**2002**) 8(4), 945-954.

129. Morris SW, Kirstein MN, Valentine MB, Dittmer K, Shapiro DN, Look AT, Saltman DL. Fusion of a kinase gene, ALK, to a nucleolar protein gene, NPM, in non-Hodgkin's lymphoma. *Science* (**1994**) 263, 1281-1284.

130. Xi S, Gooding WE, Grandis JR. In vivo antitumor efficacy of STAT3 blockade using a transcription factor decoy approach: implications for cancer therapy. *Oncogene* (**2005**) 24(6), 970-979.

131. Aggarwal BB, Kunnumakkara AB, Harikumar KB, Gupta SR, Tharakan ST, Koca C, Dey S, Sung B. Signal transducer and activator of transcription-3, inflammation, and cancer: how intimate is the relationship? *Ann N Y Acad Sci.* (**2009**) 1171, 59-76.

132. Catlett-Falcone R, Landowski TH, Oshiro MM, Turkson J, Levitzki A, Savino R, Ciliberto G, Moscinski L, Fernández-Luna JL, Nuñez G, Dalton WS, Jove R. Constitutive activation of Stat3 signaling confers resistance to apoptosis in human U266 myeloma cells. *Immunity* (**1999**) 10, 105-115.

133. Karni R, Jove R, Levitzki A. Inhibition of pp60c-Src reduces Bcl-XL expression and reverses the transformed phenotype of cells overexpressing EGF and HER-2 receptors. *Oncogene* (**1999**) 18, 4654–4662.

134. Zushi S, Shinomura Y, Kiyohara T, Miyazaki Y, Kondo S, Sugimachi M, Higashimoto Y, Kanayama S, Matsuzawa Y. STAT3 mediates the survival signal in oncogenic ras-transfected intestinal epithelial cells. *Int. J. Cancer.* (**1998**) 78, 326-330.

135. Mahboubi K, Li F, Plescia J, Kirkiles-Smith NC, Mesri M, Du Y, Carroll JM, Elias JA, Altieri DC, Pober JS. Interleukin-11 upregulates survivin expression in endothelial cells through a signal transducer and activator of transcription-3 pathway. *Lab Invest* (**2001**) 81, 327-334.

136. Liu H, Ma Y, Cole SM, Zander C, Chen KH, Karras J, Pope RM. Serine phosphorylation of STAT3 is essential for Mcl-1 expression and macrophage survival. *Blood* (**2003**) 102, 344-352.

137. Aoki Y, Feldman GM, Tosato G. Inhibition of STAT3 signaling induces apoptosis and decreases survivin expression in primary effusion lymphoma. *Blood* (**2003**) 101, 1535-1542.

138. Kanda N, Seno H, Konda Y, Marusawa H, Kanai M, Nakajima T, Kawashima T, Nanakin A, Sawabu T, Uenoyama Y, Sekikawa A, Kawada M, Suzuki K, Kayahara T, Fukui H, Sawada M, Chiba T. STAT3 is

constitutively activated and supports cell survival in association with survivin expression in gastric cancer cells. *Oncogene* (**2004**) 23, 4921-4929.

139. Konnikova L, Kotecki M, Kruger MM, Cochran BH. Knockdown of STAT3 expression by RNAi induces apoptosis in astrocytoma cells. *BMC Cancer* (**2003**) 3(23).
140. Bowman T, Garcia R, Turkson J, Jove R. STATs in oncogenesis. *Oncogene* (**2000**) 19(21), 2474-2488.
141. Battle TE, Frank DA. The Role of STATs in apoptosis. *Curr mol med* (**2002**) 2(4), 381-392.
142. Bowman T, Broome MA, Sinibaldi D, Wharton W, Pledger WJ, Sedivy JM, Irby R, Yeatman T, Courtneidge SA, Jove R. *Proc Natl Acad Sci U S A* (**2001**) 98(13), 7319-7324.
143. Turkson J, Ryan D, Kim JS, Zhang Y, Chen Z, Haura E, Laudano A, Sebti S, Hamilton AD, Jove R. Phosphotyrosyl Peptides Block Stat3-mediated DNA Binding Activity, Gene Regulation, and Cell Transformation. *J. Biol. Chem.* (**2001**) 276(48), 45443-45455

144 Masuda M, Suzui M, Yasumatu R, Nakashima T, Kuratomi Y, Azuma K, Tomita K, Komiyama S, Weinstein IB. Constitutive activation of signal transducers and activators of transcription 3 correlates with cyclin D1 overexpression and may provide a novel prognostic marker in head and neck squamous cell carcinoma. *Cancer Res* (**2002**) 62, 3351-3355.

145 . Kiuchi N, Nakajima K, Ichiba M, Fukada T, Narimatsu M, Mizuno K, Hibi M, Hirano T. STAT3 is required for the gp130-mediated full activation of the c-myc gene. *J. Exp. Med.* (**1999**) 189, 63-73.

146. Shirogane T, Fukada T, Muller JM, Shima DT, Hibi M, Hirano T. Synergistic roles for Pim-1 and c-Myc in STAT3-mediated cell cycle progression and antiapoptosis. *Immunity* (**1999**) 11, 709-719.
147. Bellido T, O'Brien CA, Roberson PK, Manolagas SC. Transcriptional activation of the p21(WAF1,CIP1,SDI1) gene by interleukin-6 type cytokines. A prerequisite for their prodifferentiating and anti-apoptotic effects on human osteoblastic cells. *J. Biol. Chem.* (**1998**) 273, 21137-21144.
148. Xie TX, Wei D, Liu M, Gao AC, Ali-Osman F, Sawaya R Huang S. Stat3 activation regulates the expression of matrix metalloproteinase-2 and tumor tumor invasion and metastasis. *Oncogene* (**2004**) 23, 3550-3560.
149. Itoh M, Murata T, Suzuki T, Shindoh M, Nakajima K, Imai K, Yoshida K. Requirement of STAT3 activation for maximal collagenase-1 (MMP-1) induction by epidermal growth factor and malignant characteristics in T24 bladder cancer cells. *Oncogene* (**2006**) 25, 1195-1204.
150. Suiqing C, Min Z, Lirong C. Overexpression of phosphorylated-STAT3 correlated with the invasion and metastasis of cutaneous squamous cell carcinoma. *J. Dermatol.* (**2005**) 32, 354-360.
151. Dien J, Amin HM, Chiu N, Wong W, Frantz C, Chiu B, Mackey JR, Lai R. Signal transducers and activators of transcription-3 up-regulates tissue inhibitor of metalloproteinase-1 expression and decreases invasiveness of breast cancer. *Am. J. Pathol.* (**2006**) 169, 633-642.
152. Gaemers IC, Vos HL, Volders HH, Van der Valk SW, Hilkens J. A stat-responsive element in the promoter of the episialin/MUC1 gene is involved in its overexpression in carcinoma cells. *J. Biol. Chem.* (**2001**) 276, 6191-6199.

153. Masciocchi D, Gelain A, Villa S, Meneghetti F, Barlocco D. Signal transducer and activator of transcription 3 (STAT3): a promising target for anticancer therapy. *Future Med Chem* (**2011**) 3(5), 367-397

154 . Shin DS, Kim, HN.; Shin, KD. *et al.* Cryptotanshinone inhibits constitutive signal transducer and activator of transcription 3 function through blocking the dimerization in DU145 prostate cancer cells. Cancer Res. 2009, *69*, 193-202.

155. Yu CL, Meyer DJ, Campbell GS, Larner AC, Carter-Su C, Schwartz J, Jove R. Enhanced DNA-binding activity of a Stat3-related protein in cells transformed by the Src oncoprotein. *Science* (**1995**) 269(5220), 81-83.

156. Keskin O, Gursoy A, Ma B, Nussinov R. Principles of protein-protein interactions: what are the preferred ways for proteins to interact? *Chem Rev.* (**2008**) 108(4), 1225-1244.

157. Wells JA, McClendon CL. Reaching for high-hanging fruit in drug discovery at protein–protein interfaces. *Nature* (**2007**) 450, 1001-1009.

158. Kwon BM, Han DC, Son KH, Shin DS. *Patent US20080051442*, 5 pp.

159. Sherf BA, Navarro SL, Hannah RR, Wood KV. *Promega Notes Magazine* (**1996**) 57, 2-8.

160. Shin DS, Masciocchi D, Gelain A, Villa S, Barlocco D, Meneghetti F, Pedretti A, Han YM, Han DC, Kwon BM, Legnani L, Toma L. Synthesis, modeling, and crystallographic study of 3,4-disubstituted-1,2,5-oxadiazoles and evaluation of their ability to decrease STAT3 activity. *MedChemComm* (**2010**), 1(2), 156-164.

161. Masciocchi D, Villa S, Gelain A, Meneghetti F, Pedretti A, Barlocco D, Kwon BM. Studies on potential STAT-3 inhibitors: reactivity and behaviour of furazan derivatives. *Hungarian-Austrian- Czech- German- Greek- Italian- Polish- Slovak- Slovenian Joint Meeting on Medicinal Chemistry* – (Budapest, 24-27 June **2009**) P-35, Book of Abstracts p.103.

162. Masciocchi D, Villa S, Gelain A, Pedretti A, Meneghetti F, Barlocco D, Kwon BM, Development on furazan derivatives as potential STAT-3 inhibitors. *XXIII Congresso Nazionale della Società Chimica Italiana* - (Sorrento, 5-10 July **2009**) FAR-PO-45, Book of Abstracts p.168.

163. Sheremetev AB, Shamshina YL, Dmitriev DE. Synthesis of 3-Alkyl-4-Aminofurazans. *Russ. Chem. Bull. Int. Ed*. (**2005**) 54, 1032-1037.

164. Sheremetev AB, Aleksandrova NS, Dmitriev DE. Synthesis and X-ray Study of Novel Azofurazan-Annulated Macrocyclic Lactams. *J. Het. Chem*. (**2005**) 42, 519-525.

165. Sheremetev AB. One Pot Synthesis of 3-Amino-4-Aryl and 3-Amino-4-heteroarylfurazans. *Russ. Chem. Bul. Int. E.* (**2005**) 54, 1057-1059.

166. Villa S, Masciocchi D, Gelain A, Meneghetti F. The influence of the substitution pattern on the molecular conformation of ureido 1,2,5-oxadiazole derivatives, related to STAT3 inhibitors: chemical behaviour and structural investigation. *Chem. Biodiv.* doi:10.1002/cbdv.201100339

167. a) Marumoto S, Kogen H, Naruto S. Absolute Configuration and Total Synthesis of (+)-Epolactaene, a Neuritogenic Agent from Penicillium sp. BM 1689-P Active in Human Neuroblastoma Cells. *J. Org. Chem.* (**1998**) *63*, 2068-2069; b) Granier T, Vasella A. Synthesis and Some Transformations of 2-

Acetamido-5-amino-3,4,6-tri-O-benzyl-2,5-dideoxy-D-glucono-1,5-lactam. *Helv. Chim. Acta* (**1998**) *81*, 865-880; c) White JD, Hrnciar P. Synthesis of Ring D Modified Morphinan Systems via Ring Expansion of a Key Codeine Intermediate *J. Org. Chem.* (**2000)** *65*, 2646-2650; d) Consonni A, Danieli B, Lesma G, Passarella D, Piacenti P, Silvani A, An Efficient Enantioselective Entry to the Piperidino-Quinolizidine Ring System of Lupine Alkaloids by Means of N-Acyliminium Ion Initiated Cyclization Reactions. *Eur. J. Org. Chem.* (**2001**) *7*, 1377-1383; e) Schrey A, Osterkamp F, Straudi A, Rickert C, Wagner H, Koert U, Herrschaft B, Harms K. Synthesis of Enantiomerically Pure Amino Acids Containing 2,5-Disubstituted tetrahydrofurane Rings in the Molecular Backbone. *Eur. J. Org. Chem.* (**1999**) *11*, 2977-2990; f) V.-D. Le, C.-H. Wong. Synthesis of 2-Substituted Polyhydroxytetrahydropyrimidines (N-Hydroxy Cyclic Guanidino-Sugars): Transition-State Mimics of Enzymatic Glycosidic Cleavage . *J. Org. Chem.* (**2000**) *65*, 2399-2409; g) Yu C, Hu L. A facile synthesis of cyclic enecarbamates using Dess–Martin periodinane. *Tetrahedron Lett.* (**2001**) *42*, 5167-5170.

168. Noonan DJ, Henry K, Twaroski ML. A high-throughput mammalian cell-based transient transfection assay. *Meth mol biol* (**2004**) *284*, 51-65.

169. Souriau C, Fort P, Roux P, Hartley O, Lefranc MP, Weill M. A simple luciferase assay for signal transduction activity detection of epidermal growth factor displayed on phage. *Nucl Acids Res* (**1997**) *25* (8), 1585-1590.

170 Dae-Seop Shin thesis: “Discovery and mechanistic study of STAT3 inhibitors in cancer cells” (October, 2007)

171. Saloumeh Kadkhodayan LOE, Mausisa G, Wallweber HA, Deshayes K, Feng B, Fairbrother WJ. *ASSAY and Drug Development Technologies* (**2007**) *5* (4), 501-514.

172. Y. Uehara, M. Mochizuki, K. Matsuno, T. Haino and A. Asai, Novel high-throughput screening system for identifying STAT3–SH2 antagonists *Biochem. Biophys. Res. Commun.* (**2009**) 380, 627-631.

173. National Cancer Institute, http://dtp.nci.nih.gov.

174. D. Masciocchi, S. Villa, F. Meneghetti, A. Pedretti, D. Barlocco, L. Legnani, L. Toma, B-M. Kwon, S. Nakano, A. Asai, A. Gelain. Biological and computational evaluation of an oxadiazole derivative (MD77) as a new lead for direct STAT3 inhibitors. Submitted 2012

175. C. K. Johnson, ORTEP 11, Report ORNL-5138, OakRidge National Laboratory, TN, 1976.

176 . a) Lee C, Yang W, Parr RG. Development of the Colle-Salvetti Correlation-Energy Formula into a Functional of the Electron Density. *Phys. Rev. B*, (**1988**) 37, 785-789; b) A. D. Becke. Density-functional thermochemistry. III. The role of exact exchange. *J. Chem. Phys.* (**1993**) 98, 5648-5652.

177. a) Cancés E, Mennucci B, Tomasi J. A new integral equation formalism for the polarizable continuum model: theoretical background and applications to isotropic and anisotropic dielectrics. *J. Chem. Phys.* (**1997**) 107, 3032-3042; b) Cossi M, Barone V, Cammi R, Tomasi J. Ab Initio Study of Solvated Molecules: a New Implementation of the Polarizable Continuum Model. *Chem. Phys. Lett.* (**1996**) 255, 327-335; c)

Barone V, Cossi M, Tomasi J. Geometry optimization of molecular structures in solution by the polarizable continuum model. *J. Comput. Chem.* (**1998**) 19, 404-417.

178. Cignarella G, Barlocco D, Pinna GA, Loriga M, Curzu MM, Tofanetti O, Germini M, Cazzulani P, Cavalletti E. Synthesis and biological evaluation of substituted benzo[h]cinnolinones and 3H-benzo[6,7]cyclohepta[1,2-c]pyridazinones: higher homologs of the antihypertensive and antithrombotic 5H-indeno[1,2-c]pyridazinones. *J. Med. Chem.* (**1989**) 32, 2277-2282.

179. Cignarella G, Barlocco D, Pinna GA, Loriga M, Tofanetti O, Germini M, Sala F. Conformationally restricted congeners of hypotensive and platelet aggregation inhibitors: 6-aryl-5-methyl-4,5-dihydro-3(2H)-pyridazinones derived from 5H-indeno[1,2-c]pyridazine. *J. Med. Chem.* (**1986**) 29, 2191-2194.

180. Gelain A, Masciocchi D, Villa S, Pedretti A, Meneghetti F, Barlocco D, Kwon BM, Shin DS, Legnani L, Toma L. Tricyclic Pyridazinone derivatives : development of new STAT-3 inhibitors. Drugs of the future. 35: Supplement A(**2010**), p. 158.

181. Frisch MJ, Trucks GW, Schlegel HB, Scuseria GE, Robb MA, Cheeseman JR, Montgomery Jr JA, Vreven T, Kudin KN, Burant JC, Millam JM, Iyengar SS, Tomasi J, Barone V, Mennucci B, Cossi M, Scalmani G, Rega N, Petersson GA, Nakatsuji H, Hada M, Ehara M, Toyota K, Fukuda R, Hasegawa J, Ishida M, Nakajima T, Honda Y, Kitao O, Nakai H, Klene M, Li X, Knox JE, Hratchian HP, Cross JB, Adamo C, Jaramillo J, Gomperts R, Stratmann RE, Yazyev O, Austin AJ, Cammi R, Pomelli C, Ochterski JW, Ayala PY, Morokuma K, Voth GA, Salvador P, Dannenberg JJ, Zakrzewski VG, Dapprich S, Daniels AD, Strain MC, Farkas O, Malick DK, Rabuck AD, Raghavachari K, Foresman JB, Ortiz JV, Cui Q, Baboul AG, Clifford S, Cioslowski J, Stefanov BB, Liu G, Liashenko A, Piskorz P, Komaromi I, Martin RL, Fox DJ, Keith T, Al-Laham MA, Peng CY, Nanayakkara A, Challacombe M, Gill PMW, Johnson B, Chen W, Wong MW, Gonzalez C, Pople JA, Gaussian 03, Revision B.04., Gaussian, Inc. Pittsburgh PA (**2003**).

182. a) Becke AD. Density-functional thermochemistry .3. The role of exact exchange. *J Chem Phys* (**1993**) *98* (7), 5648-5652; b) Lee C, Yang W, Parr RG. Development of the of the Colle-Salvetti correlation-energy formula into a functional of the electron density. *Physical Review B: Condensed Matter and Materials Physics* (**1988**) *37* (2), 785-789.

183. Cignarella G, Grella G, Curzu MM. Hydroxymethylation of 3-aroylpropanoic acids; an improved synthesis of 4-aroyl-2(3H)-dihydrofuranones and an easy approach to 3-aroyl-3-butenoic acids. *Synthesis* (**1980**) 10,825-828.

184 Laguna R, Rodriguez-Linares B, Cano E, Estevez I, Ravina E, Sotelo E. Pyridazines. XIII. Synthesis of 6-aryl-5-oxygenated substituted -3(2H)-pyridazinones and evaluation as platelet aggregation inhibitors. *Chem.Pharm.Bull*. (**1997**) 45(7), 1151-1155.

185. Lee J, Tang J, Snyder J, Preparation and dienophilicity of 3-methyl-4,5-benzofurandione *Tetrahedron Lett* (**1987**) 28(30), 3427-3430.

186. Zhang J, Duan W, Cai J. Asymmetric synthesis of 3(S),17-dihydroxytanshinone. *Tetrahedron* (**2004**) 60,1665-1669.

187. Shen Y, Tian Y, Bu X, Gu L. Natural Tanshinone-likeheterocyclic-fusedorthoquinone from regioselectiveDiels-Alderreaction: Synthesis and Cytotoxicityevaluation. *Eur J Med Chem* (**2009**) 44, 3915-3921.

188. http://www.pdb.org/

189. Becker S, Groner B, Müller CW. Three-dimensional structure of the Stat3beta homodimer bound to DNA. *Nature* (**1998**) 934(6689), 145-151.

190. Pedretti A, Villa L, Vistoli G, VEGA: a versatile program to convert, handle and visualize molecular structure on windows-based PCs. *J. Mol. Graph.* (**2002**) 21, 47-49.

191. Gasteiger J, Marsili M, Iterative partial equalization of orbital electronegativity-a rapid access to atomic charges. *Croat. Chem. Acta* (1980) 53, 601-614.

192. MacKerell Jr AD, Bashford D, Bellott M, Dunbrack Jr RL, Evanseck JD, Field MJ, Fischer S, Gao J, Guo H, Ha S, Joseph-McCarthy D, Kuchnir L, Kuczera K, Lau FTK, Mattos C, Michnick S, Ngo T, Nguyen DT, Prodhom B, Reiher III WE, Roux B, Schlenkrich M, Smith JC, Stote R, Straub J, Watanabe M, Wiorkiewicz-Kuczera J, Yin D, Karplus M. All-atom empirical potential for molecular modeling and dynamics Studies of proteins. *J. Phys. Chem. B* (**1998**) 102, 3586-3616.

193. Foloppe N, MacKerell Jr AD. All-Atom Empirical Force Field for Nucleic Acids: 1) Parameter Optimization Based on Small Molecule andCondensed Phase Macromolecular Target Data. *J. Comput. Chem*. (**2000**) 21, 86-104.

194. Phillips JC, Braun R, Wang W, Gumbart J, Tajkhorshid E, Villa E, Chipot C, Skeel RD, Kale L, Schulten K. Scalable molecular dynamics with NAMD. *J. Comput. Chem*. (**2005**) 26, 1781-1802.

195. MOPAC2009, James JP Stewart, Stewart Computational Chemistry, Colorado Springs, CO, USA, http://OpenMOPAC.net.

196. Goodsell DS, Olson AJ. Automated Docking of Substrates to Proteins by Simulated Annealing. *Proteins: Str .Func. and Genet.* (**1990**) 8, 195-202.

197. Accelrys Software Inc., San Diego, CA, USA.

198. Vistoli G, Pedretti A, Mazzolari A, Testa *B.* In silico prediction of human carboxylesterase-1 (hCES1) metabolism combining docking analyses and molecular dynamics simulations. *Bioorg. Med. Chem.* (**2010**) 18, 320-329.

199. Hussain H, Babic G, Durst T, Wright JS, Flueraru M, Chichirau A, Chepelev LL. Development of Novel Antioxidants: Design, Synthesis, and Reactivity. *J. Org. Chem.* (**2003**) 68, 7023-7032.

200. Erba E, Mai G, Pocar D. ChemInform Abstract: Triazolines. Part 32. Synthesis of 1-Alkyl-2-aminobenzimidazoles from 5-Amino-1-(2-nitroaryl)-1,2,3-triazolines. *J. Chem. Soc., Perkin Trans. 1* (**1992**) 20, 2709-2712.

201. Lloyd HA, Horning EC. Synthesis of oxindole-3-propionic acid by ring rearrangement. *J Am Chem Soc* (**1954**) *76*, 3651-3653.